

PROGRAM AND ABSTRACTS FOR CLAY MINERALS SOCIETY 28th ANNUAL MEETING



Houston, Texas
October 5-10, 1991

NASA

National Aeronautics and
Space Administration

Lyndon B. Johnson Space Center
Houston, Texas

(NASA-TM-105098) PROGRAM AND ABSTRACTS FOR
CLAY MINERALS SOCIETY 28TH ANNUAL MEETING
(NASA) 232 p CSCL 08G



LPI
N92-10248
--THRU--
N92-10256
Unclas
0046140

G3/46

The Clay Minerals Society

1990-1991

COUNCIL

EXECUTIVE COMMITTEE

Thomas J. Pinnavaia, President
Robert C. Reynolds, Jr., Vice President
Don Scafe, Secretary
Kenneth M. Towe, Treasurer
Kenneth M. Towe, Interim Editor
Brij L. Sawhney, Immediate Vice President
David R. Pevear, Vice President Elect

S. P. Altaner '91
C. V. Clemency '91
P. M. Costanzo '91
G. R. Thompson '91
B. L. Allen '92
K. S. Brady '92

F. J. Longstaffe '92
J. L. Post '92
P. F. Low '93
D. M. Moore '93
P. H. Nadeau '93
R. M. Pollastro '93

Previous Meetings

1952 University of California, Berkeley (1st Annual Clay Minerals Conference)
1953 University of Missouri
1954 Rice Institute
1955 Pennsylvania State University
1956 University of Illinois at Urbana-Champaign
1957 University of California, Berkeley
1958 U.S. National Museum, Washington, D.C.
1959 University of Oklahoma
1960 Purdue University
1961 University of Texas
1962 National Research Council of Canada
1963 Georgia Institute of Technology
1964 University of Wisconsin (1st Clay Minerals Society Meeting)
1965 University of California, Berkeley
1966 Mellon Institute
1967 University of Denver
1968 University of Indiana
1969 Dallas, Texas
1970 Miami Beach, Florida
1971 South Dakota School of Mines and Technology
1972 Woods Hole Oceanographic Institute
1973 Banff, Alberta, Canada
1974 Case Western Reserve University
1975 Mexico City, Mexico
1976 Oregon State University
1977 Kingston, Jamaica
1978 University of Indiana
1979 Macon, Georgia
1980 Baylor University, Waco Texas
1981 University of Illinois at Urbana-Champaign
1982 Hilo, Hawaii
1983 Buffalo, New York
1984 Baton Rouge, Louisiana
1985 Denver, Colorado (with AIPEA)
1986 Jackson, Mississippi
1987 Socorro, New Mexico
1988 Grand Rapids, Michigan
1989 Sacramento, California
1990 Columbia, Missouri
1991 Houston, Texas

**PROGRAM AND ABSTRACTS FOR
CLAY MINERALS SOCIETY
28th ANNUAL MEETING**

Houston, Texas
October 5-10, 1991

Hosted with
NASA Johnson Space Center
Lunar and Planetary Institute

Complied in 1991 by
Lunar and Planetary Institute
3303 NASA Road 1
Houston TX 77058-4399

The Lunar and Planetary Institute is operated by the Universities Space Research Association under Contract No. NASW-4574 with the National Aeronautics and Space Administration.

Preface

This volume contains abstracts that have been accepted for presentation at the Clay Minerals Society 28th Annual Meeting.

The Local Organizing Committee consisted of D. R. Pevear (General Chair), J. B. Dixon (Program Chair), D. W. Ming (NASA Representative), L. Simmons (LPI Representative), R. Morris and D. C. Golden (Workshop Organizers), and T. Garcia and D. W. Ming (Field Trip Organizers).

Symposia Conveners were J. J. Fripiat (Surface Chemistry), J. L. Gooding and V. L. Sharpton (The Extraterrestrial Connection), E. Eslinger and J. R. Glasmann (Geothermometers and Geochronometers), P. M. Bertsch and B. L. Sawhney (Soils and Clays in Environmental Research).

Generous financial contributions toward various specific aspects of the meeting were made by the following, to whom we offer sincere thanks: Alpha Earth Inc., ARCO Oil and Gas Co., Chevron Oil Field Research Co., CONOCO Inc., Exxon Production Research Co., Siemens X-Ray Analytical Instruments Inc., and UNOCAL Science and Technology.

Special thanks are due to David C. Black, Director of the Lunar and Planetary Institute, for his willingness to help the Clay Minerals Society have a truly multidisciplinary annual meeting, and to several loyal and hard-working LPI personnel, particularly Cathy Fischer, whose efforts, sometimes under severe time constraints, largely neutralized the Chair's lack of planning.

The General Chair thanks his employer, Exxon Production Research Co., for their willing support of his spending time organizing this meeting.

Logistics and administrative support were provided by the Program Services Department staff at the Lunar and Planetary Institute. This abstract volume was prepared by the Publications Services Department staff at the Lunar and Planetary Institute.

1991 SUSTAINING MEMBERS OF THE CLAY MINERALS SOCIETY

In 1991 the following organizations and individuals contributed \$100 or more to the Clay Minerals Society:

American Colloid Company
A. P. Green Refractories
Anglo-American Clays Corporation
Aquafine Corporation
Baroid Corporation
Burgess Pigment Company
Chevron Oil Field Research Company
Comalco Limited
CONOCO, Inc.
Engelhard Minerals and Chemical Corporation
Exxon Production Research Company
Floridin Company
Halliburton Services
J. M. Huber Corporation

Kentucky-Tennessee Clay Company
Marathon Oil Company
Nord Kaolin Company
Oil-Dri Company
Shell Development Company
Southern Clay Products Company
H. C. Spinks Company, Inc.
Thiele Kaolin Company
UNOCAL
United Catalysts, Inc.
R. T. Vanderbilt Company, Inc.
J. L. White, Inc.
W. R. Grace and Company
Wyo Ben, Inc.



Contents

PROGRAM	xvii
INDEX TO SESSIONS BY AUTHOR	xxxv
Combined Backscatter Mössbauer Spectrometer and X-Ray Fluorescence Analyzer (BaMS/XRF) for Planetary Surface Materials D. G. Agresti, T. D. Shelfer, M. M. Pimperl, E. L. Wills, and R. V. Morris	1
Sources of Clay Minerals on Mars C. C. Allen	2
A Method for the Determination of Refractive Index of Fine-Grained Mineral Powders F. Allen and P. Sennett	3
Hydrothermal Alteration in Two Active Geothermal Wells from the Phlegrean Volcanic Fields, Italy S. P. Altaner, R. H. Lander, R. E. Klimentidis, and R. F. Ylagan	4
NMR Investigation of Homo-Ionic Na- and Li-Montmorillonite D. M. Anderson	5
A Saponite-Vermiculite Intermediate in Amygdales of the Granby Basaltic Tuff, Connecticut Valley R. H. April and D. M. Keller	6
Mineralogy and Chemistry of Subsurface (900–4600 m) Mudrocks and <0.5 μm Clay Separates from the Texas Gulf Coast Paleocene-Eocene D. N. Auvillier	7
High Resolution Transmission and Analytical Electron Microscopy of the Smectite to Illite Transition in Australian Mudrocks J. C. Baker and I. D. R. Mackinnon	8
Fluid-Clay Interactions in Sandstone Reservoirs: Direct Observation J. C. Baker, P. J. R. Uwins, K. R. Martin, and I. D. R. Mackinnon	9
Clays on Mars: Review of Chemical and Mineralogical Evidence A. Banin and J. L. Gooding	10
The Internal Oxygen Isotope Fractionations in Clay Minerals: Preliminary Results and Application as Single-Mineral Geothermometers A. Bechtel	11
The Evidence for (and Against) Clay Minerals on Mars from 20 Years of Telescopic Observations J. F. Bell III	12
An Exceptional Illite from the Eureka Mine, Cordoba Province, Rep. Argentina S. R. Bertolino, C. C. Harvey, and H. H. Murray	13
Determination of Paleogeothermal and Paleohydrologic Conditions in Silicic Tuffs from Illite/Smectite Mineralogy D. L. Bish	14
Rietveld Refinement of the Dickite Crystal Structure at 12 K D. L. Bish	15
Quantitative X-Ray Diffraction Analysis of Soils: Comparison of Conventional Curve-Fitting and Rietveld Full-Pattern Methods D. L. Bish and R. C. Jones	16

Mid-IR and NIR Diffuse Reflectance of Montmorillonites as Mars Surface Analog Materials <i>J. L. Bishop, C. M. Pieters, and L. M. Coyne</i>	17
Clay Mineralogy of a Soil Climosequence Formed in Granodiorite, Sierra Nevada <i>J. L. Boettinger and R. A. Dahlgren</i>	18
Mineralogy and Mineral Equilibria of an Alfisol/Vertisol Complex in the Australian Tropics <i>J. L. Boettinger, R. A. Dahlgren, and R. J. Southard</i>	19
Low Temperature Magnetism of Goethite: Aluminum Substitution and Surface Area Effects on Mössbauer Spectra <i>L. H. Bowen, E. De Grave, P. M. A. de Bakker, and R. E. Vandenberghe</i>	20
Properties and Mechanisms of Organo-Clays as Sorbents for Pollutant Chemicals <i>S. A. Boyd</i>	21
Porosity and Index Properties Analysis of Fine-Grained Marine Sediments Using TEM <i>P. J. Burkett</i>	22
Clay Minerals in Carbonaceous Chondrites: Characterization by Cryogenic Mössbauer Spectroscopy <i>R. G. Burns and D. S. Fisher</i>	23
The Use of Illite/Smectite as a Thermal Maturity Indicator in the Northern Eromanga Basin, Queensland, Australia <i>D. C. Carmichael, R. J. Smith, and J. C. Baker</i>	24
Clay-Fluid Interactions and Flow in a Single Fracture <i>J. J. Carter, L. R. Myer, and G. Sposito</i>	25
The Mechanisms of Ionic and Non-Ionic Surfactants Adsorption-Abstraction on Heterogeneous Surfaces <i>J. M. Cases and F. Villieras</i>	26
Characterization of Interlayer Charge and Interstratification in Illite/Smectite Clays from K-Bentonites Using Alkylammonium Ion Exchange, X-Ray Diffraction and Transmission Electron Microscopy <i>K. Cetin and W. D. Huff</i>	27
Experimental Investigation of the Low Temperature Transformations of Clay Minerals in the Opalinus Shale, Switzerland <i>J. A. Chermak</i>	28
Rehydration Behavior of a Natural Analcime <i>S. J. Chipera and D. L. Bish</i>	29
Changes in U(VI) Speciation upon Sorption onto Montmorillonite from Aqueous and Organic Solution <i>C. J. Chisholm Brause, D. E. Morris, P. G. Eller, T. C. Buscher, and S. E. Conradson</i>	30
Clay Minerals as Records of the Thermal History of Sedimentary Basins <i>N. Clauer</i>	31
Sr-Nd Isotope Constraints on the Glauconitization Process <i>N. Clauer, P. Stille, and E. Keppens</i>	32
A Comparison of Methods for the Extraction of Smectites from Calcareous Rocks by Acid Dissolution Techniques <i>R. J. Cook</i>	33

Fabric Changes in Clays Permeated with Organic Liquids H. S. Cornachione, J. S. Gierke, and S. D. McDowell	34
Determining the Absolute Age of Late-Stage Thermal Maturation of Anthracite in Eastern Pennsylvania from Radiometric Dating of NH ₄ -bearing Illite E. J. Daniels, J. L. Aronson, and S. P. Altaner	35
Chlorite Geothermometry: Principles and Applications P. de Caritat, I. Hutcheon, and J. L. Walshe	36
Evaluation of Ferrous and Ferric Mössbauer Fractions for Various Natural and Synthetic Compounds E. De Grave and M. Van Alboom	37
Clay Science in Soil Environments: Recent Findings J. B. Dixon	38
Distribution of Clays in Sandstones, as Studied by Scanning Electron Microscope Image Analysis C. Durand	39
Clay Particle Sizes from Atomic Force Microscopy D. D. Eberl and A. Blum	40
Use of Illite Particle Thickness, Rather than Expandability, as a Measure of Diagenetic Grade D. D. Eberl and J. Srodon	41
Origin of the Clay Minerals at the Cretaceous/Tertiary (K/T) Boundary in Denmark W. C. Elliott and J. L. Aronson	42
Characterization of Low Temperature Silica Polymorphs in Calcium Bentonites, Sodium Bentonites and Fuller's Earths by XRD, SEM/EDS and TEM J. M. Elzea, E. K. Sprague, and I. E. Odom	43
Clay Mineral Stable Isotopes: Magnus Sandstone, North Sea A. E. Fallick, C. I. Macaulay, and R. S. Haszeldine	44
Characterisation of Jordanian and Australian Palygorskites B. S. M. Faraj, H. N. Khoury, and I. D. R. Mackinnon	45
Fine-grained Clays in Southern Hemisphere Coals: The Nature of Micrinite B. S. M. Faraj, I. D. R. Mackinnon, and M. Glikson	46
In Situ Investigation of EDB Sorption/Desorption Processes on Clay Mineral Surfaces by Diffuse Reflectance Infrared Spectroscopy W. J. Farmer, Y. Aochi, and B. L. Sawhney	47
Chromium (III) Induced Solid Phase Transformation of δ -MnO ₂ S. E. Fendorf and D. L. Sparks	48
Ammonium Fixation During Clay Mineral Diagenesis and Hydrocarbon Maturation R. E. Ferrell Jr. and L. B. Williams	49
Clay Minerals as Indicators of Paleocyanography, Paleoclimate and Diagenesis in the Upper Cretaceous Greenhorn Cyclothem of the Mancos Shale D. B. Finkelstein, R. M. Leckie, and R. F. Yuretich	50
Authigenic Illite in Silicic Tuffs of Pleistocene Lake Tecopa, California—A Cautionary Note for Clay-Mineral Geothermometry N. S. Fishman, C. E. Turner, and R. A. Sheppard	51
Electrochemical Methods for the Study of Clay Hydration A. Fitch	52

Solid-State Multinuclear NMR Studies of Reactions at the Silica-Alumina Interface in Clay Minerals <i>J. J. Fitzgerald, A. I. Hamza, S. F. Dec, C. E. Bronnimann, and G. E. Maciel</i>	53
Geochemical Computer Modelling of Clay-Pore Water Interaction as a Tool for Geothermometry <i>B. Fritz, B. Madé, and J. Duplay</i>	54
Effect of Structural Iron Reduction on the Rheological Characteristics of Na-Nontronite <i>H. Gan and J. W. Stucki</i>	55
Alkylation Reactions Using Layered Double Hydroxides as Supported Anionic Reagents <i>A.-L. Garcia-Ponce, B. Casal, and E. Ruiz-Hitzky</i>	56
The Influence of Particle Size on the Chemistry of Mica Clays <i>P. L. Gassman and L. W. Zelazny</i>	57
Intracrystalline Fractionation of Oxygen Isotopes Between Hydroxyl and Non-Hydroxyl Sites in Kaolinite: Thermal Dehydroxylation and Partial Fluorination Approaches <i>J.-P. Girard, S. M. Savin, and X. Feng</i>	58
The Importance of Late Cimmerian Meteoritic Recharge to Reservoir Quality, Rotliegendes Sandstone, Netherlands <i>J. R. Glasman</i>	59
Ionic Strength Effects on Boron Adsorption by Oxides, Clay Minerals, and Soils <i>S. Goldberg, H. S. Forster, and E. L. Heick</i>	60
Transformation Products of Submicron-Sized Aluminum-Substituted Magnetite: Color and Reductant Solubility <i>D. C. Golden, D. W. Ming, and H. V. Lauer Jr.</i>	61
The Crystal Structure of Greenalite and Caryopilite: A System of Regularly Interstratified Crystalline and Semi-Amorphous Sheets <i>S. Guggenheim, R. A. Eggleton, and I. D. R. Mackinnon</i>	62
Ionic Modeling of the Hydrogen Sites in the Kaolin Polymorphs <i>G. Guthrie and D. L. Bish</i>	63
Quantitative Analysis of Mordenite-Clinoptilolite Mixtures Using the Rietveld Method <i>G. Guthrie and D. L. Bish</i>	64
Study of the Kaolinite-rich Claystone Layer from the Cretaceous-Tertiary Boundary Using Infrared Spectroscopy <i>J. W. Happ</i>	65
Unconformity-Related K-Feldspar and Phyllosilicate Alteration at the Precambrian-Paleozoic Boundary, Southwestern Ontario <i>D. A. Harper, F. J. Longstaffe, and M. A. Wadleigh</i>	66
Mixed-Layer Clay Geothermometry in the Wairakei Geothermal Field, New Zealand <i>C. C. Harvey and P. R. L. Broune</i>	67
The Influence of Composition on the Release of Radiogenic Argon from Illitic and Glauconitic Clay Samples <i>A. A. Hassanipak and J. M. Wampler</i>	68
A Method Combining SWIR and XRD for the Identification of Clay Minerals: I. Interstratified Kaolinite/Smectite Clays <i>P. Hauff and M. Thiry</i>	69

Kaolinite was a Precursor to Diagenetic K-Feldspar of Paleozoic Age in Wisconsin R. L. Hay and J. Liu	70
Origin and Diagenesis of Chlorite Minerals in the Orcadian Basin, Scotland S. Hillier	71
Cation Exchange Staining of Clay Minerals in Thin-Section S. Hillier and T. Clayton	72
Occurrence of Expandable Clay Minerals in Contact Metamorphic Aureoles M. M. Hluchy, R. H. April, and S. L. Beebe	73
Mapping Diagenetic Fluid Flow Within a Reservoir—K/Ar Dating in the Alwyn Area, UK North Sea A. J. C. Hogg, A. E. Fallick, and M. J. Pearson	74
Modelling of the Crystal Structure of Potassium Birnessite K. Holland and J. R. Walker	75
An Experimentally Derived Kinetic Model for Smectite-to-Illite Conversion and Its Use as Geothermometer W. L. Huang, J. M. Longo, and D. R. Pevear	76
Geotechnics of Dense Clay Soils Subjected to Heat and Chemicals: Toward Predictive Model T. Hueckel and C. M. Ma	77
Diagenesis of Overpressured Tertiary and Cretaceous Mudstones from the East Shetland Basin, North Sea J. Huggett	78
Mixed-Layered Kaolinite/Expandables: Occurrence and Rates of Formation in Quaternary, Mississippi Valley Loesses R. E. Hughes, D. A. Grimley, L. R. Follmer, D. M. Moore, and W. H. Johnson	79
Synthesis of Fluorinated 2:1 Layer Silicates and Their Characterization by ^{29}Si , ^{27}Al and ^{19}F Magic Angle Spinning (MAS) Nuclear Magnetic Resonance (NMR) Spectroscopy L. Huwe, D. Saehr, P. Martin, J. Baron, and R. Le Dred	80
Hydrophobicity of Siloxane Surfaces in Smectites as Revealed by Aromatic Hydrocarbon Adsorption from Water W. F. Jaynes and S. A. Boyd	81
The Glass-to-Smectite Alteration of Tektites at the Cretaceous/Tertiary Boundary C. Jéhanno, Ph. Bonté, L. Froget, E. Robin, R. Rocchia, and H. Sigurdsson	82
AFM Study of the Surface Morphology of Muscovite Dissolved in Water P. A. Johnsson, A. E. Blum, and M. F. Hochella Jr.	83
Quantitative X-Ray Diffraction Analysis of Soils: Rietveld Full-Pattern Mineral Concentrations and Pattern Curve Fitting vs. P Sorption of Bauxite Soils R. C. Jones and D. L. Bish	84
The Smectite to Illite Reaction: Fluid & Solids Evolution Under Flow-Through Conditions G. H. Kacandes, H. L. Barnes, and L. R. Kump	85
Rehydration of Rectorite M. Kawano and K. Tomita	86
Clay Minerals in Primitive Meteorites and Interplanetary Dust II. Smectites and Micas L. P. Keller and M. E. Zolensky	87

Electron Spin Echo Modulation Studies of Transition Metal Ions in Pillared and Nonpillared Smectite Clays L. Kevan	88
Correlation of X.R.D. Crystallinity and T.E.M. Crystal Size of Synthetic Mica R. E. Klimentidis, W. L. Huang, and D. R. Pevear	89
Mössbauer Spectroscopy on the Surface of Mars G. Klingelhöfer, J. Foh, P. Held, H. Jäger, E. Kankeleit, R. Teucher, E. N. Evlanov, V. Khromov, L. M. Mukhin, O. F. Prilutski, B. Zubkov, G. V. Smirnov, J. Juchniewicz, J. M. Knudsen, M. Madsen, and C. d'Uston	90
Weathering of Impactite from Monturaqui C. B. Koch	91
K/T Boundary at Stevns, Denmark C. B. Koch and S. S. Jørgensen	92
Infrared Study of Structural OH in Good and Poorly Crystalline Kaolin and in their "Deferrated" Products at 300 K° E. Kocsardy and N. R. Shaffer	93
Soil Formation as a Solute Source for Stream Water C. J. Kornegay and R. J. Donahoe	94
K-Ar, Rb-Sr Isotopes in Clay Mineral Research in Carbonate Environments M. Kralik	95
The Role of Al in Fe(II) Transformation G. S. R. Krishnamurti and P. M. Huang	96
Decomposition of X-Ray Diffraction Patterns: A Convenient Way to Describe Complex I/S Diagenetic Evolution B. Lanson	97
Repetitive Occurrence of Potassic Diagenesis in the Region of the Upper Mississippi Valley (UMV) Mineral District: Implications for a Persistent Paleo-Hydrological Setting Favorable for Diagenesis M. Lee and J. L. Aronson	98
Environmental Restoration of DOE Sites: R & D Issues Related to Clay Sciences S. Y. Lee	99
Surface Thermodynamic Properties of Some Illites Z. Li, R. Giese, D. Eberl, and C. J. van Oss	100
Clays in Sediments of Yamato Basin, Japan Sea P.-H. Lo and T. T. Tieh	101
Mineralogical Modifications of Oil Sands During Steam Stimulation: Post-Steam Core from the Wabiskaw Member, Northeastern Alberta F. J. Longstaffe, B. N. Fialka, and G. A. Robb	102
Structural Studies of Hydroxy-Aluminosilicate Polymers Intercalated in Hectorite by Solid-State ²⁹ Si and ²⁷ Al NMR G. Lou, P. M. Huang, and J. A. Ripmeester	103
Implications of Clay-Water Isotopic Exchange During Burial Diagenesis of Shales— A Modeling Perspective P. D. Lundegard	104

Depth Related Changes in Clay Mineralogy from Frio Formation (Oligocene) Shales, Cameron, Kenedy, and Nueces Counties, Texas F. L. Lynch	105
Swelling Potential and Mineralogical Composition of Clay-Sulfate Rocks F. T. Madsen and R. Nüesch	106
Low Temperature Weathering of Basalt M. B. Madsen, L. Vistisen, N. O. Roy-Paulsen, C. B. Koch, S. Morup, and M. D. Bentzon	107
Two Scenarios for the Genesis of the Kaolinitic Vertisols on the Hawaiian Island of Lanai and Molokai H. U. Malik and R. C. Jones	108
X-Ray Absorption Spectroscopy: A Tool for Probing the Structure of Surface Complexes A. Manceau and L. Charlet	109
Contrasting Mineral/Water Reaction Pathways in Three Saline, Alkaline Lakes from Southeast Oregon J. C. Matthews and S. P. Altaner	110
Mechanism of Clay Formation on Tektites: Natural Weathering vs. Laboratory Alteration J. J. Mazer, J. K. Bates, C. R. Bradley, J. P. Bradley, and C. M. Stevenson	111
A Rapid Estimation of Layer Charge of 2:1 Expanding Silicate Clays by Alkyl Ammonium A. R. Mermut and R. J. St. Arnaud	112
Surface Chemical and Mineralogical Aspects of Colloid-Facilitated Contaminant Transport W. P. Miller and P. M. Bertsch	113
Mineralogy of Cretaceous/Tertiary Boundary Clays in the Chicxulub Structure in Northern Yucatan D. W. Ming, V. L. Sharpton, and B. C. Schuraytz	114
Characteristics of Chlorite Interlayered with a 7 Å Mineral as Found in Sandstone Reservoirs D. M. Moore and R. E. Hughes	115
Hole-Trapping Defects in Kaolinite: Origin and Use as Environmental Tracers J.-P. Muller, T. Allard, and G. Calas	116
Genetic Significance of Mn ²⁺ and VO ²⁺ Sorbed onto Natural Kaolinite J.-P. Muller, N. Malengreau, and G. Calas	117
Mössbauer Spectra of Kaolinite, Halloysite and the Firing Products of Kaolinite E. Murad and U. Wagner	118
Surface Free Energies of Kaolinites K. Murphy, C. J. Van Oss, and R. F. Glese	119
Evidence of Dissolution and Precipitation on Gibbsite Using Atomic Force Microscopy K. L. Nagy, M. F. Hochella Jr., A. E. Blum, and A. C. Lasaga	120
Hydrophobic Nature of Organo-Clays as a Lewis Acid/Base Phenomenon J. Norris, R. Giese, P. M. Costanzo, and C. J. van Oss	121
Equilibrium and Spectroscopic Characterization of Co(II) Sorption Sites on Kaolinite Surfaces P. A. O'Day, G. A. Parks, and G. E. Brown Jr.	122
Environmental Aspects of Silica Minerals in Clays and Sediments I. E. Odom and J. M. Elzea	123
Illite Age Analysis: A Method for Interpreting Shale K/Ar Ages D. R. Pevear and W. C. Elliott	124

Petrogenetic Significance of Kaolinite Nucleation and Growth on Pre-existing Mica in Sandstones and Shales <i>D. R. Pevear, R. E. Klimentidis, and G. A. Robinson</i>	125
Recent Advances in Intercalated Clay Catalysts <i>T. Pinnavaia</i>	126
Characterization of Fly Ash and the Immobilisation of Pb and Zn with Clay Minerals <i>A. Plüss and R. E. Ferrell Jr.</i>	127
The Illite/Smectite Geothermometer—Considerations and Case-History Studies in Hydrocarbon-Bearing Rocks of Miocene to Mississippian in Age <i>R. M. Pollastro</i>	128
Origin and Genesis of Clay Minerals at the Cretaceous-Tertiary Boundary Interval, U.S. Western Interior <i>R. M. Pollastro and B. F. Bohor</i>	129
Beidellite from the Black Jack-Trade Dollar Mine and Nearby Delamar Silver Mine <i>J. L. Post and B. L. Cupp</i>	130
Illite/Smectite Geothermometry of the Oronto Group, Southern Lake Superior Basin, Michigan <i>K. L. Price and S. D. McDowell</i>	131
Rietveld Refinement of a 11b-2 Clinocllore <i>J. Rakovan and S. Guggenheim</i>	132
One- and Three-Dimensional X-Ray Powder Diffraction Studies of Illite/Smectites Subjected to Different Sample Preparation Methods <i>R. C. Reynolds Jr.</i>	133
Structural and Compositional Variations in Low-Grade Metamorphic Illite and Chlorite from the Belt Supergroup, Montana and Idaho <i>P. Ryan and G. Thompson</i>	134
Respirable Quartz Determination in Kaolin by X-Ray Diffraction Methods <i>T. L. Salter and W. E. Riley</i>	135
Overview of Interactions of Organic and Inorganic Contaminants with Soils and Clays <i>B. L. Sawhney</i>	136
Far Infrared Spectroscopy of Mixed-Layer Illite/Smectites <i>P. A. Schroeder</i>	137
Trace Element Analysis of Atmospheric Aerosols Using a Synchrotron X-Ray Fluorescence Microprobe <i>D. G. Schulze, R. H. Grant, S. R. Sutton, and M. L. Rivers</i>	138
Fault Gouge Clay Dates—How Meaningful are they? <i>M. Shafiqullah and P. E. Damon</i>	139
Interaction Between Chlorohydrocarbon and Heavy Cations in the Clay Interlayer: An Example of Synergistic Effect <i>D. P. Siantar and J. J. Fripiat</i>	140
Influence of Citric Acid and Glycine on Kinetics of Mercury (II) Adsorption by Kaolinite <i>J. Singh and P. M. Huang</i>	141
The Effects of Burial Diagenesis on the Texture, Mineralogy and Properties of Source Rocks from the Permian Basin <i>S. Sivalingam</i>	142

Analytical Electron Microscopy of Illite/Smectite Clays from the Permian Basin S. Sivalingam and N. Guven	143
Estimation of Gibbs Free Energy of Formation of Clay Minerals Using Calculated Binding Energies M. Slaughter and J.-Y. Yu	144
Partial Binding Energies and Structural Properties of the Heulandite/Clinoptilolite Series M. Slaughter and J.-Y. Yu	145
Experimental Determination of the Stability and Rate of Precipitation of Authigenic Illite J. S. Small	146
Halloysite; Product of Calcium-rich Plagioclase Alteration, Riverside County, California M. C. Taylor and R. W. Berry	147
Authigenic Muscovite $^{40}\text{Ar}/^{39}\text{Ar}$ Isotopic Analyses as a Tool for Timing Pressure Solution in the Jurassic Norphlet Formation A. R. Thomas, W. M. Dahl, C. M. Hall, and D. York	148
Non-Facies Selective Clay Paragenesis of Sandstone Reservoirs, Fuller Reservoir Field, Wind River Basin, Wyoming J. Thorez, D. Bossiroy, R. M. Flores, and C. W. Keighin	149
Quantitative Whole Rock Determination of Clay Minerals in Sandstones by Combined XRD/TG/EWA D. M. Thornley and T. J. Primmer	150
Synthesis of Smectite from a Volcanic Glass, Clay Minerals and Rocks at 1 atm. K. Tomita, H. Yamane, and M. Kawano	151
Oxidation of Phenol in Acidic Aqueous Suspensions of Manganese Oxides L. Ukrainczyk and M. B. McBride	152
Textural and Compositional Variations in Size Fractionated Australian Kaolins P. J. R. Uwins and I. D. R. Mackinnon	153
"Crystallinity" and Intercalation Relationships in Size Fractionated Australian Kaolinites P. J. R. Uwins, I. D. R. Mackinnon, and J. G. Thompson	154
Artificial Weathering of Biotite and Phlogopite on Ultrathin Sections; Studied in HRTEM H. Vali, R. Hesse, and H. Kodama	155
Combined TEM Observation of Layer Structure and Surface Microtopography Applied to Study the Crystal Growth Mechanism of Clay Minerals H. Vali, R. Hesse, and J. Sródoní	156
Integrated XRD and XRF Data from a Single Instrument for Planetary-Surface Exploration D. Vaniman, D. Bish, and S. Chipera	157
Sepiolite at the Surface of Yucca Mountain, Nevada D. Vaniman, D. Bish, S. Chipera, and M. Ebinger	158
Clay and Vitrinite Kinetic Models B. Velde	159
Clay Stabilities Under Shock Pressure B. Velde	160
UV, Visible, and Near-IR Reflectivity Data for Magnetic Soils/Rocks from Brazil R. K. Vempati, R. V. Morris, H. V. Lauer Jr., and J. M. D. Coey	161

Synthesis and Properties of Ti-Substituted Goethites and Hematites R. K. Vempati, R. V. Morris, H. V. Lauer Jr., and J. DeHart	162
Clay Minerals in Subduction Zones—Role of Interlayer Water P. Vrolijk	163
Chlorite Polyttypism—A Possible Geothermometer? J. R. Walker	164
Authigenic Clay Minerals in Reservoir Sandstones of the Permian Delaware Mountain Group, West Texas S. D. Walling and T. T. Tieh	165
A Stepwise-Dissolution Technique for Potassium-Argon Analysis of Clays J. M. Wampler and A. A. Hassanipak	166
Catalytic Transformations of Amino Acids by Birnessite as Influenced by Pyrogallol M. C. Wang	167
Mechanism on Formation of Birnessite in Alkali Media M. K. Wang and D. S. Young	168
Nature of OH-Al Polymers in Commercial and Laboratory Prepared Solutions W. Wang and P. H. Hsu	169
Once a Pioneer Always a Pioneer C. E. Weaver	170
Timing of Kaolinitization in Hard Kaolins of the Huber Formation in Central and Eastern Georgia: Trace Fossil Microtextures Documented by Scanning Electron Microscopy H. Webb and E. K. Sprague	171
Paleoenvironmental Implications of Lacustrine Clay Minerals from the Double Lakes Area, Southern High Plains, Texas D. M. Webster and B. F. Jones	172
Sedimentary Structure in Gray Kaolins of Georgia G. N. White, J. B. Dixon, R. M. Weaver, and A. C. Kunkle	173
Textural Changes and Nucleation During the Early Stages of Illitization: An Experimental Study G. Whitney and B. Velde	174
Detrital Kaolinite in Sandstones of the Ancestral Yuba River (Eocene), Sierra Foothills, California J. L. Wood	175
Transmission Electron Microscopy Study of Implanted Mica Q. Xu, W.-A. Chiou, C. Tomplier, and L. Cartz	176
Transmission Electron Microscopy and Thermal Expansion Behavior of Biotite and Phlogopite Micas X. Yang, W.-A. Chiou, and L. Cartz	177
Significance of Oxygen Isotope Temperatures of Sea-Floor Hydrothermal Smectite H.-W. Yeh	178
Geometrical Structure Synthesis and Stability of Dioctahedral Clay Minerals, Including the Water Structure of Hydrated Montmorillonite J.-Y. Yu and M. Slaughter	179
Multiple-Site Modeling of Metal Ion Adsorption on Specimen and Soil Layer Silicates J. M. Zachara, C. E. Cowan, and S. C. Smith	180

Effect of Cations on the Relation Between Swelling Pressure and Interlayer Distance in Montmorillonite <i>F. Zhang, P. F. Low, and C. B. Roth</i>	181
Sorption and Desorption of Quaternary Amine Cations on Clays <i>Z. Z. Zhang and D. L. Sparks</i>	182
The Nature of the Surface Charge on Kaolinite: Constraint of Surface Charge Density <i>Z. Zhou and W. D. Gunter</i>	183
Clay Minerals In Primitive Meteorites and Interplanetary Dust I. <i>M. Zolensky and L. P. Keller</i>	184
AUTHOR INDEX	185



SUMMARY PROGRAM

DATE/TIME	EVENT/LOCATION
Saturday, October 5	
7:00 - 9:00 A.M.	Workshop Registration/Hilton Lobby
8:00 - 12:30	Workshop/Admiral Ballroom
12:30 - 1:30	Workshop Luncheon/Admiral Ballroom
1:30 - 5:00 P.M.	Workshop/Admiral Ballroom
5:00 - 6:30	Workshop Wine and Cheese/Marina Room
7:30 - 10:30	CMS Exec. Committee/Penthouse
Sunday, October 6	
9:00 - 5:30 A.M.	CMS Council Meeting/Marina Room
3:00 - 7:00 P.M.	General Registration/Hilton Lobby
5:30 - 8:30	Ice-Breaker Reception/Lakeview Manor
Monday, October 7	
7:30 - 3:30 A.M.	General Registration/ Hilton Lobby
7:30 - 8:30	Sustaining Member Breakfast/Chart Room
8:30 - 11:30	Plenary Session/Admiral Ballroom Introductions 9:00 Distinguished Member Lecture 10:00 Brindley Lecture 10:45 Pioneer in Clay Science Lecture
1:00 - 3:30 P.M.	General Session I/Admiral Ballroom, A and B
1:00 - 3:30	Surface Chemistry I/Admiral Ballroom, C
1:00 - 3:30	Extraterrestrial I/Admiral Ballroom, D
3:30 - 5:00	Posters and Refreshments/Commodore and Marina Rooms
5:30 - 7:00	Students Reception/Lakeview Manor Women in Clay Science Reception/Lakeview Manor
Tuesday, October 8	
7:30 - 3:30 A.M.	General Registration/Hilton Lobby
8:00 - 11:30	Surface Chemistry II/Admiral Ballroom, C
8:00 - 11:30	Extraterrestrial II/Admiral Ballroom, D
8:00 - 11:30	Geothermometers I/Admiral Ballroom, A and B
1:00 - 2:30 P.M.	General Session II/Admiral Ballroom, C
1:00 - 3:15	Geothermometers II/Admiral Ballroom, A and B
1:00 - 3:15	Soils/Environmental I/Admiral Ballroom, D
2:30 - 4:00	Posters and Refreshments/Marina and Commodore Rooms
4:00 - 5:00	Surface Chemistry Discussion Panel/Admiral Ballroom, C
4:00 - 5:00	Extraterrestrial Connection Discussion Panel/Admiral Ballroom, D
5:30 - 6:30	Reception/Lakeview Manor
6:30 - 8:00	Banquet/Admiral Ballroom
8:00	NASA Presentation/Admiral Ballroom

DATE/TIME	EVENT/LOCATION
Wednesday, October 9	
8:00 - 5:00 A.M./P.M.	Fieldtrip
5:00 - 7:00 P.M.	Galveston Barbecue/Appfel Park
Thursday, October 10	
8:00 - 10:30 A.M.	General Session III/Admiral Ballroom, C
8:00 - 10:30	Geothermometers III/Admiral Ballroom, A and B
8:00 - 10:30	Soils/Environmental II/Admiral Ballroom, D
10:30 - 11:30	Business Meeting/Admiral Ballroom, A and B
1:00 - 2:30 P.M.	General Session IV/Admiral Ballroom, A and B
1:00 - 2:30	Soils/Environmental III/Admiral Ballroom, C
2:30 - 4:00	Posters and Refreshments/Marina and Commodore Room
3:00 - 4:00	Soils/Environmental Discussion Panel/Admiral Ballroom, C
4:30 - 5:00	Geothermometers Discussion Panel/Admiral Ballroom D
5:00	Adjournment

Each day's posters will be up all day. Presenters will be at posters during listed times.

The Captain's Room will be available 7:00 - 5:00 for speakers to preview slides.

Monday, October 7, 1991
PLENARY SESSION
8:30 a.m. Admiral Ballroom

Presiding:	D. R. Pevear, General Chair J. B. Dixon, Program Chair
8:30 - 8:45	Introduction: D. R. Pevear Welcome: D. P. Blanchard/NASA
8:45 - 9:00	President's Remarks: T. J. Pinnavaia
9:00 - 9:45	CMS Distinguished Member: J. B. Dixon, Texas A & M University Introduction: D. W. Ming <i>Clay Science in Soil Environments: Recent Findings</i>
9:45 - 10:00	Break
10:00 - 10:45	George W. Brindley Lecture: T. J. Pinnavaia, Michigan State University Introduction: J. J. Fripiat <i>Recent Advances in Intercalated Clay Catalysts</i>
10:45 - 11:30	Pioneer in Clay Science: C. E. Weaver Introduction: D. R. Pevear <i>Once a Pioneer, Always a Pioneer</i>

Monday, October 7, 1991
GENERAL I
1:00 p.m. Admiral Ballroom, A and B

Chairs: S. Guggenheim D. L. Bish

Fundamental Properties of Minerals and Methods of Mineral Analysis

1:00 - 1:20	Bish D. L.* <i>Rietveld Refinement of the Dickite Crystal Structure at 12 K</i>
1:20 - 1:40	Rakovan J. F.* Guggenheim S. <i>Rietveld Refinement of A 11b-2 Clinocllore</i>
1:40 - 2:00	Xu Q. Chiou W.-A.* Templier C. Karioris F. G. Cartz L. <i>Transmission Electron Microscopy Study of Implanted Mica</i>
2:00 - 2:20	Yang X. Chiou W.-A.* Karioris F. G. Cartz L. <i>Transmission Electron Microscopy and Thermal Expansion Behavior of Biotite and Phlogopite Micas</i>
2:20 - 2:30	Break
2:30 - 2:50	Slaughter M.* Yu J.-Y. <i>Estimation of Gibbs Free Energy of Formation of Clay Minerals Using Calculated Binding Energies</i>
2:50 - 3:10	Slaughter M.* Yu J.-Y. <i>Partial Binding Energies and Structural Properties of the Heulandite/Clinoptilolite Series</i>

- 3:10 - 3:30 Guggenheim S.* Eggleton R. A. Mackinnon I. D. R.
The Crystal Structure of Greenalite and Caryopilite: A System of Regularly Interstratified Crystalline and Semi-Amorphous Sheets

Monday, October 7, 1991
SURFACE CHEMISTRY I
 1:00 p.m. Admiral Ballroom, C

Convener: J. J. Fripiat
 Chairs: A. Manceau L. Kevan

- 1:00 - 1:45 Kevan L.*
Electron Spin Echo Modulation Studies of Transition Metal Ions in Pillared and Nonpillared Smectite Clays
- 1:45 - 2:00 Muller J.-P.* Malengreau N. Calas G.
Genetic Significance of Mn²⁺ and VO²⁺ Sorbed Onto Natural Kaolinite
- 2:00 - 2:15 Anderson D. M.*
NMR Investigation of Homo-Ionic N_a- and L_i Montmorillonite
- 2:15 - 2:30 Lou G.* Huang P. M. Ripmeester J. A.
Structural Studies of Hydroxy-Aluminosilicate Polymers Intercalated in Hectorite by Solid-State ²⁹Si and ²⁷Al NMR
- 2:30 - 3:15 Manceau A.* Charlet L.
X-ray Absorption Spectroscopy: A Tool for Probing the Structure of Surface Complexes
- 3:15 - 3:30 Discussion Period

Monday, October 7, 1991
THE EXTRATERRESTRIAL CONNECTION I
 1:00 p.m. Admiral Ballroom, D

Conveners and Chairs: J. L. Gooding V. L. Sharpton

- 1:00 - 1:30 Banin A.* Gooding J. L.
Clays on Mars: Review of Chemical and Mineralogical Evidence
- 1:30 - 1:45 Allen C. C.*
Sources of Clay Minerals on Mars
- 1:45 - 2:00 Bishop J. L.* Pieters C. M. Coyne L. M.
Mid-infrared and Near-infrared Diffuse Reflectance of Variably Cation-Exchanged Montmorillonites as Mars Surface Analog Materials
- 2:00 - 2:15 Vaniman D.* Bish D. Chipera S.
Integrated XRD and XRF Data from a Single Instrument for Planetary-Surface Exploration
- 2:15 - 2:30 Vempati R. K.* Morris R. V. Lauer H. V. Jr. DeHart J.
Synthesis and Properties of Ti-Substituted Goethites and Hematites
- 2:30 - 3:30 Discussion Period

Monday, October 7, 1991
GENERAL POSTERS I *
3:30 p.m. - 5:00 p.m. Commodore Room

* Posters in all sessions will remain up all day. Presenters will be at posters during scheduled times.

Methods of Mineral Analysis

- Thornley D. M. Primmer T. J.*
Quantitative Whole Rock Determination of Clay Minerals in Sandstones by Combined XRD/TG/EWA
- Allen F.* Sennett P.
A Method for the Determination of Refractive Index of Fine-Grained Mineral Powders
- Hauff P.* Thiry M.
Method Combining SWIR and XRD for the Identification of Clay Minerals: I Interstratified Kaolinite/Smectite Clays
- Holland K. L. Walker J. R.*
Modelling of the Crystal Structure of Potassium Birnessite
- Hillier S.* Clayton T.
Cation Exchange Staining of Clay Minerals
- Jones R. C.* Bish D. L.
Quantitative X-Ray Diffraction Analysis of Soils: Rietveld Full-Pattern Mineral Concentrations and Pattern Curve Fitting vs. P Sorption of Bauxite Soils
- Bish D. L.* Jones R. C.
Quantitative X-Ray Diffraction Analysis of Soils: Comparison of Conventional Curve-Fitting and Rietveld Full-Pattern Methods
- Guthrie G. D. Jr.* Bish D. L.
Quantitative Analysis of Mordenite-Clinoptilolite Mixtures Using the Rietveld Method
- Cook R. J.*
Smectite Extraction from Calcareous Rocks

Monday, October 7, 1991
SURFACE CHEMISTRY POSTERS
3:30 p.m. - 5:00 p.m. Marina Room

- O'Day P. A.* Parks G. A. Brown G. E. Jr.
Equilibrium and Spectroscopic Characterization of Co(II) Sorption Sites on Kaolinite Surfaces
- Huve L.* Saehr D. Martin P. Baron J. Le Dred R.
Synthesis of Fluorinated 2:1 Layer Silicates and their Characterization by ^{29}Si , ^{27}Al and ^{19}F Magic Angle Spinning (MAS) Nuclear Magnetic Resonance (NMR) Spectroscopy
- Fitzgerald J. J.* Hamza A. I. Dec S. F. Bronnimann C. E. Maciel G. E.
Solid-State Multinuclear NMR Studies of Reactions at the Silica-Alumina Interface in Clay Minerals
- Murphy K.* van Oss C. J. Glese R. F.
Surface Free Energies of Kaolinites
- Zhou Z.* Gunter W. D.
The Nature of the Surface Charge on Kaolinite: Constraint of Surface Charge Density

Gassman P. L.* Zelazny L. W.

The Influence of Particle Size on the Chemistry of Mica Clays

Wang M. C.*

Catalytic Transformations of Amino Acids by Birnessite as Influenced by Pyrogallol

Siantar D. P.* Fripiat J. J.

Interaction Between Chlorohydrocarbon and Heavy Cations in the Clay Interlayer: An Example of Synergistic Effect

Garcia-Ponce A.-L.* Casal B. Ruiz-Hitzky E.

Alkylation Reactions Using Layered Double Hydroxides as Supported Anionic Reagents

Monday, October 7, 1991

SOILS AND CLAYS IN ENVIRONMENTAL RESEARCH POSTERS

3:30 p.m. - 5:00 p.m. Marina Room

Vali H.* Hesse R. Kodama H.

Artificial Weathering of Biotite and Phlogopite on Ultrathin Sections; Studied in HRTEM

Wang M. K.* Young D. S.

Mechanism on Formation of Birnessite in Alkali Media

Schulze D. G.* Grant R. H. Sutton S. R. Rivers M. L.

Trace Element Analysis of Atmospheric Aerosols Using A Synchrotron X-Ray Fluorescence Microprobe

Kornegay C. J.* Donahoe R. J.

Soil Formation as a Solute Source for Stream Water

Cornachione H. S.* Gierke J. S. McDowell S. D.

Fabric Changes in Clays Permeated with Organic Liquids

Burkett P. J.*

Porosity and Index Properties Analysis of Fine-Grained Marine Sediments Using TEM

Madsen F. T.* Nüesch R.

Swelling Potential and Mineralogical Composition of Clay-Sulfate Rocks

Salter T. L.* Riley W. E.

Respirable Quartz Determination in Kaolin by X-Ray Diffraction Methods

Elzea J. M.* Sprague E. K. Odom I. E.

Characterization of Low Temperature Silica Polymorphs in Calcium Bentonites, Sodium Bentonites and Fuller's Earths by XRD, SEM/EDS and TEM

Monday, October 7, 1991

Student Reception

5:30 p.m. - 7:30 p.m. Lakeview Manor (adjacent to hotel - see map)

Women in Clay Science Reception

5:30 p.m. - 7:30 p.m. Lakeview Manor

Tuesday, October 8, 1991
SURFACE CHEMISTRY II
 8:00 a.m. Admiral Ballroom, C

Chairs:	J. M. Cases A. E. Blum
8:00 - 8:45	Cases J. M. Villieras F. <i>The Mechanisms of Ionic and Non-Ionic Surfactants Adsorption-Abstraction on Heterogeneous Surfaces</i>
8:45 - 9:00	Li Z. Giese R.* Eberl D. D. van Oss C. J. <i>Surface Thermodynamic Properties of Some Illites</i>
9:00 - 9:15	Zhang F.* Low P. F. Roth C. B. <i>Effect of Cations on the Relation Between Swelling Pressure and Interlayer Distance in Montmorillonite</i>
9:15 - 9:30	Fitch A.* <i>Electrochemical Methods for the Study of Clay Hydration</i>
9:30 - 9:45	Break
9:45 - 10:00	Gan H.* Stucki J. W. <i>Effect of Structural Iron Reduction on the Rheological Characteristics of Na-Nontronite</i>
10:00 - 10:15	Jaynes W. F.* Boyd S. A. <i>Hydrophobicity of Siloxane Surfaces in Smectites as Revealed by Aromatic Hydrocarbon Adsorption from Water</i>
10:15 - 11:00	Johnsson P. A. Blum A. E.* Hochella M. F. Jr. <i>AFM Study of the Surface Morphology of Muscovite Dissolved in Water</i>
11:00 - 11:15	Nagy K. L.* Hochella M. F. Jr. Blum A. E. Lasaga A. C. <i>Evidence of Dissolution and Precipitation on Gibbsite Using Atomic Force Microscopy</i>
11:15 - 11:30	Eberl D. D.* Blum A. <i>Clay Particle Sizes from Atomic Force Microscopy</i>

Tuesday, October 8, 1991
THE EXTRATERRESTRIAL CONNECTION II
 8:00 a.m. Admiral Ballroom, D

Chairs:	V. L. Sharpton J. L. Gooding				
8:00 - 8:30	<table border="0" style="border-left: 1px solid black; border-right: 1px solid black; padding-left: 10px;"> <tr> <td style="padding-right: 10px;">Zolensky M. E.* Keller L. P.</td> <td style="padding-left: 10px;"><i>Clay Minerals in Primitive Meteorites and Interplanetary Dust I.</i></td> </tr> <tr> <td style="padding-right: 10px;">Keller L. P.* Zolensky M. E.</td> <td style="padding-left: 10px;"><i>Clay Minerals in Primitive Meteorites and Interplanetary Dust II. Smectites and Micas</i></td> </tr> </table>	Zolensky M. E.* Keller L. P.	<i>Clay Minerals in Primitive Meteorites and Interplanetary Dust I.</i>	Keller L. P.* Zolensky M. E.	<i>Clay Minerals in Primitive Meteorites and Interplanetary Dust II. Smectites and Micas</i>
Zolensky M. E.* Keller L. P.	<i>Clay Minerals in Primitive Meteorites and Interplanetary Dust I.</i>				
Keller L. P.* Zolensky M. E.	<i>Clay Minerals in Primitive Meteorites and Interplanetary Dust II. Smectites and Micas</i>				
8:30 - 8:45	Burns R. G.* Fisher D. S. <i>Clay Minerals in Carbonaceous Chondrites: Characterization by Cryogenic Mössbauer Spectroscopy</i>				

- 8:45 - 9:15 Pollastro R. M.^{*} Bohor B. B.
Origin and Genesis of Clay Minerals at the Cretaceous/Tertiary Boundary Interval, U.S. Western Interior
- 9:15 - 9:30 Happ J. W.^{*}
Study of the Kaolinite-rich Claystone Layer from the Cretaceous/Tertiary Boundary Using Infrared Spectroscopy
- 9:30 - 10:00 Break
- 10:00 - 10:15 Jéhanno C.^{*} Bonté Ph. Froget L. Robin E. Rocchia R.
Sigurdsson H.
The Glass-to-Smectite Alteration of Tektites at the Cretaceous/Tertiary Boundary
- 10:15 - 10:30 Elliott W. C.^{*} Aronson J. L.
Origin of the Clay Minerals at the Cretaceous/Tertiary (K/T) Boundary in Denmark
- 10:30 - 10:45 Ming D. W.^{*} Sharpton V. L. Schuraytz B. C.
Mineralogy of Cretaceous/Tertiary Boundary Clays in the Chicxulub Structure in Northern Yucatan
- 10:45 - 11:00 Mazer J. J.^{*} Bates J. K. Bradley C. R. Bradley J. P.
Stevenson C. M.
Mechanism of Clay Formation on Tektites: Natural Weathering vs. Laboratory Alteration
- 11:00 - 11:15 Velde B.^{*}
Clay Stabilities Under Shock Pressure
- 11:15 - 11:30 Discussion Period

Tuesday, October 8, 1991
GEOOTHERMOMETERS AND GEOCHRONOMETERS I
8:00 a.m. Admiral Ballroom, A and B

Conveners: E. Eslinger J. R. Glasmann
Chairs: S. M. Savin G. Whitney

Geothermometry: Mechanisms and Modeling

- 8:00 - 8:15 Clauer N.^{*}
Clay Minerals as Records of the Thermal History of Sedimentary Basins
- 8:15 - 8:30 Whitney G.^{*} Velde B.
Textural Changes and Nucleation During the Early Stages of Illitization: An Experimental Study
- 8:30 - 8:45 Kacandes G. H.^{*} Barnes H. L. Kump L. R.
The Smectite to Illite Reaction: Fluid & Solids Evolution Under Flow-Through Conditions
- 8:45 - 9:00 Huang W. L.^{*} Longo J. M. Pevear D. R.
An Experimentally Derived Kinetic Model for Smectite-to-Illite Conversion and Its Use as Geothermometer
- 9:00 - 9:15 Velde B.^{*}
Clay and Vitrinite Kinetic Models

9:15 - 9:30 Lundegard P. D.*
Implications of Clay-Water Isotopic Exchange During Burial Diagenesis of Shales-A Modeling Perspective

9:30 - 9:45 Break

Geothermometry: New Frontiers

9:45 - 10:00 Eberl D. D.* Srodon J.
Use of Illite Particle Thickness, Rather than Expandability, as a Measure of Diagenetic Grade

10:00 - 10:15 Bechtel A.*
The Internal Oxygen Isotope Fractionation in Clay Minerals: Preliminary Results and Application as Single-Mineral Geothermometers

10:15 - 10:30 Girard J.-P.* Savin S. M. Feng X.
Intracrystalline Fractionation of Oxygen Isotopes Between Hydroxyl and Non-Hydroxyl Sites in Kaolinite: Thermal Dehydroxylation and Partial Fluorination Approaches

10:30 - 10:45 Vali H.* Hesse R. Srodon J.
Combined TEM Observation of Layer Structure and Surface Microtopography Applied to Study the Crystal Growth Mechanism of Clay Minerals

10:45 - 11:00 Schroeder P. A.*
Far Infrared Spectroscopy of Mixed-Layer Illite/Smectites

11:00 - 11:15 Yu J.-Y. Slaughter M.*
Geometrical Structure Synthesis and Stability of Dioctahedral Clay Minerals, Including the Water Structure of Hydrated Montmorillonite

11:15 - 11:30 Walker J. R.*
Chlorite Polyttypism—A Possible Geothermometer?

Tuesday, October 8, 1991

GENERAL II

1:00 p.m. Admiral Ballroom, C

Chairs: D. G. Golden P. H. Hsu

Mineral Transformations and Kinetics: Laboratory Investigations

1:00 - 1:20 Wang W. Hsu P. H.*
Nature of OH-Al Polymers in Commercial and Laboratory Prepared Solutions

1:20 - 1:40 Krishnamurti G. S. R.* Huang P. M.
The Role of Al in Fe(II) Transformation

1:40 - 2:00 Chipera S. J.* Bish D. L.
Rehydration Behavior of a Natural Analcime

2:00 - 2:20 Golden D. C.* Ming D. W. Lauer H. V. Jr.
Transformation Products of Submicron-Sized Aluminum-Substituted Magnetite: Color and Reductant Solubility

2:20 - 2:40 Faraj B. S. M. Mackinnon I. D. R.* Glikson M.
Fine-Grain Clays in Southern Hemisphere Coals: The Nature of Micrinite

Tuesday, October 8, 1991
GEO THERMOMETERS AND GEOCHRONOMETERS II
1:00 p.m. Admiral Ballroom, A and B

Chairs: R. M. Pollastro P. D. Lundegard

Geothermometry: Case Studies

- 1:00 - 1:15 Pollastro R. M.*
The Illite/Smectite Geothermometer—Considerations and Case-History Studies in Hydrocarbon-Bearing Rocks of Miocene to Mississippian in Age
- 1:15 - 1:30 Bish D. L.*
Determination of Paleogeothermal and Paleohydrologic Conditions in Silicic Tuffs from Illite/Smectite Mineralogy
- 1:30 - 1:45 Yeh H.-W.*
Significance of Oxygen Isotope Temperatures of Sea-Floor Hydrothermal Smectite
- 1:45 - 2:00 Baker J. C.* Mackinnon I. D. R.
High Resolution Transmission and Analytical Electron Microscopy of the Smectite to Illite Transition in Australian Mudrocks
- 2:00 - 2:15 Sivalingam S.* Guven N.
Analytical Electron Microscopy of Illite/Smectite Clays from the Permian Basin
- 2:15 - 2:30 Harvey C. C.* Browne P. R. L.
Mixed-Layer Clay Geothermometry in the Wairakei Geothermal Field, New Zealand
- 2:30 - 3:15 Five Minute Introductions by Poster Presenters in Lecture Room

Tuesday, October 8, 1991
SOILS AND CLAYS IN ENVIRONMENTAL RESEARCH I
1:00 p.m. Admiral Ballroom, D

Conveners: P. M. Bertsch B. L. Sawhney
Chairs: P. M. Bertsch D. L. Sparks

- 1:00 - 1:30 Sawhney B. L.*
Overview of Interactions of Organic and Inorganic Contaminants with Soils and Clays
- 1:30 - 2:00 Boyd S. A.*
Properties and Mechanisms of Organo-Clays as Sorbents for Pollutant Chemicals
- 2:00 - 2:15 Norris J.* Giese R. Costanzo P. M. van Oss C. J.
Hydrophobic Nature of Organo-Clays as a Lewis Acid/Base Phenomenon
- 2:15 - 2:30 Zhang Z. Z.* Sparks D. L.
Sorption and Desorption of Quaternary Amine Cations on Clays
- 2:30 - 2:45 Ukrainczyk L.* McBride M. B.
Oxidation of Phenol in Acidic Aqueous Suspensions of Manganese Oxides

- 2:45 - 3:05 Farmer W. J.* Aochi Y. Sawhney B. L.
In-situ Investigation of EDB Sorption/Desorption Processes on Clay Mineral Surfaces by Diffuse Reflectance Infrared Spectroscopy
- 3:05 - 3:15 Discussion Period

Tuesday, October 8, 1991
GENERAL POSTERS II
2:30 p.m. - 4:00 p.m. Marina Room

2:1 Layer-Structured Minerals

- Mermut A. R.* St. Arnaud R. J.
A Rapid Estimation of Layer Charge of 2:1 Expanding Silicate Clays by Alkylammonium
- Tomita K.* Yamane H. Kawano M.
Synthesis of Smectite from a Volcanic Glass, Clay Minerals and Rocks at 1 atm.
- Kawano M.* Tomita K.
Rehydration of Rectorite
- Bertolino S. R.* Harvey C. C. Murray H. H.
An Exceptional Illite from the Eureka Mine, Cordoba Province, Rep. Argentina
- Finkelstein D. B.* Leckie R. M. Yuretich R. F.
Clay Minerals as Indicators of Paleocyanography, Paleoclimate and Diagenesis in the Upper Cretaceous Greenhorn Cyclothem of the Mancos Shale
- Post J. L.* Cupp B. L.
Beidellite from the Black-Jack-Trade Dollar Mine and Nearby Delamar Silver Mine

Kaolinite, Halloysite, Iron Oxides and Mineral Transformations

- Taylor M. C.* Berry R. W.
Halloysite; Product of Calcium-rich Plagioclase Alteration, Riverside County, California
- Webb H.* Sprague E. K.
Timing of Kaolinitization in Hard Kaolins of the Huber Formation in Central and Eastern Georgia: Trace Fossil Microtextures Documented by Scanning Electron Microscopy
- Kocsardy E.* Shaffer N. R.
Infrared Study of Structural OH in Good and Poorly Crystalline Kaolin and in their "Deferrated" Products at 300 K degrees
- Boettinger J. L.* Dahlgren R. A.
Clay Mineralogy of a Soil Climosequence Formed in Granodiorite, Sierra Nevada
- Uwins P. J. R.* Mackinnon I. D. R.
Textural and Compositional Variations in Size Fractionated Australian Kaolins
- White G. N.* Dixon J. B. Weaver R. M. Kunkle A. C.
Sedimentary Structure in Gray Kaolins of Georgia
- Bowen L. H.* De Grave E. de Bakker P. M. A. Vandenberghe R. E.
Low Temperature Magnetism of Goethite: Aluminum Substitution and Surface Area Effects on Mössbauer Spectra
- De Grave E.* Van Alboom M.
Evaluation of Ferrous and Ferric Mössbauer Fractions for Various Natural and Synthetic Compounds

Vaniman D.* Bish D. Chipera S. Ebinger M.
Sepiolite at the Surface of Yucca Mountain, Nevada

Hughes R. E.* Grimley D. A. Follmer L. R. Moore D. M. Johnson W. H.
Mixed-Layered Kaolinite/Expandables: Occurrence of and Rates of Formation in Quaternary, Mississippi Valley Loesses

Malik H. U.* Jones R. C.
Two Scenarios for the Genesis of the Kaolinitic Vertisols on the Hawaiian Island of Lanai and Molokai

Tuesday, October 8, 1991
GEO THERMOMETERS AND GEOCHRONOMETERS POSTERS I
3:15 p.m. - 4:30 p.m. Commodore Room

Chairs: D. Eberl B. Velde

Klimentidis R. E.* Huang W. L. Pevear D. R.
Correlation of X.R.D. Crystallinity and T.E.M. Crystal Size of Synthetic Mica

Vrolijk P.*
Clay Minerals in Subduction Zones-Role of Interlayer Water

Carmichael D. C.* Smith R. J. Baker J. C.
The Use of Illite/Smectite as a Thermal Maturity Indicator in the Northern Eromanga Basin, Queensland, Australia

de Caritat P.* Hutcheon I. Walshe J. L.
Chlorite Geothermometry: Principles and Applications

Fritz B.* Madé B. Duplay J.
Geochemical Computer Modelling of Clay-Pore Water Interaction as a Tool for Geothermometry

Hassanipak A. A. Wampler J. M.*
The Influence of Composition on the Release of Radiogenic Argon from Illitic and Glauconitic Clay Samples

Sivalingam S.*
The Effects of Burial Diagenesis on the Texture, Mineralogy and Properties of Source Rocks from the Permian Basin

Small J. S.*
Experimental Determination of the Stability and Rate of Precipitation of Authigenic Illite

Fishman N. S.* Turner C. E. Sheppard R. A.
Authigenic Illite in Silicic Tuffs of Pleistocene Lake Tecopa, California—A Cautionary Note for Clay-Mineral Geothermometry

Hillier S.*
Origin and Diagenesis of Chlorite Minerals in the Orcadian Basin, Scotland

Tuesday, October 8, 1991
THE EXTRATERRESTRIAL CONNECTION POSTERS
2:30 p.m. - 4:00 p.m. Commodore Room

Agresti D. G.* Shelfer T. D. Pimperl M. M. Wills E. L. Morris R. V.
Combined Backscatter Mössbauer Spectrometer and X-Ray Fluorescence Analyzer (BaMS/XRF) for Planetary Surface Materials

Vempati R. K.* Morris R. V. Lauer H. V. Jr. Coey J. M. D.
UV-Visible, and Near-IR Reflectivity Data for Magnetic Soils/Rocks from Brazil

Klingelhofer G.* Foh J. Held P. Jager H. Kankeleit E. Teucher R.
Evlanov E. N. Khromov V. Mukhin L. M. Prilutski O. F. Zubkov B.
Smirnov G. V. Zuchniewicz J. Knudsen J. M. Madsen M. d'Uston C.
Mössbauer Spectroscopy on the Surface of Mars

Madsen M. B.* Vistisen L. Ray-Paulsen N. O. Koch C.B. Morup S. Bentzon M. D.
Low Temperature Weathering of Basalt

Koch C. B.* Jørgensen S. S.
K/T Boundary at Stevns, Denmark

Koch C. B.*
Weathering of Impactite from Monturaqui

Tuesday, October 8, 1991
PANEL DISCUSSIONS

Surface Chemistry
4:00 p.m. - 5:00 p.m. Admiral Ballroom, C

The Extraterrestrial Connection
4:00 p.m. - 5:00 p.m. Admiral Ballroom, D

Tuesday, October 8, 1991
ANNUAL RECEPTION AND BANQUET

5:30 p.m.	Reception	Lakeview Manor (adjacent to hotel - see map)
6:30 p.m.	Dinner	Admiral Ballroom
8:00 p.m.	NASA Presentation	Admiral Ballroom

Wednesday, October 9, 1991
FIELD TRIP (departs from front of hotel)
8:00 a.m. - 5:00 p.m.

GALVESTON BEACH BAR-B-QUE
5:00 p.m. - 7:00 p.m.
(if not on Field Trip or Tour, van leaves hotel at 4:30 p.m.)

Thursday, October 10, 1991
GENERAL III
8:00 a.m. Admiral Ballroom, C

Chairs: J. L. Boettinger G. D. Guthrie, Jr.

Kaolinite, Halloysite, Iron Oxides and Mineral Transformations

- 8:00 - 8:20 Guthrie G. Jr.* Bish D. L.
Ionic Modeling of the Hydrogen Sites in the Kaolin Polymorphs
- 8:20 - 8:40 Murad E.* Wagner U.
Mössbauer Spectra of Kaolinite, Halloysite and the Firing Products of Kaolinite
- 8:40 - 9:10 Break
- 9:10 - 9:30 Reynolds R. C. Jr.
One- and Three-Dimensional X-Ray Powder Diffraction Studies of Illite/Smectites Subjected to Different Sample Preparation Methods
- 9:30 - 9:50 Uwins P. J. R.* Mackinnon I. D. R. Thompson J. G.
"Crystallinity" and Intercalation Relationships in Size Fractionated Australian Kaolinites
- 9:50 - 10:10 Hay R. L.* Liu J.
Kaolinite was a Precursor to Diagenetic K-Feldspar of Paleozoic Age in Wisconsin
- 10:10 - 10:30 Boettinger J. L.* Dahlgren R. A. Southard R. J.
Mineralogy and Mineral Equilibria of an Alfisol/Vertisol Complex in the Australian Tropics

Thursday, October 10, 1991
GEOTHERMOMETERS AND GEOCHRONOMETERS III
8:00 a.m. Admiral Ballroom, A and B

Chairs: J. M. Wampler N. Clauer

Geochronology

- 8:00 - 8:15 Pevear D. R.* Elliott W. C.
Illite Age Analysis: A Method for Interpreting Shale K/Ar Ages
- 8:15 - 8:30 Clauer N.* Stille P. Keppens E.
Sr-Nd Isotope Constraints on the Glauconitization Process
- 8:30 - 8:45 Daniels E. J.* Aronson J. L. Altaner S. P.
Determining the Absolute Age of Late-Stage Thermal Maturation of Anthracite in Eastern Pennsylvania from Radiometric Dating of NH₄-Bearing Illite
- 8:45 - 9:00 Lee M. Aronson J. L.*
Repetitive Occurrence of Potassic Diagenesis in the Region of the Upper Mississippi Valley (UMV) Mineral District: Implications for a Persistent Paleo-Hydrological Setting Favorable for Diagenesis
- 9:00 - 9:15 Break
- 9:15 - 9:30 Wampler J. M.* Hassanipak A. A.
A Stepwise-Dissolution Technique for Potassium-Argon Analysis of Clays

- 9:30 - 9:45 Thomas A. R.* Dahl W. M. Hall C. M. York D.
Authigenic Muscovite ⁴⁰Ar/³⁹Ar Isotopic Analyses as a Tool for Timing Pressure Solution in the Jurassic Norphlet Formation
- 9:45 - 10:00 Hogg A. J. C.* Fallick A. E. Pearson M. J.
Mapping Diagenetic Fluid Flow Within a Reservoir-K/Ar Dating in the Alwyn Area, UK North Sea
- 10:00 - 10:15 Glasmann J. R.
The Importance of Late Cimmerian Meteoric Recharge to Reservoir Quality, Rotliegendes Sandstone, Netherlands
- 10:15 - 10:30 Fallick A. E.* Macaulay C. I. Haszeldine R. S.
Clay Mineral Stable Isotopes: Magnus Sandstone, North Sea

Thursday, October 10, 1991
SOILS AND CLAYS IN ENVIRONMENTAL RESEARCH II
8:00 a.m. Admiral Ballroom, D

- Chairs:** W. P. Miller B. L. Sawhney
- 8:00 - 8:30 Zachara J. M.* Cowan C. E. Smith S. C.
Multiple-Site Modeling of Metal Ion Adsorption on Specimen and Soil Layer Silicates
- 8:30 - 8:45 Fendorf S. E.* Sparks D. L.
Chromium (III) Induced Solid Phase Transformation of δ -MnO₂
- 8:45 - 9:00 Goldberg S.* Forster H. S. Heick E. L.
Ionic Strength Effects on Boron Adsorption by Oxides, Clay Minerals, and Soils
- 9:00 - 9:15 Plüss A.* Ferrell R. E. Jr.
Characterization of Fly Ash and the Immobilisation of Pb and Zn with Clay Minerals
- 9:15 - 9:30 Singh J. Huang P. M.*
Influence of Citric Acid and Glycine on Kinetics of Mercury (II) Adsorption by Kaolinite
- 9:30 - 10:00 Lee S. Y.*
Environmental Restoration of DOE Sites: R & D Issues Related to Clay Sciences
- 10:00 - 10:15 Chisholm Brause C. J. Morris D. E.* Eller P. G. Buscher T. C.
Conradson S. E.
Changes in U(VI) Speciation Upon Sorption Onto Montmorillonite from Aqueous and Organic Solutions
- 10:15 - 10:30 Chermak J. A.*
Experimental Investigation of the Low Temperature Transformations of Clay Minerals in the Opalinus Shale, Switzerland

Thursday, October 10, 1991
BUSINESS MEETING
10:30 a.m. - 11:30 a.m. Admiral Ballroom, A and B

Thursday, October 10, 1991
GENERAL IV
1:00 p.m. Admiral Ballroom, A and B

Chairs: R. H. April F. J. Longstaffe

Smectite, Vermiculite, Illite, and Related Reactions

- 1:00 - 1:20 Longstaffe F. J.* Fialka B. N. Robb G. A.
Mineralogical Modifications of Oil Sands During Steam Stimulation: Post-Steam Core from the Wabiskaw Member, Northeastern Alberta
- 1:20 - 1:40 Cetin K.* Huff W. D.
Characterization of Interlayer Charge and Interstratification in Illite/Smectite Clays from K-Bentonites Using Alkylammonium Ion Exchange, X-Ray Diffraction and Transmission Electron Microscopy
- 1:40 - 2:00 Lanson B.*
Decomposition of X-Ray Diffraction Patterns: A Convenient Way to Describe Complex I/S Diagenetic Evolution
- 2:00 - 2:20 April R. H.* Keller D. M.
A Saponite-Vermiculite Intermediate in Amygdales of the Granby Basaltic Tuff, Connecticut Valley
- 2:20 - 2:30 Discussion Period

Thursday, October 10, 1991
SOILS AND CLAYS IN ENVIRONMENTAL RESEARCH III
1:00 p.m. Admiral Ballroom, C

Chairs: P. M. Bertsch TBA

- 1:00 - 1:30 Miller W. P.* Bertsch P. M.
Surface Chemical and Mineralogical Aspects of Colloid-Facilitated Contaminant Transport
- 1:30 - 1:45 Muller J.-P.* Allard T. Calas G.
Hole-Trapping Defects in Kaolinite: Origin and Use as Environmental Tracers
- 1:45 - 2:00 Hueckel T.* Ma C. M.
Geotechnics of Dense Clay Soils Subjected to Heat and Chemicals: Toward a Predictive Model
- 2:00 - 2:15 Odom I. E.* Elzea J. M.
Environmental Aspects of Silica Minerals in Clays and Sediments

Thursday, October 10, 1991
GENERAL POSTERS III
2:30 p.m. - 4:00 p.m. Marina Room

Clays in Lakes, Basins, and Reservoirs

- Webster D. M.* Jones B. F.
Paleoenvironmental Implications of Lacustrine Clay Minerals from the Double Lakes Area, Southern High Plains, Texas
- Lo P.-H.* Tieh T. T.
Clays in Sediments of Yamato Basin, Japan Sea
- Matthews J. C.* Altaner S. P.
Contrasting Mineral/Water Reaction Pathways in Three Saline, Alkaline Lakes from Southeast Oregon
- Walling S. D.* Tieh T. T.
Authigenic Clay Minerals in Reservoir Sandstones of the Permian Delaware Mountain Group, West Texas
- Faraj B. S. M. Khoury H. N. Mackinnon I. D. R.*
Characterisation of Jordanian and Australian Palygorskites
- Ferrell R. E. Jr.* Williams L. B.
Ammonium Fixation During Clay Mineral Diagenesis and Hydrocarbon Maturation
- Thorez J.* Bossiroy D. Flores R. M. Keighin C. W.
Non-Facies Selective Clay Paragenesis of Sandstone Reservoirs, Fuller Reservoir Field, Wind River Basin, Wyoming
- Moore D. M.* Hughes R. E.
Characteristics of Chlorite Interlayered with a 7 Å Mineral as Found in Sandstone Reservoirs
- Durand C.*
Distribution of Clays in Sandstones as Studied by Scanning Electron Microscope Image Analysis
- Baker J. C.* Uwins P. J. R. Martin K. R. Mackinnon I. D. R.
Fluid-Clay Interactions in Sandstone Reservoirs: Direct Observation
- Carter J. J.* Myer L. R. Sposito G.
Clay-Fluid Interactions and Flow in a Single Fracture
- Pevear D. R.* Klimentidis R. E. Robinson G. A.
Petrogenetic Significance of Kaolinite Nucleation and Growth on Pre-existing Mica in Shales and Sandstone

Thursday, October 10, 1991
GEOOTHERMOMETERS AND GEOCHRONOMETERS POSTERS II
Five Minute Introduction by Poster Presenters
2:30 p.m. - 3:15 p.m. Admiral Ballroom, D

Poster Session 3:15 p.m. - 4:30 p.m. Commodore Room

Chairs: E. Eslinger J. R. Glasmann

Awwiller D. N.

Mineralogy and Chemistry of Subsurface (900-4600 m) Mudrocks and <0.5 μ m Clay Separates from the Texas Gulf Coast Paleocene-Eocene

Altaner S. P. Lander R. H. Klimentidis R. E. Ylagan R. F.

Hydrothermal Alteration in Two Active Geothermal Wells from the Phlegrean Volcanic Fields, Italy

Harper D. A.* Longstaffe F. J. Wadleigh M. A.

Unconformity-related K-Feldspar and Phyllosilicate Alteration at the Precambrian-Paleozoic Boundary, Southwestern Ontario

Lynch F. L.*

Depth Related Changes in Clay Mineralogy from Frio Formation (Oligocene) Shales, Cameron, Kenedy, and Nueces Counties, Texas

Price K. L. McDowell S. D.

Illite/Smectite Geothermometry of the Oronto Group, Southern Lake Superior Basin, Michigan

Hluchy M. M.* April R. H. Beebe S. L.

Occurrence of Expandable Clay Minerals in Contact Metamorphic Aureoles

Ryan P. Thompson G.*

Structural and Compositional Variations in Low-Grade Metamorphic Illite and Chlorite from the Belt Supergroup, Montana and Idaho

Shafiqullah M.* Damon P. E.

Fault Gouge Clay Dates-How Meaningful Are They?

Huggett J.

Diageneses of Overpressured Tertiary and Cretaceous Mudstones from the East Shetland Basin, North Sea

Kralik M.*

K-Ar and Rb-Sr Isotopes in Clay Mineral Research in Carbonate Environments

Thursday, October 10, 1991
PANEL DISCUSSIONS

Soils and Clays in Environmental Research
3:00 p.m. - 4:00 p.m. Admiral Ballroom, C

Geothermometers and Geochronometers
4:30 p.m. - 5:00 p.m. Admiral Ballroom, D

ADJOURN, Thursday, October 10, 1991, 5:00 p.m.

Index to Sessions by Author

- Agresti D. G. The Extraterrestrial Connection Posters, Tue. p.m., Commodore Room
 Allard T. Soils and Clays in Environmental Research III, Thu. p.m., Admiral Ballroom, C
 Allen C. C. The Extraterrestrial Connection I, Mon. p.m., Admiral Ballroom, D
 Allen F. General Posters I, Mon. p.m., Commodore Room
 Altaner S. P. General Posters III, Thu. p.m., Marina Room
 Altaner S. P. Geothermometers and Geochronometers III, Thu. a.m., Admiral Ballroom, A and B
 Altaner S. P. Geothermometers and Geochronometers Posters II, Thu. p.m., Commodore Room
 Anderson D. M. Surface Chemistry I, Mon. p.m., Admiral Ballroom, C
 Aochi Y. Soils and Clays in Environmental Research I, Tue. p.m., Admiral Ballroom, D
 April R. H. General IV, Thu. p.m., Admiral Ballroom, A and B
 April R. H. Geothermometers and Geochronometers Posters II, Thu. p.m., Commodore Room
 Aronson J. L. Geothermometers and Geochronometers III, Thu. a.m., Admiral Ballroom, A and B
 Aronson J. L. The Extraterrestrial Connection II, Tue. a.m., Admiral Ballroom, D
 Awwiller D. N. Geothermometers and Geochronometers Posters II, Thu. p.m., Commodore Room
 Baker J. C. General Posters III, Thu. p.m., Marina Room
 Baker J. C. Geothermometers and Geochronometers II, Tue. p.m., Admiral Ballroom, A and B
 Baker J. C. Geothermometer and Geochronometers Posters I, Tue. p.m., Commodore Room
 Banin A. The Extraterrestrial Connection I, Mon. p.m., Admiral Ballroom, D
 Barnes H. L. Geothermometer and Geochronometers I, Tue. a.m., Admiral Ballroom, A and B
 Baron J. Surface Chemistry Posters, Mon. p.m., Marina Room
 Bates J. K. The Extraterrestrial Connection II, Tue. a.m., Admiral Ballroom, D
 Bechtel A. Geothermometer and Geochronometers I, Tue. a.m., Admiral Ballroom, A and B
 Beebe S. L. Geothermometers and Geochronometers Posters II, Thu. p.m., Commodore Room
 Bentzon M. D. The Extraterrestrial Connection Posters, Tue. p.m., Commodore Room
 Berry R. W. General Posters II, Tue. p.m., Marina Room
 Bertolino S. R. General Posters II, Tue. p.m., Marina Room
 Bertsch P. M. Soils and Clays in Environmental Research III, Thu. p.m., Admiral Ballroom, C
 Bish D. L. General I, Mon. a.m., Admiral Ballroom, A and B
 Bish D. L. General Posters I, Mon. p.m., Commodore Room
 Bish D. L. General II, Tue. p.m., Admiral Ballroom, C
 Bish D. L. Geothermometers and Geochronometers II, Tue. p.m., Admiral Ballroom, A and B
 Bish D. L. General Posters II, Tue. p.m., Marina Room
 Bish D. L. General III, Thu. a.m., Admiral Ballroom
 Bish D. L. The Extraterrestrial Connection I, Mon. p.m., Admiral Ballroom, D
 Bishop J. L. The Extraterrestrial Connection I, Mon. p.m., Admiral Ballroom, D
 Blum A. E. Surface Chemistry II, Tue. a.m., Admiral Ballroom, C
 Boettinger J. L. General III, Thu. a.m., Admiral Ballroom
 Boettinger J. L. General Posters II, Tue. p.m., Marina Room
 Bohor B. B. The Extraterrestrial Connection II, Tue. a.m., Admiral Ballroom, D
 Bonté Ph. The Extraterrestrial Connection II, Tue. a.m., Admiral Ballroom, D
 Bossiroy D. General Posters III, Thu. p.m., Marina Room
 Bowen L. H. General Posters II, Tue. p.m., Marina Room
 Boyd S. A. Soils and Clays in Environmental Research I, Tue. p.m., Admiral Ballroom, D
 Boyd S. A. Surface Chemistry II, Tue. a.m., Admiral Ballroom, C
 Bradley C. R. The Extraterrestrial Connection II, Tue. a.m., Admiral Ballroom, D
 Bradley J. P. The Extraterrestrial Connection II, Tue. a.m., Admiral Ballroom, D
 Bronnimann C. E. Surface Chemistry Posters, Mon. p.m., Marina Room
 Brown G. E. Jr. Surface Chemistry Posters, Mon. p.m., Marina Room
 Browne P. R. L. Geothermometers and Geochronometers II, Tue. p.m., Admiral Ballroom, A and B
 Burkett P. J. Soils and Clays in Environmental Research Posters, Mon. p.m., Marina Room
 Burns R. G. The Extraterrestrial Connection II, Tue. a.m., Admiral Ballroom, D
 Buscher T. C. Soils and Clays in Environmental Research II, Thu. a.m., Admiral Ballroom, D

Calas G.	Soils and Clays in Environmental Research III, Thu. p.m., Admiral Ballroom, C
Calas G.	Surface Chemistry I, Mon. p.m., Admiral Ballroom, C
Carmichael D. C.	Geothermometer and Geochronometers Posters I, Tue. p.m., Commodore Room
Carter J. J.	General Posters III, Thu. p.m., Marina Room
Cartz L.	General I, Mon. a.m., Admiral Ballroom, A and B
Casal B.	Surface Chemistry Posters, Mon. p.m., Marina Room
Cases J. M.	Surface Chemistry II, Tue. a.m., Admiral Ballroom, C
Cetin K.	General IV, Thu. p.m., Admiral Ballroom, A and B
Charlet L.	Surface Chemistry I, Mon. p.m., Admiral Ballroom, C
Chermak J. A.	Soils and Clays in Environmental Research II, Thu. a.m., Admiral Ballroom, D
Chiou W.-A.	General I, Mon. a.m., Admiral Ballroom, A and B
Chipera S. J.	General II, Tue. p.m., Admiral Ballroom, C
Chipera S. J.	General Posters II, Tue. p.m., Marina Room
Chipera S. J.	The Extraterrestrial Connection I, Mon. p.m., Admiral Ballroom, D
Chisholm Brause C. J.	Soils and Clays in Environmental Research II, Thu. a.m., Admiral Ballroom, D
Clauer N.	Geothermometers and Geochronometers III, Thu. a.m., Admiral Ballroom, A and B
Clauer N.	Geothermometer and Geochronometers I, Tue. a.m., Admiral Ballroom, A and B
Clayton T.	General Posters I, Mon. p.m., Commodore Room
Coey J. M. D.	The Extraterrestrial Connection Posters, Tue. p.m., Commodore Room
Cook R. J.	General Posters I, Mon. p.m., Commodore Room
Conradson S. E.	Soils and Clays in Environmental Research II, Thu. a.m., Admiral Ballroom, D
Cornachione H. S.	Soils and Clays in Environmental Research Posters, Mon. p.m., Marina Room
Costanzo P. M.	Soils and Clays in Environmental Research I, Tue. p.m., Admiral Ballroom, D
Cown C. E.	Soils and Clays in Environmental Research II, Thu. a.m., Admiral Ballroom, D
Coyne L. M.	The Extraterrestrial Connection I, Mon. p.m., Admiral Ballroom, D
Cupp B. L.	General Posters II, Tue. p.m., Marina Room
Dahl W. M.	Geothermometers and Geochronometers III, Thu. a.m., Admiral Ballroom, A and B
Dahlgren R. A.	General III, Thu. a.m., Admiral Ballroom
Dahlgren R. A.	General Posters II, Tue. p.m., Marina Room
Damon P. E.	Geothermometers and Geochronometers Posters II, Thu. p.m., Commodore Room
Daniels E. J.	Geothermometers and Geochronometers III, Thu. a.m., Admiral Ballroom, A and B
de Bakker P. M. A.	General Posters II, Tue. p.m., Marina Room
de Caritat P.	Geothermometer and Geochronometers Posters I, Tue. p.m., Commodore Room
De Grave E.	General Posters II, Tue. p.m., Marina Room
Dec S. F.	Surface Chemistry Posters, Mon. p.m., Marina Room
DeHart J.	The Extraterrestrial Connection I, Mon. p.m., Admiral Ballroom, D
Dixon J. B.	General Posters II, Tue. p.m., Marina Room
Dixon J. B.	Plenary Session, Mon. a.m., Admiral Ballroom
Donahoe R. J.	Soils and Clays in Environmental Research Posters, Mon. p.m., Marina Room
Duplay J.	Geothermometer and Geochronometers Posters I, Tue. p.m., Commodore Room
Durand C.	General Posters III, Thu. p.m., Marina Room
d'Uston C.	The Extraterrestrial Connection Posters, Tue. p.m., Commodore Room
Eberl D. D.	Geothermometer and Geochronometers I, Tue. a.m., Admiral Ballroom, A and B
Eberl D. D.	Surface Chemistry II, Tue. a.m., Admiral Ballroom, C
Ebinger M.	General Posters II, Tue. p.m., Marina Room
Eggleton R. A.	General I, Mon. a.m., Admiral Ballroom, A and B
Eller P. G.	Soils and Clays in Environmental Research II, Thu. a.m., Admiral Ballroom, D
Elliott W. C.	Geothermometers and Geochronometers III, Thu. a.m., Admiral Ballroom, A and B
Elliott W. C.	The Extraterrestrial Connection II, Tue. a.m., Admiral Ballroom, D
Elzea J. M.	Soils and Clays in Environmental Research Posters, Mon. p.m., Marina Room
Evlanov E. N.	The Extraterrestrial Connection Posters, Tue. p.m., Commodore Room
Fallick A. E.	Geothermometers and Geochronometers III, Thu. a.m., Admiral Ballroom, A and B
Faraj B. S. M.	General II, Tue. p.m., Admiral Ballroom, C
Faraj B. S. M.	General Posters III, Thu. p.m., Marina Room

Farmer W. J. Soils and Clays in Environmental Research I, Tue. p.m., Admiral Ballroom, D
 Fendorf S. E. Soils and Clays in Environmental Research II, Thu. a.m., Admiral Ballroom, D
 Feng X. Geothermometer and Geochronometers I, Tue. a.m., Admiral Ballroom, A and B
 Ferrell R. E. Jr. General Posters III, Thu. p.m., Marina Room
 Ferrell R. E. Jr. Soils and Clays in Environmental Research II, Thu. a.m., Admiral Ballroom, D
 Fialka B. N. General IV, Thu. p.m., Admiral Ballroom, A and B
 Finkelstein D. B. General Posters II, Tue. p.m., Marina Room
 Fisher D. S. The Extraterrestrial Connection II, Tue. a.m., Admiral Ballroom, D
 Fishman N. S. Geothermometer and Geochronometers Posters I, Tue. p.m., Commodore Room
 Fitch A. Surface Chemistry II, Tue. a.m., Admiral Ballroom, C
 Fitzgerald J. J. Surface Chemistry Posters, Mon. p.m., Marina Room
 Flores R. M. General Posters III, Thu. p.m., Marina Room
 Foh J. The Extraterrestrial Connection Posters, Tue. p.m., Commodore Room
 Follmer L. R. General Posters II, Tue. p.m., Marina Room
 Forster H. S. Soils and Clays in Environmental Research II, Thu. a.m., Admiral Ballroom, D
 Fripiat J. J. Surface Chemistry Posters, Mon. p.m., Marina Room
 Fritz B. Geothermometer and Geochronometers Posters I, Tue. p.m., Commodore Room
 Froget L. The Extraterrestrial Connection II, Tue. a.m., Admiral Ballroom, D
 Gan H. Surface Chemistry II, Tue. a.m., Admiral Ballroom, C
 Garcia-Ponce A.-L. Surface Chemistry Posters, Mon. p.m., Marina Room
 Gassman P. L. Surface Chemistry Posters, Mon. p.m., Marina Room
 Gierke J. S. Soils and Clays in Environmental Research Posters, Mon. p.m., Marina Room
 Giese R. Soils and Clays in Environmental Research I, Tue. p.m., Admiral Ballroom, D
 Giese R. Surface Chemistry II, Tue. a.m., Admiral Ballroom, C
 Girard J.-P. Geothermometer and Geochronometers I, Tue. a.m., Admiral Ballroom, A and B
 Glasmann J. R. Geothermometers and Geochronometers III, Thu. a.m., Admiral Ballroom, A and B
 Glese R. F. Surface Chemistry Posters, Mon. p.m., Marina Room
 Glikson M. General II, Tue. p.m., Admiral Ballroom, C
 Goldberg S. Soils and Clays in Environmental Research II, Thu. a.m., Admiral Ballroom, D
 Golden D. C. General II, Tue. p.m., Admiral Ballroom, C
 Gooding J. L. The Extraterrestrial Connection I, Mon. p.m., Admiral Ballroom, D
 Grant R. H. Soils and Clays in Environmental Research Posters, Mon. p.m., Marina Room
 Grimley D. A. General Posters II, Tue. p.m., Marina Room
 Guggenheim S. General I, Mon. a.m., Admiral Ballroom, A and B
 Gunter W. D. Surface Chemistry Posters, Mon. p.m., Marina Room
 Guthrie G. D. Jr. General Posters I, Mon. p.m., Commodore Room
 Guthrie G. D. Jr. General III, Thu. a.m., Admiral Ballroom
 Guven N. Geothermometers and Geochronometers II, Tue. p.m., Admiral Ballroom, A and B
 Hall C. M. Geothermometers and Geochronometers III, Thu. a.m., Admiral Ballroom, A and B
 Hamza A. I. Surface Chemistry Posters, Mon. p.m., Marina Room
 Happ J. W. The Extraterrestrial Connection II, Tue. a.m., Admiral Ballroom, D
 Harper D. A. Geothermometers and Geochronometers Posters II, Thu. p.m., Commodore Room
 Harvey C. C. General Posters II, Tue. p.m., Marina Room
 Harvey C. C. Geothermometers and Geochronometers II, Tue. p.m., Admiral Ballroom, A and B
 Hassanipak A. A. Geothermometer and Geochronometers Posters I, Tue. p.m., Commodore Room
 Hassanipak A. A. Geothermometers and Geochronometers III, Thu. a.m., Admiral Ballroom, A and B
 Haszeldine R. S. Geothermometers and Geochronometers III, Thu. a.m., Admiral Ballroom, A and B
 Hauff P. General Posters I, Mon. p.m., Commodore Room
 Hay R. L. General III, Thu. a.m., Admiral Ballroom
 Heck E. L. Soils and Clays in Environmental Research II, Thu. a.m., Admiral Ballroom, D
 Held P. The Extraterrestrial Connection Posters, Tue. p.m., Commodore Room
 Hesse R. Geothermometer and Geochronometers Posters I, Tue. p.m., Commodore Room
 Hesse R. Soils and Clays in Environmental Research Posters, Mon. p.m., Marina Room
 Hillier S. General Posters I, Mon. p.m., Commodore Room

Hillier S.	Geothermometer and Geochronometers Posters I, Tue. p.m., Commodore Room
Hluchy M. M.	Geothermometers and Geochronometers Posters II, Thu. p.m., Commodore Room
Hochella M. F. Jr.	Surface Chemistry II, Tue. a.m., Admiral Ballroom, C
Hogg A. J. C.	Geothermometers and Geochronometers III, Thu. a.m., Admiral Ballroom, A and B
Holland K. L.	General Posters I, Mon. p.m., Commodore Room
Hsu P. H.	General II, Tue. p.m., Admiral Ballroom, C
Huang P. M.	General II, Tue. p.m., Admiral Ballroom, C
Huang P. M.	Soils and Clays in Environmental Research II, Thu. a.m., Admiral Ballroom, D
Huang P. M.	Surface Chemistry I, Mon. p.m., Admiral Ballroom, C
Huang W. L.	Geothermometer and Geochronometers I, Tue. a.m., Admiral Ballroom, A and B
Hueckel T.	Soils and Clays in Environmental Research III, Thu. p.m., Admiral Ballroom, C
Huff W. D.	General IV, Thu. p.m., Admiral Ballroom, A and B
Huggett J.	Geothermometer and Geochronometers Posters II, Thu. p.m., Commodore Room
Hughes R. E.	General Posters II, Tue. p.m., Marina Room
Hughes R. E.	General Posters III, Thu. p.m., Marina Room
Hutcheon I.	Geothermometer and Geochronometers Posters I, Tue. p.m., Commodore Room
Huve L.	Surface Chemistry Posters, Mon. p.m., Marina Room
Jager H.	The Extraterrestrial Connection Posters, Tue. p.m., Commodore Room
Jaynes W. F.	Surface Chemistry II, Tue. a.m., Admiral Ballroom, C
Jéhanno C.	The Extraterrestrial Connection II, Tue. a.m., Admiral Ballroom, D
Johnson W. H.	General Posters II, Tue. p.m., Marina Room
Johnsson P.	Surface Chemistry II, Tue. a.m., Admiral Ballroom, C
Jones B. F.	General Posters III, Thu. p.m., Marina Room
Jones R. C.	General Posters I, Mon. p.m., Commodore Room
Jones R. C.	General Posters II, Tue. p.m., Marina Room
Jørgensen S. S.	The Extraterrestrial Connection Posters, Tue. p.m., Commodore Room
Kacandes G. H.	Geothermometer and Geochronometers I, Tue. a.m., Admiral Ballroom, A and B
Kankleit E.	The Extraterrestrial Connection Posters, Tue. p.m., Commodore Room
Karioris F. G.	General I, Mon. a.m., Admiral Ballroom, A and B
Kawano M.	General Posters II, Tue. p.m., Marina Room
Keighin C. W.	General Posters III, Thu. p.m., Marina Room
Keller D. M.	General IV, Thu. p.m., Admiral Ballroom, A and B
Keller L. P.	The Extraterrestrial Connection II, Tue. a.m., Admiral Ballroom, D
Keppens E.	Geothermometers and Geochronometers III, Thu. a.m., Admiral Ballroom, A and B
Kevan L.	Surface Chemistry I, Mon. p.m., Admiral Ballroom, C
Khoury H. N.	General Posters III, Thu. p.m., Marina Room
Khromov V.	The Extraterrestrial Connection Posters, Tue. p.m., Commodore Room
Klimentidis R. E.	Geothermometers and Geochronometers Posters II, Thu. p.m., Commodore Room
Klimentidis R. E.	Geothermometer and Geochronometers Posters I, Tue. p.m., Commodore Room
Klingelhofer G.	The Extraterrestrial Connection Posters, Tue. p.m., Commodore Room
Knudsen J. M.	The Extraterrestrial Connection Posters, Tue. p.m., Commodore Room
Kocsardy E.	General Posters II, Tue. p.m., Marina Room
Koch C. B.	The Extraterrestrial Connection Posters, Tue. p.m., Commodore Room
Kodama H.	Soils and Clays in Environmental Research Posters, Mon. p.m., Marina Room
Kornegay C. J.	Soils and Clays in Environmental Research Posters, Mon. p.m., Marina Room
Kralik M.	Geothermometers and Geochronometers Posters II, Thu. p.m., Commodore Room
Krishnamurti G. S. R.	General II, Tue. p.m., Admiral Ballroom, C
Kuehl S. A.	General Posters III, Thu. p.m., Marina Room
Kump L. R.	Geothermometer and Geochronometers I, Tue. a.m., Admiral Ballroom, A and B
Kunkle A. C.	General Posters II, Tue. p.m., Marina Room
Lander R. H.	Geothermometers and Geochronometers Posters II, Thu. p.m., Commodore Room
Lanson B.	General IV, Thu. p.m., Admiral Ballroom, A and B
Lasaga A. C.	Surface Chemistry II, Tue. a.m., Admiral Ballroom, C
Lauer H. V. Jr.	General II, Tue. p.m., Admiral Ballroom, C

Lauer H. V. Jr. The Extraterrestrial Connection I, Mon. p.m., Admiral Ballroom, D
 Lauer H. V. Jr. The Extraterrestrial Connection Posters, Tue. p.m., Commodore Room
 Leckie R. M. General Posters II, Tue. p.m., Marina Room
 Le Dred R. Surface Chemistry Posters, Mon. p.m., Marina Room
 Lee M. Geothermometers and Geochronometers III, Thu. a.m., Admiral Ballroom, A and B
 Lee S. Y. Soils and Clays in Environmental Research II, Thu. a.m., Admiral Ballroom, D
 Li Z. Surface Chemistry II, Tue. a.m., Admiral Ballroom, C
 Liu J. General III, Thu. a.m., Admiral Ballroom
 Lo P.-H. General Posters III, Thu. p.m., Marina Room
 Longo J. M. Geothermometer and Geochronometers I, Tue. a.m., Admiral Ballroom, A and B
 Longstaffe F. J. General IV, Thu. p.m., Admiral Ballroom, A and B
 Longstaffe F. J. Geothermometers and Geochronometers Posters II, Thu. p.m., Commodore Room
 Lou G. Surface Chemistry I, Mon. p.m., Admiral Ballroom, C
 Low P. F. Surface Chemistry II, Tue. a.m., Admiral Ballroom, C
 Lundegard P. D. Geothermometer and Geochronometers I, Tue. a.m., Admiral Ballroom, A and B
 Lynch F. L. Geothermometers and Geochronometers Posters II, Thu. p.m., Commodore Room
 Ma C. M. Soils and Clays in Environmental Research III, Thu. p.m., Admiral Ballroom, C
 Macaulay C. I. Geothermometers and Geochronometers III, Thu. a.m., Admiral Ballroom, A and B
 Maciel G. E. Surface Chemistry Posters, Mon. p.m., Marina Room
 Mackinnon I. D. R. General I, Mon. a.m., Admiral Ballroom, A and B
 Mackinnon I. D. R. General Posters II, Tue. p.m., Marina Room
 Mackinnon I. D. R. General Posters III, Thu. p.m., Marina Room
 Mackinnon I. D. R. General II, Tue. p.m., Admiral Ballroom, C
 Mackinnon I. D. R. Geothermometers and Geochronometers II, Tue. p.m., Admiral Ballroom, A and B
 Madé B. Geothermometer and Geochronometers Posters I, Tue. p.m., Commodore Room
 Madsen F. T. Soils and Clays in Environmental Research Posters, Mon. p.m., Marina Room
 Madsen M. B. The Extraterrestrial Connection Posters, Tue. p.m., Commodore Room
 Malengreau N. Surface Chemistry I, Mon. p.m., Admiral Ballroom, C
 Malik H. U. General Posters II, Tue. p.m., Marina Room
 Manceau A. Surface Chemistry I, Mon. p.m., Admiral Ballroom, C
 Martin K. R. General Posters III, Thu. p.m., Marina Room
 Martin P. Surface Chemistry Posters, Mon. p.m., Marina Room
 Matthews J. C. General Posters III, Thu. p.m., Marina Room
 Mazer J. J. The Extraterrestrial Connection II, Tue. a.m., Admiral Ballroom, D
 McBride M. B. Soils and Clays in Environmental Research I, Tue. p.m., Admiral Ballroom, D
 McDowell S. D. Geothermometers and Geochronometers Posters II, Thu. p.m., Commodore Room
 McDowell S. D. Soils and Clays in Environmental Research Posters, Mon. p.m., Marina Room
 Mermut A. R. General Posters II, Tue. p.m., Marina Room
 Miller W. P. Soils and Clays in Environmental Research III, Thu. p.m., Admiral Ballroom, C
 Ming D. W. General II, Tue. p.m., Admiral Ballroom, C
 Ming D. W. The Extraterrestrial Connection II, Tue. a.m., Admiral Ballroom, D
 Moore D. M. General Posters II, Tue. p.m., Marina Room
 Moore D. M. General Posters III, Thu. p.m., Marina Room
 Morris D. E. Soils and Clays in Environmental Research II, Thu. a.m., Admiral Ballroom, D
 Morris R. V. The Extraterrestrial Connection I, Mon. p.m., Admiral Ballroom, D
 Morris R. V. The Extraterrestrial Connection Posters, Tue. p.m., Commodore Room
 Morup S. The Extraterrestrial Connection Posters, Tue. p.m., Commodore Room
 Mukhin L. M. The Extraterrestrial Connection Posters, Tue. p.m., Commodore Room
 Muller J.-P. Soils and Clays in Environmental Research III, Thu. p.m., Admiral Ballroom, C
 Muller J.-P. Surface Chemistry I, Mon. p.m., Admiral Ballroom, C
 Murad E. General III, Thu. a.m., Admiral Ballroom
 Murphy K. Surface Chemistry Posters, Mon. p.m., Marina Room
 Murray H. H. General Posters II, Tue. p.m., Marina Room
 Myer L. R. General Posters III, Thu. p.m., Marina Room

Nagy K. L.	Surface Chemistry II, Tue. a.m., Admiral Ballroom, C
Norris J.	Soils and Clays in Environmental Research I, Tue. p.m., Admiral Ballroom, D
Nüesch R.	Soils and Clays in Environmental Research Posters, Mon. p.m., Marina Room
O'Day P. A.	Surface Chemistry Posters, Mon. p.m., Marina Room
Odom I. E.	Soils and Clays in Environmental Research Posters, Mon. p.m., Marina Room
Parks G. A.	Surface Chemistry Posters, Mon. p.m., Marina Room
Pearson M. J.	Geothermometers and Geochronometers III, Thu. a.m., Admiral Ballroom, A and B
Pevear D. R.	Geothermometers and Geochronometers III, Thu. a.m., Admiral Ballroom, A and B
Pevear D. R.	Geothermometer and Geochronometers I, Tue. a.m., Admiral Ballroom, A and B
Pieters C. M.	The Extraterrestrial Connection I, Mon. p.m., Admiral Ballroom, D
Pimperl M. M.	The Extraterrestrial Connection Posters, Tue. p.m., Commodore Room
Pinnavaia T. J.	Plenary Session, Mon. a.m., Admiral Ballroom
Plüss A.	Soils and Clays in Environmental Research II, Thu. a.m., Admiral Ballroom, D
Pollastro R. M.	Geothermometers and Geochronometers II, Tue. p.m., Admiral Ballroom, A and B
Pollastro R. M.	The Extraterrestrial Connection II, Tue. a.m., Admiral Ballroom, D
Post J. L.	General Posters II, Tue. p.m., Marina Room
Price K. L.	Geothermometers and Geochronometers Posters II, Thu. p.m., Commodore Room
Prilutski O. F.	The Extraterrestrial Connection Posters, Tue. p.m., Commodore Room
Primmer T. J.	General Posters I, Mon. p.m., Commodore Room
Rakovan J. F.	General I, Mon. a.m., Admiral Ballroom, A and B
Ray-Paulsen N. O.	The Extraterrestrial Connection Posters, Tue. p.m., Commodore Room
Reynolds R. C. Jr.	General III, Thu. a.m., Admiral Ballroom, C
Riley W. E.	Soils and Clays in Environmental Research Posters, Mon. p.m., Marina Room
Ripmeester J. A.	Surface Chemistry I, Mon. p.m., Admiral Ballroom, C
Rivers M. L.	Soils and Clays in Environmental Research Posters, Mon. p.m., Marina Room
Robb G. A.	General IV, Thu. p.m., Admiral Ballroom, A and B
Robin E.	The Extraterrestrial Connection II, Tue. a.m., Admiral Ballroom, D
Rocchia R.	The Extraterrestrial Connection II, Tue. a.m., Admiral Ballroom, D
Roth C. B.	Surface Chemistry II, Tue. a.m., Admiral Ballroom, C
Ruiz-Hitzky E.	Surface Chemistry Posters, Mon. p.m., Marina Room
Ryan P.	Geothermometers and Geochronometers Posters II, Thu. p.m., Commodore Room
Saehr D.	Surface Chemistry Posters, Mon. p.m., Marina Room
Salter T. L.	Soils and Clays in Environmental Research Posters, Mon. p.m., Marina Room
Savin S. M.	Geothermometer and Geochronometers I, Tue. a.m., Admiral Ballroom, A and B
Sawhney B. L.	Soils and Clays in Environmental Research I, Tue. p.m., Admiral Ballroom, D
Schroeder P. A.	Geothermometer and Geochronometers I, Tue. a.m., Admiral Ballroom, A and B
Schulze D. G.	Soils and Clays in Environmental Research Posters, Mon. p.m., Marina Room
Schuraytz B. C.	The Extraterrestrial Connection II, Tue. a.m., Admiral Ballroom, D
Sennett P.	General Posters I, Mon. p.m., Commodore Room
Shaffer N. R.	General Posters II, Tue. p.m., Marina Room
Shafiqullah M.	Geothermometers and Geochronometers Posters II, Thu. p.m., Commodore Room
Sharpton V. L.	The Extraterrestrial Connection II, Tue. a.m., Admiral Ballroom, D
Shelfer T. D.	The Extraterrestrial Connection Posters, Tue. p.m., Commodore Room
Sheppard R. A.	Geothermometer and Geochronometers Posters I, Tue. p.m., Commodore Room
Siantar D. P.	Surface Chemistry Posters, Mon. p.m., Marina Room
Sigurdsson H.	The Extraterrestrial Connection II, Tue. a.m., Admiral Ballroom, D
Singh J.	Soils and Clays in Environmental Research II, Thu. a.m., Admiral Ballroom, D
Sivalingam S.	Geothermometers and Geochronometers Posters I, Tue. p.m., Commodore Room
Sivalingam S.	Geothermometers and Geochronometers II, Tue. p.m., Admiral Ballroom, A and B
Slaughter M.	General I, Mon. a.m., Admiral Ballroom, A and B
Slaughter M.	Geothermometer and Geochronometers I, Tue. a.m., Admiral Ballroom, A and B
Small J. S.	Geothermometer and Geochronometers Posters I, Tue. p.m., Commodore Room
Smirnov G. V.	The Extraterrestrial Connection Posters, Tue. p.m., Commodore Room
Smith R. J.	Geothermometer and Geochronometers Posters I, Tue. p.m., Commodore Room

Smith S. C.	Soils and Clays in Environmental Research II, Thu. a.m., Admiral Ballroom, D
Southard R. J.	General III, Thu. a.m., Admiral Ballroom
Sparks D. L.	Soils and Clays in Environmental Research I, Tue. p.m., Admiral Ballroom, D
Sparks D. L.	Soils and Clays in Environmental Research II, Thu. a.m., Admiral Ballroom, D
Sposito G.	General Posters III, Thu. p.m., Marina Room
Sprague E. K.	General Posters II, Tue. p.m., Marina Room
Sprague E. K.	Soils and Clays in Environmental Research Posters, Mon. p.m., Marina Room
Srodon J.	Geothermometer and Geochronometers Posters I, Tue. p.m., Commodore Room
Srodon J.	Geothermometer and Geochronometers I, Tue. a.m., Admiral Ballroom, A and B
St. Arnaud R. J.	General Posters II, Tue. p.m., Marina Room
Stevenson C. M.	The Extraterrestrial Connection II, Tue. a.m., Admiral Ballroom, D
Stille P.	Geothermometers and Geochronometers III, Thu. a.m., Admiral Ballroom, A and B
Stucki J. W.	Surface Chemistry II, Tue. a.m., Admiral Ballroom, C
Sutton S. R.	Soils and Clays in Environmental Research Posters, Mon. p.m., Marina Room
Taylor M. C.	General Posters II, Tue. p.m., Marina Room
Teucher R.	The Extraterrestrial Connection Posters, Tue. p.m., Commodore Room
Thiry M.	General Posters I, Mon. p.m., Commodore Room
Thomas A. R.	Geothermometers and Geochronometers III, Thu. a.m., Admiral Ballroom, A and B
Thompson G.	Geothermometers and Geochronometers Posters II, Thu. p.m., Commodore Room
Thompson J. G.	General III, Thu. a.m., Admiral Ballroom
Thorez J.	General Posters III, Thu. p.m., Marina Room
Thornley D. M.	General Posters I, Mon. p.m., Commodore Room
Tieh T. T.	General Posters III, Thu. p.m., Marina Room
Tomita K.	General Posters II, Tue. p.m., Marina Room
Tomplier C.	General I, Mon. a.m., Admiral Ballroom, A and B
Turner C. E.	Geothermometer and Geochronometers Posters I, Tue. p.m., Commodore Room
Ukrainczyk L.	Soils and Clays in Environmental Research I, Tue. p.m., Admiral Ballroom, D
Uwins P. J. R.	General Posters II, Tue. p.m., Marina Room
Uwins P. J. R.	General III, Thu. a.m., Admiral Ballroom
Uwins P. J. R.	General Posters III, Thu. p.m., Marina Room
Vali H.	Geothermometer and Geochronometers I, Tue. a.m., Admiral Ballroom, A and B
Vali H.	Soils and Clays in Environmental Research Posters, Mon. p.m., Marina Room
Van Alboom M.	General Posters II, Tue. p.m., Marina Room
van Oss C. J.	Soils and Clays in Environmental Research I, Tue. p.m., Admiral Ballroom, D
van Oss C. J.	Surface Chemistry II, Tue. a.m., Admiral Ballroom, C
van Oss C. J.	Surface Chemistry Posters, Mon. p.m., Marina Room
Vandenberghe R. E.	General Posters II, Tue. p.m., Marina Room
Vaniman D.	General Posters II, Tue. p.m., Marina Room
Vaniman D.	The Extraterrestrial Connection I, Mon. p.m., Admiral Ballroom, D
Velde B.	Geothermometer and Geochronometers I, Tue. a.m., Admiral Ballroom, A and B
Velde B.	The Extraterrestrial Connection II, Tue. a.m., Admiral Ballroom, D
Vempati R. K.	The Extraterrestrial Connection I, Mon. p.m., Admiral Ballroom, D
Vempati R. K.	The Extraterrestrial Connection Posters, Tue. p.m., Commodore Room
Villieras F.	Surface Chemistry II, Tue. a.m., Admiral Ballroom, C
Vistisen L.	The Extraterrestrial Connection Posters, Tue. p.m., Commodore Room
Vrolijk P.	Geothermometer and Geochronometers Posters I, Tue. p.m., Commodore Room
Wadleigh M. A.	Geothermometers and Geochronometers Posters II, Thu. p.m., Commodore Room
Wagner U.	General III, Thu. a.m., Admiral Ballroom
Walker J. R.	General Posters I, Mon. p.m., Commodore Room
Walker J. R.	Geothermometer and Geochronometers I, Tue. a.m., Admiral Ballroom, A and B
Walling S. D.	General Posters III, Thu. p.m., Marina Room
Walshe J. L.	Geothermometer and Geochronometers Posters I, Tue. p.m., Commodore Room
Wampler J. M.	Geothermometers and Geochronometers III, Thu. a.m., Admiral Ballroom, A and B
Wampler J. M.	Geothermometer and Geochronometers Posters I, Tue. p.m., Commodore Room

Wang M. C.	Surface Chemistry Posters, Mon. p.m., Marina Room
Wang M. K.	Soils and Clays in Environmental Research Posters, Mon. p.m., Marina Room
Wang W.	General II, Tue. p.m., Admiral Ballroom, C
Weaver C. E.	Plenary Session, Mon. a.m., Admiral Ballroom
Weaver R. M.	General Posters II, Tue. p.m., Marina Room
Webb H.	General Posters II, Tue. p.m., Marina Room
Webster D. M.	General Posters III, Thu. p.m., Marina Room
White G. N.	General Posters II, Tue. p.m., Marina Room
Whitney G.	Geothermometer and Geochronometers I, Tue. a.m., Admiral Ballroom, A and B
Williams L. B.	General Posters III, Thu. p.m., Marina Room
Wills E. L.	The Extraterrestrial Connection Posters, Tue. p.m., Commodore Room
Xu Q.	General I, Mon. a.m., Admiral Ballroom, A and B
Yamane H.	General Posters II, Tue. p.m., Marina Room
Yang X.	General I, Mon. a.m., Admiral Ballroom, A and B
Yeh H.-W.	Geothermometers and Geochronometers II, Tue. p.m., Admiral Ballroom, A and B
Ylagan R. F.	Geothermometers and Geochronometers Posters II, Thu. p.m., Commodore Room
York D.	Geothermometers and Geochronometers III, Thu. a.m., Admiral Ballroom, A and B
Young D. S.	Soils and Clays in Environmental Research Posters, Mon. p.m., Marina Room
Yu J.-Y.	General I, Mon. a.m., Admiral Ballroom, A and B
Yu J.-Y.	Geothermometer and Geochronometers I, Tue. a.m., Admiral Ballroom, A and B
Yuretich R. F.	General Posters II, Tue. p.m., Marina Room
Zachara J. M.	Soils and Clays in Environmental Research II, Thu. a.m., Admiral Ballroom, D
Zelazny L. W.	Surface Chemistry Posters, Mon. p.m., Marina Room
Zhang F.	Surface Chemistry II, Tue. a.m., Admiral Ballroom, C
Zhang Z. Z.	Soils and Clays in Environmental Research I, Tue. p.m., Admiral Ballroom, D
Zhou Z.	Surface Chemistry Posters, Mon. p.m., Marina Room
Zolensky M. E.	The Extraterrestrial Connection II, Tue. a.m., Admiral Ballroom, D
Zubkov B.	The Extraterrestrial Connection Posters, Tue. p.m., Commodore Room
Zuchniewicz J.	The Extraterrestrial Connection Posters, Tue. p.m., Commodore Room

N92-10249

Combined Backscatter Mössbauer Spectrometer and X-Ray Fluorescence Analyzer (BaMS/XRF) for Planetary Surface Materials. Agresti D.G., Shelfer T.D., Pimperl M.M., Wills E.L., Physics Department, University of Alabama at Birmingham, Birmingham, AL 35294; and Morris R.V., Code SN2, NASA Johnson Space Center, Houston, TX 77058.

Introduction. We are developing a backscatter Mössbauer spectrometer (BaMS) [1] with included x-ray fluorescence (XRF) capability for the Mars Environmental Survey (MESUR) mission which has been proposed by NASA for 1998. The instrument will be suitable as well for other planetary missions such as those to the Moon, asteroids, and other solid solar-system objects. BaMS would be unique for MESUR in providing information about iron mineralogy in rocks, clays, and other surface materials, including relative proportions of iron-bearing minerals. It requires no sample preparation and can identify all the normal oxidation states of iron (3+, 2+, 0). BaMS is thus diagnostic for weathering and other soil-forming processes. Backscatter design allows the addition of XRF elemental analysis with little or no modification. The BaMS/XRF instrument complements the thermal analyzer with evolved gas analyzer (TA-EGA) and alpha-proton-x-ray spectrometer (APXS) [2] proposed (along with BaMS) for geochemical analysis on MESUR by Gooding [3].

Design Considerations. Backscatter Mössbauer spectroscopy involves the emission of γ -rays from a radioactive source (for iron work, ^{57}Co), their subsequent resonant absorption (by ^{57}Fe nuclei) in a solid matrix, and detection of fluorescent radiation (e.g. Fe $K\alpha$ x-rays) as function of source velocity (Doppler modulation of γ -ray energy). The BaMS instrument has three main components: radiation detection system, source velocity transducer (drive), and electronics for data storage and control.

The principal requirement for optimizing a BaMS for planetary missions is the overall miniaturization of these components and their integration into a single package. We have built and tested a miniature drive (90% volume reduction) of conventional, loud-speaker design [4] and are currently constructing one of comparable additional size reduction, which would be suitable for the planetary instrument. We are also investigating piezoelectric and electrostrictive transducers as alternatives. We have demonstrated the suitability of HgI_2 solid state detectors for Mössbauer spectroscopy [5] and are currently constructing a compact 2π -geometry gas-filled proportional-counter array. Work is under way to integrate all electronics onto a single board, including logic for experiment control and multichannel analysis, as well as drive and detector electronics.

References: [1] Morris et al. (1988) Sample Acquisition, Analysis, and Preservation (SAAP) Instrument Technology Workshop, Houston, Nov. 14-18; Morris et al. (1989) Lunar Planet. Sci., vol. no. 20, p. 721-722. [2] Economou T. et al. (1990) Lunar and Planetary Science, vol. no. 20, p. 307-310. [3] Gooding J.L. (1991) First MESUR Science Definition Team Meeting, NASA Ames Research Center, Feb. 22. [4] Shelfer et al. (1991) Lunar Planet. Sci., vol. no. 22, p. 1229-1230. [5] Agresti et al. (1990) Lunar Planet. Sci., vol. no. 21, p. 5-6.

SOURCES OF CLAY MINERALS ON MARS

Carlton C. Allen Lockheed ESC, C23 2400 NASA Road 1 Houston, TX 77058

The surface soil of Mars was analyzed in situ by the Viking landers and remotely by visible and near-IR reflectance spectroscopy. The soil is thought to be composed of alteration products of basic igneous rocks. Chemical compositions of fine material from both Viking landing sites are well, though not uniquely, matched by a combination of 47 wt% nontronite, 17% montmorillonite, 15% saponite, 13% kieserite, 7% calcite, and 1% rutile (1). Reflectance spectra of the landing sites are very similar to that of Fe-rich palagonite, a clay-like mineraloid produced by the alteration of volcanic soils (2). Proposed mechanisms for the formation of clays on Mars include the chemical weathering of basaltic glass and rocks and hydrothermal alteration due to volcanic or impact heating.

Chemical Weathering The present surface temperatures on Mars rarely exceed freezing, even in equatorial regions. The atmospheric pressure is approximately 1% of Earth's. Neither water nor ice is stable at most points on the surface. The atmosphere is nearly saturated with water and thin films of ice, from frost or snow, have been observed at the Viking 2 landing site (3). Planet-wide dust storms occur several times each decade.

Given these conditions, the chemical weathering of rock at the surface is expected to be extremely slow. Basaltic glass should weather much more rapidly than crystalline rock, and glass has thus been proposed as a more likely clay precursor on Mars (4). However, massive basalts do undergo weathering in the extremely cold, dry environment of the Antarctic dry valleys. Chemical reactions in thin films of snow meltwater, followed by wind scouring, result in pitted rocks with residual coatings of smectite and illite. Such a mechanism might operate, albeit much more slowly, to produce clays in martian soil (5).

Hydrothermal Alteration Clay minerals can also be produced at or beneath the surface by hydrothermal alteration of rock or glass. Much of the martian surface is thought to be underlain by permafrost which extends to a depth of several kilometers. In the vicinity of a suitable heat source significant hydrothermal activity is to be expected.

Subglacial volcanic eruptions on Earth, particularly in Iceland and British Columbia, have produced large quantities of basaltic tephra which was subsequently altered to palagonite. A model for soil formation on Mars, based on hydrothermal alteration of volcanic glass, has been proposed (6,7). The interaction of volcanism with ground ice would produce glass and the conditions for alteration to palagonite. This material is generally friable, and could be disaggregated and dispersed by the martian winds.

A second significant source of localized heat is impact cratering. On Earth impacts into water-rich rocks, such as the Ries basin in Germany, have yielded copious amounts of clay minerals. Evidence of impact-induced melting of ground ice is common on Mars, leading to models of clay formation by the same mechanism (8,9).

References 1. Baird A.K. et al. (1977) *J. Geophys. Res.*, 82, 4595-4624. 2. Singer R.B. (1982) *J. Geophys. Res.*, 87, 10159-10168. 3. Wall S.D. (1981) *Icarus*, 47, 173-183. 4. Gooding J.L. and Keil K. (1978) *Geophys. Res. Lett.*, 5, 727-730. 5. Allen C.C. and Conca J.L. (1991) *Proc. Lunar Planet. Sci. Conf.*, 21, 711-717. 6. Soderblom L.A. and Wenner D.B. (1978) *Icarus* 34, 622-637. 7. Allen C.C. et al. (1981) *Icarus*, 45, 347-369. 8. Newsom H.E. (1980) *Icarus*, 44, 207-216. 9. Allen C.C. et al. (1982) *J. Geophys. Res.*, 87, 10083-10101.

A METHOD FOR THE DETERMINATION OF REFRACTIVE INDEX OF FINE-GRAINED MINERAL POWDERS

Fred Allen & Paul Sennett
Engelhard Corporation
Iselin, New Jersey

We have developed a method for determining the average refractive index of fine-grained mineral powders such as kaolinite or other minerals which typically occur as particles too small to measure by the commonly used immersion techniques. Our procedure consists of dispersing a constant amount of the mineral powder in liquids of varying refractive index and measuring the transmission of visible light (%T) as a function of the refractive index of the suspending liquid. Maximum light transmission occurs at the point where the refractive index of the solid and liquid are equal. Because the refractive index of the liquid (RI_{liq}) is easily measured using an Abbe refractometer, the average refractive index (RI_{avg}) of the solid phase is known.

A plot of %T vs. RI_{liq} for an isotropic solid (halite) has a peak that fits best to a Lorentzian function. For a uniaxial solid (calcite) the peak is broader and fits to a Voigt function, and for a biaxial solid (kaolinite) it is broader still and fits to a Gaussian function. In each case, RI_{avg} of the solid is the point corresponding to maximum %T. For colloidal particles, RI_{avg} can be thought of as the radius of a sphere with volume equivalent to the ellipsoid representing the optical indicatrix of the solid: $(n_x n_y n_z)^{1/3}$ if biaxial, $(n_e^2 n_w)^{1/3}$ if uniaxial, and simply n if isotropic.

Average refractive indices measured for halite, calcite, and kaolin clay, agree closely with values reported in the literature (Table 1). Kaolin, when heated to temperatures in the metakaolin range, decreases in refractive index.

Table 1. Comparison of measured average refractive indices with literature values of different minerals. Data are also given for kaolins heated to different temperatures.

Mineral	RI_{avg} (meas.)	RI_{avg} (lit.)
Halite	1.549	1.544
Calcite	1.600	1.601
Kaolin, Feed	1.575	1.56-1.57
400°C	1.575	
500°C	1.560	
700°C	1.541	
850°C	1.551	
1,000°C	1.568	

HYDROTHERMAL ALTERATION IN TWO ACTIVE GEOTHERMAL WELLS FROM THE PHLEGREAN VOLCANIC FIELDS, ITALY

Stephen P. Altaner¹, Robert H. Lander², Robert E. Klimentidis², and Robert F. Ylagan¹

¹Dept. of Geology, Univ. of Illinois, Urbana, Illinois 61801 and ²Exxon Production Research, P.O. Box 2189, Houston, Texas 77252-2189

The primary authigenic minerals in the upper portions of two active geothermal wells from the Phlegrean Fields volcanic area of south-central Italy are K-feldspar, analcime, and clay minerals (smectite, chlorite, mixed-layer chlorite/smectite (C/S), mixed-layer illite/smectite (I/S), and illite), with lesser amounts of calcite, fluorite, phillipsite, clinoptilolite, laumontite, and albite. Observed depth-related reactions are the discontinuous conversion of smectite to chlorite, reaction of analcime to albite, loss of phillipsite and clinoptilolite, and formation of laumontite.

The Phlegrean Fields represent a modern geothermal system that includes active volcanism, tectonic uplift, hot springs, and a number of deep geothermal wells drilled to evaluate the geothermal energy potential of the region. The volcanic province contains multiple eruptions of Recent (<34,000 yr) pyroclastic volcanics initially of K-rich trachytic (Si-undersaturated) composition. Samples were studied from the San Vito 1 well at a depth interval of 400 to 1090 m (20° - 175°C) and from the Mofete 1 well at a depth interval of 80 - 498 m (150° - 230°C). The wells penetrate similar lithologies but very different thermal gradients. The San Vito and Mofete wells are located in the central and western portions of the Phlegrean Fields, respectively. Samples have been analyzed using XRD, SEM, and optical microscopy. Planned analytical techniques include microprobe and TEM/AEM as well as thermodynamic modeling of fluid compositions.

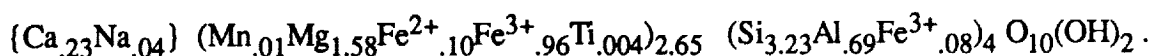
There is a discontinuous conversion of smectite to chlorite because Mg/Fe-rich smectite (or smectitic C/S with $\geq 80\%$ S) occurs in rocks below about 150°C and chlorite occurs above about 70°C. In addition, C/S occurs over a temperature interval from 100 to 170°C and contains a variable proportion of smectite layers ranging from 20 - 40% S. Therefore, there is a broad temperature interval over which smectite, chlorite, and C/S all coexist, supporting recent observations by Inoue and co-workers. The discontinuous conversion of smectite to chlorite differs with the continuous conversion of smectite to illite documented in numerous other diagenetic and hydrothermal settings. Typically, C/S only shows evidence for R1 order at a composition of about 40% S. I/S usually contains $\leq 15\%$ S and, along with illite, shows no depth-related changes. Phillipsite occurs only below about 50°C, laumontite occurs from about 110 to 150°C, and analcime is replaced by albite at ~200°C. K-feldspar is ubiquitous throughout the studied depth interval. There appears to have been multiple episodes of mineral authigenesis because in the same sample K-feldspar can precede clay mineral formation in one area and postdate clay formation in another area.

NMR INVESTIGATION OF HOMO-IONIC Na-AND Li-MONTMORILLONITE
Anderson, Duwayne M., Texas A&M University, Teague Building,
Room 326, College Station, Texas 77843-1112

Homo-ionic sodium-and lithium-saturated Wyoming bentonite at elevated water content was subjected to wide-line nuclear magnetic resonance (NMR) investigation. Proton NMR spectra were obtained as a function of temperature from room temperature to slightly below -100°C . Except for a slight departure in proton line widths in the temperature range -50°C to -90°C , the spectra are essentially identical and provide clear evidence of the existence of an unfrozen interfacial phase that steadily diminishes with temperature. However, the NMR spectra do not reveal the second order phase transitions known from scanning calorimeter data to occur in the -40°C to -80°C temperature range.

A SAPONITE-VERMICULITE INTERMEDIATE IN AMYGDALES OF THE GRANBY BASALTIC TUFF, CONNECTICUT VALLEY: Richard H. April and Dianne M. Keller, Colgate University, Hamilton, NY 13346.

Clay of apparent hydrothermal origin that fills amygdales in the Granby Basaltic Tuff (Lower Jurassic) of the Connecticut Valley was analyzed and identified as an Fe-rich, trioctahedral 2:1 expandable phyllosilicate with chemical and swelling properties intermediate between those of a smectite and a vermiculite. Based on XRF chemical analysis the structural formula of the clay is as follows:



Approximately two-thirds of the filled octahedral sites contain R^{2+} cations (most of which are Mg) resulting in an excess positive charge in the octahedral sheet of +.27. The average total layer charge of -.50 compares well with the measured CEC value of 112 meq/100 gm. These chemical results taken together with the XRD data, which include an 060 reflection at 1.538 Å and a calculated unit cell *b*-dimension of 9.23 Å, suggest that the clay should be categorized as a saponite. Additional chemical treatments, however, including saturating the clay with Ca, Mg, K, Na, and Li, heating the clay to 300°C, and exposing the clay to different relative humidities, produced diffraction results suggesting that the Granby clay is composed of both saponite and vermiculite or, alternatively, consists of diffracting domains or crystallites with layer charge heterogeneity spanning the operationally defined values for these two minerals. Because of these properties, the clay might better be described as a *saponite-vermiculite intermediate*, a term put forward by Suquet and Pezerat (1) to describe a 2:1 swelling clay showing crystallochemical properties and XRD characteristics of both minerals.

The Granby clay is of special importance, for it is one of the few naturally occurring examples of a relatively pure, Fe-rich trioctahedral 2:1 layer expandable phyllosilicate with crystallochemical and swelling properties bridging the smectite and vermiculite groups. In this respect, further study of this clay mineral will help to resolve some of the uncertainties involved in classifying trioctahedral 2:1 phyllosilicates, especially those pertaining to the distinctions between saponites and vermiculites.

1. Suquet, H. and Pezerat, H. (1988) Clays and Clay Minerals 36, 184-186.

MINERALOGY AND CHEMISTRY OF SUBSURFACE (900-4600 m) MUDROCKS AND <0.5 μm CLAY SEPARATES FROM THE TEXAS GULF COAST PALEOCENE-EOCENE:

David N. Awwiller

Dept. of Geological Sciences, The University of Texas, Austin, TX 78713

Cuttings from a well penetrating the Claiborne and Wilcox Groups (Paleocene-Eocene) in south-central Texas have been examined to identify chemical and mineralogical changes induced during burial diagenesis. Both whole rock and <0.5 μm clay separates have been examined; samples span a depth range of 900 to 4600 m of burial. Semi-quantitative whole rock XRD analyses show that K-feldspar, total clay, and calcite decrease downhole, whereas plagioclase (albite), quartz, and ankerite increase in relative abundance with increasing depth of burial. The <0.5 μm clay material shows a general decrease in discrete illite and kaolinite, and an increase in illite/smectite; chlorite appears only below ca. 2500 m of burial. Illite in I/S increases from ca. 30% at 1500 m of burial to ca. 90% at 4000 m of burial. I/S from deeper than 3200 m has ordered interstratification, ranging from R₁- to R₃-ordered.

Bulk clay chemical analyses, combined with semiquantitative XRD mineralogical analyses, allow for estimation of illite and smectite end members of interstratified I/S: $[\text{K}_{0.00}\text{X}^{+1}_{0.56}\text{Mg}_{0.39}\text{Fe}_{0.57}\text{Al}_{1.13}\text{Si}_{3.90}\text{O}_{10}(\text{OH})_2]$ and $[\text{K}_{0.53}\text{X}^{+1}_{0.18}\text{Mg}_{0.17}\text{Fe}_{0.16}\text{Al}_{2.28}\text{Si}_{3.40}\text{O}_{10}(\text{OH})_2]$, respectively. There is no obvious difference in the rate of K addition to I/S per illitic interlayer in random and ordered I/S. Substitution of Al into both tetrahedral and octahedral sites suggests that the smectite to illite reaction is a complete dissolution-precipitation reaction, rather than a simple [K + Al] for Si substitution reaction.

Although most major elemental concentrations in the whole rock samples show little or no variation as a function of depth, K₂O increases from ca. 2.0 weight percent at 1500 m of burial to ca. 3.8 weight percent at 4000 m of burial. The potassium increase cannot be accounted for without (a) large detrital variability, with the deeper samples originally containing excess detrital feldspar and/or illite; (b) importation of K derived from feldspar dissolution in interbedded Wilcox sandstones or other siliciclastic units; (c) importation of K derived from deeper in the basin, either from underlying evaporites or the metamorphic basement; or (d) shale volume loss, with preferential retention of potassium. Although the importance of downhole detrital variability has not been demonstrated, it seems most likely that a combination of processes (a) and (b) are responsible for the observed K enrichment: increase in whole rock quartz and plagioclase content is probably too great to be due solely to diagenetic modification, and the deeper (Wilcox) part of the section seems to be somewhat more sandy than the shallower (Claiborne) section. The apparent potassium transfer from sandstones into mudrocks implies that mudrocks behave as open chemical systems during burial diagenesis. A minimum of ca. 10³ pore volumes of fluid must have passed through the most K-enriched shales to have introduced the added potassium.

HIGH RESOLUTION TRANSMISSION AND ANALYTICAL ELECTRON MICROSCOPY OF THE SMECTITE TO ILLITE TRANSITION IN AUSTRALIAN MUDROCKS

Julian C. Baker and Ian D. R. Mackinnon

Electron Microscope Centre, University of Queensland,
Queensland, 4072, Australia

The smectite to illite transition in mudrocks of the Jurassic-Cretaceous Eromanga Basin and Carboniferous-Permian Galilee Basin sequences in borehole GSQ Longreach 1-1B (western Queensland) has been studied using high resolution transmission and analytical electron microscopy. The study follows the work of Green *et al.* (1991) who showed that in this borehole, over a depth interval of about 660 m, the percentage of illite interlayers in mudrock illite-smectites of the Eromanga Basin sequence progressively increases from 0 to 77%, while in mudrock illite-smectites of the underlying Galilee Basin sequence, the percentage remains constant at between 75 and 82% (see also Carmichael *et al.*, this volume).

Our preliminary results, obtained at 400kV using a JEOL 4000FX TEM with an attached EDS, show that in the shallowest samples, smectite consists of coherently stacked domains of 001 layers that commonly curve, bifurcate and pinch and swell (layer spacings range from 10 to 13Å in untreated samples). Domain sizes lie mainly between 20 and 200 Å in the basal direction. Fe and Mg are invariably present. Many crystallites also contain small amounts of K, with those containing Ca and Na being generally rare. Al to Si ratios are highly variable. In the deeper mudrocks, illite-smectite with about 60% illite interlayers typically consists of smectite layer domains which contain discrete 50 to 130 Å thick packets of illite layers. In contrast to adjacent smectite layers, these illite layers lack defects and are relatively straight, well-defined and of constant thickness. K contents are significantly higher than in the shallower samples. Illite-smectite with 70 to 80% illite interlayers in the deepest samples typically consists of subparallel, coalesced, mainly 50 to 200 Å thick packets of relatively straight, defect-free illite and completely collapsed smectite layers. Intense dark fringes showing 20 to 50 Å periodicity in some images obtained at an overfocus condition are interpreted to correspond to approximate positions of smectite interlayers (Veblen *et al.*, 1990). The proportion of imaged smectite interlayers is consistent with XRD data. In comparison to shallower illite-smectites, deep illite-smectites contain higher and lower proportions of K and Fe, respectively. Al to Si ratios are relatively consistent and are generally higher than that for the high expandability illite-smectites analysed in the shallower samples.

Despite occurring in a vastly different geologic setting, the Eromanga and Galilee Basin mudrock illite-smectites are compositionally and structurally similar to those occurring at depth in Gulf Coast sediments (c.f. Ahn & Peacor, 1986, 1989; Freed & Peacor, 1989), suggesting that smectite illitization has proceeded along similar pathways in both settings.

References:

- Ahn, J. H. and Peacor, D. R., 1986. *Clays & Clay Minerals* 34, 165-179.
 Ahn, J. H. and Peacor, D. R., 1989. *Clays & Clay Minerals* 37, 542-546.
 Freed, R. L. and Peacor, D. R., 1989. *Clay Minerals* 24, 171-180.
 Green, P. M., McKellar, J. L., Carmichael, D. C. and Smith, R. J., 1991.
Queensland Department of Resource Industries Record 1991/20.
 Veblen, D. R., Guthrie, G. D., Jr., Livi, K. J. T. and Reynolds, R. C., Jr.,
 1990. *Clays & Clay Minerals* 38, 1-13.

FLUID-CLAY INTERACTIONS IN SANDSTONE RESERVOIRS: DIRECT OBSERVATION

Julian C. Baker¹, Philippa J. R. Uwins¹, Ken R. Martin² and Ian D. R. Mackinnon¹

¹ Electron Microscope Centre, University of Queensland,
Queensland, 4072, Australia

² K. R. Martin Pty. Ltd., P.O. Box 22, Kenmore,
Queensland, 4069, Australia

An Electroscan Environmental Scanning Electron Microscope (ESEM) is currently being used to observe directly the behaviour of freshwater-sensitive clays in petroleum reservoirs in response to the introduction of salt solutions and freshwater. The ESEM makes this possible through its unique capability of allowing one to observe, under high magnification, materials and processes in their natural state. This is achieved by a series of small apertures and by differential pumping along the beam path which allows the LaB₆ electron source and upper column to remain at high vacuum while the specimen chamber can be held at pressures of up to 50 torr in fully saturated water vapour conditions. Accordingly, high resolution images of water and oil saturated, uncoated, non-conducting materials can be acquired and, moreover, by careful manipulation of chamber pressure and temperature, the natural environment of the specimen can be simulated.

For our experiments, KCl solutions were chosen because KCl/polymer drilling muds are now widely used to control clay swelling in reservoir sandstones, replacing the traditional freshwater-based bentonite muds (*e.g.* Almon & Davies, 1981). We are interested in observing, not only any differences in the clay response to KCl and freshwater, but also whether the use of excessively high concentrations of KCl results in any adverse effects within reservoir sandstones, given that formation waters in many Australian hydrocarbon basins are relatively fresh. Of particular interest is whether concentrations of KCl well above those of formation waters can cause lattice collapse leading to detachment of authigenic smectite or illite-smectite pore linings. The result of such a process could be formation damage due to pore throat blockage by the migrating clays.

Preliminary results show that smectite-rich pore-filling clays in sandstones previously immersed in a 10-15% NaCl solution for 48 hr (to simulate typical eastern Australian sedimentary basin formation waters) undergoes at least a minor morphological change when exposed to a solution containing 10% KCl. Whether this change gives rise to detachment and subsequent migration of individual crystals remains to be confirmed. Images of smectitic pore filling/lining clays in sandstones before and after treatment with KCl solutions and freshwater will be shown.

Reference:

Almon, W. R. & Davies, D. K., 1981. *Mineralogical Association of Canada, Short Course in Clays and the Resource Geologist*, F. J. Longstaffe (Ed.), 7, 81-103.

CLAYS ON MARS: REVIEW OF CHEMICAL AND MINERALOGICAL EVIDENCE

Amos Banin^{1,2} and James L. Gooding³. ¹National Research Council Senior Research Associate, MS 239-12, NASA/Ames Research Center, Moffett Field, CA 94035 USA. ²Hebrew University, Rehovot, Israel. ³SN21/Planetary Science Branch, NASA/Johnson Space Center, Houston, TX 77058 USA.

Since the 1960s, flyby, orbiter, and lander spacecraft have provided increasing knowledge about the surface of Mars. No conclusive mineral identifications have been achieved, however, and reconciliation of diverse geochemical observations remains an active area of research [1, 2]. The most important results to date were obtained from the Viking Lander 1 and 2 spacecraft which performed *in situ* analyses at two different surface locales during 1976-77. In addition, Earth-based visible (VIS) and infrared (IR) telescopic spectrophotometry, integrated over larger regions, continues to seek diagnostic absorption bands for minerals. Finally, laboratory studies of the shergottite-nakhlite-chassignite (SNC) clan of meteorites, which is suspected to represent rocks ejected from Mars by impact cratering, have provided potentially definitive information.

Mafic igneous bedrock is inferred for Mars, based on spectrophotometric evidence for pyroxene (principally in optically "dark" areas of the globe) and the pyroxenite-peridotite petrology of SNC meteorites. VIS/near-IR spectra of reddish-brown surface fines (which dominate martian "bright" areas) indicate ferric iron and compare favorably (though not uniquely) with spectra of terrestrial palagonitic soils. Some mid-IR spectral features have been provisionally assigned to hydroxyl groups in minerals such as smectites. The Viking Lander camera systems provided broad-band VIS/near-IR photometry of rocks and fine-grained sediments (hereafter denoted as "soils") but lander-based chemical analyses were limited to soil samples only. Lander photometry showed that rocks and soils exhibit similar spectral radiance curves even though the soils are brighter overall, suggesting that the rocks are partially coated with soil-like material. Insertion of magnet arrays into the soil by the Viking surface sampler mechanism confirmed occurrence of a few weight percent of one or more strongly magnetic minerals. Detailed laboratory studies of Mars-analogous mineral samples have shown that both the VIS/near-IR spectral features and magnetic susceptibilities of martian soils can be explained by certain ultrafine-grained ferric iron oxides (e.g., nanophase hematite and lepidocrocite). X-ray fluorescence spectrometry (XRFS) of soil samples at the Viking sites revealed Si and Fe as major elements with subequal minor concentrations of Al, Mg, and Ca but also significant S and Cl. Because the analytical totals were only about 90-91 percent on an oxide basis, and elements lighter than Mg could not be analyzed by the XRFS, significant concentrations of minerals bearing C, N, or Na remain as additional possibilities. Salt-subtracted corrections to the Viking XRFS data are consistent with (though not uniquely satisfied by) a nontronite + saponite mixture. A pyrolysis (gas chromatograph-mass spectrometer, GCMS) experiment, which was optimized for organic compounds but found none, confirmed soil water on the order of 1 weight percent (which is probably a lower limit). Three different chemical experiments (gas exchange, GEX; labelled release, LR; pyrolytic release, PR) on each Viking Lander were intended to test for biological activity but found, instead, evidence for highly reactive inorganic agents. Earth-based laboratory simulations of the GEX and LR results, in particular, led some investigators to conclude that trace concentrations (a few ppb or ppm by weight) of peroxides or superoxides (perhaps with maghemite as catalyst) were responsible for the unexpected behavior of the martian soil. Independent simulations showed, however, that at least for the LR and PR results, iron-exchanged smectites produced the same effects whereas palagonitic soils did not reproduce the LR data. SNC meteorites contain traces of Ca-carbonate, Ca-sulfate, and at least one example of smectite intergrown with ferric oxyhydroxides. Accordingly, both the Viking Lander and SNC results support a model for martian soil based on chemical weathering of mafic rocks to produce layer-structured silicates (clay minerals), salts, and iron oxides.

References: [1] Banin A. (1986) In Cairns-Smith A. G. and Hartman H. (Eds.), *Clay Minerals and the Origin of Life*, Cambridge, 106-115. [2] Arvidson R. E., Gooding J. L., and Moore H. J. (1989) *Rev. Geophys.*, 27, 39-60.

4 1 /

The Internal Oxygen Isotope Fractionations in Clay Minerals: Preliminary Results and Application as Single-Mineral Geothermometers; A. Bechtel, Mineralogisch-Petrologisches Institut, Universität Bonn, Poppelsdorfer Schlob, D-5300 Bonn 1, Germany.

Since the first experimental results (1,2) have been pointed out differences in isotopic composition of oxygen in different sites in hydrosilicates, recent stable isotope studies have dealt with the calibration of single-mineral thermometers (3,4,5). To determine the oxygen isotope ratios of hydroxyl groups in silicate minerals, a vacuum extraction technique was worked out (5). The results of this method from minerals, which contain no ferrous iron, and by use of a modified partial fluorination technique (2) agree within the limits of error. A preliminary empirical calibration of the internal illite-OH fractionation was derived by studies on natural, hydrothermally formed illites in the temperature range of 200°-300°C (5). Its accuracy mainly suffers from the uncertainty of the formation temperature of the investigated samples.

To obtain better calibrations, it is necessary to use mineral samples synthesized under fixed experimental conditions. In this study kaolinite was crystallized at 250°, 300° and 350°C from a gel in a hydrothermal-apparatus (6). The comparison of the derived kaolinite-water fractionation values with the calibration curve (7) show significant differences. Despite this, the internal ¹⁸O fractionations of the synthesized samples were measured by vacuum extraction. The results of the oxygen isotope investigations of the kaolinites suggest a linear correlation between the internal fractionation and the temperature of formation. The equation for the internal oxygen isotope fractionation of kaolinite was calculated by "least squares" method.

The mineral-OH fractionations of a hydrothermally formed dickite and a commercial kaolinite (probably an alteration product under near-surface conditions) were determined to test the fractionation curve for applicability to natural samples, as well as to temperature conditions outside the investigated range. The calculated temperatures from internal oxygen isotope fractionation data are in agreement with temperature assessments from geological and petrological results.

- (1) Savin S.M. (1967) Ph D Diss, California Inst of Technology
- (2) Hamza M. and Epstein S. (1979) Geochim Cosmochim Acta, 44, 173-182
- (3) Pickthorn W.J. and O'Neil J.R. (1985) Geol Soc Am Abstr Progr, 17, 689
- (4) Yapp C.J. (1986) Geochim Cosmochim Acta, 51, 355-364
- (5) Bechtel A. and Hoernes S. (1990) Contrib Mineral Petrol, 104, 463-470
- (6) Noll W. (1936) N Jahrbuch Mineral, Suppl 70 / A, 65-115
- (7) Land L.S. and Dutton S.P. (1978) J Sediment Petrol, 48, 1167-1176

THE EVIDENCE FOR (AND AGAINST) CLAY MINERALS ON MARS FROM 20 YEARS OF TELESCOPIC OBSERVATIONS: James F. Bell III (Planetary Geosciences Division, University of Hawaii, 2525 Correa Rd., Honolulu 96822; e-mail: jimbo@ruth.pgd.hawaii.edu).

Summary: Considerable debate still exists about the nature, origin, and even the occurrence of clay minerals on Mars. This abstract reviews the evidence for and against the occurrence of clays on Mars and attempts to determine whether any conclusive data exist from the past twenty years of telescopic near-infrared reflectance spectroscopy that can be used to definitively address this issue. The interpretations of many telescopic data sets are at odds with the interpretations of many Mariner and Viking experiments. This may be in part due to large differences in spatial and spectral resolution and measurement goals between groundbased and spacecraft studies; alternately, a continuum of crystalline and amorphous clay and clay-like phases may exist on Mars that do not have good terrestrial analogs.

Much evidence has been presented for the existence of clays on Mars. The existence of bound water and thus of hydrated minerals has been known for some time based on the very strong Mars 3.0- μm absorption feature [1-3]. Mariner 9 IRIS spectral features near 9.0 μm were interpreted as montmorillonite [4] or a basalt-montmorillonite mixture [5], although other minerals were also shown to exhibit these features [6]. Viking XRF chemical analyses were best matched with the smectites nontronite (50%) and montmorillonite (20%) as major components [7,8]. Thermodynamic calculations have shown that "gas-solid weathering of mafic silicates (of volcanic or impact origin) may...favor the production of metastable Fe-rich montmorillonite clays" [9]. Simulations of the Viking Lander LR and PR experiments found that iron- and hydrogen-enriched nontronite and montmorillonite successfully reproduced the results from Mars [10,11]. These same materials were also found to be good spectral analogs to Mars in the UV through near-IR based on the available data [10,12].

Despite several spacecraft missions and many laboratory and theoretical studies and simulations, telescopic reflectance spectroscopy remains as the primary source of mineralogic information on Mars. Data in the 1.0-4.0 μm region (near-IR) are sensitive to clay mineralogies since this region contains numerous vibrational modes and combination and overtone bands of H_2O and OH^- [13,14]. Perhaps the most diagnostic spectral region is between 2.2-2.5 μm where weak cation- OH^- absorptions occur in a highly transparent window in the terrestrial and martian atmospheres [see review by 15]. Telescopic spectra obtained prior to 1971 [reviewed by 16] are of relatively low signal-to-noise (S/N) and show no evidence for clay-type absorption bands. Data obtained in 1976 and 1978 [17-19] showed a complex absorption feature near 1.95 μm that was interpreted as being composed of several lattice vibrational modes of clay minerals like montmorillonite and kaolinite, supporting these authors' suggestion that most of the features in the 1.0-2.2 μm region are caused by ice+mineral hydrate mixtures. Small, distinct absorption bands in the 2.2-2.5 μm region can be seen in the spectra of [18,19]. These authors attribute weak features near 2.3 μm and possibly 2.4 μm to Mg-OH in sheet silicates (serpentine, talc, Mg-smectites) or amphiboles (anthophyllite, actinolite). They interpret the lack of a 2.2 μm feature (characteristic of Al-OH) as evidence that montmorillonite or other dioctohedral clays are not a major component of the martian soil since its reflectance signature is not at all like that of the nontronite is not a major component of the martian soil since its reflectance signature is not at all like that of the available data. However, the presence of other iron-poor clays (such as montmorillonite) could not be totally excluded. Relative reflectance spectra obtained during the 1986 opposition [21] showed some evidence of spectral variability in the 2.2-2.5 μm region, but these data suffer from low S/N and await further re-calibration efforts. Interpretation of data obtained during the 1988 opposition [22] have suggested that the weak features in the 2.3 μm region (and possibly elsewhere in the 1.0-2.2 μm region) are not caused by hydroxylated minerals but are due to absorptions by atmospheric CO and the mineral scapolite in abundances varying from 0-2% to 10-20% depending on the region. The 2.3 μm feature has been resolved into at least 5 components that are not consistent with any single clay-type mineral. This interpretation has not been confirmed by recent Phobos-2 ISM observations of Mars [23], which detected a small absorption feature near 2.35 μm and found it to be predominantly caused by CO. Finally, new imaging spectroscopy data acquired during the 1990 opposition [24,25] shows evidence for weak absorptions near 2.2 and 2.25 μm that are definitely not correlated with CO abundance and may be indicative of Fe-OH bands. Further calibration of this and another high spectral resolution (R=1500) data set [26] in the 2.1-2.5 μm region is progressing and will be discussed along with previous data and interpretations in more detail at the conference.

References: [1] Sinton W.M. (1967) *Icarus*, 6, 222. [2] Houck J.R. et al. (1973) *Icarus*, 18, 470. [3] Pimentel, G.C. et al. (1974) *JGR*, 79, 1623. [4] Hunt G.R. et al. (1973) *Icarus*, 18, 459. [5] Toon O.B. et al. (1977) *Icarus*, 30, 663. [6] Aronson J.R. and A.G. Emslie (1975) *JGR*, 80, 4925. [7] Baird A.K. et al. (1976) *Science*, 194, 1288. [8] Toulmin P. et al. (1977) *JGR*, 82, 4625. [9] Gooding J.L. and K. Keil (1978) *GRL*, 5, 727. [10] Banin A. and J. Rishpon (1979) *J. Mol. Evol.*, 14, 133. [11] Banin A. and L. Margulies (1983) *Nature*, 305, 523. [12] Banin A. et al. (1985) *JGR*, 90, C771. [13] Hunt G.R. and J.W. Salisbury (1970) *Mod. Geol.*, 1, 283. [14] Clark R.N. et al. (1990) *JGR*, 95, 12653. [15] Roush T.L. et al. (1991) in *Remote Geochemical Analyses*, (C. Pieters & P. Englert, eds.) in press. [16] McCord T.B. et al. (1971) *Icarus*, 14, 245. [17] McCord, T.B. et al. (1978) *JGR*, 83, 5433. [18] Singer R.B. et al. (1979) *JGR*, 84, 8415. [19] McCord T.B. et al. (1982) *JGR*, 87, 3021. [20] Singer, R.B. (1982) *JGR*, 87, 10159. [21] Bell J.F. III and T.B. McCord (1989) *Icarus*, 77, 21. [22] Clark R.N. et al. (1990) *JGR*, 95, 14463. [23] Erard S. et al. (1991) *PLPSC 21st*, 437. [24] Bell J.F. III and D. Crisp (1991) *LPSC XXII*, 73. [25] Bell J.F. III and D. Crisp (1991) submitted to *Icarus*. [26] Bell J.F. III and D. Crisp (1990) unpublished data.

**AN EXCEPTIONAL ILLITE FROM THE EUREKA MINE, CORDOBA PROVINCE,
REP. ARGENTINA**

Silvana R. Bertolino^{1,2}, Colin C. Harvey² and Haydn H. Murray²

¹ CONICET. Fac. Cs. Ex. Fís. y Nat. Universidad Nacional de Córdoba. Av Velez Sarsfield 299. (5000) Córdoba. Rep. Argentina.

² Department of Geology, Indiana University, 1005 East Tenth St. Bloomington, IN 47405.

A well crystallized dioctahedral illite 2M1 is reported from the Eureka Mine, Cordoba Province, Argentina. This occurrence is unusual in the fact that pure illites are remarkably rare in nature. The illite is the in situ alteration product from a fault zone in a quartz-muscovite rich pegmatite, located on the West slope of the Achala Batholith in the Sierras Pampeanas Ranges.

The bulk mineralogy is quartz, muscovite, illite with accessory feldspars and minor hematite and soluble salts of Na, K and Ca. The <2 μ m fraction is variable ranging from 7 to 43%, with illite content increasing with depth. The purity of the illite in this fraction ranges from 90 to 100% with 10 to 0% of quartz. XRD analysis revealed symmetrical and sharp basal reflections consistent with very well crystallized dioctahedral illite 2M1. SEM studies showed the illite to be composed predominantly of well formed laths with minor quantities of irregularly shaped particles.

The structural formula, calculated from the chemical composition of the <2 μ m fraction is:



This calculation assumes: an anionic charge of -44; that total iron is in the Fe³⁺ state and that K, Na and Ca are in the interlayer site. The net layer charge is -1.83 while the interlayer cation (K+Na+Ca) charge is +1.86. This discrepancy of 0.03 in the charge balance may be due to, either a proportion of Fe²⁺ in the octahedral sites of the layer, or alternatively, the Ca and Na may be present as minor amounts in soluble salts. Traces of soluble salts have been detected and are considered to be the most likely explanation. In a compositional ternary diagram (Newman and Brown, 1987) the composition plots midway between muscovites and hydromuscovites.

This illite may have special applications in ceramics since, it is naturally white to greyish white and it fires white. Its DTA curve is similar to that of dioctahedral muscovite.

Because of the mineralogical and chemical purity of the Cordoba Illite it should be considered as a standard reference material for illite.

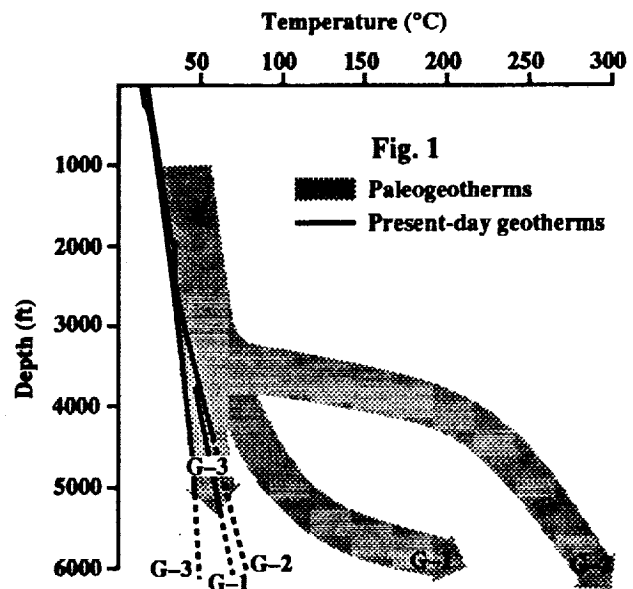
DETERMINATION OF PALEOGEOTHERMAL AND PALEOHYDROLOGIC CONDITIONS IN SILICIC TUFFS FROM ILLITE/SMECTITE MINERALOGY

David L. Bish

Earth & Environmental Sciences, MS D469, Los Alamos National Lab., Los Alamos, NM 87545

Yucca Mountain, Nevada, is being investigated as a potential site for the nation's first high-level radioactive waste repository. The political and scientific complexity of the Yucca Mountain Site Characterization Project requires a thorough understanding of past alteration events as predictors of possible future alteration processes. The paleogeothermal conditions in the Miocene (12-14My) silicic tuff sequence from Yucca Mountain have been investigated using a combination of illite/smectite (I/S) mineralogy, K/Ar dating, and fluid inclusion analysis. The illite/smectites in the northernmost drill hole (USW G-2) exhibit a transition from R0 to R \geq 3 I/S and illite with depth, and fluid inclusions in the deep calcites yield temperatures over 200°C. The R0-to-R \geq 3 transition is shifted to greater depths to the south in drill hole USW G-1 and is not observed in the southernmost hole (USW G-3). The spatial relations in mineralogy and the I/S K/Ar dates (10.7 ± 0.8 Ma; $n = 8$) [1] suggest that the alteration at depth in Yucca Mountain is related to intracaldera hydrothermal activity associated with the Timber Mountain caldera to the north (10.7 Ma). The paleogeotherms inferred from the I/S and fluid inclusion temperatures (Fig. 1) closely resemble those from modern-day geothermal sites such as Newberry Volcano, Oregon. For example, drill hole GEO N-1 from the southern flank of Newberry Volcano has a nearly constant temperature to ~3300 ft, at which point the temperature rapidly increases from ~8°C to ~50°C and then takes on a conductive nature [2]. The shallower, constant-temperature regime has been interpreted as a rain-curtain effect, and the abrupt rise in gradient is attributed at least partially to variations in permeability.

The similarity in form between the northernmost Yucca Mountain paleogeotherms and modern geotherms in geothermal wells suggests that they have several genetic features in common. The relatively constant inferred temperature in drill hole USW G-2 to ~3500 ft depth, much deeper than the present static water level (~1712 ft), suggests that either a rain-curtain effect existed and/or the rocks deeper than 3500 ft were relatively impermeable and were not affected by the regional groundwater flow. In support of a rain-curtain effect, limited climatological data suggest that this area was much wetter ~11 My ago, before uplift of the Sierra Nevada. In addition, there is a probable major fault near 3510 ft in USW G-2, and the primary minerals below this depth are mostly altered to secondary minerals. The deepening southward of this transition zone is likely due to a combination of distance from the hydrothermal source and the consequent variations in alteration and permeability. These studies at Yucca Mountain show that the alteration assemblage present today evolved shortly after deposition of the tuffs, in a thermal and hydrologic regime significantly different than existing today.



- [1] Aronson, J. L., and Bish, D. L. (1987) 24th Annual CMS meeting, p. 25.
 [2] Swanberg, C. A., and Combs, J. (1986) EOS, Trans. AGU, 578-580.

RIETVELD REFINEMENT OF THE DICKITE CRYSTAL STRUCTURE AT 12 K

David L. Bish

Earth & Environmental Sciences, MS D469, Los Alamos National Lab., Los Alamos, NM 87545

Although the basic structure of dickite is well known, recent low-temperature infrared (IR) spectra showing more than the four allowed O-H stretching bands below ~60 K (1) suggest a need to re-evaluate the structure. In addition, considerable uncertainty remains regarding the orientation of the OH groups that are so important in determining and understanding the details of the interlayer bonding. For example, published O-H bond lengths in dickite range from 0.72 Å to 1.25 Å, whereas accurate refinements of similar materials at room temperature yield O-H bond distances of 0.97 ± 0.2 Å. In an attempt to understand the structural details yielding the IR spectra, time-of-flight neutron diffraction data were obtained at 12 K on the <325-mesh fraction (<44 μm) of dickite from St. Claire, Pennsylvania, using the Neutron Powder Diffractometer (NPD) at the Los Alamos Neutron Scattering Center (LANSCE).

The Rietveld refinement program GSAS was used to refine the structure, using the non-H atom positions of (2) as a starting model. Initially, scale factors and profile and lattice parameters were refined, with the positions of the non-H atoms fixed and no H atoms included. Difference-Fourier maps were then calculated, and they indicated the existence of four sizable regions of negative density with no significant anisotropy evident, unlike the maps obtained for kaolinite (3). The four apparent H positions were then added to the asymmetric unit, and Rietveld refinement proceeded with the application of soft distance constraints. Anisotropic profile coefficients and a preferred orientation correction ([001]) were then refined, followed by isotropic temperature factors for groups of similar atoms (all O atoms, all hydroxyl O atoms, all H atoms, all Al atoms, and all Si atoms grouped together, respectively). The absorption correction did not function properly due to the highly absorbing nature of the fully hydrogenated sample; diffraction may have been occurring only near the outside of the V can. The correction was refined in subsequent cycles, but it is obvious that problems with its refinement led to inaccurate values for atomic temperature factors, some of which were negative. A final set of cycles (overall $R_{wp} = 2.55\%$, $\chi^2 = 1.86$) with anisotropic H atoms revealed only minor anisotropy.

The resulting non-hydrogen structure in Cc is very similar to those previously published, but the refined H positions differ significantly from literature values. In addition, the refined lattice parameters [$a = 5.1496(5)$ Å; $b = 8.9424(9)$ Å; $c = 14.396(2)$ Å; $\beta = 96.484(1)^\circ$] differ from those reported most recently by (2), but refinements using room-temperature X-ray powder diffraction data sets for several different dickite samples suggest that their reported values are in error. O-H distances range from 0.937 to 0.969 Å, Si-O distances vary from 1.607 to 1.623 Å, and Al-O distances extend from 1.887 to 1.957 Å. Because of the excellent fit to the data with this structural model, further refinement in a lower space group which would allow >4 independent H positions was not attempted. There is no evidence in the powder pattern to support a lower symmetry, and the lack of significant splitting of the individual H positions does not argue for a lower symmetry. In addition, recently obtained low-temperature IR spectra of this dickite sample (C. Johnston, personal communication) show only three bands, suggesting that the sample used by (1) may have been impure.

- (1) Prost, R., Dameme, A., Huard, E., Driard, J., and Leydecker, J. P. (1989) *Clays & Clay Minerals*, 37, 464-468.
- (2) Joswig, W., and Drits, V. A. (1986) *N. Jb. Mineral. Mh.*, 19-22.
- (3) Bish, D., and Von Dreele, R. (1990) 27th Annual CMS Meeting Abstracts, 25.

QUANTITATIVE X-RAY DIFFRACTION ANALYSIS OF SOILS: COMPARISON OF CONVENTIONAL CURVE-FITTING AND RIETVELD FULL-PATTERN METHODS

D. L. Bish and R. C. Jones

Earth & Environmental Sciences, MS D469, Los Alamos National Lab., Los Alamos, NM 87545

Dept. of Agronomy and Soil Science, Univ. of Hawaii, Honolulu, HI 96822

A suite of Hawaiian bauxites taken from the surface to 290-cm depth was examined by X-ray powder diffraction methods to determine variations in total quantitative mineralogy and any systematic changes in the individual minerals. Digital X-ray powder data were obtained with Co K α radiation from 10 to 78° 2 θ using a fixed 1° divergence slit and 0.025°- 2 θ steps. The quantitative mineralogy of the samples was first determined using integrated intensities found by curve fitting in conjunction with XRF chemical data. In addition, the profile refinement results suggested a general trend in diffracting domain size with depth, with domain size decreasing downward in the section.

Subsequently, the data were analyzed by the Rietveld refinement method which fits the complete diffraction pattern with one calculated based on a structural model. The Rietveld quantitative analyses used a modified version of the program DBW 3.2. Although these samples represent complex (up to eight phases) and poorly crystalline mixtures, the refinements converged to consistent values and the resultant fits were excellent. The quantitative results were more consistent with the chemical data than those obtained by conventional curve fitting. Integrated peak intensities for the goethite 110 reflection found by curve fitting correlated very well with the quantitative results from Rietveld refinement ($r^2 = 0.96$). In addition, the Rietveld refinements yielded precise lattice parameters for the major phases; for example, the goethite parameters suggested an Al content between 28 and 35%, and the maghemite parameters showed that the maghemites were 75 to 80% oxidized towards end-member maghemite. However, the refinements with DBW 3.2 clearly showed that the goethite reflections were anisotropically broadened, so further refinements were conducted with the Rietveld program GSAS which can model anisotropically broadened reflections. The results of the GSAS refinements suggested that the goethite reflections had a significant strain-broadening component in addition to a finite crystallite size component. The crystallite size broadening was primarily perpendicular to the (001) plane, whereas the strain broadening was principally in the a - b plane. The GSAS program employs the March function preferred orientation correction which appears to work well with platy materials, but the refinement showed that the major phases in these samples did not exhibit significant preferred orientation, probably because of their fine-grained nature.

Considerable information can be extracted from the diffraction data on these complex and poorly crystalline materials using conventional quantitative analysis methods and profile refinement. However, in addition to quantitative analyses, the Rietveld method can provide precise lattice parameters and information on the nature of peak broadening for the major phases by simultaneously analyzing the complete diffraction pattern.

MID-IR AND NIR DIFFUSE REFLECTANCE OF MONTMORILLONITES AS MARS SURFACE ANALOG MATERIALS: J. L. Bishop, C. M. Pleters and L. M. Coyne.

Brown University, Chemistry Dept., Box H, Providence, RI 02912

The focus of these laboratory spectroscopic studies is to examine a) the relationship between exchangeable Fe^{3+} , Fe^{2+} , Mg^{2+} , Ca^{2+} and Na^+ and both interlayer surface and self H-bonded water, and b) the effect of structural Al^{3+} , Fe^{3+} and Mg^{2+} on the spectral properties of structural OH in clays in relationship to environmental moisture and exchangeable cation. A growing body of evidence shows that none of these variables is independent, and that Fe in particular exhibits anomalous behavior in amounts both below and above the cation exchange capacity (CEC) of montmorillonite. The study of Fe-rich clays is of special interest because Fe is one of the primary components found by Viking in the martian surface regolith. Our objective is to provide a better understanding of the factors influencing the spectral features of clays, which will enable us to develop ground-based truths for remotely interpreting clay and moisture content, and perhaps some aspects of the surface chemistry of martian aeolian material.

Soft-pressed pellets (3 mm path length) of variably cation-exchanged SWy montmorillonite (<125 μm particle size) were prepared and diffuse reflectance was measured using the RELAB spectrometer (0.3 - 3.6 μm) and Nicolet 740 FTIR (1 - 25 μm) at Brown University. RELAB spectra were obtained under ambient atmospheric humidity, in contrast to spectra taken on the Nicolet where the sample chamber was purged with air free of carbon dioxide and water. The energy of those water molecules firmly coordinated to cations through hydrogen bonding was found to vary with exchangeable cation as suggested originally by Russell and Farmer (1964). We measured this vibrational energy at 1632 cm^{-1} for H-SWy, 1629 cm^{-1} for Na-SWy and Fe-SWy, 1626 cm^{-1} for Ca/Fe-SWy and 1625 cm^{-1} for Ca-SWy under low humidity conditions. The NIR combinations at 1.4 and 1.9 μm at low and ambient humidity are consistent with this trend, showing a decrease in vibrational energy from the Na- to the Fe- to the Ca-form of this clay. Our measurements for these features are similar to values reported by Cariati *et al.* (1983) and Sposito *et al.* (1983). It is also interesting to note that although the clays were measured under identical moisture conditions the intensities of these strongly surface H-bonded water features (1.4, 1.9, 6 μm) vary. In fact, a pattern in the intensity of these features under our experimental conditions was repeated: $\text{Na} < \text{Fe} < \text{Ca}$. A number of factors are under consideration which are of importance to the implications of this trend.

Since the Fe composition of the martian surface soil could support an iron/clay ratio several times the exchange capacity, Fe-rich montmorillonites were prepared at Fe-contents exceeding this capacity. An interesting reversal in these highly Fe-loaded montmorillonites was observed in the intensities of the 1.4, 1.9 and 6 μm features of clays examined under constant, low humidity. Initially the band intensities increased with increasing interlayer Fe content, until 200 to 400 % of the CEC was achieved, after which additional Fe actually suppressed the intensity of these features. We have previously reported a significant decrease in the intensity of the 1.9 μm , and perhaps the 1.4 μm , band of 100 % Fe-SWy in comparison to its Ca-, Ca/Fe- and natural Na/Ca- forms. The energy due to the bending vibrations of the firmly cation H-bonded water molecules gradually decreased from 1629 cm^{-1} for the 100 % Fe- to 1627 cm^{-1} for 600 % Fe-SWy clays. A parallel shift towards lower energies for the Fe-rich clays, measured under ambient conditions, as well as under dry air, was exhibited in the NIR combination features at 1.4 and 1.9 μm . This suggests a complex Fe-water relationship in Fe-rich clays which complicates spectral quantification of iron and water in clays when they are both present. Fe-rich montmorillonites may serve as a template for the formation of iron-water complexes and micro-crystallization of hydrous iron minerals.

As the structural OH vibrations in clays are not obscured by atmospheric bands, they are of particular interest relative to remote spectral identification of Mars. To study the effects of structural Al^{3+} , Fe^{3+} and Mg^{2+} on these M-OH spectral features we selected three natural montmorillonites (SWy, STx and SAz) which have varying ratios of Al/Fe/Mg occupying octahedral sites. As measured by Farmer (1974) and Salisbury (1987), three separate M-OH bending vibrations were observed at 920, 880, 850 cm^{-1} corresponding to Al_2OH , AlFeOH and AlMgOH . The intensities of these three features measured at low humidity correlate well with the Al, Fe, and Mg octahedral site compositions determined through XRF analyses. The 2.2 μm combination band shifted in shape and intensity corresponding to the varying compositions of these three montmorillonites as expected.

CLAY MINERALOGY OF A SOIL CLIMOSEQUENCE FORMED IN GRANODIORITE, SIERRA NEVADA.

Janis L. Boettinger and Randy A. Dahlgren

Department of Land, Air & Water Resources, Univ. of California, Davis, CA 95616.

The clay mineralogy of five granodiorite-derived soils was investigated to evaluate the effects of orographic climate on the rates and pathways of mineralogical weathering. Soils were sampled at various elevations along an east-west transect across the central Sierra Nevada. The climate ranges from 17°C and 330 mm precipitation at 200 m elevation, to 4°C and 1011 mm precipitation at 2865 m elevation. Most of the precipitation occurs during the winter months with the high elevation sites receiving the bulk of the precipitation in the form of snow. The clay fractions were separated by centrifugation, mounted as oriented aggregates, and analyzed with XRD. Selective dissolution analysis was used to determine the relative amounts of Fe and Al in crystalline, short-range-order, and organically complexed phases. Soil solutions were equilibrated for 100 h using an automatic vacuum extractor assembly. Solutions were analyzed by ICP, AA, and IC. Soils at lower elevations are dominated by kaolinite and mica. No mica was found in the clay-sized fraction in the mid- to upper-elevations in spite of the high concentrations of mica in the parent material. At the mid-elevation (1389 m), kaolin minerals are dominant: kaolinite content decreases with depth in the soil profile, as halloysite increases with depth. At the higher elevations where soil pH values ranged between 5 to 6, gibbsite and hydroxy-Al interlayered 2:1 minerals become more prevalent and kaolinite decreases. Gibbsite appears as a well-crystalline dominant mineral in the soil at 2194 m. The clay minerals appear least crystalline at the highest elevation. The optimal climate for chemical weathering, as determined by the depth of the soil profile, clay contents, and free iron oxide concentrations, occurs at the mid-elevation site. Weathering rates are inhibited by lack of moisture at the lowest elevation site, and inhibited by cold temperatures and perhaps low effective moisture at the higher elevations. Despite the clay mineral assemblages detected with XRD, nearly all soil horizons possessed equilibrium Si activities falling in the stability field of kaolinite. The gibbsite at the higher elevations is an anomaly considering the low degree of weathering indicated by the very small degree of pedogenic development expressed by various soil properties in the higher elevation soils.

MINERALOGY AND MINERAL EQUILIBRIA OF AN ALFISOL/VERTISOL COMPLEX IN THE AUSTRALIAN TROPICS.

Janis L. Boettinger, Randy A. Dahlgren, and Randy J. Southard

Department of Land, Air & Water Resources, Univ. of California, Davis, CA 95616

The clay mineralogy and mineral equilibria of soils in an Alfisol/Vertisol complex were studied to evaluate the effects of mineralogy on soil formation. Black Vertisols occur adjacent to red Alfisols on an upland pediment in the subhumid and seasonally dry tropics of Queensland, Australia. Field evidence indicates that Alfisols are being transformed to Vertisols. Two Vertisol and two Alfisol pedons were sampled to characterize the soil end-members. A 6-m trench exposing the boundary between the Alfisol and Vertisol was excavated, and profiles were sampled by horizon at 0.5 m intervals along the soil continuum. The clay mineralogy of each sampled horizon or weathered rock layer was determined and compared to mineral equilibria data. Clays were fractionated and analyzed as oriented aggregates with x-ray diffraction. Solutions were equilibrated with each soil/weathered rock sample by adding distilled water to soil columns, and circulating the resultant solution through the columns for a soil/solution residence time of 100 h. Solutions were characterized with ICP, IC, and AA. The dominant clay mineral in the typical Vertisol is smectite, whereas the Alfisols are dominated by kaolinite. Along the continuum from Alfisol to Vertisol, there is a gradual transition in dominant mineralogy from kaolinite to smectite. Along the first part of the continuum, soil solutions were in equilibrium with kaolinite, and the activity of basic cations increased. At approximately 2/3 of the distance along the soil boundary towards the Vertisol, Si activity increased sharply. Silica activity continued to increase until it was within the stability field of smectite at the Vertisol end of the continuum. The solutions equilibrated with Alfisol surface horizons were very high in silica ($10^{-3.14}$ M), but no smectite was evident with XRD. Highly soluble opal phytoliths were found in these horizons. These phytoliths are apparently controlling the Si activities in these horizons, and may play an important role in supplying the Si necessary for kaolinite transformation to smectite.

LOW TEMPERATURE MAGNETISM OF GOETHITE: ALUMINUM SUBSTITUTION
AND SURFACE AREA EFFECTS ON MOSSBAUER SPECTRA

L.H. Bowen¹, E. De Grave², P.M.A. de Bakker²,
and R.E. Vandenberghe²

1. Dept. of Chemistry, North Carolina State University, Raleigh, USA
2. Laboratory of Magnetism, Gent State University, Gent, Belgium

Goethite, α -FeOOH, is often found in soil clays substituted with Al, which has profound effect on its properties. In the present work we used two series of goethites: low surface (LS) with surface areas under $100 \text{ m}^2/\text{g}$, and high surface (HS) with surface areas greater than $140 \text{ m}^2/\text{g}$. For both, the Al content varied up to 30 mole percent. The objective was to use Mössbauer spectroscopy in an external magnetic field to study the effect of Al and surface area on the low temperature magnetic properties.

The Mössbauer spectra were fitted with a bidimensional distribution for both the intrinsic field and the angle between the intrinsic and the applied field. Preliminary results from LS samples (1) showed that Al substitution affected the distribution of spins in an external field. The present experiments were undertaken in order to distinguish between the effects of Al and those due to particle size. All the experiments reported here were obtained at 4K.

With no applied field, both the mean intrinsic field and the field of maximum probability decrease with increasing Al, but the HS goethites have a lower intercept by about 0.5-1.0T. This behavior is also seen in the spectra with 6T applied field. The field of maximum probability varies from 49 to 51T, and for the HS samples with high Al (20-30 %) there is a second maximum in the probability distribution at about 44T. The distribution of angle between external and intrinsic fields exhibits striking variations. The angle of maximum probability for the LS samples increases with increasing Al, corresponding to a non-random orientation of spins. However for the HS samples, surface area has as much of an effect as Al content on this angle. In addition, a bimodal distribution becomes noticeable for the samples with both high Al (19-29%) and high surface ($150\text{-}170 \text{ m}^2/\text{g}$). In this case, there is greater probability for angles both greater and less than 90° . This effect is in distinct contrast to pure goethite (2) where the external field has almost no effect on the orientation of spins. For these high Al, high surface goethites there must be an appreciable number of antiferromagnetic spin pairs which partially line up with the applied field.

1. Bowen L.H., De Grave E., de Bakker P.M.A., and Vandenberghe R.E. (1990) Hyp. Int. 54, 467-472.
2. De Grave E. and Vandenberghe R.E. (1986) Hyp. Int. 28, 643-646.

PROPERTIES AND MECHANISMS OF ORGANO-CLAYS AS SORBENTS FOR POLLUTANT
CHEMICALS: Boyd, S.A.

Dept. of Crop & Soil Sciences, Michigan State University, East Lansing, MI 48824-1325

We have shown that the sorptive capabilities of clays for removing nonionic organic contaminants (NOCs) from water can be greatly improved by replacing naturally occurring inorganic exchange cations (e.g., Na^+ , Ca^{2+}) with quaternary organic cations (QUATS) of the general form $[(\text{CH}_3)_3\text{NR}]^+$. In general, the organo-clays we have studied fall into two groups depending on the size or hydrophobicity of the "tail", or R-group, of the QUAT. The first major class of organo-clays is based on the use of QUATS with relatively large aliphatic R-groups, and these are referred to as organophilic clays. Hexadecyltrimethylammonium (HDTMA)-smectite, where R is a C_{16} hydrocarbon, represents this class of organo-clays. Members of the second class of organo-clays are derived from smaller organic cations such as tetramethylammonium (TMA) or trimethylphenylammonium (TMPA) cations. These clays are functionally and mechanistically distinct from organophilic clays, and are referred to as adsorptive clays.

Organophilic Clays. The mechanistic function of the HDTMA-derived organic phase in these clays can be described as a partition medium for NOCs(1). The dissolution of NOCs into this phase is mechanistically similar to liquid-liquid partitioning, except that here the HDTMA organic partition phase is fixed on the clay surfaces. Consistent with this concept, the sorption isotherms are linear and the $\log K_d$ values for NOC sorption by these clays are similar to the corresponding $\log K_{ow}$ values. One application of this research is the in situ modification of soil clays to increase NOC sorption and retard NOC transport in contaminated soils(2). Thus it is important to establish the sorptive properties of different HDTMA-clays because on-site soil materials would usually contain a variety of clay mineral types. Our results have shown that HDTMA vermiculite, illite and smectites were all highly effective sorbents for NOCs, whereas Mg-smectite was ineffective. Generally, the higher basal spacings and greater HDTMA-contents of high charge clays increased NOC sorption(1).

Adsorptive clays. When comparatively smaller organic cations such as TMA or TMPA, are used to form organo-clays, these cations exist as isolated discrete entities on the smectite layers, and are separated by free (uncovered) planar aluminosilicate mineral surfaces. Sorption isotherms for the uptake of benzene by TMA-smectite are Langmuir type isotherms suggesting a surface adsorptive mechanism(3). TMA-smectite shows excellent affinities for benzene but also displays strong shape selectivity resulting in progressively lower uptake of larger solutes like toluene and ethylbenzene. TMPA-smectite exhibits high affinity for benzene as well as other water soluble alkylbenzenes and naphthalene, which commonly occur as cocontaminants(4). Three other related QUATS, benzyltrimethyl-, benzyltriethyl- and benzyltributyl-ammonium were found to result in less effective sorptive properties than TMPA-smectite.

Recently, we examined the nature of the adsorptive site in TMPA-smectite. This study clearly established that the aromatic hydrocarbons were sorbed from water directly to the siloxane mineral surfaces. The TMPA exchange ions in these clays functioned as compact, non-hydrated pillars that allow the aromatic species to interact directly with mineral surface(5).

These results show that organo-clays are promising fundamental materials for use in a variety of environmental applications including: chemical waste stabilization, as components of clay barriers for hazardous waste reservoirs, as liners for petroleum storage tanks, and in the development of in-situ soil restoration technologies.

1. Jaynes, W.F. and Boyd, S.A. 1991. Soil Sci. Soc. Amer. J. 55:43-48.
2. Lee, J.F., Crum, J., and Boyd, S.A., 1989. Environ. Sci. Technol. 23:1365-1372.
3. Lee, J.F., Mortland, M.M., Chiou, C.T., Kile, D.E. and Boyd, S.A. 1990. Clays and Clay Miner. 38:113-120
4. Jaynes, W.F., and Boyd, S.A. 1990. J. Air Waste Manag. Assoc. 40:1649-1653.
5. Jaynes, W.F., and Boyd, S.A. 1991. Clays and Clay Miner. In press.

POROSITY AND INDEX PROPERTIES ANALYSIS OF FINE-GRAINED MARINE
SEDIMENTS USING TEM

Patti Jo Burkett

Department of Oceanography, College of Geosciences
Texas A&M University, College Station, TX 77843

Fine-grained marine sediments, comprised primarily of smectite and illite, were cored from three sites: the South Atlantic Ocean, Weddell Sea's South Orkney Continental Margin, and the Western Atlantic Barbados Accretionary Complex. After preparation, according to methods of Bennett (1) and Baerwald *et. al.*, (2) ultra-thin samples were examined using transmission electron microscopy. Mosaics, each representing an area of approximately $2500 \mu\text{m}^2$, were constructed to provide a more accurate view of the "big picture". Previous microfabric analyses (3, 4) have demonstrated several advantages of using mosaics instead of individual micrographs. The most obvious advantage of utilizing mosaics is the improved ability to detect spatial features such as trends in orientation of particles, micro-channels for fluid flow and small particle transport, grain size and sorting, and mineral composition. Micrographs were laser-scanned and analyzed using imaging software for the Macintosh. This allowed, for the first time, a micro-scale analysis of *in situ* porosity and void ratio of both total area and components of matrix, individual grains and/or aggregates. Interestingly, a broad variation of values was noted indicating localized variance of properties. Pore characteristics such as geometry, size, permeability, and calculated intra/inter-granular porosity were analyzed revealing a complex three dimensional network of micro-channels characterized by channels surrounding aggregates and cutting through matrix constituents.

- 1) Bennett, R.H. (1977) Clay Fabric and Geotechnical Properties of Selected Submarine Sediment Cores from the Mississippi Delta, NOAA Professional Paper 9.
- 2) Baerwald, R.J., Burkett, P.J., and Bennett, R.H. (1991) Techniques for the Preparation of Submarine Sediments for Electron Microscopy: in *Microstructure of Fine-Grained Sediments From Mud to Shales*, Springer-Verlag.
- 3) Burkett, P.J., et. al. (1987) SANDIA REPORT -SAND86-2492-UC-70.
- 4) Burkett, P.J., Bennett, R.H., and Bryant, W.R. (1991) The Role of the Microstructure of Pacific Red Clays in Radioactive Waste Disposal: in *Microstructure of Fine-Grained Sediments From Mud to Shales*, Springer-Verlag.

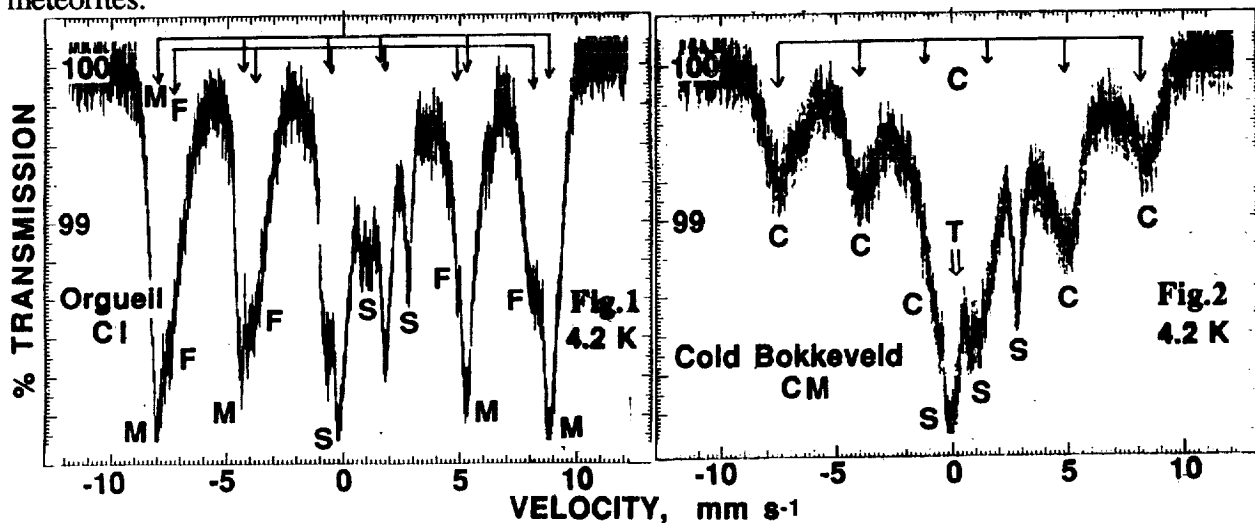
CLAY MINERALS IN CARBONACEOUS CHONDRITES: CHARACTERIZATION BY CRYOGENIC MÖSSBAUER SPECTROSCOPY

Burns, R. G. and Fisher, D. S. [Department of Earth, Atmospheric and Planetary Sciences., Massachusetts Institute of Technology, Cambridge, MA 02139].

Introduction. The presence of ferric-bearing assemblages, including phyllosilicates, oxide hydroxides and magnetite, in matrices of some carbonaceous chondrites, specifically those classified as CI and CM, indicates that these meteorites underwent pre-terrestrial sub-aqueous oxidation reactions. However, the low temperature aqueous alteration that must have occurred on meteorite parent bodies are poorly understood. The intimate intergrowth on a sub-micron scale of several clay silicates (serpentines including cronstedtite; smectites including saponite) and poorly crystalline phases (tochilinite, ferrihydrite) in CI and CM meteorites have made it very difficult to estimate the relative proportions of ferrous and ferric iron and the modal mineralogy of carbonaceous chondrite matrices using conventional electron microbeam analytical techniques. However, Mössbauer spectroscopy, particularly measurements made at very low temperatures, have enabled variations of Fe^{3+}/Fe^{2+} ratios and iron-bearing phases to be determined in suites of several meteorite-types, including CI and CM carbonaceous chondrites.

Procedures. Specimens used in Mössbauer spectral measurements at room temperature, 30 K and 4.2 K included 50-100 mg samples of the CI meteorites Orgueil, Alais, Ivuna and Tonk, and the CM meteorites Murchison, Murray, Cold Bokkeveld and ALH 83100 from Antarctica.

Results. Representative Mössbauer spectra of CI and CM meteorites are illustrated in figure 1 (Orgueil) and figure 2 (Cold Bokkeveld). Magnetite peaks (M) and a Fe^{3+} doublet dominate the 295 K spectra of CI meteorites. At 4.2 K, however, two magnetic sextets originating from magnetite (M) and ferrihydrite (F) appear (fig.1), together with ferrous and ferric doublets indicative of Fe^{2+} - Fe^{3+} smectite (S). Remarkably similar Mössbauer spectral profiles are shown by each the four CI meteorites studied, with only minor variations of ferrihydrite and smectite Fe^{3+}/Fe^{2+} ratios. Greater variations are seen in Mössbauer spectral profiles of CM meteorites. The complex 4.2 K spectra (fig.2) contain broad peaks attributed to cronstedtite (C), the magnetic ordering temperature of which is ≤ 8 K, in addition to tochilinite (T) and serpentine (S) peaks. At 295 K, only Fe^{2+} and Fe^{3+} doublets are present, relative intensities of which differ for each CM meteorite. The relative peak intensities also show temperature variations due to electron delocalization in cronstedtite. Since such electron hopping is quenched at very low temperatures, Fe^{3+}/Fe^{2+} ratios and tochilinite proportions of the CM meteorites were estimated from Mössbauer spectra measured at 30 K. The Fe^{3+}/Fe^{2+} ratios and cronstedtite proportions decrease in the order: Cold Bokkeveld > Murchison > Murray >> ALH 83100, with tochilinite occurring in comparable amounts in each of these CM meteorites.



Figures 1 & 2. Mossbauer spectra of CI and CM carbonaceous chondrites at 4.2 K.

Left:- Orgueil (CI): M = magnetite; F = ferrihydrite; S = Fe^{2+} - Fe^{3+} smectite

Right:- Cold Bokkeveld (CM): C = cronstedtite; T = tochilinite; S = serpentine

THE USE OF ILLITE/SMECTITE AS A THERMAL MATURITY INDICATOR IN THE NORTHERN EROMANGA BASIN, QUEENSLAND, AUSTRALIA

David C. Carmichael¹, Raymond J. Smith¹ and Julian C. Baker²

¹ Department of Resource Industries, 61 Mary Street, Brisbane, Queensland, 4000, Australia

² Electron Microscope Centre, University of Queensland, Queensland, 4072, Australia

The thermal maturity of the Jurassic Birkhead Formation in the northern Eromanga Basin, Queensland has been determined using the percentage of illite interlayers in mudrock illite/smectites together with vitrinite reflectance. X-ray diffraction and high resolution transmission and analytical electron microscopy (HREM) were used to establish illite/smectite compositions. Illite interlayer percentages for 17 wells were plotted against vitrinite reflectance to determine the relationship between the two maturation indices. A least squares linear regression analysis of the data produced the following relationship:

$$Y = 134.2X - 42.2$$

where Y = percent illite layers and X = mean maximum reflectance of telovitrinite; correlation coefficient, $R^2 = 0.76$.

In the study area, kerogen in the Birkhead Formation consists mainly of vitrinite with inertinite and some liptinite. It is generally accepted that peak oil generation from such a maceral assemblage occurs when vitrinite reflectance is in the range 0.70 to 0.90 percent. In the northern Eromanga Basin, these percentages correspond to illite interlayer values of 52 and 79 percent, respectively.

A computer generated contour map of illite interlayer percentages depicts areas in which the Birkhead Formation is within the peak oil generation window.

The composition and structure of illite/smectite from regions of high and low thermal maturity are compared using HREM.

Illite interlayer percentage versus depth profiles are shown for three fully-cored boreholes drilled in the northern Eromanga Basin. The trends shown in these plots are similar to those found in sedimentary basins elsewhere in the world.

CLAY-FLUID INTERACTIONS AND FLOW IN A SINGLE FRACTURE

J.J. Carter*
Dept. Material Science and
Mineral Engineering
UC Berkeley

L.R. Myer
Earth Sciences Division
Lawrence Berkeley Laboratory

G. Sposito
Dept. Soil Science
UC Berkeley

Laboratory experiments were conducted to investigate the relationship between electrolyte concentrations and hydraulic conductivity of a fracture, the walls of which are coated by Na-montmorillonite clay. Model clay-coated rock fracture surfaces were simulated by sedimenting and air-drying a thin (approx. $13\mu\text{m}$ thick) layer of Na-montmorillonite onto two glass plates. Prior to sedimentation a stock suspension of sodium-saturated montmorillonite ($2\mu\text{m}$ size) in a 0.01M NaCl solution was prepared and the glass plates were chemically cleaned to remove organic contaminants. Simulated fracture apertures were created by separating the clay-coated glass plates with mylar shims of 124, 186, and $258\mu\text{m}$ thickness. Hydraulic conductivity measurements were made by measuring fluid flow under hydraulic heads which varied from 15mm to 65mm of water. Effective hydraulic apertures were calculated assuming laminar flow between parallel plates. Flowing fluids constituted NaCl solutions ranging from 0.50M to 0.75M and CaCl_2 solutions of $7.8 \times 10^{-3}\text{M}$ and 0.05M.

Reduction in electrolyte concentration from 0.75M to 0.50M NaCl resulted in large decreases in effective hydraulic aperture which were attributed to volume expansion in the clay layer. For example, at 0.5M NaCl, the apparent volume change was 6 to 7 times the thickness of the sedimented layer. Apparent increases observed in clay volume were supported by gravimetrically determined water contents. Volume expansion was also non-linear with NaCl concentration, increasing more rapidly at 0.5M than at 0.75M. In addition, the increase in clay volume is very much larger than can be predicted by double-layer interactions. The results of this experiment suggest that particle associations other than stacks of parallel plates are present in the swollen clay and are strongly dependent on electrolyte concentration. Volume expansion during flow of $7.8 \times 10^{-3}\text{M}$ CaCl_2 was similar to that for 0.5M NaCl, indicating accordance with the Schulze-Hardy Rule. Ion exchange during flow of 0.05M CaCl_2 resulted in a stabilized clay coating which exhibited only limited swelling when the flowing fluid was switched to deionized water.

Transmission electron microscopy, employing freeze fracture techniques, was used in an attempt to visualize the resulting structure in the clay layers. Differences in structure between samples exposed to 0.5M NaCl and 0.75M NaCl were observed. The images were, however, quite different from those which have been obtained previously on vacuum-dried samples, and further work is required for non-ambiguous interpretation.

* (presently at Levine-Fricke, Inc. Engineers, Hydrogeologists & Applied Scientists, of Emeryville, California)

4174

THE MECHANISMS OF IONIC AND NON-IONIC SURFACTANTS ADSORPTION-ABSTRACTION ON HETEROGENEOUS SURFACES

J. M. CASES and F. VILLIERAS
L. A. 235 "Environnement et Minéralurgie"
ENSG - Institut National Polytechnique de Lorraine
B.P. 40 54500 Vandœuvre Cedex France

ABSTRACT:

The mechanisms of adsorption abstraction of surfactants on heterogeneous surfaces can be described by taking into account :

1) the importance of lateral bonds that favours the formation of aggregates through a cooperative process on surfaces,

2) the intensity of normal adsorbate-adsorbent bond that favours either the formation of two-dimensional aggregates (patches) in the monolayer range and at higher concentration the formation of a bilayer if the interaction with the solid is strong or if the temperature is lower than the Krafft point or the formation of micelles in the case of weak interaction with the solid surface ($T > T_K$),

3) the importance of energetic surface heterogeneity which controls the size of patches,

4) the possible association of ionic surfactants with ions in solution that leads to bulk or surface precipitation (three-dimensional condensation on substrate).

The importance of the selection of a reference phase and the specific methods to determine the nature of the adsorbed-abstracted phase will be discussed.

The use of ionic surfactants, in the case of high normal adsorbate adsorbent bond, as a probe to study surface heterogeneity will be emphasized and the importance of such use to determine the percentage of broken edge faces of phyllosilicates demonstrated.

ORIGINAL PAGE IS
OF POOR QUALITY

CHARACTERIZATION OF INTERLAYER CHARGE AND INTERSTRATIFICATION IN ILLITE/SMECTITE CLAYS FROM K-BENTONITES

Kenan Cetin, Warren D. Huff
Department of Geology, University of Cincinnati, Cincinnati,
Ohio 45221 U.S.A.

Alkylammonium ion exchange and X-ray diffraction (XRD) have been used to study the layer charge characteristics of the expanding component in a suite of fourteen illite/smectite (I/S) clays from K-bentonites, representing random (R0) to long-range ordered (R3) interstratification and ranging in expandability from 70% to less than 5%. The mean layer charge of the expandable component in the samples with more than about 15% expandability was estimated from the systematic increase of basal spacings with increasing alkyl chain length. The mean layer charges, varying between 0.32 and 0.45 equivalents/unit formula, indicate that expandable interlayers even in samples containing significant populations of 20, 30 and 40Å thick illite particles are smectitic. This result supports the layer transformation mechanism for the conversion of smectite to illite in the >15% expandability range.

XRD patterns of alkylammonium treated samples of more illitic composition (less than 15% expandability) show, in addition to a stable illite peak at 10Å, a vermiculite-like component that expands nearly linearly between 24 and 32Å with alkyl chain length. High resolution transmission electron microscope (HRTEM) lattice fringe images obtained from a well-dispersed, R3 ordered I/S clay displaying a 30Å XRD peak when treated with heptadecylammonium ions, confirm the presence of a vermiculite-like component. This component consists of 10Å thick silicate layers regularly alternating with about 20Å thick interlayers, and has an estimated layer charge of 0.7-0.9. HRTEM also shows: (1) subparallel illite particles mostly 30, 40, and 50Å in thickness that are separated by interparticle areas of about 30Å; and (2) individual particles 300-700Å thick and 2000-3000Å long that consist mostly of 20 to 60Å packets, presumably of illite, separated by 15-20Å thick interlayers. A few 10Å thick layers also were present. Some particles appear to have disintegrated along expanded interlayers.

These observations collectively support the notion that fundamental smectite and illite particles of Nadeau and coworkers¹ result from disintegration of primary crystals. The presence of a vermiculite-like component in highly illitic I/S clays indicates the continuation of a transformation mechanism from smectite to illite in the more illitic end of I/S series in K-bentonites. This, however, does not exclude a neoformation mechanism.

1

Nadeau et al. (1985). Mineral. Mag., 49, 393-400.

EXPERIMENTAL INVESTIGATION OF THE LOW TEMPERATURE TRANSFORMATIONS OF CLAY MINERALS IN THE OPALINUS SHALE, SWITZERLAND

J. A. CHERMAK, Mineralogisch-Petrographisches Inst., University of Bern, Switzerland

Shales, due to their high sorption properties, and low permeabilities are being considered as suitable rocks for low and high level radioactive waste repositories. Very little experimental data exists on the effects of the interaction of the waste form and the host shales (such as changes in temperature and solution composition). The presence of concrete barriers could significantly alter the in-situ pH, solution composition, and mineralogy of the shales. Possible mineralogical changes include: quartz and calcite dissolution and precipitation, the alteration of clay minerals, and the formation of zeolite minerals. The formation of clay (especially smectite) and zeolite minerals is quite important when assessing the waste storage potential of shales. To investigate these possibilities experiments were conducted using the Opalinus clay formation (middle Jurassic) in Mont Terri, Northern Switzerland.

Batch experiments were run in small volume teflon bottles (7 ml, perfluoralkoxy) which were loaded with charges and then placed within 50 ml titanium hydrothermal reactor vessels (2 per vessel). These reactors were sealed, and placed onto a rotisserie unit inside an oven set at 175°C for reaction times of up to 17 days. Individual reactors were removed at specific intervals, quenched in cold water, and opened. The solution pH was measured at 25°C using a Ross combination pH electrode, and the solids were separated from the solutions. Each reactor was charged with 0.14 grams of the 80-200 mesh size fraction of Opalinus clay, and 7 ml of solution of varying composition (NaOH, KOH, and NaOH/KOH). The solids were characterized and analyzed by x-ray diffraction and scanning electron microscopy. Mineral composition of the starting shale as determined by x-ray diffraction is: 40% quartz, 20% kaolinite, 15% muscovite/illite, 15% calcite, 5% chlorite, 3% mixed layer smectite/illite, 2% siderite and trace pyrite.

The table below gives quench pH and reaction products versus time data for 0.1m NaOH, 0.1m KOH, and 0.1m NaOH/KOH (0.05m Na and K) solutions. Solid phase transformations as determined by x-ray diffraction in experimental runs after 17 days include the disappearance of kaolinite, and chlorite and the formation of clay and zeolite phases. The precipitation of these clay and zeolite minerals will greatly enhance the sorption capabilities of the Opalinus shale.

Time, Days	quench pH, 25°C	Reaction Products
0.1m NaOH solution		
0.00	12.73	*****
1.00	12.67, 12.70	analcime
3.00	12.13, 12.17	analcime, smectite
10.01	11.37	analcime, smectite, mica/smectite
17.04	11.23, 11.29	analcime, smectite, mica/smectite
0.1m KOH solution		
0.00	12.73	*****
10.01	11.90	kspat, phillipsite
17.04	11.55, 11.56	kspat, mica/smectite
0.1m NaOH/KOH solution		
0.00	12.81	*****
3.00	12.66, 12.66	phillipsite
10.0	11.75, 11.74	phillipsite, mica/smectite

REHYDRATION BEHAVIOR OF A NATURAL ANALCIME

Steve J. Chipera and David L. Bish

Earth & Environmental Sciences Division, Mail Stop D469, Los Alamos National Lab., Los Alamos, NM 87545

The dehydration-rehydration behavior of natural zeolites is important in a variety of applications, and the observed behavior varies considerably from zeolite to zeolite. Whereas some zeolites with large structural exchange-site cavities rehydrate readily, those with small cavities, such as analcime, rehydrate very slowly. In order to understand the effects of water-vapor pressure and temperature on natural zeolites, we have studied the rehydration behavior of a natural analcime from Wikieup, Arizona.

The analcime was first dehydrated in a 300°C oven for 3 days and splits of dehydrated analcime were then placed into teflon vessels with de-ionized water. Three vessels were placed into ovens at 50, 75, and 100°C, and a fourth vessel was left at the prevailing room temperature (~20-30°C). A fifth split was placed in an environmental chamber kept at a temperature of 25-30°C and relative humidity (RH) of ~50%.

To monitor the progress of rehydration, the samples were periodically removed and examined on a Siemens D-500 powder diffractometer, scanning from 2 to 140° 2θ with a 0.02° step size and count times of at least 8 seconds/step using Cu radiation and a solid-state Si(Li) detector. Samples were then placed back into their proper vessels for continued rehydration. The water occupancy for each analcime analysis was determined using Rietveld refinement techniques, although the intensity ratio between the 15.9 and 26.0° analcime diffraction peaks proved to be an accurate empirical indicator of the state of hydration and can be readily calibrated using calculated diffraction patterns.

The analcimes at room temperature rehydrated slowly, with projected trends suggesting that it would take years for them to attain their initial pre-dehydration state (Fig. 1). The analcime in the environmental chamber at 25-30°C and 50% RH reached only 48% of its initial hydrated state after 259 days. The analcime in the room temperature vessel with de-ionized water reached 44% of its initial hydrated state after 42 days and 67% after 200 days. Analcime in the 50°C vessel reached 68% of its rehydrated state after 34 days and 91% after 213 days. The split rehydrating at 100°C reached the initial hydrated state after ~35 days.

The slow rate at which analcime rehydrates is attributed to the small kinetic diameter of the structural tunnels (2.6Å) relative to that of a water molecule (2.65Å)⁽¹⁾. With increasing temperature, the structure expands to facilitate the entry of water molecules as evidenced by the increased rate of hydration.

(1) Breck, D.W. (1974) *Zeolite Molecular Sieves*, John Wiley & Sons, New York.

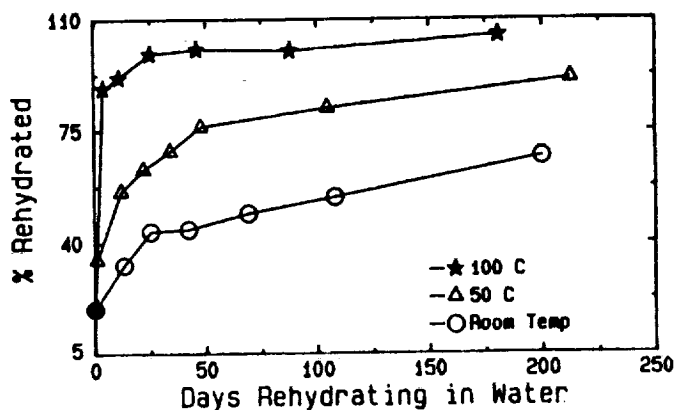


Fig. 1

CHANGES IN U(VI) SPECIATION UPON SORPTION ONTO MONTMORILLONITE FROM AQUEOUS AND ORGANIC SOLUTIONS

C. J. Chisholm Brause, D. E. Morris, P. G. Eller,
T. C. Buscher, and S. E. Conradson

Los Alamos National Laboratory, Los Alamos, NM, USA

Past waste management practices at U.S. Department of Energy complexes have resulted in significant levels of organic solvents, neutral-donor extractants, and actinides in the underlying soil and groundwater. To evaluate the mobility and fate of such "co-contaminant" (actinide/organic) wastes in clay-rich soils and groundwaters, we have conducted spectroscopic experiments on a model system: U(VI) in aqueous or 20% tributyl-phosphate (TBP)/dodecane solutions, and sorbed on montmorillonite (SAz-1 from the Missouri Clay Repository) from these solutions.

Raman, luminescence, and extended x-ray absorption fine structure (EXAFS) spectroscopic data for U(VI) in aqueous solution and sorbed on SAz-1 indicate that the U(VI) sorption complexes are different than U(VI) solution species, and that the nature of the sorption species changes with changes in U(VI) concentration and pH. Luminescence data for aqueous U(VI) sorbed on montmorillonite suggest that a single U(VI) sorption complex is present when formed from solutions with low U(VI) concentrations ($\leq 10^{-4}$ M), but at least two species are present at higher concentrations. Raman spectra for 0.05M U(VI) in solution indicates the presence of three species, consistent with predictions of aqueous U(VI) species based on thermodynamic calculations. In contrast, Raman spectra for U(VI) sorbed on SAz-1 from this solution indicates that there are only two sorption species, and that these sorption species are distinct from those in solution. These differences between the spectra for the aqueous solution and sorption sample suggest that the two sorption species are not simply monomeric and multimeric species analogous to those in solution.

Analysis of EXAFS data for U(VI) sorbed on SAz-1 from aqueous solution show that the average numbers and distances of equatorial oxygens ("O_{eq}") increase with increasing U(VI) concentration, suggesting a change in speciation as also inferred from the luminescence data. Furthermore, at high total U(VI) concentrations (0.05M), two different U-O_{eq} distances are observed, which indicates either two (or more) different species with distinct U-O_{eq} distances or a single sorption complex with variable U-O_{eq} distances. The average U-O_{eq} distance increases slightly at higher pH for 0.05M U(VI) sorbed on SAz-1; the number of O_{eq} atoms is similar at all pH values for these sorption samples. The EXAFS results also indicate that the aqueous sorption complexes studied have fewer equatorial oxygen atoms on average than the U(VI) solution complexes. These conclusions support the Raman results that the aqueous sorption and solution species are different.

FTIR, TGA, XRD, and elemental analysis show that TBP readily intercalates SAz-1, with expansion of the d₀₀₁ spacing to 25.3Å. The weight percent loading of TBP can be as high as 25%. Comparison of the EXAFS results for U(VI) in 20% TBP/dodecane solution and sorbed on clay (from this organic solution) shows changes in the local coordination environment of U(VI) similar to that described above for aqueous systems. Preliminary analysis of the EXAFS data suggests that the number of equatorial oxygen ligands decreases from six in solution (consistent with the complex, UO₂(TBP)₂(NO₃)₂, determined from potentiometric titration studies), to about four in the sorption complex. The average U-O_{eq} distance is shorter for sorbed U(VI), consistent with the decrease in coordination number. The lower coordination number may indicate loss of one or more ligands, and/or ligand exchange with interlayer water.

In summary, there are pronounced changes in speciation of U(VI) upon sorption onto clay from aqueous and organic solutions. Furthermore, there is evidence for different sorption complexes at different total U(VI) concentrations and pH values. The significance of these changes in speciation will be discussed in detail.

CLAY MINERALS AS RECORDS OF THE THERMAL HISTORY OF SEDIMENTARY BASINS

Clauer N.

Centre de Géochimie de la Surface, Strasbourg, France

The diagenetic changes occurring in sedimentary rocks after deposition are mainly induced by pressure and temperature and are known to influence the porosity and permeability of the rocks. The overall evolution of any sedimentary basin can, therefore, be considered in terms of episodic versus continuous processes and physical versus chemical conditions for alterations occurring during burial. These aspects will be discussed from examples on some major sedimentary basins.

The clay material contained in sedimentary rocks represents a widely used index for control of the evolutionary history of the basins. XRD studies, for instance, have been extensively applied to suggest continuous evolution with progressive increase of burial despite the s-shaped trend often found for the illite-smectite mixed-layer evolution relative to depth. The reorganization process of the illite-smectite mixed-layer modifies mainly the stacking of the layers, and seems to be litho-dependent: solid-state transformation in shales and dissolution-recrystallization in sandstones.

Rb-Sr and K-Ar isotope systematics of the clay material are rather in favor of episodic processes often induced by migrations of hot brines. Stable isotope geochemistry of the clay materials provide information of their crystallization temperatures, but the data depend also strongly on the water to rock ratios, and therefore allows evaluation of the differential influence of the hot migrating fluids onto the rocks relative to the major faulting systems in the basins (drains). The same diagenetic/hydrothermal episode is imprinted differently in the sedimentary rocks depending on lithology and location. We also use computed isotope simulation programs together with analytical data to obtain information on the duration of the thermal events.

While combined studies on clay materials and associated authigenic cements from buried sedimentary rocks provide useful information on the paleo-history of sedimentary basins, the chemistry and isotopic analyses of the present-day formation waters give insights to the recent water-rock interactions. We are also currently testing a technique for reconstruction of paleo-fluids which would allow estimations of the mass transfers.

Chemical and isotopic data on carefully separated and characterized clay materials, associated cements and formation waters represent a powerful tool to differentiate overall burial from local and episodic thermal events which might produce concentrations of economically interesting matters in sedimentary basins.

Sr-Nd ISOTOPE CONSTRAINTS ON THE GLAUCONITIZATION PROCESS

Clauer N., Stille P. and Keppens* E.

Centre de Géochimie de la Surface, Strasbourg, France;

*Vrije Universiteit, Brussels, Belgium

Sr and Nd isotopes of present-day glauconitic pellets off shore from the Congo river delta were analyzed following leaching in 1N HCl for about 15 minutes. The residues containing up to 4% K₂O yielded identical $^{87}\text{Sr}/^{86}\text{Sr}$ and $^{143}\text{Nd}/^{144}\text{Nd}$ ratios, which are significantly different from those of sea water but very similar to those of the leached detrital clay fraction in the mud serving as the potential precursor of the glauconies. The $^{87}\text{Sr}/^{86}\text{Sr}$ ratios of the leachates were close to that of sea water, but the $^{143}\text{Nd}/^{144}\text{Nd}$ ratios were significantly lower than that of sea water but higher than that of the detrital clay. Measurements obtained on residues of more evolved glaucony fractions (K₂O: 4-7 wt.%) yielded Sr and Nd isotopic composition values which approximate those of the surrounding sea water. Sm-Nd isotope investigations on residues resulting from a leaching experiment including four successive steps on the same glauconite fraction (H₂O, 0.1 N HAc and twice 1 N HCl) suggest that the glauconies contained three isotopically distinct components. In a Sm-Nd isochron diagram all leachates define a straight line between sea water $^{143}\text{Nd}/^{144}\text{Nd}$ and $^{147}\text{Sm}/^{144}\text{Nd}$ ratios and another endmember with Sr close to sea water and Nd being similar to the detritus. Its $^{147}\text{Sm}/^{144}\text{Nd}$ ratio (>0.15) is much higher than that of the detrital component (0.10). It could correspond to the dissolved river load which Sm and Nd concentrations are 11 to 17 times higher than those of sea water, while the Sr concentration of river water can be about 100 times lower than that of sea water. Thus, glauconies forming in front of the Congo delta may have kept the dissolved REE from the river water adsorbed on the clay particles, while they trapped Sr from sea water. The Sr-Nd isotope data suggest that the glauconitization process involves at least two steps: (1) an early dissolution-crystallization process of the clay material delivered by the rivers in equilibrium with a precursor-dominated (REE from detrital smectite and river loads) chemical environment occurring in a closed chemical system without any seawater influence, and (2) a crystal growth of the authigenic clay material in equilibrium with seawater (open system).

This model underscores the persistence of a genetic link between detrital clay and authigenic glauconies. It requires a chemical system isolated during the first step from the marine environment with elemental compositions highly dependent on the detrital and river load components. It also explains why isotopic dating of glauconies is only possible when the K₂O content exceeds 6%. The reason is not persistence of detrital relicts in the pellets but evolution in a closed system during initial pellitization.

A Comparison of Methods for the Extraction of Smectites from Calcareous Rocks by Acid Dissolution Techniques: R. J. Cook
PRIS, The University, P.O. Box 227, Whiteknights, Reading
RG6 2AB, U.K.

ABSTRACT: Four methods of extracting clays from calcite-rich samples are compared: (i) sodium acetate buffer solution, (ii) lithium acetate buffer solution, (iii) hydrochloric acid, (iv) liquid cation exchange acid. The methods were tested on mixtures consisting of 80% calcite, 10% quartz and 10% hectorite. Potassium had previously been exchanged onto the interlayer sites of the clay.

XRD traces of the extracted clays appeared identical with those of the original clays except for a sharpening of the 001 reflection. The bulk chemistry of the clay was unchanged except by the hydrochloric acid extraction, which appeared to cause a stripping of the octahedral cations. With all of the methods the exchangeable cation content was altered. The sodium acetate method, for example, retained only 17% of the original exchangeable K^+ , the other methods all retaining less than 10%.

FABRIC CHANGES IN CLAYS PERMEATED WITH ORGANIC LIQUIDS

H. S. Cornachione, J. S. Gierke, and S. D. McDowell

Michigan Technological University, Dept. of Geological Engineering,
Geology, and Geophysics, Houghton, Michigan 49931

Saturated, compressed clays exhibit increases in permeability after exposure to concentrated solutions (70 to 100 percent) of both miscible and immiscible organic liquids. This behavior is observed in kaolin and bentonite clays, as well as various naturally occurring soil types. Both polar and non-polar organics liquids have been shown to produce an increase in permeability, often following an initial permeability decrease. Some experimentalists have attributed the increase in permeability to observed cracking of the clays, while others have observed permeability increases without visually-detected changes in the appearance of the substrate. Field studies of leaky clay liners have also been inconclusive regarding the combined impact of the organic contaminant chemical properties and clay mineralogy to the problem. This presentation summarizes the objectives and methodology for quantifying permeability changes in clay soils based on the mineralogy and physical properties of the soil (e.g. confining stresses, porosity, particle size distribution) and the physical properties of the organic contaminants. Better understanding of clay-water-organic interactions will increase predictive capabilities for various engineering applications such as liner design, contaminant transport and soil remediation.

The study consists of three phases: (1) literature search, selection of substrate and organic liquids, and development of techniques to view the fabric of contaminated clays; (2) dynamic permeation studies using flow-through cells in both rigid- and flexible-wall permeameters; and (3) model development of organic permeation and fabric permeability changes. The modeling phase will include vapor transport studies. Results of Phase I will be presented in this session and will have a direct influence on the design of the permeation experiments and the model developments. Data obtained from the initial phase of the study will be shown, including X-ray diffraction data (XRD), scanning electron micrographs (SEM) and photomicrographs from thin-section microscopy. Preliminary XRD patterns using simple vapor adsorption onto thin sections suggests that contamination of the clay minerals proceeds by preferential pathways. This has important implications for both transport and remediation considerations.

Determining the Absolute Age of Late-Stage Thermal Maturation of Anthracite in Eastern Pennsylvania from Radiometric Dating of NH₄-bearing Illite

¹Daniels, Eric J., ²Aronson, James L., and ¹Altaner, Stephen P.

¹Department of Geology, Univ. of Illinois, Urbana, IL 61801

²Department of Geology, Case Western Reserve Univ., Cleveland, OH 44106

NH₄-bearing illite (with 20-80 mol% NH₄⁺ substitution for K⁺), a common mineral in anthracite-rank coal beds and associated organic-rich shale from northeastern Pennsylvania, serves as a geochemical indicator of pore fluids during burial and establishes a direct link between organic maturation and illite formation. The ubiquity of this mineral in these sediments is due to the release of N from organic matter during coalification concurrent with the dissolution (instability) of kaolinite at T>200 °C, which resulted in the general reaction:



Other interlayer cations in NH₄-bearing illite include K⁺, Rb⁺ and Sr²⁺.

Cleat (joints restricted to coal beds) in coal samples with R_{max} (maximum vitrinite reflectance) < 3.0 % contain only authigenic kaolinite (± quartz). Cleat in higher rank coal (3.0% ≤ R_{max} ≤ 6.3%) from this region contain a variety of phyllosilicates, including NH₄-illite, that have replaced precursor kaolinite. R_{max} values of 3.0-6.3% suggest minimum burial temperatures of ~200-275 °C for anthracite formation and kaolinite replacement reactions. Previous studies suggest that anthracite rank was attained during a relatively short thermal event within 15 m.y. after peat deposition because the vitrinite reflectance fabrics of late Pennsylvanian (~280 Ma) organic matter in this region were established largely prior to and, to a lesser extent, during Alleghanian-age (~265 Ma) deformation. Thus, NH₄-illite is a promising candidate for radiometric age-dating of low-grade metamorphism in this region because all interlayer cations were incorporated into the illite structure at T≥200 °C during one relatively short thermal event, and no interlayer cations could have been inherited from precursor kaolinite. This reaction path contrasts with the normal smectite illitization process, in which interlayer K may be inherited or fixed over a broad range of temperatures. Furthermore, NH₄-bearing illite from coal fractures is regarded as a highly reliable sample type for age-dating because of the absence of detrital minerals and the certainty of the precursor mineral, kaolinite, in the fractures. In comparison, the <0.5 μm size fractions of samples from coal matrices and adjacent shale units contain contaminating phases (illite and Na-rich illite) that are of uncertain origin.

Absolute age-dating of NH₄-bearing illite via analyses of K/Ar and Rb/Sr isotopic signatures should yield an absolute age for late-stage coalification in this region because NH₄⁺ in this mineral is directly linked to the coalification process. K/Ar ages of 236 Ma (±12 Ma) and 254 Ma (±13 Ma) were measured for two NH₄-illite samples from the coal fractures, and 265 Ma (±13Ma) was determined for the <0.5 μm size fraction of one shale sample. The radiometric dates determined from NH₄-illites from coal cleat are close to, but somewhat younger than, the predicted age of coalification. The age derived from the shale sample may be older than those of the fracture samples because of the presence of detrital illite and/or early-stage authigenic illite. The theoretical closure temperature for retention of Ar in (K-rich) illite layers has previously been estimated to be ~150-180 °C. Thus, the younger dates may be due to Ar leakage from illite interlayers during the time of peak metamorphism, and may represent the time at which the rocks cooled below 150-180 °C. We are currently obtaining Rb/Sr age determinations to test whether the K/Ar dates accurately represent the time of peak metamorphism or if they represent a younger age due to Ar diffusional loss at high temperatures.

CHLORITE GEOTHERMOMETRY: PRINCIPLES AND APPLICATIONS

Patrice de Caritat¹, Ian Hutcheon¹, John L. Walshe²

¹*Department of Geology & Geophysics, Univ. of Calgary, Calgary, Alberta T2N 1N4, Canada*

²*Department of Geology, Australian National University, Canberra, ACT 2601, Australia*

Chlorites forming in the subsurface record information about their precipitation conditions, such as temperature, bulk rock composition, and fluid composition. Among these, the temperature is of particular interest, and both empirical and theoretical attempts to relate temperature of formation to chlorite composition have been made in the past, and are reviewed here. Failure to predict reasonable temperatures from chlorite composition for some areas of known thermal history, using either empirical or theoretical geothermometers, may be caused by: 1) interlayering of chlorite with other clay minerals, introducing a bias in the electron probe analysis; and 2) the effect of bulk rock composition on chlorite composition, which prevents the generalization of established theoretical or empirical geothermometer models to rocks of different composition to those from which these models were calibrated (e.g., Salton Sea). Additional factors which influence chlorite composition and are an obstacle to the development of an accurate chlorite geothermometer model include: poor thermodynamic data, particularly for Fe-chlorites, and poorly constrained activity-composition models; identifying the octahedral sites in which substitutions (Al, Fe, Mg) take place (i.e., in the "brucite"- or "talc"-layer); and the little known $\text{Fe}^{2+}/\text{Fe}^{3+}$ ratios in natural chlorites, which reflect their oxidation state, and which must regulate to some extent the octahedral substitutions that are possible.

Problems with interlayering and bulk rock composition can be reduced, or perhaps even eliminated, by respectively: 1) using chlorite composition data acquired with analytical TEM rather than electron probe, thus permitting any interlayering with non-chloritic clays to be noticed; and 2) better understanding the relationship between bulk rock composition and chlorite composition. Here, we present some suggestions as to how to deal with the bulk rock composition-chlorite composition problem. Additionally, a detailed survey of chlorite composition and geothermometry from a sedimentary basin, the Denison Trough in Australia, is presented and compared with chlorite compositions from other basins (North Sea, Venture Field).

EVALUATION OF FERROUS AND FERRIC MÖSSBAUER FRACTIONS FOR VARIOUS NATURAL AND SYNTHETIC COMPOUNDS.

E. De Grave* and A. Van Alboom

Laboratory of Magnetism, University of Gent, B-9000 Gent, Belgium.

The quantitative analysis of mixtures of iron-containing compounds and the determination of the $\text{Fe}^{2+}/\text{Fe}^{3+}$ ratio in a given compound, are important environmental applications of ^{57}Fe -Mössbauer spectroscopy. Both mentioned data are evaluated from the relative areas of the corresponding spectral components, assuming in most cases equal recoilless fractions f for the involved iron nuclei. In this contribution, the authors present their evaluation of f fractions for a large number of various oxides and oxyhydroxides, silicates (incl. a clay mineral) and carbonates, showing that f for Fe^{2+} is generally lower than for Fe^{3+} in structurally related substances.

The f values were obtained from the temperature variation of the center shift δ , i.e. $\delta(T) = \delta_1 + \delta_{\text{SOD}}(T)$, with δ_1 the intrinsic isomer shift, commonly considered not depending on T , and δ_{SOD} the second-order Doppler shift which originates from the non-zero mean square velocity of the emitting and absorbing nuclei. Using the Debye approximation for the lattice-vibrational spectrum, a relatively simple expression for $\delta(T)$ is obtained (1). It contains the parameter Θ_M , the so-called *characteristic Mössbauer temperature*, which can be evaluated by adjusting the theoretical expression to the experimental $\delta(T)$ curve. Once Θ_M is known, its value can be used to calculate f at any given temperature (1).

It was found that all f values at room temperature (RT) are in the range 0.8 - 0.9 for Fe^{3+} and 0.6 - 0.75 for Fe^{2+} . Typical results are 0.84 for Fe^{3+} in hematite and 0.70 for Fe^{2+} in hedenbergite. This significant difference would mean that errors of up to 20% could occur if the quantitative analysis assumes equal recoilless fractions. The deviation is less important at low temperatures: at 80K, f is calculated to be 0.92 and 0.88 for hematite and hedenbergite respectively.

Using standard mixtures of hematite with selected ferric or ferrous compounds, relative Mössbauer fractions were derived from the areas of the corresponding subspectra and compared to the results obtained indirectly from $\delta(T)$. It was found that the latter method yields an underestimation of the ferrous-to-ferric f ratio, reducing possible errors to 10%. It is concluded that this underestimation is due to the temperature dependence of δ_1 , the slope being different for Fe^{2+} and Fe^{3+} .

Reference

1. Frauenfelder H (1963) *The Mössbauer Effect*. W.A. Benjamin Inc., New York, pp 1-336.

* Senior Research Associate, National Fund for Scientific Research, Belgium.

CLAY SCIENCE IN SOIL ENVIRONMENTS: RECENT FINDINGS

J. B. Dixon

Department of Soil and Crop Sciences, Texas A&M University,
College Station, 77843-2474.

Soil systems are largely composed of crystals and the diversity of soils environments yields many minerals both pedogenic and inherited. Some of them are formed under acid and others under alkaline conditions. Both oxidation and reduction influence the variety of minerals formed in soils. The occurrence of low concentrations of minerals in soils has led to the adoption of methods of determining crystal phases based on selective physical and chemical methods (e.g. high resolution transmission electron microscopy (HRTEM) and differential x-ray diffraction (DXRD)).

The question of pedogenic origin of minerals often has been addressed. Recent investigations have shown the growth of euhedral kaolinite crystals in an acid sulfate soil and in recrystallized kaolins of Georgia. These findings reveal clay mineral formation at greater depths than in traditional soil profiles.

It has been established that the substitution of Al for Fe in the structures of Fe oxides contributes to their occurrence in the clay-size fraction (<2 microns). More recently the cyclical reduction and oxidation of Vertic soils in rice-paddy environments have been shown by HRTEM and DXRD to form lepidocrocite and ferrihydrite with short-range-order in a few weeks. Thus indicating that transient Fe oxides are involved in the chemical and physical behavior of wetland soils. Evidence for bacterial origin of some of these short-range-order Fe oxides adds further to the complexity of the system.

Manganese oxides are seldom abundant in soils but their selective ion retention and vast range of occurrences makes them important to understanding and utilizing soils. Three Mn oxides are of interest in soil and rock-weathering systems: todorokite, birnessite, and lithiophorite. Todorokite and lithiophorite form well developed crystals in certain environments suggesting that they may approach equilibrium there. Yet birnessite generally does not develop crystals that have distinctive morphology or are large enough to give strong x-ray diffraction patterns. Limited data support the hypothesis that birnessite is formed by fungi in soils and the crystals are thin and crumpled. The occurrence of todorokite in rock-weathering and young soil environments, of birnessite in soils of intermediate weathering states, and lithiophorite in mature soils (e.g. Ultisols and Oxisols) makes them useful indicator minerals.

The analytical demands of complex soil systems have led to the development of many innovative methods and principles that are useful in the wider fields of clay science and technology. The great variety of soil environments offer continuing opportunity to explore new manifestations of clay mineralogy and the solutions to existing and potential problems.

**DISTRIBUTION OF CLAYS IN SANDSTONES, AS STUDIED
BY SCANNING ELECTRON MICROSCOPE IMAGE ANALYSIS**

C. DURAND

Dept. de Physique et Analyses, Institut Francais Du Petrole,
BP 311 G2506 Rueil-Malmaison, France

Quantitative evaluation of the amount of clays in sandstones is, although tedious, feasible (1). But, even in small amounts, clays may be of great influence on the transport of fluids, depending of their distribution in the porosity. Numerous studies have already shown localisation of clays as coating, bridging or filling the pores. Quantitative evaluation of the distribution can be of interest in the description of sandstones with some clay content.

Combining backscattered electron microscope images and chemical local analyses allows identification of clays. Use of image analysis, granulometry of pores as well as covariograms, allows a quantitative description of the clay distribution, and of its influence on porosity. Several images are analyzed for each sample, in order to evaluate representativity.

Several sandstones, model ones as well as oil reservoirs, are studied.

(1) C. Durand, J.L. Renaud, R. Szymanski, (1991), Rev. IFP, vol. 46, n° 3, p. 295.

CLAY PARTICLE SIZES FROM ATOMIC FORCE MICROSCOPY

D. D. Eberl¹ and Alex Blum²¹U.S. Geological Survey, Mail Stop 404, Federal Center, Denver, CO 80225²U.S. Geological Survey, Mail Stop 420, 345 Middlefield Rd., Menlo Park, CA 94025

The atomic force microscope (AFM) can be used to measure the sizes and shapes of fundamental clay particles, and of stacks of fundamental clay particles (MacEwan crystallites). This method is easier, faster, and more accurate than previous methods that employ the transmission electron microscope (TEM) and Pt-shadowing. Fundamental clay particles of known thicknesses can be used to calibrate the AFM in the vertical direction. For example, measurements of fundamental illite particles (sample RM30) and elementary smectite particles (Na-saturated Wyoming bentonite) have shown that the manufacturer's calibration of the piezoelectric crystal, calibrated by using an interferometer in the range 450 to 900 nm, overestimates vertical distances in the range of many clay particle thicknesses (1 to 20 nm). Using a revised calibration, single, elementary flakes of Na-smectite give thicknesses of about 12.5 Å when imaged on a muscovite substrate, thereby indicating that the particles are composed of a single 2:1 layer plus a single water layer. The water layer probably is located between the 2:1 layer and the mica substrate. Any water absorbed on top of the 2:1 layers appears to be too weakly bonded to be imaged during AFM analysis, and therefore does not contribute to the measured particle thicknesses. The thickness of stacks of elementary Na-smectite layers are multiples of the thickness of a single smectite layer ($n \times 12.5 \text{ \AA}$, $\pm 1 \text{ \AA}$). Measurements of the sizes of fundamental clay particles in the horizontal plane (ab plane) are identical for the AFM and the TEM techniques.

The AFM appears to be an excellent tool for measuring directly clay particle sizes and clay particle size distributions, for swelling or non-swelling clay, under a variety of environmental conditions. The instrument may be particularly useful for monitoring changes in clay particle thicknesses during illitization.

USE OF ILLITE PARTICLE THICKNESS, RATHER THAN EXPANDABILITY, AS A MEASURE OF DIAGENETIC GRADE

D. D. Eberl¹ and Jan Srodon²

¹U.S. Geological Survey, Mail Stop 404, Federal Center, Denver, CO 80225, U.S.A.

²Institute of Geological Sciences, Polish Academy of Science, 31-002 Krakow, Senacka 3, Poland

The reaction of smectite to illite in burial diagenetic and in hydrothermal systems most often is studied by measuring the expandability (i.e. percentage smectite layers) of mixed-layer illite/smectite (I/S). Expandability decreases as the reaction proceeds through randomly interstratified and then regularly interstratified I/S. Although expandability is a sensitive indicator of diagenetic grade, it can not be used for detailed thermodynamic, kinetic, and mass balance interpretations because it is subject to a severe artifact known as the "short stack effect." Standard XRD techniques for measuring expandability almost always overestimate the percentage of illite layers in a sample, because the tops and bottoms of MacEwan crystallites (i.e. stacks of fundamental illite particles that diffract coherently) are not counted as swelling layers. Illite particle thickness is a better measurement for following these reactions. Particle thickness distributions can be measured directly by high resolution transmission electron microscopy (HRTEM) and by atomic force microscopy (AFM), or less directly by use of Pt-shadowed samples and the transmission electron microscope (TEM), or by use of the Warren-Averbach X-ray peak broadening analysis technique. The present paper attempts to recast expandability measurements and chemical analyses found in the literature into illite particle thickness measurements to see how this change affects geologic interpretations of illite diagenesis. Two methods are used to recast literature data. The first method makes use of the equation: $\log \text{thickness (in nm)} = 1.385 - 0.689(\log \text{ expandability})$. This equation comes from an empirical comparison between XRD and TEM measurements for a set of I/S samples, and may not be valid for all I/S. A second method is based on the observation that illite layers have a constant fixed potassium content of 0.9 equivalents per $\text{O}_{10}(\text{OH})_2$. For this method the following equation can be used if the I/S has been chemically analyzed: $\text{thickness (in nm)} = 1/(1-(\text{fixed K}/0.9))$.

The Origin of the Clay Minerals at the Cretaceous/Tertiary (K/T) boundary
in Denmark:

W. Crawford Elliott, and James L. Aronson

Department of Geological Sciences
Case Western Reserve University
Cleveland, Ohio 44106

We present evidence showing that the clay minerals themselves at the K/T boundary at Denmark are not derived from meteorite impact. A magnesian (5.0 wt% MgO) smectite is the predominant clay mineral in the K/T marls at Stevns Klint (informally known as the Fish Clay) and at Nye Kløv. Illite is also found in trace amounts within these K/T boundary marls. This Mg-smectite is also the predominant clay mineral in a Tertiary marl approximately 8 meters above the K/T boundary, and this Tertiary marl does not contain anomalous concentrations of Ir. Thus, this Mg-smectite is not unique to the K/T boundary, and therefore we suggest that this Mg-smectite is not derived from meteorite impact. Moreover, pyroclastic plagioclase is found within the red-colored pyritic layer in the Fish Clay, and we suggest that basaltic volcanism might be a common progenitor for both the plagioclase as well as the Mg-smectite. The clay minerals are either epiclastic (i.e. derived from volcanism predating the K/T boundary) or detrital. Illite is clearly detrital based on the K/Ar ages of the coarse clay fractions.

We do not reject the impact hypothesis. Our results however indicate the clay minerals themselves are not derived from impact. The K/T boundary marls are thus viewed as the accumulation of sediment having detrital, impact-derived (i.e. shocked quartz), and volcanic sources.

CHARACTERIZATION OF LOW TEMPERATURE SILICA POLYMORPHS IN CALCIUM BENTONITES, SODIUM BENTONITES AND FULLER'S EARTHS BY XRD, SEM/EDS, AND TEM: J.M. Elzea*, E.K. Sprague*, and I.E. Odom*

*McCrone Associates, Inc., 850 Pasquinelli Drive, Westmont, IL 60559, *American Colloid Company, 1500 West Shure Drive, Arlington Heights, IL 60004

Two low temperature silica polymorphs have been identified in 10 Na and Ca bentonite deposits and Fuller's Earths ranging in age from Jurassic to Miocene. These polymorphs may be differentiated based on crystallographic, chemical, and morphological observations made by XRD, SEM/EDS, and TEM. One polymorph is characterized by: 1) a sharp, intense (101) reflection centered near 4.04 Å, 2) relatively large crystallites that tend to occur in small masses along the edges of clay flakes, 3) trace amounts of Al and Fe in addition to Si. The second polymorph is distinguished based on: 1) a broader, less intense (101) reflection centered near 4.07 to 4.10 Å, 2) much smaller crystallites that form large agglomerates or lepispheres between clay flakes, 3) the absence of elements other than Si. These minerals correspond to opal-C and opal-CT respectively as described by Jones and Segnit (1). Both polymorphs exhibit a shift in d-spacing, an increase in intensity, and a sharpening of the (101) peak when heated to 1050°C for 24 hours.

A comparison of two Cretaceous deposits, one a sodium bentonite and the other a calcium bentonite, indicates that the type of parent material from which the deposit altered may have the greatest influence on secondary silica mineralogy. Volcanic glass appears to dissolve and reprecipitate as opal-C. Biogenically precipitated opal-A appears to preferentially recrystallize as opal-CT. These silica polymorphs exhibit different X-ray diffraction patterns depending on degree of order. Younger deposits tend to contain opaline silica that is very poorly ordered. Degree of ordering tends to increase with age and is reflected by an increase in peak sharpness, number of peaks present, and peak intensity. TEM observations suggest that the crystallites increase in size with age.

The more ordered opal-C may be misidentified as true α -cristobalite. The simple heating test described above will quickly reveal whether or not the mineral in question is crystalline (quartz, tridymite, cristobalite) or one of the hydrous polymorphs (opaline silica) that commonly occur in clay deposits. It is important to make this distinction because crystalline silica is classified as a probable human carcinogen.

- (1) Jones, J.B. and E.R. Segnit, 1971, J. Geol. Soc. Aust., 18(1), pp. 57-68.2

CLAY MINERAL STABLE ISOTOPES: MAGNUS SANDSTONE, NORTH SEA.

A.E. FALLICK, C.I. MACAULAY AND R.S. HASZELDINE

Isotope Geology Unit, SURRC,

Department of Geology and Applied Geology, Glasgow University

The Magnus oilfield, located 116km north-east of the Shetland Islands in the North Sea, is comprised of Upper Jurassic subarkosic sandstones deposited as a prograding submarine fan. During the Cretaceous there was tectonic uplift, tilting and erosion with meteoric water penetrating the reservoir. Subsequently, a seal was formed by a one kilometer or so thickness of Upper Cretaceous muds and marls. There was rapid subsidence until the late Tertiary, and the reservoir is now at its maximum burial depth. We have studied the diagenetic history of Magnus in three wells separated by a total distance of 3km laterally. The first well (211/12-1) is taken to be representative of the crestal region of the structure; the second (211/12a-M1), representing the flank, is similar in many respects to the first, and these two contrast in some ways with the third well (211/12a-9) characterising conditions downdip. The maximum difference in depth of the Magnus sandstone amongst the three wells studied is 400m; for a thermal regime controlled by conduction this corresponds to a temperature difference of 14 to 18°C. The grain size of the sandstones is very similar in the three wells and they have comparable paragenetic sequences. The deep, downdip well is more shale-rich, has more abundant diagenetic illite and kaolinite and intersects the oil-water contact. From a stable isotope study of five sequential diagenetic minerals in the sandstone, Macaulay et al (1991) have concluded that the pore fluid regime was isotopically distinct in the deep and crestal parts of the reservoir, with a stronger meteoric water influence updip persisting from early diagenesis through to hydrocarbon emplacement around 55Ma. Here, we consider the systematics and implications of oxygen and hydrogen isotope data on late diagenetic kaolinite and illite. Whereas in the crestal and flank wells the kaolinite is predominantly vermiform in character, the kaolinite found downdip is of blocky morphology. There is a consistent and systematic difference in $\delta^{18}\text{O}$ and δD in that average values in 211/12a-9 (downdip) are enriched in ^{18}O (by 3 to 4‰) and D (by 20 to 30‰) compared to the other two wells. Taking the data from all three wells together, there are statistically significant correlations between $\delta^{18}\text{O}$ and δD for both illite and kaolinite:

ILLITE: $\delta\text{D} = 5.9\delta^{18}\text{O} - 159$ ($n=11$; $r=0.78$ which is significant above 99%)KAOLINITE: $\delta\text{D} = 6.1\delta^{18}\text{O} - 169$ ($n=12$; $r=0.66$ which is significant above 95%)

Pooling all 23 data gives a correlation significant above the 99.9% level. No clay mineral isotopic composition approaches closely the equilibrium lines for illite or kaolinite with sea-water. Based on considerations of the burial history curve for Magnus sandstone, together with geochemistry and the constraints afforded by stable isotopic analyses of other diagenetic phases (quartz overgrowths, magnesian siderites, and ankerites), we estimate mean formation temperatures of approximately 80°C for kaolinite and 100°C for illite. If clay minerals have linearly correlated stable isotope ratios ($\delta\text{D} = A\delta^{18}\text{O} + B$) and a constant temperature of precipitation is assumed, the locus of formation waters in $\delta^{18}\text{O}$ - δD space can be calculated (assuming no post-precipitation isotopic exchange):

$$\delta\text{D}_w = A \alpha_D^{18} \delta^{18}\text{O}_w + 10^3 \left(\alpha_D^{18} \frac{A}{\alpha_D} + \frac{1-A-10^{-3}B}{\alpha_D} - 1 \right)$$

where α^{18} and α^{D} are, respectively, the oxygen and hydrogen isotope fractionation factors between the appropriate clay mineral and water, at the precipitation temperature. Using α values recommended by Savin and Lee (1988) and the suggested Magnus temperatures leads to:

ILLITE: $\delta\text{D}_w = 6.1\delta^{18}\text{O}_w - 57$ KAOLINITE: $\delta\text{D}_w = 6.3\delta^{18}\text{O}_w - 45$

Within error, these are identical and so we propose that Magnus sandstone basinal fluids during late diagenesis can be represented by $\delta\text{D}_w = 6.2\delta^{18}\text{O}_w - 50$. We note that this line intersects the present day meteoric water line at a value which is not characteristic of any water likely to have had access to the sandstone. The measured isotopic compositions of the clay minerals correspond to extreme water compositions of (-4‰, -76‰) at the crest and (+4‰ - 24‰) downdip. Given a best estimate of Cretaceous meteoric water of (-7‰, -46‰) and of Jurassic seawater of (-1‰, -10‰), it is clear that an assumption of approximate temperature constancy for each clay mineral requires a porefluid isotopic evolution which resulted in an increase in $\delta^{18}\text{O}$ but a decrease in δD .

CHARACTERISATION OF JORDANIAN AND AUSTRALIAN PLYGORSKITES

Basim S.M. Faraj¹, Hani N. Khoury² and Ian D.R. Mackinnon¹

¹Electron Microscope Centre, The University of Queensland, St. Lucia, QLD 4072
Australia

²Dept. of Geology and Mineralogy, University of Jordan, Amman, Jordan

Palygorskite is a rare aluminum-magnesium hydrosilicate containing pyroxene like chains in a 2:1 inverted ribbon¹. Economic deposits of palygorskite are known in the Georgia/Florida region in the USA, in the Palygorsk Range in the Ural mountains in the USSR, Senegal, Spain and South Africa².

Palygorskite was discovered for the first time in Azraq basin, during an investigation of the clay minerals in Azraq basin. Samples from the shallow intervals (5-30m) of four exploration oil wells in the area were studied by a range of techniques including SEM, XRD, bulk chemical analysis and organic matter characterisation³. All samples indicated the presence of palygorskite in an area of approximately 35 square km. Palygorskite occurs in the Samra Formation (Pleistocene) as interwoven fibrous mats and pore-bridging cements in dolomitic marls. The fibres are sub-micron in diameter and many tens of microns long. A similar texture was observed in samples from two Australian deposits at Lake Nerramyne, Western Australia and at Garford Formation in the Southern Coober Pedy area, South Australia. Both the Jordanian and Australian palygorskites were precipitated from solutions via evaporation of shallow alkaline lakes in a semi-arid climate^{2,4}.

Semi-quantitative elemental analyses show that these palygorskites are composed of the following elements Si, Al, Mg, Fe, O, K, similar to the Attapulgit PF1-1 Source Clay. X-ray diffraction and scanning electron microscopy (SEM) show that palygorskite is the dominant clay mineral. In addition, non-clay minerals such as dolomite, gypsum and halite are also present and are more dominant in the Azraq and Garford samples than in the Lake Nerramyne samples. The Lake Nerramyne deposits are superior in terms of quality and quantity, with proven reserves of 4 million tonnes and possible reserves of 100 million tonnes². The Attapulgit Source Clay, PF1-1, shows similar chemistry and purity of sample to the Lake Nerramyne deposit. Palygorskite is a valuable commercial mineral which has numerous uses in industrial applications including molecular sieves, in paints, absorbents, drilling muds, pharmaceuticals and for the purification of water^{2,5}.

References:

1. Brindly, C.H. and Brown, G. (eds), (1984), **Mineralogical Society Monograph No. 5**, 495 pp.
2. Rakich, P. B. (1990) **Proceedings of the 9th Industrial Minerals International Conference**, Sydney, p.165-169.
3. Faraj, B.S. (1988), **Natural Resources Authority Internal Report No. BG-007**, Amman, Jordan, 13 pp.
4. Khoury, N.H. (1980), **Dirasat**, vol. no. 7, p. 21-31, Amman, Jordan.
5. Callen, R.A. and Singer, A. (eds), (1978), **Elsevier Sci. Co.** 352 pp.

FINE-GRAINED CLAYS IN SOUTHERN HEMISPHERE COALS: THE NATURE OF MICRINITE

Basim S.M. Faraj¹, Ian D.R. Mackinnon¹ and Miryam Glikson²¹Electron Microscope Centre, The University of Queensland, St. Lucia, QLD 4072
Australia²Department of Geology and Mineralogy, The University of Queensland, St. Lucia, QLD
4072 Australia

Micrinite is a rare, but important component of bituminous coal sequences in both Hemispheres and has been principally defined on the basis of reflected light microscopy observations of polished sections. The operating definition used by most organic petrologists is a finely particulate, submicron size "maceral" component with reflectance comparable to fusinite and semi-fusinite¹. Micrinite also exhibits a granular to porous texture and occurs in association with important macerals such as desmocollinite and sporinite¹. Micrinite has been observed in coals from the Callide and Greta coal seams in Eastern Australia, as well as in seams in Antarctica and New Zealand. In all Australian coals, micrinite occurrences are primarily in seams which have been deposited in a comparatively aerobic environment in sedimentary basins formed on stable cratonic basement rocks². In contrast, Northern Hemisphere coals rarely show micrinite in coal seams rich in vitrinite and exinite³.

Interest in the hydrocarbon capacity of coal seams has prompted a detailed study of key maceral phases in order to better define their provenance. In this work, a range of complementary petrographic techniques including SEM, AEM and conventional optical microscopy have been rigorously applied to precisely defined areas of coal samples from the Callide Basin. The fine-grained size ($< 1\mu\text{m}$) and uncommon abundance of micrinite (e.g. ~1% in Callide samples) inhibits ready characterisation by techniques other than electron microscopy. Nevertheless, there is still ambiguity from electron microscopy studies, due primarily to the lack of supporting elemental analyses on individual coal components^{4,5}.

SEM/EDS analyses of fine-grained, porous regions previously defined optically as micrinite showed a high abundance of Al, Si and O. Elemental mapping of micrinite in vitrinite showed that Al, Si and O were concentrated solely in the micrinite regions and that C-rich material occurred in the vitrinite areas. Micrinite was examined as microtomed thin sections using a Jeol 4000FX with attached windowless Si(Li) EDS. Selected area electron diffraction of these samples showed a characteristic 0.73nm layer silicate basal spacing and typical lath-like morphology. Thin-film EDS analyses showed the presence of Al, Si and O in all cases. Thus, precise elemental, morphological and structural data provide unambiguous evidence for the presence of kaolinite in the coal component known as micrinite. It appears that micrinite in Southern Hemisphere coals consists predominantly of fine-grained kaolinite (>90% of the component) and, as such, should not be considered a maceral.

References:

1. E. Stach *et al.*, *Stachs' Textbook of Coal Petrology*, Gebruder Borntraeger, Berlin, 1975; 2. M. Shibaoka, *Fuel*, 57, 73-77, 1983; 3. M. Teichmuller, *Geol. Mitt.*, 12, 219-254, 1973; 4. G.H. Taylor and S.Y. Liu, *Intl. Jour. Coal Geology*, 14, 29-46, 1989; 5. M. Glikson and C. Fielding, *Intl. Jour. Coal Geology*, 17, in press, 1991.

In situ Investigation of EDB Sorption/Desorption Processes on Clay Mineral Surfaces
by Diffuse Reflectance Infrared Spectroscopy

Walter J. Farmer, Yukiko Aochi
University of California, Riverside
Brij L. Sawhney
The Connecticut Agricultural Experiment Station

The occurrence of organic contaminants as environmental pollutants is often associated with the unexpected long-term persistence of the compound. An example of this is the reported (1) detection of 1, 2-dibromoethane (EDB) in Connecticut soils up to 19 years after the last known application, although the chemical and physical properties of this soil fumigant would predict a much lower persistence. Recent investigations of EDB sorption and desorption from the vapor phase onto clay mineral surfaces led to the conclusion that both processes were comprised of rapid and slow components (2). In the present investigation, a controlled environment diffuse reflectance accessory was used to follow the same processes at the molecular level. Infrared spectra were collected periodically as EDB vapor and/or N₂ gas flowed through samples held within the accessory. The spectral results indicated the presence of EDB in two conformations, anti and gauche, within a liquid phase associated with the clay mineral surface. The abundance of the gauche conformer was consistently higher during both the sorption and desorption phases of the experiment indicating preferential retention of the gauche conformer. The relative retention of the two conformers was also influenced by the type of clay being used. The preferential retention of one conformer relative to another is consistent with the observed macroscopic results and could help explain the unexpectedly high retention of EDB by soils. Molecular isomerism is a common phenomena and may be an important factor in predicting the environmental behavior of some organic chemicals.

1. Steinberg, S.M., Pignatello, J.J. and Sawhney, B.L. Environ. Sci. Technol. 1987, 21, 1201-1208.
2. Sawhney, B.L. and Gent, M.P.N. Clays Clay Min. 1990, 38, 14-20.

CHROMIUM(III) INDUCED SOLID PHASE TRANSFORMATION OF δ -MnO₂

Fendorf S.E.* and Sparks D.L.

Dept. of Plant & Soil Science, Univ. of Delaware, Newark DE 19717-1303

In order to evaluate the hazard of heavy metals it is necessary to determine their reaction pathways in surficial environments. Chromium is a heavy metal which is stable in two oxidation states under surface environmental conditions, Cr(III) and Cr(VI). The trivalent form is benign and rather immobile in soil and water systems due to its low solubility in all but acidic conditions, in addition to its high affinity for solid surfaces. In contrast, Cr(VI) is more toxic and very mobile in the environment as it readily forms anionic species. Therefore, to assess the hazard of Cr in a system one must determine the speciation of Cr and any reaction pathways which will allow for transformations between oxidation states (redox reactions).

Manganese oxides appeared to be the oxidant of Cr(III) present in the soils (1), and are the only naturally occurring substances which are capable of oxidizing Cr(III) under commonly occurring environmental conditions (2). Various phases of Mn-oxides have the capacity to oxidize Cr(III) (2-4). Amacher and Baker (4) used a commonly occurring form of Mn-oxide, δ -MnO₂, to investigate the oxidation of Cr(III). Chromium(III) was readily oxidized by the δ -MnO₂, but the oxidation rate decreased with increased pH--contradicting thermodynamically expected trends. It was hypothesized that Mn(II) liberated in the redox reaction was re-adsorbing on the surface and inhibiting Cr(III) sorption and subsequent oxidation by the oxide. However, Mn(II) was shown not to inhibit the oxidation of Cr(III) (5); Fendorf and Zasoski (3) hypothesized that the decrease in extent and rate of Cr(III) oxidation by δ -MnO₂ with increasing solution pH values and Cr(III) concentrations was due to the formation of a surface precipitate of Cr(OH)₃. The Cr-hydroxide precipitate thus induced a barrier to the electron transfer between Cr(III) and δ -MnO₂, and was itself thermodynamically redox stable. The resulting electrophoretic mobilities of the conglomerated colloid were representative of the Cr-hydroxide as opposed to the δ -MnO₂.

The hypothesized formation of a surface precipitate has been based on macroscopic data; therefore, the inhibition mechanism of Cr(III) oxidation remains in question. Here, we have used high resolution transmission electron microscopy (HRTEM) to investigate the possible formation of a surface precipitate at higher solution pH values and Cr(III) concentrations. High-resolution TEM images show that the unreacted MnO₂ was partially crystalline (6). Interspersed with amorphous material, there are layers of parallel atomic planes exhibiting severe bends and twists which in some cases form distinctive needle-shaped protrusions characteristic of synthetic birnessites. Conventional selected area electron diffraction yields patterns show well defined but rather broad rings having prominent 2.4 Å and 1.4 Å spacings, and a spacing of roughly 7.3 Å can also be discerned. After reacting with Cr(III), HRTEM images of the δ -MnO₂ show a marked change in the crystal structure. Electron diffraction confirms this, producing patterns containing sharp, well defined rings throughout. A dramatic change in the crystal structure is apparent after the oxidation/reduction reaction of Cr(III) and MnO₂. The solid surface post-reaction is not redox reactive and thus Cr(III) oxidation is terminated upon its formation. The results of these findings have important implications for environmental quality. The highly redox reactive δ -MnO₂ is transformed into a redox stable crystalline solid; thus, the potential for Cr(III) oxidation to the more hazardous Cr(VI) species is eliminated. Currently work is underway to determine the identity of this newly formed solid phase resulting from the Cr(III)/MnO₂ reaction.

References

- (1) Bartlett, R.J., and B. James. 1979. *J. Environ. Qual.* 8:31-35.
- (2) Eary, L.E., and D. Rai. 1987. *Environ. Sci. Technol.* 21:547-552.
- (3) Fendorf, S.E., and R.J. Zasoski, 1991. *Environ. Sci. Technol.* *In Press*.
- (4) Amacher, M.C., and D.E. Baker. 1982. DE-AS08-77DPO4515. Inst. for Res. on Land and Water Res., Penn State Univ, PA.
- (5) Fendorf, S.E., R.J. Zasoski, and R.G. Burau. 1991. Submitted to: *Environ. Sci. Technol.*
- (6) Fendorf, M., Fendorf, S.E., Sparks, D.L., and Gronsky, R. 1991. *Proceedings of the 49th Annual Meeting of the Electron Microscopy Society of America*, (ed. Bailey, G.W.) *In Press* (San Francisco Press, Inc., San Francisco, 1991).

AMMONIUM FIXATION DURING CLAY MINERAL DIAGENESIS AND HYDROCARBON MATURATION: R. E. Ferrell, Dept. of Geol. & Geophys., Louisiana State University, Baton Rouge, LA and L. B. Williams, Dept. of Geol., Arizona State University, Tempe, AZ.

Fixed-NH₄ in deeply buried organic-rich sediments is potentially useful in increasing our understanding of hydrocarbon maturity and migration pathways. In these normally reducing environments, N is predominantly in the form of the ammonium ion (NH₄⁺), which substitutes for K⁺ in aluminosilicates. NH₄⁺ integral to a silicate structure is called "fixed-NH₄" and it is protected from environmental fluctuations that might affect dissolved, organic, and exchangeable forms of N. Once fixed, NH₄⁺ becomes an indicator of the chemical environment existing when the mineral formed. Our initial investigations have demonstrated that fixed-NH₄ anomalies are associated with hydrocarbon occurrences and can be used to indicate levels of hydrocarbon maturation and to trace paths of hydrocarbon migration. N-speciation and the identity of the host mineral are important to consider in all interpretations. Topics reviewed and the general findings include:

1.) **Results of Laboratory Experiments.** Three CMS reference clays were each reacted in a 0.05M NH₄Cl aqueous solution at 25, 60, and 80°C at pH 4 or 8 under reducing conditions for 128 days. The greatest NH₄-fixation occurred in mixed-layered I/S (Standard ISMT-1) at pH=4. The quantity of NH₄⁺ fixed is directly proportional to temperature, but equilibrium was not attained in any case. Charge heterogeneity associated with I/S mixed-layered clays and the conversion of smectite to illite are important in controlling the quantities of fixed-NH₄.

2. **Surface vs Subsurface Fixed-NH₄.** Fixed-NH₄ concentrations in shallow cores near a Holocene oil seep in the Green Canyon area were compared to two producing reservoirs at ≈4 km depth in Fordoche Field, Pointe Coupee Parish, Louisiana. The concentrations within mudstones are twice as high at depth and intervals of the sandstone from which oil is extracted contain anomalously high fixed-NH₄ concentrations.

3. **Fixed-NH₄ in Oil, Gas and Dry Wells.** Two cores were examined from the Wilcox Group in Fordoche Field; one from a well producing crude oil, and one from an abandoned gas well at the edge of the field. Core samples from a dry hole in Hurricane Creek Field were also studied. Concentrations of fixed-NH₄ from organic-rich mudstones show a general increase with depth, coincident with increasing organic maturity. Reservoir sandstones containing crude oils show a two-fold increase over background, while fixed-NH₄ concentrations in the gaseous portion of the reservoir are three times background. High values in non-productive intervals suggest migration occurred.

4. **Ammonium substitution relative to illite authigenesis.** Samples from the contact aureole of the basaltic Walsen dike which intrudes the Cretaceous organic-rich Pierre Shale were studied to learn more about the fixation process. Fixed-NH₄ concentrations increase (to ≈1100 mg/kg clay) with the quantity of authigenic illite formed during the smectite->illite transformation, but the maximum NH₄-fixation per unit of illite formed occurs within the "oil window" where thermal breakdown of organic matter is rapid.

5. **Fixed-NH₄ in a high temperature gradient: Salton Sea, California.** Fixed-NH₄ was analyzed in samples from the US DOE Salton Sea Scientific Drilling Project, where the geothermal gradient is steep. Fixed-NH₄ concentrations in this core decrease with depth, but samples below 1200m are metamorphosed (T>300°C) and fixed-NH₄ concentrations approach the minimum detection limit. Ammonia (NH₃) is the dominant form of N at high temperatures and low pH, and it does not interact with silicates.

6. **Fixed-NH₄ in a high-N gas reservoir: Sorrento Field, Colorado.** Analyses revealed no fixed-NH₄ anomalies; samples contained fixed-NH₄ concentrations approximately equal to background levels of fixed-NH₄ observed in the Wilcox cores. Only background levels of fixed-NH₄ are expected where N₂ gas predominates.

7. **Fixed-NH₄ in a high organic-N source area: Monterey Fm.** Very high fixed-NH₄ (up to 1.3% of the illite) was found in organic-rich, quartz-grade siliceous rocks of the Miocene Monterey Formation from the Santa Maria and San Joaquin basins, California. Fixed-NH₄ was found to correlate with the amount of diagenetic illite layers in the I/S. Mineralization of NH₄⁺ is apparently promoted by the coincident release of abundant NH₄⁺ associated with oil generation and the illitization of smectite.

CLAY MINERALS AS INDICATORS OF PALEOCEANOGRAPHY,
PALEOCLIMATE AND DIAGENESIS IN THE UPPER CRETACEOUS GREENHORN
CYCLOTHEM OF THE MANCOS SHALE

¹Finkelstein, David B., ²Leckie, R. Mark, and ²Richard F. Yuretich

¹Department of Geology, Univ. of Illinois, Urbana, IL 61801

²Department of Geology and Geography, Univ. of Mass., Amherst, MA 01003

The distribution of clay minerals in the Greenhorn Cyclothem of the Cretaceous Mancos Shale across the western side of the Western Interior Seaway reflects paleoceanographic, paleoclimatic, and, to a lesser degree, diagenetic controls. Stratigraphic sections were studied at Lohali Point (LP) in the Black Mesa Basin, Arizona, Mesa Verde (MV), Colorado, and Rock Canyon (RC), Colorado, which represent shallow to progressively deeper water conditions, respectively. Observed clay minerals include kaolinite, illite, mixed-layer illite/smectite (I/S), and minor chlorite.

The relative amount of kaolinite shows similar changes within each of the sections which is interpreted to reflect primary depositional variations. In the basal transgressive units of all three sections studied, the kaolinite abundance progressively decreases up section. During the upper regressive interval, kaolinite progressively increases up section at LP and MV. There is a pulse of kaolinite associated with peak transgression of the Greenhorn Sea, and it is thought to be a paleoclimate signal and not a shoreline indicator because of the distance to shoreline during peak transgression of the Sea.

There are also major differences in clay mineralogy among the three studied sections, which is interpreted to reflect differences in source area, associated paleoclimate, and degree of diagenesis. The clay mineralogy is relatively uniform at LP and RC, consisting mainly of highly expandable I/S that is randomly interstratified, indicating that both sections were neither buried very deeply nor subjected to high geothermal gradients. At MV, kaolinite and illite are the dominant clays and I/S shows major changes through the section. I/S varies from 40% illite with random interstratifications, at the top of the section, to 85% illite with long-range order at the bottom. MV is further distinguished by the presence of chlorite, which shows no systematic variation throughout the section. The large change in I/S mineralogy over a small stratigraphic interval suggests that the section was subjected to a high geothermal gradient.

The presence of larger amounts of illite and chlorite at MV, suggests that the source for the clays in the section could be from a more northern source area. The expanding Greenhorn Sea may have modified regional climate patterns with approach of peak transgression. The increase of kaolinite during peak transgression at both LP and MV possibly indicates that a northern push of warm southern waters produced a wetter climate, which increased the rate of chemical weathering.

Authigenic illite in silicic tuffs of Pleistocene Lake Tecopa, California--

A cautionary note for clay-mineral geothermometry

Neil S. Fishman, Christine E. Turner, and Richard A. Sheppard

U.S. Geological Survey, Box 25046, MS 939, Denver, CO 80225

Authigenic illitic mixed-layer illite/smectite (I/S) occurs in three distinct altered tuff beds in Pleistocene Lake Tecopa, an ancient alkaline, saline lake complex in eastern California. Within each tuff a concentric zonation of diagenetic mineral zones forms a crude bulls-eye pattern, from fresh glass along the margins of Lake Tecopa, to zeolites (chiefly phillipsite and clinoptilolite) farther basinward, to potassium feldspar in the center of the lake. The illitic clays (0-30% expandable layers) occur in tuffs in both the potassium feldspar and zeolite zones. Smectitic I/S (70-100% expandable layers) occurs in the fresh glass zone, where it is the only authigenic aluminosilicate present, and also in some zeolitized tuffs, but it is rare in tuffs that contain potassium feldspar.

Preliminary SEM observations indicate that the illitic clays are fibrous, postdate the authigenic zeolites, and appear to have precipitated directly from solution. Compositionally, the illitic clays are iron-bearing, as indicated by SEM-EDS analyses, weak 5 Å peak intensities, and the position of d(060) reflections (1.5090-1.5095 Å).

The illitic-bearing tuffs in Lake Tecopa have never been buried to depths in excess of about 50-75 m, suggesting that elevated temperatures due to burial did not play a role in the formation of these clays. Instead, the distribution of the illitic clays in the tuffs and their association with authigenic zeolites and feldspar argue strongly for pore-water chemistry as the main control on illite formation. Because pore waters at near-surface temperatures can control formation of authigenic illite, caution should be exercised before using illitic phases in clay geothermometry.

Electrochemical Methods for the Study of Clay Hydration:
Fitch A., Dept. of Chemistry, Loyola University of Chicago,
6525 N. Sheridan Road, Chicago, IL 60626

A single film wall-jet clay-modified electrode can be used to study reversible clay interlayer dimensions in the long range swelling regime. Transport of the electroactive anions $\text{Fe}(\text{CN})_6^{3-}$ or IrCl_6^{2-} is dependent upon the total porosity of the film (1-3) which correlates well with X-ray diffraction data of Norrish (4) suggesting that the diffusion limited current observed at an underlying Pt electrode is thus related to the interlayer spacing. The clay-modified electrode exhibits rapid swelling on exposure to progressively more dilute electrolytes. No comparable shrinking of the film is observed on exposure to concentrated NaCl. However, a pulse of N_2 can be used in situ to reproducibly dry the electrode. The technique is robust, allowing for repetitive cycling (swell in electrolyte, shrink with N_2 stream) between electrolytes for an extended period of time. A first application of the technique is to follow the shrink/swell dynamics corresponding to the exchange of K^+ for Na^+ in SWy-1 montmorillonite.

- (1) Fitch, Alanah and Fausto, C. L. Fausto (1988) *J. Electroanal. Chem.*, 257, 299.
- (2) Lee, S. A. and Fitch, Alanah (1990) *J. Phys. Chem.*, 94, 4998.
- (3) Wieglos, Todd and Fitch, Alanah (1990) *Electroanalysis*, 2, 449-454.
- (4) Norrish, K. (1954) *Trans. Farad. Soc.*, 18, 120-134.

SOLID-STATE MULTINUCLEAR NMR STUDIES OF REACTIONS AT THE SILICA-ALUMINA INTERFACE IN CLAY MINERALS. John J. Fitzgerald and Abdullatef I. Hamza, South Dakota State University, Brookings, SD 57007; and Steven F. Dec, Charles E. Bronnimann and Gary E. Maciel, Department of Chemistry, Colorado State University, Fort Collins, CO 80523.

Reactions of clay minerals in the solid-state and at the solid/solution interface are important to numerous chemical processes used to produce specialized chemicals, clay-based materials and ceramics. Multinuclear solid-state NMR studies of several reactions of the clay minerals kaolinite, pyrophyllite and montmorillonite are described. The dehydration and dehydroxylation of these minerals up to 750°C has been examined. Related studies of solid-state reactions leading to silica-alumina phase separation and the formation of various high-temperature phases up to 1350°C have also been examined. In addition, the dealumination of these native and various calcined clay-derived materials produced by the solid/solution "interfacial" reaction with HCl(aq) are described.

¹H CRAMPS (Combined Rotation and Multiple Pulse Spectroscopy) NMR techniques have been particularly useful to examine the proton populations during the dehydroxylation of kaolinite and pyrophyllite, to elucidate the structure of the dealuminated kaolinite solids and to describe the mechanism of its dealumination in acidic aqueous media. In addition, CP/MAS and FT/MAS ²⁹Si NMR studies have been used to describe the structural nature of the aluminum and silicon sites in these solids as a function of degree of dealumination.

The simultaneous use of MAS ²⁹Si NMR and high-speed MAS ²⁷Al have also provided unique insights into the dehydroxylation process and the high-temperature thermal transformations of these three clay minerals in the temperature range 750°C-1350°C. The structural nature of both the aluminum and silicon sites in the various intermediate dehydroxylated clay-derived materials is described. In addition, plausible mechanisms of phase separation and subsequent solid-state reactions at the silica-alumina interface in these minerals is discussed.

These investigations suggest fruitful areas for future investigations of the solid-state dehydroxylation and high-temperature reactions at the silica-alumina interface, as well as related solid/solution dealumination processes for other clay minerals.

GEOCHEMICAL COMPUTER MODELLING OF CLAY-PORE WATER INTERACTION AS A TOOL FOR GEOTHERMOMETRY

Fritz B. Madé B. and Duplay J.

Centre de Géochimie de la Surface (CNRS), STRASBOURG, France.

The chemical interaction between clay minerals and aqueous solutions is a major problem for geochemists who try to model the evolution of sedimentary rocks under diagenetic and/or hydrothermal conditions. The corresponding interactions are strongly influenced by (P,T) conditions like for any other type of mineral phase, but with a higher level of complexity when considering clay minerals. These phases behave like solid solutions: their chemical composition tends to adapt to the evolution of the chemistry of the aqueous solution along a given process producing clay minerals as secondary particles or transforming preexisting clay particles.

For that reason the introduction of clay minerals with variable composition has been done progressively in our geochemical codes and still remains a challenge if not a controversy.

Any evolution of the chemical characteristics of clays in a given water rock system is of course induced by activity potentials (thermodynamic conditions). For that reason, the first approach of clay minerals through computer codes followed what had been done previously for simple minerals, by applying the Mass Action Law to the equilibrium condition between an aqueous solution producing a given clay as a "defined compound". In that approach the representativity of the model with respect to natural condition is extremely simplified and poor. As an example, in diagenetic conditions one would consider a mean composition for one smectitic phase (detrital) and a mean composition for the illite one (secondary). This binary model shows in diagenetic conditions that smectite will transform into illite along a positive thermal gradient: this will not produce a real geothermometer but only predict this general tendency.

The solid solution approach adds a degree of complexity between the two end-members S (smectite) and I (illite). If one still considers equilibrium conditions while using a binary smectite-illite solid solution model, the thermal dependence of the solubility products of the two end-members becomes a kind of geothermometer: for a given chemical composition of the reacting system (solutions + rock) the composition of the S-I complex phase depends on the temperature of reaction.

The generalized solid solution approach introduces a large number of possible end-members resulting from the combination of several substitutions of cations in each of the three types of possible sites in the clay layers (tetrahedral, octahedral and interlayer sites). This approach helps to describe the relation between chemical compositions of solutions and clay particles in the population of clay micro-particles contained in each clay macro-sample. For a given aqueous chemistry the trend in chemical composition within a population of particles, stable with respect to that type of solution, is an indirect function of temperature.

Finally, the introduction of kinetics in the geochemical code still needs a lot of additional theoretical developments concerning the nucleation phenomenon in particular, but opens a large field of application for understanding why a clay sample is a population of particles with domain of composition depending strongly on the temperature of formation.

EFFECT OF STRUCTURAL IRON REDUCTION ON THE RHEOLOGICAL CHARACTERISTICS OF NA-NONTRONITE: Huamin Gan and Joseph W. Stucki, University of Illinois, Urbana, IL 61801

A rotational viscometer was used to investigate the rheological behavior of suspensions of Na-nontronite as affected by different concentrations of clay, electrolyte, and structural Fe(II). The effects of different particle sizes were also studied. Results were interpreted in light of a theoretical equation ($\theta = kN^2E_a/2$) which relates the extrapolated shear stress, θ , to the number of particles, N , per unit volume and the interparticle bond energy, E_a . Reduction of structural Fe yielded a greater value of θ than observed in oxidized clay suspensions, indicating that interparticle attractive forces are much greater in reduced than in oxidized clays. Results also revealed that the value of θ for oxidized Na-nontronite increased with increasing electrolyte concentration until 0.01 M , at which point flocculation occurred. This behavior is opposite to that of Upton montmorillonite, and may be attributed to the origin of layer charge. For clay suspensions with the limited particle-size range of 0.5 to 2 μm , θ was greater than for the entire $< 2 \mu m$ size fraction.

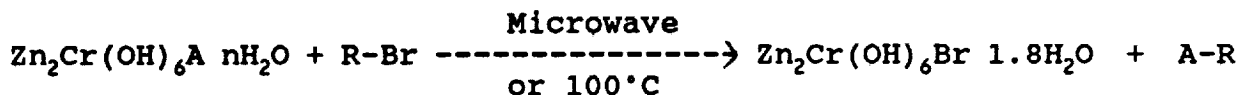
ALKYLATION REACTIONS USING LAYERED DOUBLE HYDROXIDES AS SUPPORTED ANIONIC REAGENTS.

García-Ponce, A.L.; Casal, B. and Ruiz-Hitzky, E.
Instituto de Ciencia de Materiales, C.S.I.C.; C/ Serrano, 115 bis, 28006 Madrid, Spain.

Layered double hydroxides (LDH) are an important group of host materials with anionic-exchange properties ("anionic clays"). They are layered brucite-like compounds of general formula $[M_x^{II}M_y^{III}(\text{OH})_{2x+2y}]A_{y/n} z\text{H}_2\text{O}$ with positive charge, due to the substitution of octahedral divalent cations by trivalent cations. This layered charge is compensated by hydrated anions located in the interlayer space. The combinations of M^{II} , M^{III} cations, and A^n anions, provide a wide range of different hydrotalcite-like compounds.

Different properties of this kind of compounds have been studied in relation to their applications as: ionic conductors, pillared materials, catalysts, or supported anionic reagents. In this last case, LDHs act at the same time as support materials and as sources of activated anions. It is generally known that inorganic solid supports have a positive influence in anionic activation processes. Therefore it is possible to get higher reaction yields and better selectivity than when the reactions are carried out in homogeneous media.

In this work, we present the results of anionic alkylation reactions of two organic halide compounds. $\text{Zn}_2\text{Cr}(\text{OH})_6A \cdot n\text{H}_2\text{O}$ was the LDH used, with acetate (Ac^-) and benzoate (Bz^-) as interlayered anions (A), and 1-bromooctane ($\text{C}_8\text{H}_{17}\text{-Br}$) and benzyl bromide ($\text{C}_6\text{H}_5\text{CH}_2\text{-Br}$) as reaction substrates. The model of reaction was as follow:



Different conditions were investigated. In some cases when the reaction was activated by microwave irradiation (2450 MHz), the rate was between 20 and 30 times faster than by conventional heating (100°C). When the reactions were carried out for too long, the decomposition of A-R ester became significant. This phenomenon is more substantial for the n-octyl acetate, yielding important amounts of n-octanol, specially in the case of microwave activation (45%). In the synthesis of benzyl esters, appeared benzyl alcohol, and, to a lesser extend, two other secondary compounds. They can be related to the oxidation of this aromatic alcohol although the role of the solid in this last reaction is no clear.

The Influence of Particle Size on the Chemistry of Mica Clays

Gassman, P.L.* and L.W. Zelazny²

Geosciences Department, Battelle Pacific Northwest Laboratory, Richland, WA 99352

²Dept. of Crop and Soil Environmental Sciences, Virginia Polytechnic Institute
Blacksburg, VA 24061

To assess the effect of particle size on composition and charge characteristics of 2:1 micas, mechanically produced clay separates of muscovite and biotite were analyzed for total chemical composition by electron probe microanalysis (EPMA) and dissolution analysis (ICP & flame AA). Thermogravimetric analysis (TGA) was used to determine coordinated water contents of the clays. Infinitely thick, salt-free clay isolates of each particle size (0.2-2.0 μm , 0.08-0.2 μm , <0.08 μm) were analyzed as bulk samples, with eighteen elements determined by EPMA. Salt free clay separates were also used in HF/aqua regia dissolution analysis by ICP/AA. Mechanical comminution of 2:1 micas significantly reduced interlayer cation content and increased levels of coordinated water as particle size decreased. Interlayer cation site occupancy was lowered in both muscovite and biotite, with reductions of about 42% of site occupancy from coarse (0.2-2.0 μm) to fine (<0.08 μm) clay size. Excellent agreement of elemental compositions was obtained by the two methods, although calculated water contents by EPMA were lower than by thermogravimetry, and slightly higher elemental abundances were consistently obtained by EPMA. With the exception of the interlayer cation loss, there is no evidence of alteration of the natural stoichiometry of the clay separates across particle sizes. There were no significant perturbations of occupancies of tetrahedral and octahedral sites. However, loss of interlayer cation requires compensatory charge reduction via coordination of external ions at clay surfaces or structural transformations. The identity and location of compensatory charge were not determined in this study but elemental analysis may suggest that the additional coordinated water may exist as the hydronium ion.

* corresponding author

INTRACRYSTALLINE FRACTIONATION OF OXYGEN ISOTOPES BETWEEN HYDROXYL AND NON-HYDROXYL SITES IN KAOLINITE: THERMAL DEHYDROXYLATION AND PARTIAL FLUORINATION APPROACHES.

Jean-Pierre Girard, Samuel M. Savin and Xiahong Feng.

Department of Geological Sciences, Case Western Reserve University, Cleveland, Ohio 44106.

Thermal dehydroxylation and partial fluorination techniques were used to measure the intracrystalline fractionation of oxygen isotopes between hydroxyl and non-hydroxyl sites in kaolinite. Similar experiments were performed on gibbsite and brucite. Although both techniques need further refinement and testing the results suggest that the thermal dehydroxylation technique may be suitable for analysis of OH groups in fine grained (< 1 μm) kaolinite. Partial fluorination appears less suitable.

Several aliquots of a fine-grained kaolinite from Macon, GA, were dehydroxylated *in vacuo* by heating with a resistance furnace. Various combinations of heating procedures (single-step, two-step and multi-step), heating rates (between about 1°C/min to 200°C/min), and ultimate temperatures (between 500 and 1000°C) were investigated. Measured $\delta^{18}\text{O}$ values of both the liberated water and the dehydroxylated residue are very consistent, within 1 permil or less, over a wide range of target temperatures and heating rates when dehydroxylation is performed in a single step fashion. Similar single-step dehydroxylation experiments were performed on gibbsite, brucite and a series of six relatively coarse-grained kaolinites. The results indicate that, 1) gibbsite dehydroxylation occurs with a substantial isotopic fractionation, probably due to its complex, multi-reaction dehydroxylation pathway, 2) dehydroxylation of brucite, which follows a single-reaction pathway very similar to kaolinite, occurs without significant fractionation and, 3) some kaolinites do and others do not yield consistent $\delta^{18}\text{O}$ values over the range of temperature and heating rates. The results of these experiments suggest that either no significant fractionation or a constant fractionation of the OH oxygen occurs during single-step thermal dehydroxylation of fine-grained kaolinite. Oxygen exchange during diffusion of water through large particles may be responsible for all or part of the inconsistencies observed during dehydroxylation of coarse grained kaolinites. Two-step and multi-step dehydroxylation procedures appear to be accompanied by significant fractionation and/or isotopic exchange between different oxygen sites or between the liberated water and the dehydroxylated residue.

Partial fluorination of fine-grained kaolinite in the presence of excess fluorine at low temperatures yields (< 185°C) highly inconsistent $\delta^{18}\text{O}$ values. When performed at high temperatures (220-240°C) in the presence of insufficient fluorine $\delta^{18}\text{O}$ values are systematically lower than the bulk $\delta^{18}\text{O}$ value and increase nearly linearly with the percent stoichiometric yield. Interpretation of the results in terms of internal fractionation measurements is premature at this time. Further partial fluorination experiments on kaolinite, gibbsite and brucite are underway.

THE IMPORTANCE OF LATE CIMMERIAN METEORIC RECHARGE TO RESERVOIR QUALITY, ROTLIEGENDES SANDSTONE, NETHERLANDS

J. Reed Glasmann

Unocal Science and Technology, 376 S. Valencia Ave., Brea, CA 92621

Diagenesis of the Permian Rotliegendes Sandstone in the vicinity of the Broad Fourteens basin, offshore Netherlands, was strongly influenced by late Jurassic - early Cretaceous paleogeography related to late Cimmerian tectonic events. Late Cimmerian erosion along the flanks of the Broad Fourteens basin resulted in aggressive meteoric recharge of shallow Rotliegend reservoirs and was associated with precipitation of kaolinite and dissolution of carbonate cements and feldspar. The oxygen isotopic composition of kaolinite in the Rotliegend in the vicinity of eroded paleohighs (avg. $\delta^{18}\text{O} = 18.3$ permill, $n=30$) is consistent with low temperature precipitation from meteoric pore water ($\delta^{18}\text{O} = -7$ to -8 permill, SMOW). Diagenetic illite, which occurs in subordinate amounts in kaolinitic sandstones, has a similar isotopic composition to kaolinite ($\delta^{18}\text{O}$ illite = 18 to 19 permill) and yields K-Ar ages that indicate illite precipitation during shallow burial. Basinward from eroded paleohighs, the diagenetic modification of Rotliegend reservoirs changes significantly, primarily due to the absence of kaolinite and presence of abundant illite. Illite K-Ar ages have no relationship to the time of maximum pre-Laramide burial of the Broad Fourteens basin, but generally indicate cementation in response to rapid late Cimmerian subsidence (ca 150 - 130 Ma). The oxygen isotopic composition of illite from the Broad Fourteens basin shows a strong relationship to depth of burial at the time of diagenesis, ranging from about 12.5 permill in the deepest reservoirs to about 17 permill in reservoirs flanking structural highs. Results of basin thermal history modeling suggest that illite in the Broad Fourteens basin precipitated from a pore water of fairly uniform isotopic composition ($\delta^{18}\text{O} = +3.5$ to $+4.5$ permill, SMOW) over a wide range of temperature (80 - 180°C). Good reservoir quality in the Rotliegendes Sandstone is dependent upon meteoric flushing and can be roughly predicted from late Cimmerian paleogeographic reconstructions.

Ionic Strength Effects on Boron Adsorption by Oxides, Clay Minerals, and Soils: Goldberg S., Forster H. S., and Heick E. L.
USDA-ARS, U.S. Salinity Laboratory, 4500 Glenwood Drive, Riverside, CA 92501

Boron adsorption on the iron oxide, goethite, the aluminum oxide, gibbsite, the clay minerals, kaolinite and montmorillonite, and two arid zone soils was investigated as a function of solution pH (3-11) and ionic strength of the background electrolyte (0.01-1.0 M NaCl). Boron adsorption on the oxides and kaolinite increased from pH 3 to 7.5, exhibited a peak at pH 7.5 to 8.5, and decreased from pH 8.5 to 11. For boron adsorption on montmorillonite and the soils, the adsorption maximum was located near pH 9. Ionic strength dependence of the adsorption maximum increased in the order: goethite < kaolinite < gibbsite < kaolinitic soil < montmorillonite \cong montmorillonitic soil. Boron adsorption decreased with increasing ionic strength below the zero point of charge (ZPC) and increased with increasing ionic strength above the ZPC. The use of ionic strength effect studies to distinguish adsorption mechanisms will be evaluated. The ability of a surface complexation model to describe boron adsorption data will be presented.

N 9 2 - 1 0 2 5 1

TRANSFORMATION PRODUCTS OF SUBMICRON-SIZED ALUMINUM-SUBSTITUTED MAGNETITE: COLOR AND REDUCTANT SOLUBILITY. D.C. Golden¹, D.W. Ming¹, and H.V. Lauer Jr.². ¹NASA-Johnson Space Center, Houston, TX 77058 and ²Lockheed ESC, Houston, TX 77058.

Magnetite when present as fine particles is soluble in acid ammonium oxalate (pH=3); however, the commonly-used extractant for free iron oxides (i.e., citrate-dithionite-bicarbonate (CDB)) is not very effective in dissolving magnetite in soils and geologic materials. Upon oxidation, magnetite transforms to maghemite and at elevated temperatures maghemite inverts to hematite. This transformation causes a change in color from black to red and may affect the reductant solubility as well. The objectives of this study were to examine the color and reflectance spectral characteristics of products during the transformation of magnetite to maghemite to hematite and to study the effect of Al-substitution in magnetite on the above process. Reductant solubility of Al-substituted magnetite, maghemite and hematite was also studied.

Submicron-sized aluminum-substituted magnetite was synthesized in the laboratory by mixing appropriate ratios of molar $\text{Fe}(\text{Cl})_2$, $\text{Fe}(\text{Cl})_3$ and $\text{Al}(\text{Cl})_3$ solutions; the magnetite was precipitated in concentrated NH_4OH . The mole ratio of $\text{Al}/(\text{Al} + \text{Fe})$ in the initial mixture ranged from 0 to 0.4. The precipitates were dialyzed for 48 hrs to remove excess salts and then freeze-dried. Products were examined using X-ray diffraction (XRD), infrared spectroscopy (IR), transmission electron microscopy (TEM), and reflectance spectra in the region of 0.2 to 2.2 μm wavelength. Solubility of magnetite and its oxidation products were determined by using ammonium oxalate (pH=3) and CDB as extractants. Mineralogy of synthesized samples was magnetite except when the $\text{Al}/(\text{Al} + \text{Fe})$ mole ratio was > 0.25 ; a trace of goethite or ferrihydrite precipitated along with magnetite at the higher $\text{Al}/(\text{Al} + \text{Fe})$ ratios. The color of magnetite was black regardless of the Al-substitution. Maghemite, formed by oxidation of magnetite when heated to 400°C, had a redder hue than magnetite; the Munsell color for maghemite ranged from 5R 2/2 for $\text{Al}/(\text{Al} + \text{Fe})$ mole ratio of 0 to 10R 3/4 for $\text{Al}/(\text{Al} + \text{Fe})$ mole ratio of 0.4. The color of hematites formed by heating the maghemite to 500°C was not noticeably different from the parent maghemites. This suggested that the color change during magnetite transformation to maghemite is determined mainly by the oxidation state of Fe rather than by the crystal structure, as the crystal structure remains unchanged during the transformation process. Reflectance in the near IR region increased with an increase in $\text{Al}/(\text{Al} + \text{Fe})$ mole ratio for magnetite and maghemite. A greater Fe^{2+} content in the structure of magnetites and a decrease in particle size resulted in an increase in oxalate solubility of magnetites.

Mean crystallite dimensions (MCDs) of the magnetites as determined by using the Sherrer formula increased with the $\text{Al}/(\text{Al} + \text{Fe})$ mole ratio. Magnetites with $\text{Al}/(\text{Al} + \text{Fe})$ mole ratio between 0.15 to 0.25 had a maximum MCD value of 37 nm and then decreased slightly with further increase in Al. Heating magnetite to 400°C did not increase the MCDs significantly; however, hematite MCDs were much larger than those of maghemite or magnetite from which it was derived.

In summary, the transformation of magnetite to maghemite was accompanied by a change in color from black to red because of the oxidation of structural Fe^{2+} to Fe^{3+} . The phase change maghemite to hematite had a relatively minor effect on color and the reflectance spectra.

THE CRYSTAL STRUCTURE OF GREENALITE AND CARYOPILITE: A SYSTEM OF REGULARLY INTERSTRATIFIED CRYSTALLINE AND SEMI-AMORPHOUS SHEETS

STEPHEN GUGGENHEIM, Dept. of Geol. Sci., Univ. of Illinois at Chicago, Chicago, Illinois 60680, R.A. EGGLETON, Dept. of Geology, Australian National University, Canberra, Australia, and IAN D. R. MACKINNON, Electron Microscope Centre, Univ. of Queensland, St. Lucia, Queensland, Australia.

Greenalite, the Al-poor and Fe²⁺-rich serpentine, and its Mn analogue, caryopilite, form a series of closely related modulated layer silicates. High-resolution transmission electron microscope (TEM) images confirm that there is a modulated tetrahedral sheet in both structures, with two planes of Si tetrahedral cations between adjacent Fe or Mn-rich octahedral sheets, respectively. The tetrahedra have a complete lack of long range positional regularity along *X* and *Y*, although limited short-range order exists. On the average, equal numbers of tetrahedra coordinate to adjacent octahedral sheets.

Diffraction data can be interpreted as from a one-dimensional imperfect crystal along the three *Y** directions, where the distance between successive domain centers of six-fold silicate rings varies about an average value within the (001). The "unit cell" as it relates to the superlattice is a meaningless concept. The tetrahedra are distributed semi-randomly within the (001); thus, tetrahedral sheets may be considered "semi-amorphous".

Electron diffraction patterns of individual crystals show discrete *IT* and *IM* polytypes. Thus, an earlier suggestion that intergrowths may be essential to the stability of the structural system of greenalite and caryopilite is not plausible. The *IT* polytype may be derived following stacking rules for the serpentines, but the *IM* polytype requires shifts along $+a/3$ (or pseudohexagonal *a* axes) in contrast to $-a/3$ shifts for the ideal *IM* polytype in the common serpentines. The relative abundance of each polytype in a sample is related to chemistry, with the dominant polytype being the more stable based on the severity of lateral misfit between the octahedral and tetrahedral sheets. However, neither the *IT* nor the *IM* are restricted to either greenalite or caryopilite compositions, respectively. Stacking in greenalite and caryopilite describes the relative positions of adjacent octahedral sheets, and therefore, it is possible to place limits on the displacements of neighboring domains of silicate rings within the (001).

Modifications to an earlier model are proposed: the essential difference involves the avoidance of the use of a unit cell. Domain boundary linkages cannot be described precisely, although four-fold and eight-fold rings probably dominate.

Ionic Modeling of the Hydrogen Sites in the Kaolin Polymorphs

G. D. Guthrie, Jr. and D. L. Bish

Geology/Geochemistry, MS D469, Los Alamos National Laboratory, Los Alamos, NM 87545

The positions of hydrogen atoms can be extremely difficult to determine in minerals, particularly in clay minerals for which large single crystals or pure, well-crystallized samples are not available. Ionic modeling of the hydrogen-oxygen interactions in a mineral is another approach that may allow prediction of hydrogen positions in minerals. Furthermore, ionic modeling of atomic interactions can provide information pertaining to the energy potential around an atomic site. We developed a method to describe short-range interactions between hydrogen and oxygen (1), thereby permitting the ionic modeling of hydrogen in minerals. The short-range interaction is formulated as a Born-Mayer exponential, $W_{ij} = \lambda \exp[-r_{ij}/\rho]$, where the constants λ and ρ are functions of the site potential of the oxygen. In other words, the model allows for isotropic changes to the electron density of oxygen. We have used this method to model and produce energy maps of the hydrogen positions in the kaolin polymorphs.

Energy minimization and energy mapping were done with the program WMIN. The non-hydrogen part of the structures for each polymorph was fixed to a reported structure. The initial positions of the hydrogen atoms were set to the positions of the hydroxyl oxygens, and the hydrogen positions were varied until a minimum-energy configuration was achieved. The site potentials for each oxygen were recalculated after each minimization cycle, and the process was repeated. Once an absolute minimum was obtained for a hydrogen, energy maps were calculated by moving the hydrogen about the minimum-energy position and calculating the total electrostatic energy.

The model worked very well for kaolinite and nacrite. Positions of the inner-surface hydrogens were reproduced successfully. The predicted bond lengths were in the range 0.97–0.99 Å, and O–H vectors were within 5.5° of the observed vectors. Energy mapping of these sites showed that the energy wells were disk-shaped, with the disks parallel to (001). This is consistent with the observed anisotropy in the temperature factors for these hydrogens. The predicted bond length of the inner hydrogen (the one that occupies the empty octahedral site) was 1.02 Å, but the orientation of the O–H vector was 20.5° away from the observed vector. Energy mapping of this site showed that the energy well was sausage-shaped and oriented approximately parallel to [001]. This is consistent with the observed anisotropy in the temperature factor for this hydrogen. The predicted position was at one end of the energy well, and the observed position is at the other. In other words, the energies of the predicted and observed positions were very close, and the hydrogen may be oscillating within an energy well. Predicted O–H bond lengths for nacrite were in the range 0.92–1.04 Å, but the positions differed significantly from those predicted by Giese and Datta (2).

The model was not successful at reproducing the hydrogen positions in dickite. Predicted O–H bond lengths were too large, and O–H vectors deviated significantly from observed vectors. In fact, the model predicted minimum-energy positions such that each inner-surface hydrogen was equidistant from two oxygens. The failure of the model to predict hydrogen positions in dickite may indicate that (1) atomic interactions that were not considered in the model are significant in dickite; (2) the reported structure (either the positions of the hydrogen atoms or the entire structure) is incorrect; or (3) the model does not work. The latter two possibilities seem unlikely, since (a) the various reported refinements for dickite give similar non-hydrogen positions; and, (b) the model has previously been shown to work in a wide range of structures, including two kaolin polymorphs.

1 Guthrie, G. D., Jr., Bish, D. L., and Burnham, C. W. (1991) *Eos*, 72:144.

2 Giese, R. F. and Datta, P. (1973) *Am. Mineral.*, 58:471.

Quantitative Analysis of Mordenite–Clinoptilolite Mixtures Using the Rietveld Method

G. D. Guthrie, Jr. and D. L. Bish; Geology/Geochemistry, MS D469, Los Alamos National Laboratory, Los Alamos, NM 87545

Samples of natural zeolites typically are mixtures of numerous minerals, which often include several zeolites. The mineralogy of such samples can be determined quantitatively, however, using X-ray powder diffraction. For mordenite–clinoptilolite mixtures, the use of the relative intensity ratio (RIR) method is difficult, due to severe overlap of peaks between the two minerals. The Rietveld method is an alternate procedure for determining the mineralogy, and the method explicitly accounts for peak overlap. We have evaluated the use of the Rietveld method for quantitative analysis of mordenite–clinoptilolite mixtures by analyzing known mixtures. We have also analyzed two unknown “mordenite” samples that have been used as mordenite standards in biological experiments.

Standard mixtures of mordenite–clinoptilolite were prepared by mechanically mixing a purified mordenite (Poona, India; Ward's Scientific) and a purified clinoptilolite (#27163; Death Valley Junction, CA; Minerals Research). One gram of each of 3 mixtures was prepared and mixed with 0.25-g Al_2O_3 as an internal standard, thus producing the following mixtures: 72% mordenite–8% clinoptilolite–20% Al_2O_3 ; 40–40–20; and, 8–72–20. Each sample was ground under acetone for 10 minutes in a Brinkmann grinder. Back-packed mounts were prepared from each, and data were collected on a Siemens D500 θ – θ diffractometer using $\text{CuK}\alpha$ radiation and scanning from 2–150° 2θ at 0.02° 2θ /step and 4 s/step. Earlier refinements used data collected to only 70° 2θ , but these data were insufficient to allow refinement of all necessary parameters.

The Rietveld program DBW was used to refine the model, which consisted of clinoptilolite, mordenite, and corundum. Refinement proceeded as follows: scale factors and background parameters; lattice parameters; sample displacement; profile parameters (with those for the two zeolites constrained to one another); overall temperature factor; occupancies of the cage-sites in the zeolites. Though both mordenite and clinoptilolite orient preferentially (even in a back-packed mount), no preferred orientation correction was added to the model. This led to seemingly large residuals in the final model; however, the omission of a preferred orientation correction did not significantly affect the accuracy of the results. The final model reproduced the known amounts to better than 12% relative and 1.5 wt. % absolute.

Following a similar procedure, we analyzed two “mordenite” samples used in studies to assess the pathogenicity of mineral dusts: (a) “HM mordenite,” (1) and, (b) “S mordenite,” (2). Each was mixed with Al_2O_3 (20 wt. %) and ground under acetone for 10 minutes in a Brinkmann grinder. Data were collected as described above. The initial models included clinoptilolite, mordenite, and corundum. However, peaks consistent with other phases were present in the patterns. Hence, sanidine, albite, cristobalite (used to simulate opal CT), and quartz were added to both models; gypsum was added to the model for S mordenite.

The final models indicated that both “mordenite” samples contained at most 50% mordenite (HM mordenite 49.9%; S mordenite 36.5%). The remaining material consisted of clinoptilolite, feldspar, silica, and gypsum (S mordenite only). The dilution of mordenite by these other minerals may have resulted in an incorrect estimate of the pathogenicity of mordenite, *i.e.*, only the biological activities of the two natural mordenite-bearing samples were determined correctly. In light of its fibrous habit and the poor quality of the samples that have been studied, mordenite should be restudied in greater detail as a potential carcinogen.

- 1 *e.g.*, Hansen, K. and Mossman, B. T. (1987) *Cancer Res.* 47:1681; Palekar, L. D., Most, B. M., and Coffin, D. L. (1988) *Environ. Res.* 46:142.
- 2 *e.g.*, Suzuki, Y. (1982) *Environ. Res.* 27:433.

STUDY OF THE KAOLINITE-RICH CLAYSTONE LAYER FROM THE CRETACEOUS-TERTIARY BOUNDARY USING INFRARED SPECTROSCOPY: Happ J. W., Shenandoah University, 1460 University Drive, Winchester, VA 22601.

A thin 1-2 cm thick kaolinitic clay bed and its associated iridium-rich impact layer occur at the Cretaceous-Tertiary boundary in continental rocks at numerous sites east of the Rocky Mountains from Alberta to New Mexico. For this study, kaolinite claystone samples have been collected from 13 previously documented K-T boundary sites at Trochu, Alberta; Hell Creek, Montana; and the Raton Basin of Colorado and New Mexico.

Additional data regarding the structure of kaolinite in the claystone boundary layer is provided by analysis using fourier transform infrared spectroscopy. The infrared spectra of kaolinite is characterized by strong absorption bands in the OH-stretch and SiO-stretch regions. The relative intensities of these bands depend not only upon the nature of the kaolinite-group clay but also upon the shape of the particles, their orientation and the angle of incidence of radiation upon the preparation examined in the spectrometer.

The ratio of absorptions of frequency bands in the OH-stretch and SiO-stretch regions of the spectrum of randomly oriented kaolinite preparations from boundary and non-boundary sites have been compared. Analysis of the comparison suggests an interesting contrast between boundary and nonboundary kaolinites. This relationship is not evident from analysis of X-ray diffraction data or other published analyses. Experiments have been carried out to determine the nature of the difference and to determine the extent to which structure and particle size are responsible.

The position of the kaolinite upon a plot of the ratio of absorptions of frequency bands provides information regarding the type of kaolinite in the claystone boundary layer.

UNCONFORMITY-RELATED K-FELDSPAR AND PHYLLOSILICATE ALTERATION AT THE PRECAMBRIAN-PALEOZOIC BOUNDARY, SOUTHWESTERN ONTARIO

D.A. Harper¹, Longstaffe¹, F.J. and Wadleigh, M.A.²

¹Department of Geology, University of Western Ontario, London, Ontario Canada N6A 5B7;

²present address: Department of Earth Science, Memorial University of Newfoundland, St. John's, Newfoundland Canada A1B 3X7.

Grenvillian (Precambrian) granitoid gneisses are unconformably overlain by Paleozoic sedimentary rocks in the subsurface of southwestern Ontario. Alteration of variable thickness (tens of cm to m) and intensity occurs in the Precambrian rocks adjacent to the unconformity. The alteration zone is immediately recognizable because of reddening and an increase in porosity, both features probably resulting from ancient weathering. In a detailed profile through one tonalitic gneiss, the alteration zone can be petrographically characterized by the appearance of secondary minerals including abundant K-feldspar plus illite, chalcedony, carbonates (calcite and dolomite) and chlorite. K-feldspar occurs as overgrowths on, and replacements of, pre-existing mineral grains in the granitoid rocks, and as fracture-fillings (multiple generation?) displaying both microcrystalline and adularia habits. The K-feldspar is chemically pure (Or 99-100) and is non-cathodoluminescent, features that suggest low temperature formation. Textural relationships among illitized and chloritized minerals, and the secondary K-feldspar that has overgrown and/or replaced some of these grains, suggest that phyllosilicates were precursors to the secondary K-feldspar. Some secondary K-feldspar has been subsequently coated by illitic clays.

Abundant diagenetic K-feldspar is also a striking feature of the immediately overlying Cambrian/Ordovician mixed quartz arenites, dolomitic quartz sandstones, dolomitic arkoses and sandy dolostones (1). The diagenetic feldspar occurs as overgrowths, as euhedral, neofomed crystals, as fine-grained matrix, and in association with illite. All feldspar varieties are enriched in K and depleted in Na and Ba relative to detrital K-feldspar in the same rocks. Illite, chlorite, calcite, dolomite and quartz overgrowths are also present in pore space; some lithologies also contain pelloidal glauconite. Diagenetic K-feldspar crystallized early in the paragenetic sequence, disrupting quartz overgrowths, and coating some quartz grains. Most K-feldspar formation predated all but initial development of some grain-coating illite.

Oxygen-isotope analyses of bulk-rock samples through the alteration profile in the Precambrian tonalitic gneiss confirm that massive, low-temperature alteration has occurred. The $\delta^{18}\text{O}$ values shift from +7.5 ‰ (SMOW) in unaltered gneiss to +18.2 ‰ adjacent to the Precambrian-Paleozoic boundary. This change is proportional to the amount of secondary K-feldspar in the samples. The secondary K-feldspar has dramatically high $\delta^{18}\text{O}$ values (+18.9 to 21.4 ‰) relative to primary minerals. The $\delta^{18}\text{O}$ values for quartz (+7.3 to +8.6 ‰), plagioclase (+7.2 to +7.8 ‰), hornblende (+4.8 to 6.0 ‰) and biotite (+0.3 to 2.0 ‰) vary in the order expected for meta-igneous minerals approaching high temperature equilibrium.

We conclude that crystallization of secondary K-feldspar in the Precambrian gneisses resulted from low-temperature interaction between phyllosilicates formed during earlier weathering and porewaters focussed along the Precambrian-Paleozoic boundary, early in the diagenetic evolution of the Cambro-Ordovician sediments. This interaction may be a part of a wider phenomenon of secondary K-feldspar formation known throughout midcontinental North America (e.g., 2-4).

1. Longstaffe, F.J. Wadleigh, M.A., Frapce, S.K. and McNutt, R.H. (1990) Ontario Geological Survey Miscellaneous Paper 150, p. 143-152.
2. Stablein, N.K. and Dapples, E.D. (1977) *Journal of Sedimentary Petrology*, vol. 47, p. 1512-1538.
3. Hearn, P.P. and Sutter, J.K. (1985) *Science*, vol. no. 228, p. 1529-1531.
4. Duffin, M.E. (1989) *Geology*, vol. no. 17, p. 765-768.

MIXED-LAYER CLAY GEOTHERMOMETRY IN THE WAIRAKEI GEOTHERMAL FIELD, NEW ZEALAND

Colin C. Harvey* and Patrick R.L. Browne

Geothermal Institute and Department of Geology,
University of Auckland, Private Bag, Auckland, New Zealand

Mixed-layer clays of variable composition and structure occur in core samples from two wells (WK207 and WK210) in the Te Mihi sector of the Wairakei geothermal field.

The clays were identified by X-ray diffraction analysis of glycolated, oriented sample fractions at less than 2 micrometers and less than 0.2 micrometers.

Low permeability lacustrine sediments encountered by drillhole WK207 contain a well-developed sequence of mixed-layer clays. The shallowest downwell appearance of mixed-layered illite/smectite ($I_{0.6}/Sm$) occurred at 146 m depth where the bore temperature is only 100°C. Mixed-layered illite-chlorite ($I_{0.7}/Chl$) occurred at 244-250 m depth in association with highly ordered illite/smectite ($I_{0.9}/Sm$) where prevailing formation temperatures are 170°C. Discrete illite was present only below 297m (above 200°C) in the finest size fraction (less than 0.2 micrometers). Chlorite first appeared in association with illite-smectite at 177m depth (110°C).

The lithology in drillhole WK210 is predominantly ignimbrites and rhyolites. The fluid flow in these rocks is dominated by conduit flow. Within these rocks a sequence of interlayered clays is poorly developed, with illite present at only 244 m. Temperatures range from 140 to 226°C.

Differences in the identity of clay minerals present in a geothermal reservoir, where conditions are otherwise the same, demonstrate the strong control that the type of fluid flow can have on their formation. In low permeability sediments where diffuse fluid flow prevails, a well-defined sequence of mixed-layer clays occurs. These are absent where conduit flow prevails.

* Present Address:

Dept of Geology, Indiana University, 1005 East Tenth St, Bloomington, IND 47405, USA

The Influence of Composition on the Release of Radiogenic Argon from Illitic and Glauconitic Clay Samples

A. A. Hassanipak¹ and J. M. Wampler²

¹Mining Engineering Department, Faculty of Engineering, Tehran University, Tehran, Iran.

²School of Earth and Atmospheric Sciences, Georgia Institute of Technology, Atlanta, GA 30332-0340.

We have studied the release of radiogenic argon by stepwise heating (under vacuum) of various clay samples, including highly smectitic mixed-layer clays. Argon-release "spectra," based on 24-hour heating intervals at 250, 375, and 500°C and 20-minute heating at 1000°C, for illitic and glauconitic samples are distinctly different from one another. The glauconitic samples studied released 50-86% of their radiogenic argon in the first two heating steps (to 375°C) and had released nearly all (90-99%) such argon after heating at 500°C. In contrast, the illitic samples released only a small fraction (18% or less) of their radiogenic argon during the first two steps, and even after 24 hours at 500°C they retained most of their radiogenic argon (60% on average).

The radiogenic-argon release patterns obtained for various size fractions (four fractions in the size range 2 to <0.1 μm) of the individual illitic and glauconitic samples are nearly the same, indicating that the argon release rate is not a function of particle size for the size ranges studied. The argon release patterns are dependent on composition, however. The rate of argon release at a given temperature is inversely related to potassium content but is directly related to iron content. The rate of release of argon under these laboratory conditions is apparently controlled by the rate of thermal decomposition of these materials, which depends on composition but evidently not on particle size.

The K-Ar apparent ages of some highly smectitic samples from Eocene claystones in Georgia are greater than the stratigraphic ages of the samples, indicating that inherited argon is present in a detrital component. Even for the finest fraction (<0.1 μm) the inherited argon is evident. Stepwise heating of these samples indicates the presence of detrital illite and provides a basis for estimation of the amount of such illite in each size fraction. For the <0.1- μm size fraction, the proportion of detrital illite is small enough that correction for its presence changes the apparent age to a value close to the stratigraphic age. Our results indicate that <0.1- μm mixed-layer clays can retain radiogenic argon well enough to be useful in geochronometry.

A METHOD COMBINING SWIR AND XRD FOR THE IDENTIFICATION OF CLAY MINERALS: I. INTERSTRATIFIED KAOLINITE/SMECTITE CLAYS

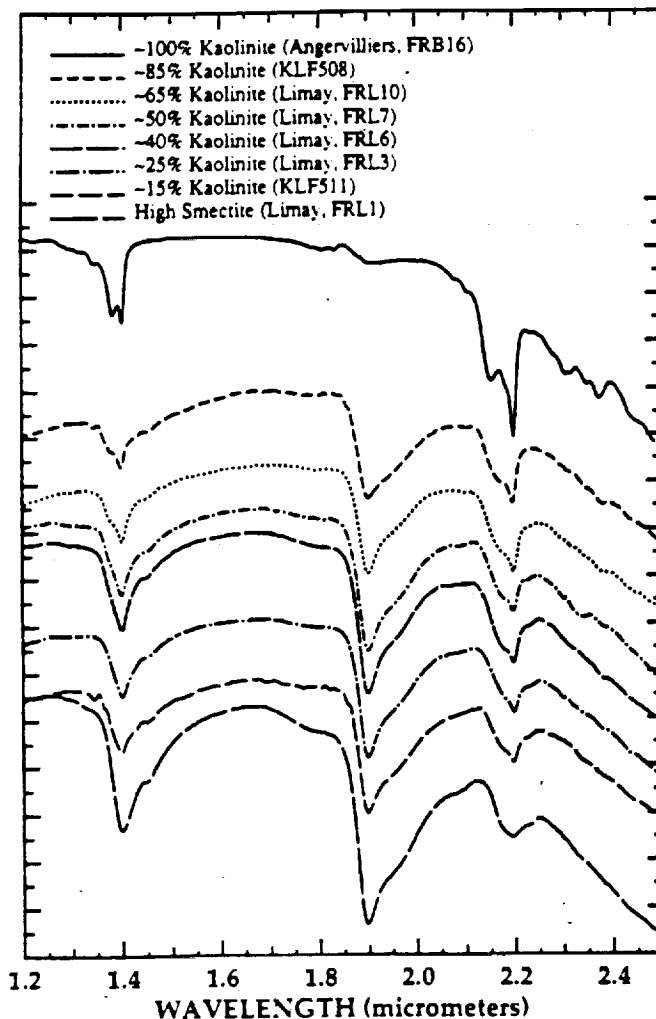
PHOEBE HAUFF AND *MÉDARD THIRY

Spectral Research, Lafayette, Colorado, USA

*École des Mines de Paris, CGGM, Fontainebleau, FRANCE

X-ray diffraction has long been a primary and reasonably accurate means for the identification of clay minerals. It is a time consuming process involving complex sample preparation and analysis with laboratory based instrumentation. The method developed combines the accuracy of XRD with the speed and flexibility of a field portable Short Wave Infrared Reflectance (SWIR) spectrometer. SWIR techniques detect phyllosilicates, carbonates and sulfates which have absorption features in the 1.3 - 2.5 micrometer wavelengths of the electromagnetic spectrum. The method is rapid, taking approximately one minute per spectra and self-calibrating to an internal standard. The spectrometer weighs about twenty pounds and with an internal light source, is independent of solar illumination.

A unique sample set of kaolinite/smectite(K/S) clays from the Paris Basin, France illustrates the field application. The entire paragenetic sequence of kaolinite/smectite interstratified clays exists in quarries within 100km of Paris. Smectites formed in weathering profiles developed within the Argiles Plastique Formation deposited on flint-bearing chalk. Weathering of the chalk with leaching under alkaline soil conditions produced the interstratified kaolinite/smectite clays while the acidic environments associated with weathering of argillaceous and sandy sediments produced kaolinites.



Laboratory characterization of this complex suite was done using XRD, DTA (Differential Thermal Analysis), chemical analysis, and SEM (Scanning Electron Microscopy). SWIR techniques are very sensitive to the discrimination of species components within interstratified clays. Each clay mineral has a diagnostic combination of the spectral features for hydroxyls (1.4 μ m), water (1.9 μ m), Al-OH (~2.2 μ m), Fe-OH (~2.25 μ m) and Mg-OH (~2.35 μ m). The figure illustrates how the spectra change with different layer component ratios. Note how the 1.4 μ m, 1.9 μ m and 2.2 μ m feature profiles reflect these compositional variations. With profile analysis, a digital value can be calculated for each feature and equated to the layer percentages. The different clays can therefore be detected in the field with the portable SWIR unit and a map of the mineralogy constructed with sample positions determined by a GPS (Global Positioning System) detector, which integrates with the spectrometer computer. This paper summarizes the geology for the kaolinite/smectites and describes in detail the integration of XRD with laboratory and field SWIR for the rapid identification of K/S clays.

KAOLINITE WAS A PRECURSOR TO DIAGENETIC K-FELDSPAR OF PALEOZOIC AGE IN WISCONSIN

R. L. Hay and Junzhe Liu
Department of Geology, University of Illinois
1301 West Green St., Urbana IL 61801

Authigenic K-feldspar replaces kaolinite in an alteration profile developed on Precambrian granites beneath the Mt. Simon Sandstone (Upper Cambrian) in Wisconsin. The profile is commonly 1-3 m thick and is interpreted as a pre-Mt. Simon paleosol overprinted by diagenetic reactions with pore fluids from the Mt. Simon Sandstone. At Irvine Park, in western Wisconsin, residual spheroids of weathered plagioclase granite in a saprolite have a kaolinitic interior and a cortex in which the kaolinite is largely replaced by K-feldspar of low-temperature origin. Where a saprolite is lacking, as in quarries near Neillsville, Wisconsin, the upper zone of the alteration profile, about 1 m thick, has abundant authigenic K-feldspar and overlies a kaolinitic zone. Associated spheroids of exfoliating granite are zoned from cores of fresh plagioclase-microcline granite through a kaolinitic zone into a cortex in which authigenic K-feldspar is the dominant feldspar. Potassium for the K-feldspar of the alteration profile was supplied by large-scale fluid movements, and silica was at least partly supplied by dissolution of quartz in the altered granites.

Kaolinite may have been a precursor to K-feldspar in the enigmatic K-feldspar-rich beds of the Readstown Member of the St. Peter Sandstone (Ordovician). Dissolution of quartz is commonly associated with the K-feldspar, and shapes of some K-feldspar aggregates are suggestive of replaced kaolinite macrocrystals.

Authigenic K-feldspar below the pre-Mt. Simon unconformity was probably formed in the early Devonian episode of K-feldspar authigenesis in Cambrian and Ordovician rocks of the Upper Mississippi Valley. K-feldspar of altered granite from a Neillsville quarry yielded a K-Ar date of 411 ± 10 Ma, which compares with 394 ± 6 Ma for authigenic K-feldspar in the Mt. Simon Sandstone in northwest Illinois, 377 - 402 Ma for enigmatic K-feldspar-rich beds of the St. Peter Sandstone in eastern Wisconsin, and 390 ± 7 to 400 ± 6 Ma for authigenic K-feldspar in altered vitric tuffs of Ordovician age in southeast Minnesota and northeast Iowa. Authigenic K-feldspar from a Neillsville quarry has a $\delta^{18}\text{O}$ value of $+21.3\text{‰}$, which falls within the range of 21.0 - 21.4‰ for authigenic K-feldspar in Ordovician rocks of Wisconsin and Minnesota.

ORIGIN AND DIAGENESIS OF CHLORITE MINERALS IN THE ORCADIAN BASIN, SCOTLAND: S. Hillier, Laboratoire de Geologie, L'Ecole Normale Supérieure, 24 rue Lhomond, Paris 75231 Cedex 05 France

Chlorite minerals are common in lacustrine mudrocks from the Devonian Orcadian Basin, but have a variable stratigraphic and regional distribution. Vitrinite reflectance data show that this distribution is related to diagenetic grade. In areas where mean vitrinite reflectance is $> 1.3\%$, chlorite minerals are ubiquitous, whereas in areas with lower maturity, they are generally absent. This relationship indicates that the majority of chlorite minerals found throughout the Orcadian Basin are authigenic and were formed during burial diagenesis/metamorphism. Detrital chlorite appears to be only a minor component or absent.

Semi-quantitative mineralogical and chemical analyses of Orcadian mudrocks indicate that authigenesis of chlorite minerals occurred by a reaction between the original detrital dioctahedral clay minerals and original lacustrine dolomite. Reactions between detrital clay minerals and carbonates during burial diagenesis may explain the occurrence of corrensite and chlorite in other evaporite basins. In the Orcadian Basin corrensite occurs in rocks with vitrinite reflectance between about 1 and 3% and always occurs with chlorite, though chlorite may occur without corrensite. X-ray diffraction data, and electron microprobe analysis appear to indicate that some minerals are intermediate between corrensite and chlorite.

CATION EXCHANGE STAINING OF CLAY MINERALS: S.Hillier and

T.Clayton Laboratoire de Geologie, L'Ecole Normale Supérieure, 24 rue Lhomond, Paris
75231 Cedex 05 France

Clay minerals in thin-sections can be 'stained' by cation exchange. The technique is illustrated by a series of clay minerals from reservoir sandstones which have been cesium (Cs) exchanged. After Cs exchange the clay minerals have been analysed by electron microprobe. The amount of Cs found by analysis can be helpful in distinguishing good microprobe analyses from those which represent a mixture or are contaminated with other phases. The cation exchange capacity of the clay can be calculated and the exchangeable cations in the natural state are indicated by comparison with analyses made before Cs exchange. Swelling clays are readily identified and their distribution can be studied by using the probe to map for Cs.

OCCURRENCE OF EXPANDABLE CLAY MINERALS IN CONTACT METAMORPHIC AUREOLES

Hluchy, Michele M., Alfred University, Geology Dept., Alfred, NY 14802;
April, Richard H., and Beebe, Stephanie L., Colgate University, Geology
Dept., Hamilton, NY 13346.

Contact metamorphism is being investigated in dike-intruded sediments from Emery County, Utah. At this location a swarm of Tertiary-aged basaltic dikes intrude Jurassic-aged Carmel Formation sediments. The metamorphic effect of these intrusions on several different sedimentary lithologies is being studied with emphasis on clay mineral transformations.

Samples of various sedimentary lithologies were collected at increasing distances from the basalt-country rock contact. Mineralogic trends observed thus far indicate that the expandable clay mineral smectite is stable close to the dikes and increases with proximity to the intrusions. Clay mineral suites in the unaltered country rock vary with lithology and the transformation reaction, which results in the formation of smectite in the contact aureole, may not be the same in all rock types. The type of smectite forming near each dike is also different and mixed-layered phases (e.g., C/S and/or I/S) sometimes show increased proportions of expandable layers close to the intrusions.

The results of this study indicate that expandable clays, such as smectites, can form as alteration products in contact metamorphic systems. It is suggested that formation of expandable clays in the Utah study area may be controlled by the geochemistry of the hydrothermal system, especially the pH of the fluids associated with the intrusions. Further work is continuing to characterize the precise thermal and geochemical conditions for smectite formation in this environment.

MAPPING DIAGENETIC FLUID FLOW WITHIN A RESERVOIR-K/Ar DATING
IN THE ALWYN AREA, UK NORTH SEA: Hogg A. J. C., Fallick A.
E., and Pearson M. J., Reservoir Appraisal Branch, BP
Research, Chertsey Rd., Sunbury-on-Thames, Middx TW16 7LN UK

The paragenetic sequence and isotope geochemistry of diagenetic cements are used to reconstruct the pore fluid history of the Middle Jurassic Brent reservoir sandstones in the Alwyn South Field, of the UK North Sea. This reconstruction is used to determine the controls on the distribution of diagenetic cements and variations in reservoir quality within the relatively limited area of three adjacent reservoir panels at successively higher structural levels.

The cement assemblage of quartz, kaolinite and illite has resulted in severe deterioration of otherwise good reservoir quality. Early precipitation of vermiform and late blocky kaolinite was succeeded by a relatively intense illitization. Quartz cementation took place in as many as five phases through much of the later diagenetic history.

Vermicular kaolinite and subsequently blocky kaolinite were precipitated from meteoric fluids which invaded the reservoir during late Jurassic emergence and were flushed to around 1km depth during continued burial. Illite formation took place between 60 and 38 Ma bp from compositionally homogeneous waters with marine isotope compositions ($\delta^{18}\text{O}$ 0-2% SMOW) and salinity (3-4wt% NaCl) at temperatures of 105-120°C. This indicates that the early meteoric fluids were replaced by saline pore-water probably derived from compacting argillaceous rocks at depth. The fluids precipitating illite were the precursors of hydrocarbon emplacement which began between the Middle Eocene and Lower Oligocene.

Fluid migration into the reservoir was probably along the deep seated Alwyn-South-Ninian Fault system. K-Ar dating of illites shows that migration between reservoir panels proceeded from the deepest reservoirs up-structure. Wells adjacent to fluid inlet are extensively silicified. Within panels the pattern of fluid movement is facies dependent. In lithologically homogeneous reservoirs fluid circulation was relatively simple and illitization proceeded from the base of the well upwards at rates of approximately 5.5mMa^{-1} . The duration of illite formation at any one level was between 2 to 5Ma. In heterolithic reservoirs fluid migration occurred initially along high permeability fairways and consequently illite ages do not vary systematically with depth.

Overall variation in reservoir quality between reservoirs depends on proximity to the source of diagenetic fluids. Variation in the timing of diagenesis and reservoir quality within panels is the result of facies control on fluid migration pathways.

MODELLING OF THE CRYSTAL STRUCTURE OF POTASSIUM BIRNESSITE

Kerry L. Holland and Jeffrey R. Walker

Department of Geology and Geography, Vassar College, Poughkeepsie, NY 12601

Birnessite is a poorly crystallized phyllosulfate which readily oxidizes highly toxic As(III) to less toxic As(V). X-ray diffraction experiments using unreacted, reacted, and heated/reacted samples of synthetic K-birnessite were designed to study structural changes occurring upon reaction and heating and increase understanding of the crystal structure. Results of the diffraction analyses were modeled and refined by hand with the following computer programs: POWD10 (D. K. Smith) and BIRNDIF and TURBOBIRN (both modified from the programs of R. C. Reynolds). All modeling was based on the monoclinic unit cell where $a=5.149 \text{ \AA}$, $b=2.843 \text{ \AA}$, $c=7.4131 \text{ \AA}$, and $\beta=100.76^\circ$. Two peaks which appeared only in the heated and/or reacted patterns were tentatively identified as peaks from the Mn-As hydrate complex hoernesite. The first and second peaks in the heated/reacted pattern had a significantly smaller d-value signifying collapse of the interlayer upon heating. No significant collapse was observed in the reacted pattern. In each pattern, the 2.4 \AA , 1.4 \AA , and 1.2 \AA peaks had diffraction bands on their high-angle sides. In the heated/reacted pattern, the diffraction band on the high-angle side of the 2.4 \AA peak was partially modulated. Through refinement of an ordered theoretical pattern, it was determined that each peak with a diffraction band is not in the 00/ series. In each case, an hk peak is found at the approximate location of the 00/ position whereas the 00/ peak is at or near extinction. Through trial and error, a mean defect-free distance δ , and the number of cells coherently stacked along the a-, b-, and c-axes, N_1 , N_2 , and N_3 were varied in order to model the disorder of the unreacted sample. The values which produced a pattern closest to that of the experimental pattern were: $\delta=2.5$, $N_1=1$, $N_2=5$, and $N_3=18$. Small values of N_1 and N_2 also indicate extreme disorder along the a- and b-axes and that the nature of the disorder is anisotropic. Ordered and disordered theoretical patterns were overlain and combined with theoretical data output to determine which reflections contribute to the large 2.4 \AA peak and the diffraction band on its high-angle side.

AN EXPERIMENTALLY DERIVED KINETIC MODEL FOR SMECTITE-TO-ILLITE
CONVERSION AND ITS USE AS GEOTHERMOMETER

W. L. Huang, J. M. Longo and D. R. Pevear

Exxon Production Research Company
P. O. Box 2189, Houston, Texas 77001

The smectite-to-illite conversion during shale diagenesis has been recently used to constrain the estimate of a basin thermal history. We have systematically investigated the kinetics for the conversion of a Na-saturated montmorillonite (SWy-1) to a mixed-layer smectite/illite (S/I) as a function of KCl concentration (from .1 to 3 moles/liter) over a temperature range of 250 to 325°C at 500 bars in cold-seal pressure vessels using gold capsules as the sample container.

The results show that the conversion rate can be described by a simple empirical rate equation:

$$-dS/dt = A * \exp(-E_a/RT) * [K^+] * S^2$$

where S = fraction of smectite layers in the S/I estimated by its expandability (NEWMOD modeling) using x-ray diffraction data, t = time in seconds, A = frequency factor = 80800 sec⁻¹, exp = exponential function, E_a = activation Energy = 28000 cal/mole, R = gas constant, 1,987 cal/deg-mole, T = temperature (degree Kelvin), [K⁺] = K⁺ concentration in molarity (M) in the fluid.

We found that by assuming a range (100-300 ppm) of K⁺ concentrations similar to the value typically reported in oil field brines, the present kinetic model can reasonably predict the extent of the smectite-to-illite conversion for a number of shales from various depths and age. This narrow range of potassium concentrations, therefore, is used to model the smectite-to-illite conversion in shale when the actual chemical information of pore fluid is not available.

The kinetic equation has been tested by modeling shale diagenesis using field data from a large variety of geologic settings worldwide (Gulf of Mexico, East Taiwan Basin, Vienna Basin, Salton Sea Geothermal System, South Caspian Basin etc). The results show the equation to reasonably predict the extent of the reaction within our knowledge of the variables involved (burial history, thermal gradients, potassium concentration).

**GEOTECHNICS OF DENSE CLAY SOILS SUBJECTED TO HEAT AND CHEMICALS:
TOWARD PREDICTIVE MODEL**

T. Hueckel and C.M. Ma

Department of Civil and Environmental Engineering
Duke University, Durham N.C. 27706

When subjected to heat or certain chemicals some clay minerals and clay soils increase their permeability from two to four orders of magnitude when not loaded. Mechanical load can invert completely this tendency and when sufficient, the permeability can even decrease up to one order of magnitude. Hypothetical microscopic mechanisms of interaction between the permeants and the mineral, as well as of the action of heat are discussed in terms of an engineering model for soil under stress in the elastoplastic range. Inter-constituent mass transfer from solid to liquid simulates the degradation of adsorbed water due to temperature or chemical attack. Changes in permeability are modeled by coupling it to changes in effective porosity through Kozeny-Carman equation.

Diagenesis of overpressured Tertiary and Cretaceous mudstones
from the East Shetland Basin, North Sea

Jenny Huggett, Dept Geology, Imperial College, London,
SW7 2BP UK

This poster describes the petrography, mineralogy and diagenesis of an overpressured Tertiary and late Cretaceous mudrock sequence from a single well in the East Shetland Basin (North Sea). These mudrocks are brown and unconsolidated down to a depth of approximately 1475m, below this depth they are lithified and their colour shows a gradual transition to grey. The matrix is ash dominated above 1400m and smectite dominated below. The smectite content increases with depth due to alteration of volcanic ash, shards and grains which commences almost immediately after deposition and is still not complete at burial depths of over 2300m. There is no evidence of alteration of the smectite to illite despite a locally available supply of K^+ in the form of K feldspar. K feldspar is increasingly leached with depth, and although observed in the electron microscope in all samples is not detected by XRD below 1450m. Calcic plagioclase is increasingly replaced by albite with depth. Quartz shows no depth trends and appears to have been neither leached or precipitated. Illite and minor kaolinite show no obvious trends with increasing depth, though BSEM indicates that much of the kaolinite has replaced mica. Microfossil tests filled with authigenic clays such as have been observed in other Tertiary mudrocks in the North Sea, were not observed, though a few fossil cavities are filled with carbonate cements. Authigenic carbonates have a patchy distribution, probably related to the distribution of detrital carbonate.

MIXED-LAYERED KAOLINITE/EXPANDABLES¹: OCCURRENCE AND RATES OF FORMATION IN QUATERNARY, MISSISSIPPI VALLEY LOESSES

R. E. Hughes^{1*}, D. A. Grimley², L. R. Follmer¹, D. M. Moore¹, and W. H. Johnson²

¹ Illinois State Geological Survey, 615 E. Peabody, Champaign, IL 61820

² Department of Geology, University of Illinois, Urbana, IL 61801

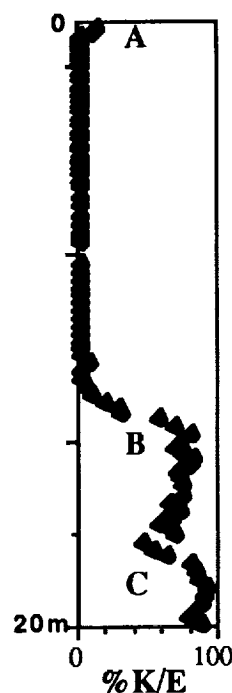
Thick (20 m+) loess deposits along the Mississippi River contain a modern soil and several paleosols. The clay and nonclay mineral contents for the modern soil and two paleosols suggest that the parent materials for the three profiles were similar. The three profiles contain pedogenic mixed-layered kaolinite/expandables (K/E)¹ proportional to the intensity and duration of soil formation. Furthermore, both the amount of this mineral and its ratio of kaolinitic to expandable layers (fig. 1) vary proportionally with the assumed length of weathering. Broadening and "smearing" of the 17Å_{eg} peak² are associated with K/E and are proportional to degree of weathering. This peak smearing results from the growth of kaolinitic interlayers within the 17Å_{eg} phase. Indices of weathering based on the 17Å peak are most useful for samples with low K/E contents. Vermiculite is also associated with the early stages of formation of K/E and is another clue that minor amounts of K/E may be present.

The distribution of feldspars and carbonates in these profiles is a second measure of weathering intensity. Approximately a third to a half of the feldspars in the Sangamon and Yarmouth Geosols is altered to kaolinite. Because clay minerals are illuviated in the profiles, weathering intensity estimates based on nonclays provides a useful corroboration of clay-based estimates.

A comparison of local and regional profile descriptions and mineral and particle size distributions within profiles, when combined with deep sea data on Quaternary climatic fluctuations, make refined estimates of climate and length of pedogenesis in the region possible. These estimates provide essential information for discussions about variations in Quaternary climates, recent anthropogenic changes in global climate, and their causes.

¹This is our suggestion to broaden the definition of mixed-layered kaolinite/smectite.

²Mostly smectite-rich I/S in unaltered samples of presumed parent material.



SYNTHESIS OF FLUORINATED 2:1 LAYER SILICATES AND THEIR CHARACTERIZATION BY ^{29}Si , ^{27}Al AND ^{19}F MAGIC ANGLE SPINNING (MAS) NUCLEAR MAGNETIC RESONANCE (NMR) SPECTROSCOPY:
 HUVE L., Saehr D., Martin P., Baron J., and Le Dred R.,
 Ecole Nationale Supérieure de Chimie de Mulhouse 3, rue A.
 Werner 68093 Mulhouse Cedex France

2:1. Layer silicates are usually synthesized from neutral to basic hydrogels containing the framework-forming elements such as Si, Al, Mg (1), (2). The hydrothermal way is the most commonly used for these synthesis where hydroxide ions are involved as mobilizing agent of the structural elements. Guth et al. have shown that this role may also be played by fluoride ions (3). The present paper reports hydrothermal synthesis in fluoride medium of 2:1 di- and trioctahedral layer silicates, their characterization by X-Ray Diffraction (XRD) and Solid State ^{29}Si , ^{27}Al and ^{19}F MAS NMR. The 2:1 layer silicates were prepared hydrothermally at 220 °C under autogeneous pressure in Teflon-lined stainless steel autoclave during several days. The reactants were powder silica, aluminium oxyhydroxide or magnesium acetate, fluorinated salts (NaF , NH_4F ,...), fluorhydric acid and distilled water. The hydrogels had typically the following formula : $1 \text{ SiO}_2 ; x \text{ Al}_2\text{O}_3$ and/or $y \text{ MgO} ; z \text{ CF} ; \omega \text{ HF} ; 48 \text{ H}_2\text{O} ; \text{C}$ was a monovalent cation (Na^+ , NH_4^+ ,...). The products were washed, dried at room temperature and first characterized by XRD. According to their di- or trioctahedral nature, their powder diffraction patterns show a (060) band at nearly 1.49 Å or 1.53 Å, respectively. Solid state MAS NMR spectroscopy is a very good tool to study these products (4). ^{29}Si MAS NMR authorizes a good determination of tetrahedral Si/Al ratio for layer silicates as synthesized and the observed chemical shifts (relative to TMS) at nearly - 92.6, - 88 and - 83 ppm for dioctahedral ones and at nearly - 95 ppm for trioctahedral ones confirmed their nature according to literature's data. ^{27}Al MAS NMR allows an evaluation of the $\text{Al}_{\text{IV}}/\text{Al}_{\text{VI}}$ ratio but the results should be considered with care according to possible quadrupolar interactions (5). The ^{19}F MAS NMR is a new way to study F for OH substitutions in relationship with the nature of the layer silicates (di- or trioctahedral) and the octahedral layers composition. ^{19}F MAS NMR signals at nearly - 176 ppm and - 132 ppm (relative to CFCl_3) may be easily attributed to structural fluorine in trioctahedral - Mg layer silicates and dioctahedral - Al ones, respectively. Fluoride medium synthesis and ^{19}F MAS NMR are new ways to synthesize 2:1 layer silicates and study their octahedral layers composition.

Références :

- (1) BARRER, R.M. and DICKS, LWR (1967), J. Chem. Soc. (A) , p. 1523-1529
- (2) TORII, K. and IWASKI, T. (1986), Chem. Lett., p. 2021-2024
- (3) GUTH, J.L. et al. (1989), Zeolite Synthesis, ACS Symposium Series, 398 (13) , p. 176-195
- (4) SANZ, J and SERRATOSA, J.M. (1984) J. Am. Chem. Soc, vol. 106 , p. 4790-4793
- (5) WEISS et al. (1987), Am. Miner. vol. 72 , p. 935-942.

HYDROPHOBICITY OF SILOXANE SURFACES IN SMECTITES AS REVEALED
BY AROMATIC HYDROCARBON ADSORPTION FROM WATER

W. F. Jaynes*, and S. A. Boyd

Crop & Soil Science Department, Michigan State University,
East Lansing, MI 48824

The adsorption of aromatic hydrocarbons from water by organo-clays was used to evaluate the nature of the siloxane surfaces in smectites. Organo-clays were prepared by replacing the hydrophilic, inorganic exchange cations of a series of smectites with the small, hydrophobic organic cation, trimethylphenylammonium (TMPA). Smectites with a range in charge densities were used which resulted in different TMPA contents in the organo-clays. Adsorption isotherms of benzene, alkylbenzenes, and naphthalene from water by the TMPA-smectites indicated that sorption was inversely related to TMPA content. The Langmuir form of the isotherms suggests that the aromatic compounds adsorb to the clay surface. Possible adsorptive sites in TMPA-smectites are limited to the TMPA cations and the siloxane oxygen surfaces. Because sorption increased as layer charge and TMPA content decreased, the organic compounds must adsorb to the siloxane surfaces.

Calculations based on an adsorbed compound monolayer, which was estimated by fitting adsorption data to the Langmuir equation, and the N₂ specific surface area of each TMPA-clay indicate, that the surface area occupied by each adsorbed molecule increases as the planar area of the molecule increases. This suggests that the planar surfaces of the compounds adsorb directly to the clay surface. Apparently, the TMPA cations function to keep the smectite interlayers open. Interactions between the phenyl groups of the TMPA cations on opposing interlayer clay surfaces may act to increase the size of the adsorptive regions. These results show that the siloxane surfaces of smectites can effectively adsorb aromatic hydrocarbons from water if the hydrophilic, inorganic exchange cations are replaced with small, hydrophobic organic cations.

The glass-to-smectite alteration of tektites at the Cretaceous/Tertiary boundary
 Jéhanno C., Bonté, Ph., Froget L., Robin E., Rocchia R., Sigurdsson H., Centre des Faibles Radioactivités CEA/CNRS, 91198 Gif-sur-Yvette, France.

The K/T boundary mass extinction has probably been produced by the collision of a huge asteroid or a comet. The collisional scenario implies that a significant mass of target material has been dispersed on a wide geographical scale. This ejecta is not easily identifiable in most sections. However, in North American sections the boundary is marked by a 1-2 cm thick exotic clay layer which suggests that the collision occurred in a nearby site. The presence in the section of Beloc (Haïti) of a 20-50 cm thick glass spherule bed provides additional support to this view and points to a collision in the Caribbean area. The section has been first described by Maurrasse (1). The tektite-bearing Haiti layer of impact ejecta is associated with other K/T boundary markers (Ir, magnesioferrite and shocked quartz), but these components are not found inside the glass spherule layer, but just above it (2). The glassy spherules have been shown to be tektites, consisting of two compositional types (3), representing fusion of continental crust and evaporite deposits. The very good preservation of the tektites provides the opportunity to study the composition of the target material and its alteration products.

Glasses: The spherules consist of a glass core, surrounded by a smectite shell. About 98% of the glasses have a high-silica composition and 2% are highly enriched in Ca and S. These two types of glasses give constraining conditions about the location of the impact and indicate an continental crustal source with a significant contribution from an evaporitic deposit (4). The $^{87}\text{Sr}/^{86}\text{Sr}$ values of glasses fall on a mixing line with two end-members: one with a high isotopic ratio (0.7095; high-silica glass) and the other with the isotopic signature of a late Cretaceous marine deposit (0.7080; high-Ca glass).

Clay mineralogy: At the site which shows least reworking (B1), the top and base of the spherule layer are lighter in colour and contain abundant smectite and a significant fraction of clinoptilolite. The center of the layer, 15-20 cm thick, consists of nearly pure smectite spherules, resulting from the alteration of the original glass spherules. Chemical composition and X-ray diffraction indicate that the smectite is iron-beidellite. At site B2, the unaltered glass cores are surrounded by a thin (10 micron) layer of palagonite, the beidellite precursor, and the palagonite is in turn encased in a thick smectite shell. The palagonite is amorphous, isotropic and forms thin lamellae. The smectite is massive, generally yellowish brown in colour.

Chemistry: The alteration of glass to smectite has resulted in significant chemical changes. In the alteration products, Fe and Mg are enriched with respect to the glass, whereas Ti, Al and Si show no significant change. On the other hand, Ca, Na and K are highly depleted in the smectite with respect to the glass, by a factor of ten or more. The composition of palagonite is generally similar to that of the glass. The glass-to-smectite alteration has resulted in major remobilization of trace elements, notably REE. Rare earth content of smectite is generally order of magnitude lower than in the source glass (Fig.), but the REE pattern is very similar to that of kaolinite claystone from continental K/T boundary sites in North America (5). We suggest that the precursor of the KT boundary clay is in general tektite glasses of the type found in Haiti.

REFERENCES: (1) Maurrasse et al., *Transactions of the Fourth Latin American Geological congress*, 328-337, 1979. (2) Jéhanno et al., *Proc. Lunar Planet. Sci. Conf.* 22, 641-642, 1991. (3) Sigurdsson et al., *Nature* 349, 482-487, 1991. (4) Sigurdsson et al., *Nature*, submitted 1991. (5) Izett, *Geol. Soc. Amer. Spec. Paper* 249, 1990.

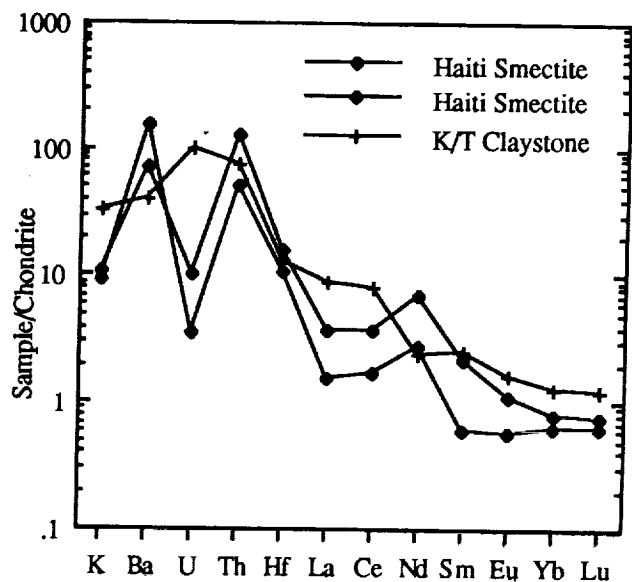


Figure: Chondrite-rare earth and other trace element patterns in Haiti smectites, compared to kaolinite claystone from the K/T boundary in the Raton Basin.

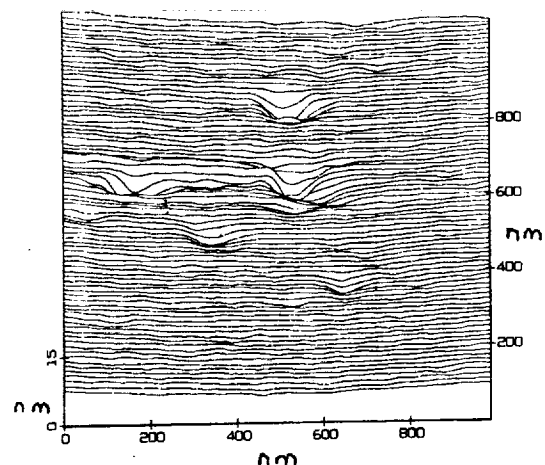
AFM STUDY OF THE SURFACE MORPHOLOGY OF MUSCOVITE DISSOLVED IN WATER.

Johnsson, Patricia A. (Applied Earth Sciences Dept., Stanford Univ., Stanford, CA 94305);
Blum, Alex E. (U.S. Geological Survey, 345 Middlefield Rd. MS420, Menlo Park, CA
94025); Hochella, Michael F. Jr. (Dept. of Geology, Stanford Univ., Stanford, CA 94305)

As part of a study of muscovite surface reactivity, we have used the atomic force microscope (AFM) to image in air the surface topography of the basal (001) surfaces of muscovite which were freshly cleaved and then exposed to deionized water for time periods ranging from 2 hours to 10 days. Freshly cleaved surfaces show atomically flat topography with no pits at any scale. Within a few hours, small (<100 nm diameter, <5 nm deep) pits appeared in some locations on the surface. The figure below is a surface line plot of a typical muscovite cleavage surface dissolved in distilled water for 2 hours, with the axis in nm. Following 10 days of dissolution, pits with diameters 200 - 500 nm and <10 nm depth were abundant. The rapid formation of pits on the basal plane may provide an explanation for the high initial muscovite dissolution rates observed during the first hours of laboratory dissolution experiments¹. In addition, etch pit formation on the basal surfaces suggests that dissolution from the basal surface contributes to the overall muscovite dissolution rate. This raises questions about the commonly held idea that it is kinetically much more favorable to dissolve and precipitate on the edges of sheet silicates, rather than on the basal surfaces. However, the relative rates of basal versus edge dissolution remain to be determined.

The observed pits tend to occur in small clusters. The shape of the pits is approximately oval without any apparent crystallographic control of the pit shape. The lack of apparent spiral structures suggests that growth of the pits is not controlled by screw dislocations. Previous dissolution experiments indicate that Fe is preferentially released during muscovite dissolution with Fe/Al ratios ~ 5 times greater than the ratios in the muscovite samples^{1,2}. This suggests that the observed pits may result from preferential dissolution in regions with elevated levels of Fe impurity. XPS (X-ray photoelectron spectroscopy) analysis of fresh cleavage surfaces indicates that Fe is present in this muscovite.

The basal surface of muscovite commonly is used as an AFM standard because of its atomic-scale flatness and the ease with which molecular-scale images may be reproduced. However, the observed reactivity of the basal surface suggests that caution is warranted in using muscovite as an inert substrate for aqueous experiments.



- 1: Lin F. and Clemency C. V., 1981, *Geochemica et Cosmochimica Acta*, vol. 45, p. 571-576.
- 2: Huang W. H. and Keller W. D., 1970, *American Mineralogist*, vol. 55, p. 2076-2094.

QUANTITATIVE X-RAY DIFFRACTION ANALYSIS OF SOILS:
RIETVELD FULL-PATTERN MINERAL CONCENTRATIONS AND PATTERN
CURVE FITTING VS. P SORPTION OF BAUXITE SOILS

R. C. Jones and D. L. Bish

Dept. of Agronomy and Soil Science, Univ. of Hawaii, Honolulu, HI 96822
EES Division, MS D469, Los Alamos National Lab, Los Alamos, NM 87545

A suite of Hawaiian bauxites collected from a vertical section at a bauxite reclamation experimental site were analyzed by X-ray powder diffraction and by incremental additions of CaHPO_4 for their phosphate sorption capacities. ΔpH was determined as an assessment of positive charge on the Fe and Al-bearing minerals by measuring pH in 10:1 water and in 10:1 1N KCl. The pH values ranged from near neutral at the surface to 3.5 at 270 cm. ΔpH values ranged from 0.0 at the surface to 1.6 pH units at 270 cm. An index of net positive charge was taken as $\sinh(1+\Delta\text{pH})$ inasmuch as mineral pH-dependent surface charges describe a hyperbolic sine distribution.

Step-scanned X-ray diffraction patterns collected by $\text{Co K}\alpha$ radiation were analyzed by Rietveld refinement to obtain a quantitative measure of the minerals present. The patterns were then curve fit by use of computer program Pi'o Pili Pa'a. In all cases the peak profiles were fit with pseudo-Voigt functions, therefore, size broadening as associated with Cauchy widths was distinguished from strain broadening which is associated with Gaussian widths. Gibbsite showed no size or strain broadening. The Scherrer equation was applied to the Cauchy portion of the goethite (110) peak for each sample. Goethite percentages found by Rietveld refinement were divided by the mean goethite needle circumference found by curve fitting. These values were then added to 10% of the gibbsite percentages found by Rietveld refinement to approximate crystallite edge effects.

Without taking into consideration the effect of positive charge, the correlation of P sorption with goethite surface area index or of gibbsite edges or of the sum of goethite and gibbsite, was poor. When taken as the product of the sum of the effects of mineral surface areas and positive charge ($\sinh(1+\Delta\text{pH})$), there was a very good correlation with P sorption.

Our conclusions are: In order to use X-ray diffraction to explain chemical properties of soils, quantitative techniques such as Rietveld refinement must be used first to determine the mineral concentrations. By peak parameter refinements, mean indices of surface area can be estimated. Differences in concentrations of surface OH groups can then be estimated. Finally, the determination of charge characteristics are necessary to determine the extent of surface OH protonation--the conversion of OH groups to HOH^+ sites that will react with anions.

THE SMECTITE TO ILLITE REACTION: FLUID & SOLIDS EVOLUTION UNDER FLOW-THROUGH CONDITIONS

Kacandes G.H., Barnes H.L. and Kump L.R.

Department of Geosciences, Penn State University, University Park, PA 16802

We are investigating the kinetics of the smectite to illite reaction using a hydrothermal flow-through apparatus. The flow-through design permits control of input solution composition and continuous monitoring of output solutions. Additionally, the present apparatus allows periodic sampling of solids without perturbing experiment conditions. Pressure is controlled independently of temperature by using a backpressure regulator. The reaction cell itself is cylindrical (100 cc) and capped by 2" diameter, $0.5 \mu\text{m}$, metal filters. The reactants inside are kept well-mixed by maintaining a fluidized bed and by rotating the reaction cell in a reciprocating fashion. This design minimizes concentration gradients that could lead to diffusion-limited kinetics.

We have reacted the 1-2 μm fraction of the Wyoming Bentonite (SWY-1, K^+ -saturated) with 0.05 M KCl solution ($\text{pH} \approx 7$) at 250 °C and 145 bars. The flow rate was 0.25 cc/min and the water/clay mass ratio in the cell was 80. Outlet concentrations of aqueous K^+ and H^+ remained near input values throughout the duration of the experiment. Mg^{2+} , ΣAl^{3+} , and $\text{SiO}_{2(\text{aq})}$ were released during reaction then stabilized at steady state concentrations (40 days). Stable values of $\log[\text{K}^+]/[\text{H}^+]$, $\log[\text{Mg}^{2+}]^{0.5}/[\text{H}^+]$, and $\log[\text{SiO}_{2(\text{aq})}]$ were 5.7, 4.9, and -3.4, respectively. In the bulk solids, the content of K, Mg, and Al increased with time, while the Si content decreased. XRD analyses of these same samples document the progressive reaction of smectite to illite. The initial smectite/illite produced was randomly ordered. This was later replaced by an R1-ordered phase and finally, at approximately 50 days, by 100% illite. The other phases identified were chlorite and boehmite. Stabilized aqueous activity ratios plot near equilibrium boundaries for these three phases. Quartz, a minor phase identified in the starting material, was not observed in the final products.

In this experiment, illitization occurred in the company of an undersaturated input solution; constituents of the product phases were derived from initial smectite and quartz. The illitization rate was considerably greater than published rates for closed-system experiments conducted at similar temperatures. By controlling input solution composition, the experiments of this series will be used to provide kinetic data on maximum rates of illitization. These data can be used to more effectively isolate the chemical and physical factors which influence illitization in sedimentary basins.

REHYDRATION OF RECTORITE: M. KAWANO and K. TOMITA

Dept. of Environmental Sci. & Tech., Faculty of Agriculture, Kagoshima Univ.
1-21-24, Korimoto, Kagoshima 890, Japan

The rehydration properties of Ca-, Mg-, Na-, and K-saturated homoionic rectorites were studied. The rehydrated materials were prepared as follows. The homoionic rectorites were heated at various temperatures for 1 hr and were maintained in a wet state for 1 day at room temperature. The rehydrated materials pre-heated at $<400^{\circ}\text{C}$ apparently recovered the same hydration states as those of original samples, whereas rehydrated materials which were pre-heated at $>500^{\circ}\text{C}$ exhibited quite different hydration states. The characteristic rehydration properties of the materials pre-heated at $>500^{\circ}\text{C}$ are: (1) the basal spacings of H_2O -, ethylene glycol-, and glycerol-complexes changed to about 22.5, 26.85, and 27.65\AA respectively, independently of saturating cations under 50% RH; (2) the Ca- and Mg-materials exhibited single layer hydrate under $<50\%$ RH, whereas K-material showed double layer hydrates at 80% RH; (3) the IR absorption spectra due to interlayer H_2O exhibited the same or very close absorption intensities and frequencies to each other; (4) the DTA-TGA indicated that the amounts of rehydrated H_2O approached about 4.2 Wt% with increasing pre-heated temperature; and (5) the interlayer cations of expandable layers were fixed by heating at $>500^{\circ}\text{C}$. These results represent that the effect of interlayer cation on formation of water layers in the interlayer space has been reduced by heating at $>500^{\circ}\text{C}$. This strongly supports the idea of rehydration mechanism of rectorite reported previously.

N 9 2 - 1 0 2 5 2

CLAY MINERALS IN PRIMITIVE METEORITES AND INTERPLANETARY DUST II. SMECTITES AND MICAS. L. P. Keller and M. E. Zolensky, Planetary Science Branch, NASA Johnson Space Center, Houston, TX 77058.

INTRODUCTION. In the accompanying abstract [1], we briefly summarized the classification of stony meteorites and cosmic dust, and described the mineralogy and chemistry of serpentine group minerals. Here we focus on the occurrence of smectites and micas in extraterrestrial materials.

The characterization of fine-grained minerals in meteorites and IDPs relies heavily on electron beam instruments, especially the transmission electron microscope (TEM). Typically, phyllosilicates are identified by a combination of high resolution imaging of basal spacings, electron diffraction, and chemical analysis. Smectites can be difficult to differentiate from micas because the smectites lose their interlayer water and the interlayers partly collapse in the high vacuum of the TEM. In HRTEM images, smectite basal spacings vary from 1 nm (fully collapsed) up to 1.5-nm, while micas show only 1- or 2-nm basal spacings.

SMECTITES. Smectites occur in CI, CM (rarely), CR, CV and ungrouped carbonaceous chondrites, ordinary chondrites, and in chondritic IDPs [2-9]. In CV and ordinary chondrites, and in IDPs, smectite is the dominant clay mineral present. Smectites are derived from a variety of precursors including olivine, pyroxene, feldspar, and glass. The smectites are Mg-rich and correspond to trioctahedral, Fe-bearing saponites with Na as the main interlayer cation. Saponite compositions extend from near end member saponite to ~ 60 mol% Fe-saponite. Smectites with the highest reported Fe contents are found in certain ordinary chondrites, where nontronitic smectites have been described [7]. Most of the saponites exhibit only a slight (<10%) dioctahedral character. The typical crystallite size (measured in TEM images) is ~500 nm perpendicular to the c- axis, but varies from <5nm up to several μ m. Unlike the serpentine group minerals, smectites often show crystallographic relationships to their host minerals. Saponite in CV chondrites commonly occurs in epitactic intergrowths with host olivine, such that the c-axis of saponite is parallel to the a-axis of olivine [5,10]. These intergrowths are texturally similar to terrestrial "iddingsite". Saponite also forms oriented intergrowths with pyroxenes (both high- and low-Ca), where the c-axis of saponite parallels the a-axis of pyroxene. This reaction is common because the saponite inherits part of the pyroxene structure during the reaction [4].

Smectites are typically associated with minor quantities of Fe-rich minerals such as FeNi-sulfides, magnetite, ferrihydrite, or maghemite; minor differences in the oxidation state during alteration control the mineralogy of these Fe-rich phases. Fine-grained carbonates, including calcite, magnesite-siderite solid solutions, and dolomite are also commonly associated with smectites.

MICAS. Micas have only been reported from CV chondrites where they occur in Ca- and Al-rich inclusions and olivine aggregates. Micas in these meteorites are compositionally heterogeneous with both di- and trioctahedral types present. Several micas have been described including Na-phlogopite, margarite, clintonite, and muscovite. Na and Ca are the main interlayer cations. Electron diffraction shows that different mica polytypes are present; phlogopite and clintonite occur as 1M polytypes while mixed 1M and 2M polytypes are present in margarite. The Na-phlogopite occurs in coherent intergrowths with minor aluminous serpentine. Like the smectites, micas show crystallographic relationships to their hosts; for example, margarite occurs as oriented lamellae in anorthite and the (001) planes of phlogopite parallel the (100) planes of pyroxene. Petrographic evidence and thermodynamic calculations indicate that the micas in CV meteorites result from gas:solid reactions at relatively low temperatures (400-500K) early in the history of our solar system [11]. It is unclear whether the aluminous serpentines result from gas:solid reactions like the micas or if they result from a later aqueous alteration event.

REFERENCES. [1] Zolensky and Keller, this volume. [2] Tomeoka and Buseck (1988) GCA 52, 1627. [3] Zolensky (1991) Meteoritics, in press. [4] Keller and Buseck (1990) GCA 54, 2113. [5] Tomeoka and Buseck (1990) GCA 54, 1745. [6] Zolensky and Lindstrom (1992) Proc. 22nd Lunar Planet. Conf., in press. [7] Alexander, C. *et al.* (1989) GCA 53, 3045. [8] Thomas *et al.* (1991) Lunar Planet. Sci. Conf. XXII, 1395. [9] Bradley (1988) GCA 52, 889. [10] Keller and Thomas (1991) Lunar Planet. Sci. Conf. XXII, 708. [11] Keller and Buseck, (1991) Science 252, 946.

Electron Spin Echo Modulation Studies of Transition Metal Ions
In Pillared and Nonpillared Smectite Clays

Larry Kevan
Department of Chemistry
University of Houston, Houston, Texas 77204-5641

Electron spin echo modulation (ESEM) can measure weak electron-nuclear dipolar interactions in powders, and is becoming increasingly useful for probing the surroundings of paramagnetic transition metal ions in a variety of oxide surfaces of catalytic importance. The following examples the detailed structural information from ESEM about ion location and coordination in smectite clays.

ESR studies on $[\text{Pd}(\text{NH}_3)_4]^{2+}$ -doped Al_{13} -pillared Laponite clay activated in flowing oxygen at 250 to 500 °C indicate that Pd(III) is generated at the lower activation temperature and that Pd(I) is generated at the high activation temperatures. ESEM analyses indicate that at low activation temperatures a Pd(III) species is located close to an Al_{13} -pillar in the interlayer space and that it migrates from the Al_{13} -pillar at higher temperatures. At still higher temperatures Pd(I) is increasingly formed and migrates to a hexagonal pocket of the tetrahedral sheet of a tetrahedra-octahedral-tetrahedral three-sheet Laponite layer where it interacts with ${}^7\text{Li}$ nuclei in the central octahedral sheet.

Fluorohectorite containing lattice Cu(II) has been synthesized and characterized by ESR and ESEM spectroscopy. Three Cu(II) species termed A, B and C are identified. From ESEM measurements Cu(A) and Cu(B) are assigned to Cu(II) in octahedral sites without and with neighboring Li(I), respectively. Cu(C) is assigned to coordinatively unsaturated Cu(II) at edge sites of the crystallites.

Radiolytic reduction of Ag(I)-exchanged synthetic beidellite generates two paramagnetic Ag(0) species termed A and B. By ESEM analysis Ag(A) interacts with Al(III) in the tetrahedral sheet and is coordinated to only two water molecules. Thus Ag(A) is near one surface of the beidellite interlayer in which the Ag(A) is coordinated to two basal surface oxygen atoms and two water molecules at all levels of hydration. Analysis of Ag(B) indicates direct coordination to four water molecules and no interaction with Al within 0.6 nm. Thus Ag(B) is located more in the center of the interlayer space.

CORRELATION OF X.R.D. CRYSTALLINITY AND T.E.M. CRYSTAL SIZE OF SYNTHETIC MICA.

R.E. Klimentidis, W.L. Huang, D.R. Pevear.

EXXON Production Research Co., P.O.Box 2189, Houston, TX 77001

Mg-micas with a variety of crystallinities were synthesized from SWy-1 montmorillonite in 0.6M KHCO_3 (solution/rock mass ratio of 5) at temperatures ranging from 275 to 450°C using gold capsules at 500 bars in cold-seal pressure vessels. The crystallinity index in terms of degrees two-theta of the neoformed Mg-mica 001 peak first increases rapidly from 1.5 for 5 hours run duration to 0.53 for 3 days, then slowly to 0.38 for 110 days at 400°C. Similar kinetic behavior has been observed at different temperatures which show that the crystallinity increases with temperature at constant time. The experimental results confirm that both temperature and time are major factors influencing the crystallinity of mica. Electron microscopy and X-ray diffraction analyses were used to study the mechanisms of mica re-crystallization.

T.E.M. observations show good correlation between mean particle thickness obtained by high resolution lattice imaging ($n= 4$ to 23) and the Kubler index (from 1.25 to 0.38°2 θ). X-ray diffraction peak fitting and particle size analyses using Warren-Averbach and NEWMOD processing techniques are under investigation to test agreement between observed particle thickness distribution (crystallite thickness under the T.E.M.) and X-ray diffraction calculation from peak width measurements. Preliminary results show peak width and spacing calculated by NEWMOD, using T.E.M. data for n , match those of the experimental patterns.

Other particle dimensions such as length, width, equivalent diameter, and area demonstrate that mica crystallites grow larger and more euhedral with increasing thickness. Particle shapes vary from anhedral or rounded to sub-equant euhedral. In each sample a portion of the grains displays partially rounded to well-rounded outlines suggesting that some dissolution is taking place. This observation may be in agreement with the Ostwald ripening process.

MÖSSBAUER SPECTROSCOPY ON THE SURFACE OF MARS

G. Klingelhöfer¹, J. Foh¹, P. Held¹, H. Jäger¹, E. Kankeleit¹, R. Teucher¹, E.N. Evlanov², V. Khromov², L.M. Mukhin², O.F. Prilutski², B. Zubkov², G.V. Smirnov³, J. Juchniewicz⁴, J.M. Knudsen⁵, M. Madsen⁵, C. d'Uston⁶

¹Institut für Kernphysik, Technical University Darmstadt, 6100 Darmstadt, Germany; ²Space Research Institute, USSR Academy of Sciences, Moscow, USSR; ³Kurchatov Institute of Atomic Energy, Moscow, USSR; ⁴Space Research Center, Polish Academy of Sciences, Warszawa, Poland; ⁵H.C.Oerstedt Institute, University of Copenhagen, Denmark; ⁶Centre d'Etude Spatiale des Rayonnements, Toulouse, France;

The elemental composition of Martian soil was determined by x-ray fluorescence analysis during the Viking mission, but not its mineralogical composition. One believes, that the Martian surface is composed mainly of iron-rich clay minerals, with an iron content of about 14(±2)%. Also the experiments indicate that the soil contains about 5 wt.% of a strongly magnetic mineral, probably maghemite (Fe₂O₃) or magnetite (Fe₃O₄). Of extremely great interest is the oxidation state of the iron and the mineral composition of the Mars surface. These two questions can be answered by Mössbauer spectroscopy.

The Mössbauer spectrometer will be installed on a Mars Rover. The main parts of this system, proposed for the Mars-94/96 mission of the USSR, are the electromechanical vibrator, the detector system consisting of silicon photodiodes, the electronics for the driving unit and the detector, and a multilayer radiation shield for the ⁵⁷Co Mössbauersource.

The weight (~50g) and dimensions (length ~45mm; diameter ~20mm) of the new velocity transducer are drastically reduced in comparison to standard systems.

The proposed detector system consists of at least 4 silicon-diodes, each of them provided with its own preamplifier-amplifier-ADC-circuit, because of noise reduction and required high energy resolution. For Mössbauer spectroscopy applications standard PIN-photo-diodes (useful energy range between ~4 keV and about 100 keV) are sufficient. But for the interpretation of the Mössbauerspectra it is important to resolve at least the Ti x-ray's (4.51 keV) to determine its amount. This application needs improved silicon-photo-diodes or other high resolution x-ray detectors. Besides Mössbauerspectroscopy this system allows simultaneously X-ray fluorescence measurements. Also the possibility of measuring vibrations transferred to the Mars-rover and therefore the Mössbauer Spectrometer, in using the drive control signal, is in discussion.

The whole system is controlled by a Transputer.

This work is partly supported by DARA and BMFT (Germany).

References

- [1] J.M. Knudsen, S. Moerup, J. Galazha-Friedman, *Mössbauer Spectroscopy and the Iron on Mars*, Hyp.Int. 57(1990)2231
- [2] E.N.Evlanov, L.M.Mukhin, O.F.Prilutski, G.V.Smirnov, J.Juchniewicz, E.Kankeleit, G.Klingelhöfer, J.M.Knudsen, C.d'Uston, *Mössbauer Backscatter Spectrometer for Mineralogical Analysis of the Mars Surface for Mars-94 Mission*, in: Lunar and Planetary Science XXII, Houston, USA, March 1991
- [3] J. Foh, P. Held, H. Jäger, E. Kankeleit, G. Klingelhöfer, U. Imkeller, *Mössbauer Spectrometer for mineralogical Analysis of the Mars Surface*, XVI General Assembly of European Geophysical Society, Wiesbaden, April 1991, Annales Geophysicae Supplement to Vol.9

Weathering of impactite from Monturaqui: C. Bender Koch.

Laboratory of Applied Physics, Technical University of Denmark,
Lyngby, Denmark

The Monturaqui meteorite crater in Chile is situated at very high altitude (ca. 3500 m) in a climate which presently is very dry.

Previous investigations of the impact material have revealed the presence of Fe/Ni metal spherules of various size imbedded in the glassy phase.

Fe/Ni oxides formed from weathering of metal spherules are present along cracks and linings of vacuoles. Average composition of the oxides is 90 wt. % Fe_2O_3 and 10 wt. % NiO. In addition to Fe and Ni, the oxides contain small amounts of Si possibly adsorbed to the surface of the oxides. Although weathering of the glass cannot be observed the Si in the Fe/Ni bands presumably originates from this phase rather than from a percolating solution.

K/T boundary at Stevns, Denmark: C. Bender Koch and S. Storgaard Jørgensen
Laboratory of Applied Physics, Technical University of Denmark, Lyngby,
Denmark

The mineralogy of the K/T boundaries has attracted much interest due to the controversy on the cause of the mass-extinction at/or close to this boundary: Was it due to an extraterrestrial body impacting of the Earth or due to increased terrestrial volcanic activity? Both scenarios possibly would effect huge masses of inorganic materials and important clues to a detailed evaluation of the two explanations might thus be hidden in the inorganic mineralogy of these boundaries.

Earlier investigations have shown that smectite-type minerals dominates both the $< 2\mu\text{m}$ fractions of the K/T boundary itself and also the surrounding limestones. This resemblance has been taken as indication of a terrestrial origin of the clay minerals.

One study has designated the clay mineral in the boundary layer as a beidellitic montmorillonite. In this study we have characterized the clay minerals using Mg, K and Li saturations and find only evidence of montmorillonitic layers.

Other important minerals of $2 < \mu\text{m}$ fractions are apatite and goethite (at the boundary only).

INFRARED STUDY OF STRUCTURAL OH IN GOOD AND POORLY CRYSTALLINE KAOLIN AND IN THEIR "DEFERRATED" PRODUCTS AT 300 K^o

Kocsardy, E. and Shaffer, N. R.

Geological Sciences Department, Indiana University, Bloomington, Indiana, USA

The Fe position in kaolinite was investigated by chemical dissolution techniques and infrared spectroscopy, using both traditional IR spectrophotometer and FT-IR spectrometer. Well crystallized English China clay (Hinkley Index [HI]=0.810, total Fe₂O₃=1.33%) and Cretaceous age Georgia kaolin (HI=0.922, total Fe₂O₃=0.365%) have four bands in OH region (3695 ± 3; 3670; 3653; 3620 cm⁻¹). Two poorly crystalline kaolins, one from Jari Brazil (HI=undetectable; total Fe₂O₃=1.78%) and one Tertiary age kaolin from Georgia (HI=0.202, total Fe₂O₃=0.87%) have three bands (3692 ± 2; 3653; 3620 cm⁻¹) and a shoulder at 3669 cm⁻¹. Only in Brazilian fine, secondary, weathered kaolin can be detected γAlOHFe at 3604 ± 4 cm⁻¹ and δAlOHFe at 879 cm⁻¹ respectively.

The position of inner hydroxyl at 3620 cm⁻¹ is very stable, it doesn't change with "crystallinity, Fe content, or deferration process.

The position of inner surface hydroxyl at 3692 is increased to 3698 cm⁻¹ in the poorly crystalline kaolinite, indicating changes in H-bonds lengths. The "deferration" process produces no difference on the position of inner surface OH groups. The position of the 3670 and 3653 cm⁻¹ bands are stable independent of crystalline state or deferration.

The AlOHFe bands at 3604 (γAlOHFe) and (δAlOHFe) were detected in the Jari Brazil kaolin with total Fe₂O₃=1.78 and "structural" Fe₂O₃=1.5%. The position of AlOHFe bands are stable after the deferration process. The SiO out of plane bands position at 1100 cm⁻¹ were changed only in good crystalline kaolin (English China Clay and cretaceous Georgia) shifting this band to 1115 cm⁻¹.

Using intensity ratios of γOH bands three K "crystallinity" indexes can be calculated. Based on several hundred measurements after^{2,3} an evaluation table for the relationship of K-indexes can be constructed and estimation of five classes or degrees of order (very good, good, moderate, poor, very poor) in kaolinite can be made.

From study of γOH bands intensity in IR spectra can be made a classification of our samples: in the English China clay and cretaceous Georgia kaolin the degree of order is between good and very good, and in Jari, Brazil moderate to good and the Tertiary Georgia kaolin shows a poor degree of order.

After the magnetic and chemical separation the degree of order in "deferrated" samples doesn't change-inside of the error of measurement-indicating, that the usual industrial separation does indeed clean the iron-bearing phases between and on the kaolin platelets, but does not affect "structural" iron closed in the kaolinite framework.

References:

1. E. MENDELOVICI, S. H. Yariv (1979) Iron-bearing kaolinite in Venezuelan laterites: Clay Minerals (1979) 17, 323.
2. E. KOCSARDY, A. HEYDEMANN (1980) Characterisation of kaolin minerals of different origin: Acta Miner.-Petr. XXIV/1980 p. 91-99.
3. M. FOLDVARY, E. KOCSARDY (1982) Factor influencing the IR spectrometric determination of crystallinity state of kaolinite: Hungarian Geology Inst. 1982 p. 417-422.

SOIL FORMATION AS A SOLUTE SOURCE FOR STREAM WATER

Kornegay, Celeste J. and Donahoe, Rona J.

Department of Geology, The University of Alabama,
Tuscaloosa, Alabama 35487-0338

The process of soil formation is being studied in a stream ecosystem in order to evaluate solute contributions to stream water chemistry from inorganic and organic processes. The stream basin is underlain by Pottsville sandstone bedrock and is located in the Plateau structural province of northern Alabama. Soil samples were collected vertically to depths of 48 inches and analyzed by X-ray diffraction (XRD). Bedrock was collected to obtain weathered and unweathered samples and analyzed by XRD. XRD analyses of the weathered and unweathered portions of the bedrock were compared with the soil XRD analyses to qualitatively determine the weathering products and possible weathering reactions. Petrographic and SEM data provided verification of weathering reactions suggested by the XRD work. Porous ceramic cup soil lysimeters installed at 24, 36, and 48 inch depths were used to collect soil water samples. Throughfall precipitation and stream water samples were also collected. Water samples were analyzed for cation and anion content, alkalinity, and pH.

A variety of clays and clay minerals are produced by chemical weathering of the sandstone. Primary feldspars (albite and microcline) are undergoing hydrolysis to form kaolinite, providing some sodium, potassium, and silicic acid to solution. Primary muscovite is apparently altering to illite with or without kaolinite. Chlorite is weathering to corrensite, releasing some iron to solution. Primary hematite is weathering to form goethite. Electron microprobe analyses of primary and secondary phases are in progress. Balanced chemical reactions will be written to quantitatively determine the contribution of solutes from chemical weathering.

Preliminary mass balance calculations indicate that inorganic weathering reactions alone cannot provide the concentrations of calcium, sodium, and magnesium observed in the stream water. These alkaline elements are observed to vary significantly with season in throughfall precipitation samples and have decreasing concentrations with depth in soil water. It is proposed that calcium, sodium, and magnesium are progressively removed from the soil solution with depth by adsorption mechanisms. These trends suggest that the primary contribution of calcium, sodium, and magnesium is from the leaf canopy and soil litter zone rather than chemical weathering. In contrast, silica concentrations in soil water are fairly uniform with depth. Despite significant biotic contribution of the more soluble elements, mass balance calculations indicate that relatively small dilutions are needed to derive the stream water chemistry from soil water.

K-AR, RB-SR ISOTOPES IN CLAY MINERAL RESEARCH IN CARBONATE ENVIRONMENTS

KRALIK, M.

**Environmental Geology, Geotechnical Institute, Federal
Research Institute-Arsenal, P.O.Box 8, A-1030 VIENNA,
AUSTRIA**

Potassium, Argon, Rubidium and Strontium are assumed to be more or less strongly bound in interlayer positions or more loosely attached to surfaces of clay minerals. K and Rb are in important cations in ubiquitous illites and glauconites as well as celadonites. Sr is more frequent in smectites and chlorites. Kaolinites and vermiculites incorporate these ions in traces only.

The still ongoing natural radioactive decay of the isotope ^{40}K to ^{40}Ar (half-life $T_{1/2}=1.25$ Ga billion years) and of ^{87}Rb to ^{87}Sr ($T_{1/2}=48.8$ Ga) offers the possibility to solve several time related problems in clay mineral research. In addition, the strontium isotope ratio $^{87}/^{86}$ can be used as tracer for interlayer exchange and recrystallization mechanisms in clay mineral research. Basically, these methods have been applied in clay mineral research for source area studies, for investigations of diagenetic interlayer exchange or recrystallization, for isotopic exchange in metamorphic, hydrothermal or tectonic events as well as tool in studies of clay mineral growth.

THE ROLE OF AL IN FE(II) TRANSFORMATION: Krishnamurti G. S. R. and Huang, P. M., Department of Soil Science, University of Saskatchewan, Saskatoon, Sask., Canada.

The ionic environment present in the soil system during the formation of Fe oxides, from Fe(II) liberated upon the weathering of primary minerals, is expected to have a profound influence on the kinetics of Fe(II) oxidation and the resultant precipitation products. The influence of anions on the kinetics of Fe(II) oxidation was earlier studied (1, 2). A few reports are available on the influence of cations (i.e., Ca, Mg, Mn, Al) on the nature of Fe oxides formed from the oxidation of Fe(II) solutions (3). However, no study has been carried out so far on the influence of Al, one of the most abundant cations present in soil environment, on the kinetics of Fe(II) oxidation. The influence of Al (as 0.1 M aluminum perchlorate) on the kinetics of Fe(II) (as 0.01 M ferrous perchlorate) oxidation was studied at pHs of 6.0 and 8.0 and different Al/(Al+Fe) molar ratios (0, 0.09 and 0.33), and both at the dissolved oxygen level of < 0.1 ppm and under ambient conditions. The nature of the hydrolytic products of oxidation was arrived at by XRD, IR spectroscopic and chemical analyses.

The presence of Al accelerated the Fe(II) oxidation, which followed first order kinetics with respect to the Fe(II) concentration. At pH 6.00, the rate constant increased from 0.20 to 0.42 min⁻¹ and from 7.06 to 7.32 min⁻¹ as the Al/(Al+Fe) molar ratio increased from 0 to 0.33 at the dissolved oxygen level of < 0.1 ppm and under ambient conditions, respectively. At pH 8.00, the corresponding increase was from 0.27 to 0.50 min⁻¹ and 7.50 to 14.26 min⁻¹, respectively. In the absence of Al, lepidocrocite with a small amount of goethite formed at pH 6.00 under ambient conditions and no precipitate was observed at the dissolved oxygen level of < 0.1 ppm; whereas maghemite was the crystalline product formed at pH 8.00, both at the dissolved oxygen level of < 0.1 ppm and under ambient conditions. At an Al/Al+Fe molar ratio of 0.09, goethite formed at pH 6.00 under ambient conditions, whereas no precipitate was observed at the dissolved oxygen level of < 0.1 ppm; lepidocrocite with a small amount of maghemite formed at pH 8.00 at the dissolved oxygen level of < 0.1 ppm, whereas maghemite formed under ambient conditions. Higher amounts of Al (Al/Al+Fe = 0.33) perturbed the crystallization processes resulting in the formation of poorly crystalline goethite under ambient conditions, and X-ray noncrystalline Fe oxides at the dissolved oxygen level of < 0.1 ppm at pH 8.00; whereas both at the dissolved oxygen level of < 0.1 ppm and under ambient conditions X-ray noncrystalline Fe oxides formed at pH 6.00. The perturbation of the crystallization processes of the oxidation products of Fe(II) increased with an acceleration of Fe(II) oxidation kinetics in the presence of an increasing amount of Al.

1. Krishnamurti G. S. R. and Huang P. M. 1991. *Clays and Clay Miner.* 39: 28-34.
2. Krishnamurti G. S. R. and Huang P. M. 1991. *Proc. 9th. Int. Clay Conf. (Strasbourg)* (in press).
3. Schwertmann U. and Taylor R. M. (1989) In: Minerals in Soil Environments, J.B. Dixon and S.B. Weed, eds., Soil Sci. Soc. Amer., Madison, WI, 379-438.

DECOMPOSITION OF X-RAY DIFFRACTION PATTERNS: A CONVENIENT WAY TO
DESCRIBE COMPLEX I/S DIAGENETIC EVOLUTION.

Bruno LANSON

U.S. Geological Survey; Mail Stop 404; Box 25046; Federal Center; Denver, Co, 80225

Most of the methods used to identify mixed-layered illite/smectite and to quantify their smectite content are based on the positions of mixed-layered XRD peaks. In XRD patterns of diagenetic samples the I/S 001 peaks frequently are overlapping with peaks of other phases, making it difficult to separate the different contributions to the diffraction pattern, which is an essential step for these methods. Other peak position methods also require measurements based on higher angle peaks which are difficult to perform routinely because of the low intensity of these peaks. Moreover, these methods are, to say the least, difficult to perform when there is more than one mixed-layer phase.

The decomposition treatment described in this paper includes smoothing, background stripping, and fit of elementary peaks on the experimental pattern. Each elementary peak, assumed to be symmetrical, is associated with a single clay phase.

The identification step is performed by comparing position-width values of elementary peaks fitted on experimental patterns with those measured on simulated patterns.

Some fundamental assumptions have to be kept in mind while using this powerful method in order to obtain valid results. However, this method, because of its minor experimental limitations, is a powerful and reliable tool to describe X-ray patterns.

Repetitive Occurrence of Potassic Diagenesis in the Region of the Upper Mississippi Valley (UMV) Mineral District: Implications for a Persistent Paleo-hydrological Setting Favorable for Diagenesis

Lee, M¹ and Aronson, J.L.²

¹Mobil Research and Development Corporation, P.O. Box 819047, Dallas, TX 75381;

²Department of Geological Sciences, Case Western Reserve University, Cleveland, OH 44106.

Several potassic diagenetic events have occurred within Paleozoic sandstones and bentonites in the Upper Mississippi Valley mineral district and the adjacent area on the northern edge of the Illinois basin. K/Ar ages of diagenetic illitic clays and K-feldspar fall into several groups: 400MA, 380-360 MA, 340MA, and less than 300 MA. Each episode is defined with distinct, but partly overlapping regions. The repetitive occurrence of potassic events suggests that the paleo-hydrological setting allowed basin-wide diagenetic fluids to be focused up into the district over a prolonged period of time.

The 400 MA episode is defined by ages of diagenetic K-feldspar in Ordovician tuffs and illitic clay and K-feldspar in the Cambrian Mt. Simon and Ordovician St. Peter Sandstones, and suggests that diagenetic fluids might have moved along the unconformity above the basement. The area affected by this event is extensive, several hundred kilometers in diameter. A younger diagenetic event at 360 MA is revealed by the ages of illitic clay (ordered I/S with 65-85% illite layers) in Ordovician K-bentonites in a smaller region of Minnesota, Iowa and Wisconsin, including the mineral district. Isotopic data indicate a cooler diagenetic temperature or isotopically heavier water for the 360 MA event as compared to the 400 MA event. Within the UMV mineral district, ages of the finest illitic clays from the Ordovician bentonites fall into a narrow range at 340 MA, while the coarser fractions give ages at 360 MA. The 340 million-year age illite also characterizes the finest clay fraction of the clay-rich and highly bioturbated Upper St. Peter samples within the UMV district. The 340 MA episode correlates with that of extensive diagenetic clay alteration reported for the Upper St. Peter samples in the Michigan Basin (e.g. Barnes et al., 1990), indicating that this episode affected a large area, from the northern Illinois Basin, across the Wisconsin Arch and into the Michigan Basin. Lastly, clays from the St. Peter sandstones at Shullsberg, Wisconsin, the most mineralized region within the district, give an even younger age, around 310-300 MA, that probably registers one of the main Pb-Zn mineralization events. Even younger diagenetic illite ages between 230-215 MA were found in the St. Peter and Mt. Simon sandstones of the nearby UPH wells, on the Wisconsin Arch.

This record of repetitive diagenetic alterations over a 200 m.y. period within the UMV district and the surrounding area is unusual compared to most cases reported in the literature. Apparently the paleo-hydrological setting of the UMV district has maintained a geometry favorable for the episodic movement of diagenetic fluids into this region. The timings of the episodes that triggered fluid flow in the continental interior coincide with that of the Acadian, Appalachian/Quachita orogenies and the opening of the Atlantic on the east and southeast continental margin.

ENVIRONMENTAL RESTORATION OF DOE SITES: R&D ISSUES RELATED TO CLAY SCIENCES*

S. Y. Lee

Environmental Sciences Division, Oak Ridge National Laboratory, Oak Ridge, Tennessee

The Department of Energy (DOE) of United States has started a major environmental restoration effort to reduce the environmental and health risks resulting from past low-level radionuclide waste disposal and management at more than 3,700 facilities across the country. The General Accounting Office has estimated that cleaning up the radioactive contamination produced over the decades by these facilities would take 50 years and cost \$200 billion or more. A group of scientists have identified five major categories of basic research needs for the environmental restoration: (1) environmental transport and transformations; (2) advanced sampling, characterization, and monitoring methods; (3) new remediation technologies; (4) performance assessment; and (5) health and environmental effects (DOE/ER-0482T¹). Some of these issues are directly or indirectly related to behavior of clays and minerals as components of soils and sediments or engineering materials. However, direct involvement of clay mineralogists on the environmental restoration R&D program has been limited. In this presentation, the scientific issues of the DOE Environmental Restoration Program will be discussed from a clay mineralogist's perspective. On-going investigations, such as a radiocobalt migration study at the Oak Ridge National Laboratory, an uranium contaminated soil decontamination demonstration program at Fernald, and a plutonium contaminated soil characterization study at the Nevada Test Site, will be discussed as examples of decontamination approaches for environmental restoration.

¹Basic Research for Environmental Restoration, DOE/ER-0482T, Office of Energy Research, U.S. Department of Energy.

*Research sponsored by Office of Technology Development, U.S. Department of Energy, under contract DE-AC05-84OR21400 with Martin Marietta Energy Systems, Inc.

SURFACE THERMODYNAMIC PROPERTIES OF SOME ILLITES: Li Z., Giese R., Eberl D., and van Oss C. J., Geology-SUNY 4240 Ridge Lea Road, Amherst, NY 14226

Interfacial phenomena, particularly at the interface between water and a mineral, are of great geological importance. These phenomena are determined by the surface thermodynamic properties of the solid and liquid acting across the interface. The surface thermodynamic properties of solids and liquids are characterized by the surface tension which is composed of two distinct factors: the apolar Lifshitz-van der Waals surface tension component (γ^{LW}) and the polar electron acceptor (γ^{\ominus}) and electron donor (γ^{\oplus}) properties as described by the Lewis acid/base theory. These quantities are accessible through the measurement of contact angles of liquid drops on solid surface by means of the Young equation. If such surfaces are not available, the cosine of the contact angle can be derived from measurements of the rate of capillary rise of the test liquid through a thin, uniform film of a powder using the Washburn equation. In addition to the surface tension properties, there are the electrostatic (EL) properties which can be measured separately by an electrokinetic experiment.

The illite samples in this study were: 1) the Silver Hill illite (IMt-1), 2) RM-30 and 3) SG-4 (the latter two samples are from the Silverton caldera, Colorado). The $< 2 \mu\text{m}$ fraction of each sample was separated by Stokes settling, and a thin layer was deposited on a clean glass slide from a 2% suspension in water. The slides were dried overnight and stored in a dessicator until needed. The illite samples were too porous for direct contact angle measurements so the technique of thin layer wicking was used. The test liquids were α -bromonaphthalene, diiodomethane, water, formamide, and ethylene glycol. The contact angles obtained from the wicking experiments were used to solve the Young equation for the surface tension components of each illite sample. These values (in mJ/m^2) along with the average particle thickness (in nm) as determined by a Warren-Averback analysis of the X-ray diffraction pattern are shown below. For comparison, surface tension values for the cleavage surface of muscovite and for an oriented film of SWy-1 (both by contact angle measurements) are shown.

Sample	thickness	γ^{LW}	γ^{\ominus}	γ^{\oplus}
Silver Hill	4.6	33.6	0.2	13.4
RM-30	10.4	29.2	0.2	10.3
SG-4	17.6	35.1	0.0	16.9
SWy-1	-	41.5	0.7	36.2
muscovite	-	36.8	0.05	61.9

All three illite samples have a small or zero Lewis acid surface tension parameter; they are primarily Lewis bases. The LW surface tension components for the illites lie below the values of muscovite and SWy-1, and the Lewis base parameters for the illites are substantially smaller than both SWy-1 and muscovite. Given these differences in γ^{LW} and γ^{\ominus} , it is difficult to see how the illites of this study could be considered as some sort of mixture of mica and montmorillonite. One simple explanation of the curious surface properties of these illites is that the outermost layer of each crystallite is different, either chemically or structurally (or both), from the bulk of the material.

CLAYS IN SEDIMENTS OF YAMATO BASIN, JAPAN SEA

Lo, Pei-hua and Tieh, Thomas T.
Department of Geology, Texas A&M University
College Station, TX 77843

Cored interval from Ocean Drilling Program Leg 127, Site 797, located in Yamato Basin of Japan Sea, consists dominantly of clays and clayey siltstones, with minor amounts of sandstones. The interval ranges in depth from 200 to 850 meters below the sea floor (mbsf), representing an age span of early Pliocene to early Miocene. The complete sedimentary sequence suggests that deposition evolved from a slope to a basin environment. Forty samples representative of all lithological types of the interval were selected and studied for mineralogical and textural characteristics in order to determine the origin and post-depositional alteration of these sediments,

Except for the few sandy samples, in which the sand is mostly of volcanogenic origin, all samples are dominated by clay-size particles. The clay fractions were separated and studied by x-ray diffraction and scanning electron microscopy methods, supplemented by analyses of cation exchange capacity and atomic absorption spectrophotometry.

Major constituents of the clay fractions are clay minerals, silica minerals, and feldspars; minor minerals include authigenic pyrite, zeolite, carbonates, and titanium oxides. In the more deeply buried, middle to late Miocene sediments, chlorite is the dominant clay mineral. In contrast, from late Miocene to early Pliocene, smectite and kaolinite become increasingly abundant. Associated with these changes are also depth-related opal-A \rightarrow opal-CT and opal-CT \rightarrow quartz transformations of biogenic silica. The occurrence of authigenic pyrite, zeolite, carbonates, and titanium oxides appears to be texturally controlled; these minerals form mostly in sands and silts where fluid-mineral interactions have been intensive.

Mineralogical variations in terrigenous in-put, especially the amount of volcanogenic materials, control the clay mineralogy of sediments of the Yamato Basin sediments. However, during burial, significant post-depositional alterations have modified the original mineralogy. The study of these modifications will provide useful information concerning clay diagenesis and its relation to basin evolution.

MINERALOGICAL MODIFICATIONS OF OIL SANDS DURING STEAM STIMULATION: POST-STEAM CORE FROM THE WABISKAW MEMBER, NORTHEASTERN ALBERTA

E.J. Longstaffe¹, B.N. Fialka² and G.A. Robb²

¹Department of Geology, University of Western Ontario, London, Ontario Canada N6A 5B7;

²AEC Oil and Gas Company, 2400, 639-5th Avenue, S.W., Calgary, Alberta T2P 0M9

Most technologies for *in situ* recovery of bitumen from Cretaceous oil sand and heavy oil reservoirs in northeastern Alberta involve hot water/rock interaction. One method utilizes cyclic steam injection to heat and mobilize bitumen. Potential for reservoir damage during steaming includes permeability loss related to formation of swelling clays, and partial dissolution of impermeable calcite-cemented sandstones which can be used to channel and confine injected hot fluids. In this paper, XRD data are used to document mineralogical changes that occurred in the Wabiskaw Member (basal Clearwater Formation) oil sands at a locality about 100 km north of Cold Lake, Alberta, during eighteen months of steaming. Post-steam core was obtained <2 m from the steam-injection well. Temperatures as high as ~275°C were achieved at the base of the reservoir, decreasing to ~100°C near its top at the start of each steam cycle.

Pre-steam Wabiskaw sands are composed of litharenite or feldspathic litharenite. Framework grains consist mostly of quartz, chert, feldspar (plagioclase > K-feldspar), and sedimentary plus volcanic rock fragments ± minor glauconite. Kaolinite is the most abundant cement, but siderite streaks are also common. Most calcite-cemented intervals are entirely bitumen-free. The clay fraction (<2 µm) is dominated by kaolinite (79%), with lesser amounts of illitic clay (13%) and minor amounts of chlorite (3%) and smectitic clay (4%). Their relative abundances do not vary significantly throughout the reservoir.

The upper portion of the post-steam core remains heavily saturated with bitumen (**unswept**), but the lower portion contains three zones which are bitumen-free (**swept**), consisting of a melange of sand, partially lithified sand fragments, and shaly clasts. The upper and lower portions of the core are separated by a calcite-cemented sandstone, as are two of the three zones within the swept interval. Siderite was not detected in the swept or unswept sands. A substantial decline in average feldspar content (10% vs 27%) and an increase in average clay content (16% vs 8%) of steam-swept versus pre-steam samples has occurred. In contrast, no significant differences in feldspar and total clay contents were observed between post-steam, unswept sands and pre-steam sands, probably due to lack of direct contact with steam in the former case. In the <2 µm fraction, both swept and unswept post-steam samples show a substantial increase in the abundance of illitic (40%, 33%) and smectitic clays (41%, 53%), and a decline in kaolinite content (14%, 9%), relative to pre-steam values. Bulk and <2 µm fraction mineralogies return to pre-steam values <0.5 m below the lowermost calcite-cemented sandstone. Steam was introduced immediately above this sandstone, and it remained effective as a vertical barrier to fluids.

Unswept portions of the post-steam core are characterized by an interstratified swelling clay with a superlattice diffraction at ~29-31Å (Ca-glycol). This clay shows variable behaviour upon drying, rehydration and heating in the K-saturated form. Most abundant, however, is a mixed-layer swelling clay (~80% smectitic layers) which does not collapse completely to 10Å upon K-saturation and heating to 107°C. This behaviour may result from development of poorly crystallized, Fe hydroxy-interlayer material in the swelling clay. Within the swept portion of the core, a similar mixed-layer swelling clay containing ~65-70% smectitic layers is present. However, no clay with a superlattice diffraction was detected in the swept interval. On average, the cumulative abundance of swelling clay layers in the swept portions of the post-steam core is much lower than in the unswept portion of the reservoir. This behaviour, and the concomitant increase in the abundance of 10Å clays in the swept interval, may reflect the influence of a proprietary steam additive, the greater availability of K⁺ from K-feldspar dissolution, and/or the higher temperatures achieved in those portions of the core directly contacted by steam.

STRUCTURAL STUDIES OF HYDROXY-ALUMINOSILICATE POLYMERS INTERCALATED IN HECTORITE BY SOLID-STATE ^{29}Si AND ^{27}Al NMR: Lou, G., Huang, P.M., and Ripmeester, J.A., Department of Soil Science, University of Saskatchewan, Saskatoon, Canada and Steacie Institute for Molecular Science, National Research Council of Canada, Ottawa, Canada.

Hydroxy-aluminosilicate (HAS) interlayered and hydroxy-Al interlayered hectorite were prepared by reacting $< 2 \mu\text{m}$ Ca-hectorite with HAS solution (1.4 mM Si and 3.0 mM Al) and hydroxy-Al solution (3.0 mM), respectively. The reaction products were examined by chemical analysis, x-ray diffraction, and infrared (IR) and solid-state ^{29}Si and ^{27}Al NMR spectroscopies.

HAS-hectorite complexes exhibited a basal spacing of 17.2\AA upon K-saturation and heating at 110°C for 2 h, which indicated an interlayer thickness of 7.6\AA . Differential IR spectrum showed that the dominant species adsorbed by hectorite from HAS solution was orthosilicate in nature. The adsorbed species had a Si/Al molar ratio of 0.48, which was in good agreement with the theoretical ratio for "proto-imogolite" (0.5).

Solid-state ^{29}Si NMR spectrum of HAS-interlayered hectorite showed a peak at -78.0 ppm, indicative of the presence of "proto-imogolite" structure, which was formed through the displacement of an orthosilicate group for three OH groups surrounding a vacant octahedral site in a gibbsite-like sheet of Al hydroxide. The Al in both HAS and hydroxy-Al interlayers was predominantly octahedrally coordinated as indicated by the strong ^{27}Al NMR peaks at 1.0 and 5.0 ppm, respectively. Very weak peaks at about 58 ppm were apparent in the ^{27}Al NMR spectra of both HAS and hydroxy-Al intercalated hectorite, which were attributable to the formation of a trace amount of tetrahedrally coordinated Al as a result of local alkalinity created during the preparation of HAS and hydroxy-Al solutions. The low peak area ratios of Al(4)/Al(6) (0.067 for HAS and 0.043 for Al interlayers) and low basal spacings (17.2\AA for HAS and 13.7\AA for Al interlayers) suggested that hydroxy- Al_{13} was not the dominant species adsorbed. Rather, the interlayer thickness of 7.6\AA as shown by x-ray diffraction analysis was consistent with the thickness of a "proto-imogolite" fragment, i.e., the overall thickness of a gibbsite-like sheet of Al hydroxide and Si tetrahedra attached to one of its 001 faces.

The present solid-state NMR evidence substantiated the evidence of the intercalation of "proto-imogolite" in hectorite.

IMPLICATIONS OF CLAY-WATER ISOTOPIC EXCHANGE DURING BURIAL DIAGENESIS OF SHALES - A MODELING PERSPECTIVE

Lundegard, P. D.

Unocal Science and Technology, 376 S. Valencia Ave., Brea, CA 92621

Pore waters of sedimentary basins generally differ in their isotopic composition from the initial, or depositional, pore waters. Multiple processes can affect the post-depositional isotopic composition of pore water in basins. These processes include solution-reprecipitation, membrane filtration, and fluid mixing. Many shales contain more structural oxygen in clay minerals than in the water molecules which occupy their pore space. It is widely known that the expandable clays in shales undergo mineralogical change during burial which according to current theories results in isotopic exchange with the pore water. This isotopic exchange between clay and water during shale diagenesis can have a very significant impact on both the oxygen and hydrogen isotopic composition of pore water in compacting, shaly basins containing reactive detrital clays. The possible consequences of clay-water isotopic exchange are evaluated via a simple computer model for a range of initial clay and water isotopic compositions, geothermal gradients, reactive clay fractions, porosity-depth relationships, and isotopic exchange scenarios.

For fractional exchange scenarios, where isotopic exchange is implicitly linked to the progress of the illite/smectite reaction, the isotopic composition of pore water is mostly dependent on the initial isotopic composition of the reacting clay and the amount of reactive clay in the shale. The final pore water composition is only weakly influenced by the initial pore water composition when the reactive clay fraction exceeds 0.5. Changes in the bulk clay oxygen isotopic composition of more than 3 per mil are not likely to be produced by closed system clay diagenesis if the reactive clay fraction exceeds 0.5. Consideration of fractional, total, and punctuated exchange scenarios suggests that the temperature trends in bulk clay isotopic composition will be similar. However, these exchange scenarios will produce different isotopic distributions at a given temperature.

Depletion of the hydrogen isotopic composition of basin pore waters, relative to their initial composition, is often attributed to the influx of meteoric water. It can be shown, however, that hydrogen isotopic depletions of 10 to 15 per mil can readily be produced by isotopic exchange during shale diagenesis.

Depth Related Changes in Clay Mineralogy from Frio Formation (Oligocene) Shales, Cameron, Kenedy, and Nueces Counties, Texas.

F. Leo Lynch, Department of Geological Sciences, The University of Texas at Austin, Austin Texas, 78713.

The <1 um fraction of shale cuttings from three central and south Texas Gulf coast wells were analyzed by X-ray diffraction in order to investigate the composition and diagenetic modification of the clay minerals. The wells studied are the Atlantic #1 Mustang Island from Nueces county, the Mobil State Tract #406 from Kenedy county, and the Shell #1 Continental & Fee from Cameron county. The depth range investigated is 7145 ft. to 18,085 ft. Based on the 52 samples analyzed, the clay mineralogy of the <1 um fraction of an "average" Frio shale is 68% mixed-layer illite/smectite (I/S), 17% discrete illite, 7% chlorite, and 8% kaolinite, however, these values are highly variable. There is noticeably less illite and more kaolinite present in the samples from Nueces county.

The composition of the I/S changes from R=0, 40-75% I in the more shallow samples to R>1, 70-85% I in the deeper samples. The change from random to ordered interstratification occurs close to the depth of geopressure in all three wells. Below this depth the composition of the I/S changes very little. There is an increase in the molar abundance of I/S with depth in the samples from Nueces and Cameron counties. The molar abundance of I/S from Kenedy county remains essentially unchanged.

The molar abundance of chlorite decreases slightly with depth in Nueces and Cameron counties and increases slightly in Kenedy county. The molar abundance of discrete illite increases slightly in Kenedy county and shows a significant decrease in the other two wells. The molar abundance of kaolinite also shows a significant decrease in Nueces and Cameron counties.

A few shallow Miocene age samples from the Cameron county well were also analyzed. The I/S from these samples ranges from 10-60% I and is always R=0. The molar abundances of I/S and illite are unchanged with depth and the amounts of chlorite and kaolinite increase.

SWELLING POTENTIAL AND MINERALOGICAL COMPOSITION OF CLAY-SULFATE ROCKS

Fritz T. Madsen and Rolf Nüesch

Laboratory for Clay Mineralogy
Geotechnical Engineering
Swiss Federal Institute of Technology (ETH)

Since the construction of the first tunnels in Switzerland more than 100 years ago, problems with swelling rocks causing damage mainly by heave of the tunnel-floor and convergence of the abutments have been well known.

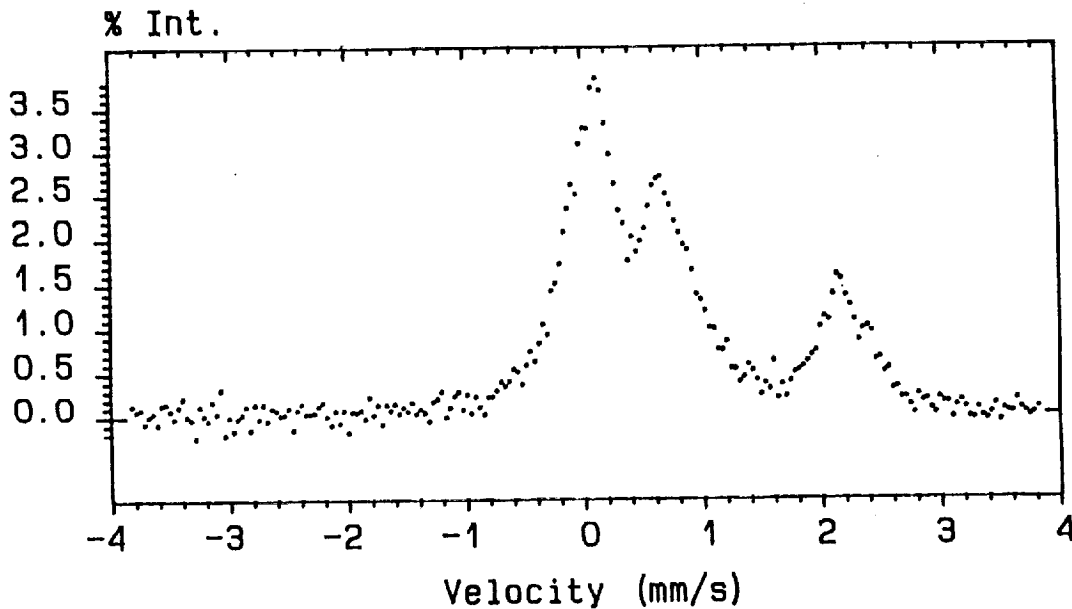
Swelling of rock is understood as a time dependent volume increase involving physico-chemical reactions with water. Whereas the swelling process of rocks containing only clay is well understood, the swelling process involving transition of anhydrite (calciumsulfate) into gypsum is not.

The swelling behaviour of clay-containing sulfate rocks, is, in addition to the influence of the overburden pressure, mainly dependent on the mineralogical composition and the texture of the rock. The clay-swelling process is stated as an osmotic uptake of water caused by differences in the ion concentration between the double layer of the clay particles and the pore solution. The swelling mechanism of clay-containing sulfate rocks also includes the transition of anhydrite to gypsum. The solubility of anhydrite in water is about 2.7 grams/liter and that of gypsum about 2.4 grams/liter. The transition of anhydrite into gypsum is therefore understood as a dissolution of anhydrite succeeded by a precipitation of gypsum. A complete transition of anhydrite into gypsum will cause a volume increase of about 60% if the water is added to the system. The solubility of anhydrite and gypsum is influenced by the presence of other ions such as sodium.

Rocks containing only anhydrite do not swell, whereas, rocks containing 5 percent clay may develop a swelling stress of more than 1 MPa. The maximum swelling potential was found in rocks containing 10 to 15 percent clay and 70 to 75 percent anhydrite. With this latter composition, a swelling stress greater than 4 MPa and swelling strain greater than 120% was determined after a testing time of 6 and 3 years respectively. Samples containing more than 15 percent clay tended to show a smaller swelling potential. The time-swelling behaviour is determined by the amount of clay and the texture of the rock. The investigation showed that a larger amount of clay caused a larger amount of anhydrite to convert into gypsum in the same period of time.

LOW TEMPERATURE WEATHERING OF BASALT: Madsen M. B., Vistisen L., Roy-Paulsen N. O., Koch C. B., Morup S., and Bentzon M. D., Physics Laboratory, H. C. Orsted Institute, Universitetsparken 5, DR-2100 Copenhagen O, Denmark

In arctic and antarctic regions a reddish stained rind is commonly observed on basaltic stones. Because the surface temperatures prevalent on Mars are similar to those of the polar regions on Earth, it is of interest to investigate weathering products of basalts from these regions. The surface varnish of a weathered piece of basaltic rock from Lindsay's Nunatak, Greenland has been studied by ^{57}Fe Conversion Electron Mössbauer Spectroscopy (CEMS).



^{57}Fe Conversion Electron Mössbauer Spectrum of arctic basaltic rock.

In this spectrum the ferrous components have the isomer shifts and quadrupole splittings typical of pyroxene and olivine. The ferric component(s) cannot be identified unambiguously by a room temperature spectrum alone. A detailed investigation of different fractions of the same rock by ^{57}Fe transmission Mössbauer spectroscopy, X-ray powder diffraction and electron microscopy showed that both pyroxene and olivine are present in the parent rock. But no crystalline ferric components were detected, that could explain the origin of the reddish rind. However, at low temperatures (5 K) transmission Mössbauer spectra of powdered samples from the reddish rind contained a broad lined component, whose Mössbauer parameters are similar to those of ferrihydrite. This assignment is corroborated by the ^{57}Fe Conversion Electron Mössbauer Spectrum.

TWO SCENARIOS FOR THE GENESIS OF THE KAOLINITIC VERTISOLS ON THE HAWAIIAN ISLANDS OF LANAI AND MOLOKAI

H. U. Malik and R. C. Jones

Dept. of Agronomy and Soil Science, Univ. of Hawaii, Honolulu, HI 96822

Soils classified as kaolinitic Vertisols occur on the islands of Lanai and Molokai in Hawaii. Soils clay minerals illite, interstratified illite/smectite, dehydrated halloysite, and a small amount of kaolinite have been identified (Malik, 1990). We have also found >10 percent illite in the soils in northeast Lanai. Since Hawaiian basalts, the most probable parent material, contain very little potassium, there is a question as to the origin of the illite found in the soils.

The first scenario is the importation of illite by tropospheric winds from the Asian Continent. There is growing evidence that quartz, mica, feldspars, and clay minerals are deposited as tropospheric dust on Hawaiian soils. Although the highest rates of deposition are in areas of high rainfall, the highest concentrations of illite is in areas that are relatively dry. Estimates from the literature place the rate of tropospheric dust deposition at 0.4 to 2.0 mm/10³ years over the open Pacific. If Lanai and Molokai received the same rainfall as the open Pacific, and using an age of about 1.5 million years for the islands, there could be a dust accumulation 1.44 to 1.75 meters thick. These figures, of course, ignore losses by erosion.

The second scenario is the illitization of smectite. During the glacial periods over the life of the islands, the sea-stand was below the shallow saddle between the islands of Maui, Lanai, and Molokai. There are several trachyte cones on West Maui that could have deposited ash and pumice in the saddle between the islands. Because smectite has been identified in an ash deposit of 1924 on the island of Hawaii, where fresh ash is produced continuously, we know that smectite can form rapidly under the right conditions. There is then a good possibility that smectite illitization has occurred as the result of trachyte weathering and potassium release under the estuary conditions that existed in the saddle. The clays could have then been transported to the islands by wind.

The most probable scenario is that tropospheric dust is mixed with illitized smectite from the saddle between the islands. If there is a mixture of illite from the two possible sources, K-Ar dating may be inconclusive.

X-RAY ABSORPTION SPECTROSCOPY: A TOOL FOR PROBING THE STRUCTURE OF SURFACE COMPLEXES. Alain MANCEAU¹ and Laurent CHARLET²

1- Laboratoire de Minéralogie-Cristallographie, Tour 16, 4 place Jussieu, Paris 75252, France.
2- Institut für Anorganische Chemie, Freiestrasse 3, 3000 Bern, Switzerland.

The molecular-level description of sorption mechanisms of diluted species at solid surfaces is of great importance in a variety of fields, including geochemistry, catalysis, environmental engineering (i.e. waste water treatment), and material science. Surface reactions have been continuously studied for two decades by chemists and, in the absence of structural data, surface complexation models have been developed to account for macroscopic measurements. These models can now be validated thanks to the recent development of the synchrotron-based fluorescence-yield X-ray absorption spectroscopy (XAS = EXAFS + XANES), which makes feasible a mechanistic description of surface phenomena.

After a short technical presentation of the method, the talk will aim at showing how information gains at the molecular-level helps understanding basic macroscopic measurements. Three case studies will be presented: the sorption mechanisms of UO_2^{2+} and Cr(III) by hydrous Fe oxides (HFO), and the molecular mechanism of the Cr(III) oxidation to Cr(VI) at the MnO_2 /water interface.

Hydrous ferric oxides (HFO) formed through the hydrolysis of iron in natural waters are known to be efficient scavengers of uranium. The enrichment factor of uranyl ions on HFO measured in batch experiments is as high as 10^5 - 10^6 . EXAFS results indicate that uranyl complex bonds Fe gels through a mononuclear bidentate linkage, i.e. edge-sharing linkage. This bonding mechanism arises from a quite perfect match between the lengths of the O-O edges in the sorbent (2.8-3.0Å) and in the sorbate ($2.89\text{Å} < \text{O}_e\text{-O}_e < 3.05\text{Å}$). In other words, the very strong affinity of uranyl ions for HFO, as measured at the macroscopic level, is accounted for, at the microscopic level, by a steric fitting between the sorbate and the sorbent.

Chromium behaves differently with Fe and Mn oxides: the former immobilizes it, and the latter oxidizes and then solubilizes it. The high Cr for HFO affinity is commonly used to eliminate Cr^{3+} from tannery sludges. At the opposite, the result of the high Cr for Mn oxides affinity is an increase of the chromium toxicity.

On HFO, Cr(III) ions bond to the surface like a Fe(III) ion, i.e., through mononuclear bidentate and binuclear bidentate linkages. This structural mimesis is explained by the existence of isostructural Fe and Cr oxides polymorphs (e.g. αFeOOH and αCrOOH) with close unit-cell parameters. Nevertheless, strong structural differences are observed as to whether Cr(III) is, sorbed onto, or coprecipitated with, HFO, and explain why chromium is much more efficiently removed from water by the latter mechanism.

The Cr(III)→Cr(VI) oxidation rate is speeded by several orders on Mn oxides compared to the homogeneous oxidation. The molecular mechanism of this surface catalyzed oxidation process has been elucidated at the birnessite ($\text{Na}_4\text{Mn}_{14}\text{O}_{27}\cdot 9\text{H}_2\text{O}$) surface by a kinetics study of the Cr sorption. It can be mechanistically depicted as follows: 1) Cr(III) aqua ions diffuse towards Mn(IV) vacancies of the lattice; 2) the coupled Cr(III) oxidation/Mn(IV) reduction occurs; 3) Cr(VI) and Mn(II) ions are released in the solution. Once more, this mechanism is feasible owing to a steric fitting between the sorbate and the active site of the sorbent, as both Mn(IV) and Cr(III) ions have similar ionic radii: in a certain sense, the vacant octahedral cages of birnessite act as a molecular sieve for Cr(III) free ions.

These examples illustrate how the structure of the sorbent, through the nature of the reactive surface sites, control the speciation of metals in aqueous media. More generally, this new approach highlights the importance of gaining information on surface reactions at the molecular-level for discussing more confidently macroscopic, i.e. thermodynamic and kinetic, measurements.

CONTRASTING MINERAL / WATER REACTION PATHWAYS IN THREE SALINE, ALKALINE LAKES FROM SOUTHEAST OREGON

James Matthews and Stephen Altaner

Department of Geology, University of Illinois, Urbana, IL 61801.

Different reaction pathways were observed in 6 m deep cores from three playa lakes (Alkali, Abert, and Alvord) in southeast Oregon. The important variables controlling the pathway are the pore fluid composition and the detrital mineral composition which in turn is strongly related to parent rock composition. Detrital dioctahedral smectite and randomly interstratified (R=0) illite/smectite (I/S) reacts to trioctahedral R=0 kerolite/stevensite in the two most saline playas. However, in the most dilute pore fluids at Alvord Lake, trioctahedral smectite and smectite with b-axis dimensions intermediate between di- and tri-octahedral (here termed intermediate smectite) appear to react to form an R=0 intermediate smectitic mixed layer clay.

The chemical and isotopic composition of pore fluids from each playa appear to reflect mixing between evaporatively concentrated brine at the surface and more dilute water at depth. Pore fluids from each playa are predominantly Na and Cl -rich brines that become increasing more dilute with depth (e.g. at Alkali Lake, TDS ranges from 152,000 ppm in the top 5 cm to 2,700 ppm at 650 cm depth). In addition, δD and $\delta^{18}O$ values systematically decrease with depth (e.g. at Alkali Lake, δD and $\delta^{18}O$ values relative to SMOW range from -80.8 and -5.7 respectively in the top 5 cm to -113.2 and -13.1 at 650 cm depth). Pore fluids from each basin span a different range of TDS and pH values, probably due to different degrees of evaporative concentration in each basin.

Alkali Lake brines are the most concentrated and have the highest pH of the three basins studied. The reaction pathway at Alkali Lake involves dioctahedral and intermediate R=0 I/S and yields trioctahedral R=0 smectitic kerolite/stevensite and clinoptilolite. The thin soils developed on silicic to basaltic extrusive volcanics contain dioctahedral to intermediate R=0 smectitic I/S and significant opal. Playa sediments contain trioctahedral R=0 kerolite/stevensite, abundant clinoptilolite, and trace amounts of kaolinite, erionite, and illite. Trona, halite, and thin layers of Magadiite in the sediment support the fluid composition data which indicate extreme evaporative concentration of pore fluids.

The reaction pathway in Lake Abert playa sediments (which contain brines of intermediate TDS and pH) also involves reaction of dioctahedral smectite and R0 I/S to trioctahedral kerolite/stevensite. Soils developed on basaltic and intermediate volcanics contain dioctahedral smectite and R=0 I/S with small amounts of kaolinite, R=0 kaolinite/smectite, and discrete illite. Playa clays contain a smectite-rich trioctahedral R=0 kerolite/stevensite with lesser amounts of trioctahedral smectite and traces of kaolinite and illite.

Pore fluids from the Alvord Lake playa are the most dilute and have the lowest pH of the three playas studied. The reaction pathway at Alvord Lake involves the reaction of trioctahedral and intermediate smectite to an R=0 intermediate smectitic mineral. Soils developed on basaltic and intermediate lavas contain trioctahedral and intermediate smectite and lesser R=0 I/S and illite. Playa sediments contain an intermediate ($d(060)=1.51 \text{ \AA}$) smectitic R=0 $10\text{\AA}/17\text{\AA}$ mixed layer mineral, and small amounts of kaolinite and illite.

Mechanism of Clay Formation on Tektites: Natural Weathering vs. Laboratory Alteration

MAZER, J. J., BATES, J. K., BRADLEY, C. R. Chemical Technology
 Division, Argonne National Laboratory, Argonne, IL 60439;
 BRADLEY, J. P., Mc Crone Assoc., 850 Pasquinelli Dr., Westmont,
 IL, 60559; STEVENSON, C. M., Archaeological Service
 Consultants, P. O. Box 02095, Columbus, OH 42302

Tektite alteration to clay phases has been proposed as the genesis of clay microspherules found at the Cretaceous-Tertiary boundary and evidence of an impact event [1-3]. Previous experimental studies of tektite/water interactions have reported that the reaction mechanism consists solely of surface etching [4,5]. We have undertaken a detailed study of naturally and experimentally altered tektites to resolve this issue. The hydration of indochinite tektite is described for 100% relative humidity experiments at temperatures between 150 and 225°C for up to 256 days. Birefringent hydration layers formed on the tektite surfaces and their thicknesses increased at a rate proportional to the square root of time. The activation energy of the process, over the range of conditions examined, is 91 ± 2 kJ mol⁻¹. Characterization of the hydration layers with analytical electron microscopy, secondary ion mass spectrometry and optical microscopy suggest that the reaction mechanism in these experiments is dominated by molecular water diffusion with some evidence for the initial formation of Fe-rich clay (glaucinitic illite?). The reaction mechanism for naturally altered tektite includes significant subaerial secondary mineral formation, including kaolin, Fe-bearing rutile, alpha quartz, hematite and a Fe-rich clay (glaucinitic illite?). Our results provide an experimental basis for proposing that tektites can transform into clay phases, as with microspherules found at the Cretaceous-Tertiary boundary. Our observations of birefringent layer formation on experimentally altered tektite are unique in the literature [6,7] and highlights the importance of reaction conditions, specifically the glass surface area to solution volume ratio in affecting glass reaction processes. Clay formation on tektites can also be helpful in deducing the past soil environments.

References

1. Montanari A., Hay R., Alvarez W., Asaro F., Michel H., Alvarez L. and Smit J. (1983) *Geology*, vol. 11, p.668-671.
2. Margolis S., Claeys P. and KYTE F. (1991) *Science*, vol. 251, p. 1594-1597.
3. Pollastro R. M. and Pillmore C. L. (1987) *J. of Sed. Pet.*, vol. 57, p. 456-466.
4. Barkatt A. A., Boulos M. S., Barkatt Al., Sousanpour W., Boroomand M. A., Macedo P. B. and O'Keefe J. A. (1984) *Geochim. Cosmochim. Acta*, vol. 48, p.361-371.
5. LaMarche P. H., Rauch F. and Lanford W. A. (1984) *Journal of Non-Cryst. Solids*, vol. 67, p. 361-369.
6. Ewing R. C. (1979) in Scientific Basis for Nuclear Waste Mgmt. I, p. 57-68
7. Berger R. and Ericson J. (1974) in Recent Advances in Science and Technology of Materials, A. Bishay ed., Plenum Press, New York, p.187-189.

A RAPID ESTIMATION OF LAYER CHARGE OF 2:1 EXPANDING SILICATE CLAYS BY ALKYL AMMONIUM

A.R. Mermut, and R.J. St. Arnaud

University of Saskatchewan, Saskatoon, Sask., S7N 0W0, Canada.

The alkylammonium ion-exchange technique is still not widely used for routine determination of layer charge of 2:1 silicate clays. Several suggestions have been made to refine the original technique developed first by Weiss (1963) and Lagaly and Weiss (1969). According to a modified technique by Rühlicke and Kohler (1981), clay minerals are saturated with alkylammonium ions of varying chain length, and the charges are calculated on the basis of the expansion in the spacing, which is measured by X-ray diffraction analysis. Several difficulties still exist in the calculation of internal charges of 2:1 expanding clays. This paper investigates the possibility of rapidly estimating mean layer charges by determining the nitrogen content of the clays following the alkylammonium saturation.

The following phyllosilicates with known chemical characteristics and cation exchange capacity were saturated with alkylammonium cations: Biotite (interlayer K exchanged with Ba), phlogopite, Santa Olalla Vermiculite, Illite Montana Vermiculite, Idaho Vermiculite, Na montmorillonite and Ca montmorillonite. Charge distribution in octahedral and tetrahedral sheets were also determined by blocking the octahedral charge using the LiCl saturation technique. Nitrogen determination of the clays saturated with alkylammonium having chain lengths between 6 and 16 resulted in consistent nitrogen contents. It is concluded that the method may be utilized to estimate rapidly the mean layer charge of smectites and vermiculites.

REFERENCES:

1. Lagaly, G. and Weiss, A. 1969. Proc. Int. Clay Conf., Tokyo, 173-187
2. Rühlicke, G. and Kohler, E.E. 1981. Clay Min. 10:305-307
3. Weiss, A. 1963. Clays and Clay Miner. 10:191-224

SURFACE CHEMICAL AND MINERALOGICAL ASPECTS OF COLLOID-FACILITATED CONTAMINANT TRANSPORT: Miller W. P. and Bertsch P. M., Agronomy Dept., Plant Science Bldg., Univ. of Georgia, Athens, GA 30602

Environmental contaminants such as metals, pesticides, and radionuclides have sometimes been observed to be more mobile in soil-aquatic systems than might be predicted from their chemical solubilities and adsorption behavior. Migration of contaminants associated with mobile colloidal materials has been suggested as a potential explanation for these phenomena. Such colloid-facilitated transport has been observed in surface waters, where rainfall runoff has transported dispersed colloids and adsorbed pesticides and nutrients to streams and lakes. Recent evidence also suggests that downward migration of colloids may be responsible for aquifer contamination under conditions where colloids with adsorbed radionuclides were dispersed and transported through intact soils (1).

Conceptual models describing the process of colloid-facilitated contaminant transport involve 1) partitioning of the contaminant to the colloid via adsorption; 2) initial mobilization of the colloid from the soil matrix, or formation of the colloid *in situ*; 3) transport to a surface or subsurface water body. Assuming that desorption is a relatively slow process, the extent of colloid transport is determined by processes within 2) and 3).

The generation of colloidal suspensions may occur by detachment of matrix colloids, or by formation in the water system via precipitation (1). While the later may be more important in deep burial of contaminants where the chemistry has been altered (i.e., landfills), mobilization of colloids at the soil surface by raindrop impact is primarily responsible for potential movement of surface-applied contaminants. Shear forces induced by water flowing in pores may also be involved, but are poorly understood.

The stability of the colloidal suspension is crucial to its capacity to be transported over or through the soil without attenuation. The use of DLVO theory in describing the effect of repulsive forces acting between charged particles has had some qualitative success in describing the flocculation process (2). Mineralogical analyses of suspended colloids has shown high-charge minerals to be dominant over kaolinite, but kaolinite may also be dispersive. Specifically adsorbed compounds such as organics may increase surface charge and double layer repulsion, greatly enhancing stability compared to reference clays (3). Organic coatings also enhance sorption of contaminants (4). Filtration theory, often used to describe straining of particles, does not describe well the attenuation of these finely dispersed particles, particularly in macro-porous soils (5).

Several case studies illustrate the problems involved in fully understanding and modelling colloid-facilitated transport: the movement of pesticides in runoff waters from cultivated soils (6), and the occurrence of radionuclides in groundwaters below nuclear test sites in the Western US (7). Further understanding of processes governing the formation and stabilization of soil-derived colloidal suspensions will be required before adequate management-remediation strategies can be devised.

1. McCarthy, J.F., and Zachara, J.M. (1989) *Environ. Sci. Technol.* 23:496-502.
2. Gregory, J. (1989) *Crit. Rev. Environ. Control* 19:185-230.
3. Miller, W.P., Frenkel, H., and K.D. Newman. (1990) *Soil Sci. Soc. Am. J.* 54:346-351.
4. Murphy, E.M., Zachara, J.M., and Smith, S. (1990) *Environ. Sci. Technol.* 24:1507-1516.
5. McDowell-Boyer, L., Hunt, J.R., and Sitar, N. (1989) *Water Resour. Res.* 22:1901-1921.
6. Pionke, H.B., and G. Chesters. (1973) *J. Environ. Qual.* 2:29-45.
7. Penrose, W.R., et al. (1990) *Environ. Sci. Technol.* 24:228-234.

V92-10253

MINERALOGY OF CRETACEOUS/TERTIARY BOUNDARY CLAYS IN THE CHICXULUB STRUCTURE IN NORTHERN YUCATAN; D. W. Ming¹, V.L. Sharpton², and B.C. Schuraytz². ¹NASA Johnson Space Center, SN14, Houston, TX, 77058, and ²Lunar and Planetary Institute, Houston, TX, 77058.

The Cretaceous/Tertiary (K/T) boundary clay layer is thought to be derived from ejecta material from meteorite impact [1], based on the anomalous concentrations of noble metals in the layer. Because of recent findings of a half-meter thick ejecta deposit at the K/T boundary in Haiti [2], efforts have focused on locating a large impact feature in the Caribbean and the Gulf of Mexico. One of the leading candidates for the site of a large impact is the "Chicxulub structure" located on the northern Yucatan Peninsula in Mexico [3,4,5]. The Chicxulub structure is a subsurface zone of upper Cretaceous igneous rocks, carbonates, and breccias. The structure has been interpreted to be a 200 km diameter impact crater [4,5]; however, there is some question to the size of the structure or to the fact that it even is an impact feature [6]. Little is known about the mineralogy of this structure; therefore, the objective of this study was to determine the clay mineralogy of core samples from within the Chicxulub structure.

MATERIALS AND METHODS: Core samples from upper Cretaceous through Eocene were obtained from Pemex drill-hole Yucatan-2, located approximately 130 km southeast of the structure's center. Sample identification, core interval, and lithology are listed in Table 1. Clay fractions ($<2 \mu\text{m}$) were separated from carbonate-free materials (treated with N NaOAc buffered to $\text{pH}=5$) by sedimentation and centrifugation techniques. Mineralogy of the clay fraction was determined by x-ray diffraction analysis of Mg- and K-saturated samples using standard techniques.

RESULTS AND DISCUSSION: The clay mineralogy of Yucatan-2 core samples is summarized in Table 1. The location of the K/T boundary in Yucatan-2 is not known because cores were taken intermittently and recovery was low; however, the K/T boundary is believed to occur between 250 and 300 meters below sea level. A sample of particular interest is located below the K/T boundary (N6) that has been interpreted to represent an 80 m thick ejecta blanket [5]. A chlorite-vermiculite randomly interstratified mineral (or possibly a hydroxy-interlayered vermiculite) appears to be the predominant clay mineral as suggested by a shift in x-ray d-spacing from a 1.25 nm peak (K-saturated clay at 25, 110, & 300°C) toward a 1.05 nm peak upon heating to 550°C. Smectite was the predominant clay mineral in core samples below N6. Very little clay material ($<4 \text{ wt. } \%$) occurred in core samples located above N6.

ACKNOWLEDGEMENTS: We thank A.E. Weidie (University of New Orleans) for providing samples from Pemex drill-hole Yucatan-2.

REFERENCES: [1] Alvarez L.W. et al. (1980) *Science*, 208, 1095-1108. [2] Hildebrand, A.R., and W.V. Boynton (1990) *Science*, 248, 843-847. [3] Penfield, G.T., and A. Camargo (1981) 51st An. Mtg. Soc. Explor. Geophys. Abstr., 448-449. [4] Pope, K.O. et al. (1991) *Lunar Planet. Sci. Conf.* 22, 1083-1084. [5] Hildebrand, A.R., and W.V. Boynton (1990) *EOS*, 71, 1424-1425. [6] Sharpton, V.L. et al. (1991) *Lunar Planet. Sci. Conf.* 22, 1223-1224.

TABLE 1. Lithology and clay mineralogy ($<2 \mu\text{m}$) of samples from drill-hole Yucatan-2.

Sample	Interval (m)	Lithology	Clay Mineralogy
N-3	204-207	porous sparry micrite	illite
N-5	254-257	vuggy micrite	no XRD detectable phase found
-----K/T Boundary-----			
N-6	301-303	anhydrite/dolomite conglomerate	interstratified chlorite-smectite
N-9	500-503	anhydrite/dolomite conglomerate	smectite
N-11	701-704	anhydrite/dolomite conglomerate	smectite, illite, chlorite

CHARACTERISTICS OF CHLORITE INTERLAYERED WITH A 7Å MINERAL AS FOUND IN SANDSTONE RESERVOIRS

D. M. Moore and R. E. Hughes

Illinois State Geological Survey, 615 E. Peabody, Champaign, IL 61820

X-ray diffraction measurements on chlorites from five different petroleum reservoir sandstones allow a consideration of the relations of variations in chlorites to reservoir characteristics. This clay mineral is diagenetic and coats quartz grains. The peak positions, intensities, and widths were measured for the first five orders of this clay mineral and for the quartz peaks for spacings of 4.26Å and 3.33Å. In some samples the amount of kaolinite, illite, illite/smectite or some combination of these exceeded the amount of chlorite present. Interferences were dealt with by measuring the half-width of the peak of interest from the center of the peak to the side away from the interference at half the maximum height above background and then doubling that value. Broadening of the odd-ordered peaks caused by the interlayering of a 7Å phase with chlorite could be measured in 112 of the 122 sandstones analyzed. The amount of peak broadening is directly related to the amount of 7Å material interlayered in the chlorite. The amount of broadening seems unrelated to the amount of Fe in this mineral. Iron content was determined by a ratio of the area of the 002 peak plus the area of the 004 peak divided by the area of the 003 peak. The d(001) measurements of the 7Å/chlorite mineral were determined by averaging the positions of the five orders of peaks after adjustment using the first quartz peak as an internal standard.

ANOVA treatment of the data can be used to distinguish one oil field from another or one formation from another. No geographic trends were apparent. The earlier expectation that there would be a correlation between the amount of peak broadening (reflecting amount of 7Å material present) and porosity has not been found. There is, however, based on only five samples, a preliminary indication of a correlation between the amount of peak broadening and permeability.

HOLE-TRAPPING DEFECTS IN KAOLINITE: ORIGIN AND USE AS ENVIRONMENTAL TRACERS

Jean-Pierre Muller, Thierry Allard, Georges Calas

Laboratoire de Minéralogie-Cristallographie, URA CNRS 09, Tour 16/26
Universités Paris 6 et 7, 4 Place Jussieu, 75252 Paris Cedex 05, France

Natural kaolinites are known to incorporate defects of various types, either extended or localized. Several structural point defects may be directly studied through their paramagnetic character, by using Electron Paramagnetic Resonance (EPR). EPR spectra of all natural kaolinites we have investigated exhibit a complex, narrow signal at high magnetic field. The variable shape and intensity of this signal has been interpreted in terms of variable concentrations of hole-trapping-centers within the kaolinite lattice (1) (2) (3). Three types of centers (designated A, A' and B) are identified after spectral analysis of X- and/or Q-band spectra.

We have related the EPR spectra of natural kaolinites to those obtained after artificial irradiation of natural kaolinites from various environments (weathering, hydrothermal and sedimentary) (3) (4). In order to approach natural radioactivity effects, three types of irradiation have been used: γ -rays, He⁺ and Pb²⁺ beam implantation. Although the various radiations have a variable efficiency, the only effect of artificial irradiation is an increase of concentrations of the pre-existing centers. This demonstrates the irradiation origin of hole-trapping centers in natural kaolinites. Moreover, annealing experiments evidence that these centers can be separated with respect to their relative stability (A>A'>B), the A-center being stable up to 450°C, then over geological periods. Because of their different thermal stability, the different centers observed in natural kaolinites can be then considered as formed at different periods.

Kaolinite is then a unique tool for tracing the dynamics of the transfer of radionuclides in kaolinite-containing clayey formations: the use of kaolinite as a sensitive environmental tracer will be illustrated by three examples chosen in different geological settings:

(1) studies of kaolinites from lateritic weathering profiles (1) (3) show that the absolute concentration of hole-trapping defects is related to background radioactivity. At the same time, this allows an efficient fingerprint determination of the successive generations of kaolinites during the weathering processes

(2) studies of kaolinites from hydrothermally altered tuffs from Mexico (4) bring into evidence variations of the relative concentration of defects as a function of kaolinites location. Compared to petrological data, these variations allow to distinguish successive irradiation of kaolinites, and then successive transits of radionuclides, during hydrothermal history

(3) studies of sedimentary kaolins show that an irradiation of kaolinite has been effective during the deposit of kaolins and the development of associated diagenetic processes (5)

Finally, because of the geological settings chosen for nuclear wastes are located in environments containing kaolinites, dosimetry of trapping-holes defects could be directly useful to a safety assessment of these wastes (6) (7).

(1) Muller J. P. and Calas G. (1989) *Econ. Geol.*, vol. 84, P. 694-707; (2) Muller J. P., Ildefonse P. and Calas G. (1990) *Clays and Clay Minerals*, vol. 6, p. 600-608; (3) Muller J. P., Clozel B., Ildefonse Ph. and Calas G. (1991) *Applied Geochem.*, Supplement no 1 (in press); (4) Clozel B. (1991) Unpub. Thesis, Univ. Paris 7, Paris; (5) Muller J. P. and Calas G. (1991) *Keller Kaolin 90 Symposium*, W. Bundy and H. H. Murray eds., *Clay Miner. Soc.* (accepted); (6) Ildefonse P., Muller J. P., Clozel B. and Calas G. (1990) *Engineering Geology*, vol. 29, p. 413-439; (7) Ildefonse P., Muller J. P., Clozel B. and Calas G. (1990) *Mat. Res. Soc. Symp. Proc.*, vol. 212, p. 749-756

GENETIC SIGNIFICANCE OF Mn^{2+} and VO^{2+} SORBED ONTO NATURAL KAOLINITES

Jean-Pierre Muller, Nathalie Malengreau and Georges Calas

Laboratoire de Minéralogie-Cristallographie, URA CNRS 09, Tour 16-26, 2ème étage, Universités Paris 6 et 7, 4 Place Jussieu, 75252 Paris Cedex 05, France

Paramagnetic trace elements and defect centers (trapped holes) have been investigated, using electron paramagnetic resonance (EPR), in more than 350 kaolinite samples from weathering, sedimentary and hydrothermal environments (1). A special attention has been paid to the location of these paramagnetic species inside or at the surface of the kaolinite lattice and to their genetic significance. Sorbed divalent manganese and tetravalent vanadium have only been detected in kaolinites from tropical soils and sedimentary rocks, respectively.

The characteristic 6-line hyperfine structure (HFS) of Mn^{2+} ions have been recognized on Q-band EPR spectra of kaolinites from ferruginous nodules located within an intermediate zone of lateritic weathering profiles (2). A detailed analysis of the EPR signal shows that spectra of two Mn^{2+} -species are superimposed: the one is related to Mn^{2+} ions substituted in octahedral sites of ancillary muscovite; the other corresponds to $[Mn(H_2O)_6]^{2+}$ outer-sphere surface complexes similar to those found in zeolites (sodalite supercage). The EPR parameters remain unchanged after several washings, chemical treatments (deferration, oxidation, Na^+ -saturation) and heating up to 400°C. Mn^{2+} ions in natural kaolinites are protected from external modifications. They may be trapped in the closed folders observed by HR-TEM in some natural kaolinites between adjacent layers inside kaolinite lattice could act as traps for these ions, subsequently to crystal growth.

The characteristic 8-line hyperfine structure of V^{4+} is easily recognized at X-band on the only EPR spectra of sedimentary kaolins (1). The EPR spectra exhibit an orientation dependence respective to the magnetic field: vanadium, actually vanadyl complexes VO^{2+} , is sorbed as inner-sphere complexes with a well-defined orientation respective to the kaolinite surface. While vanadyl ions experimentally sorbed on hydrated kaolinite indicate outer-sphere, freely tumbling vanadyl species, EPR spectra of sedimentary kaolinites remain unaffected by external treatments such as drying, oxydation and formation of kaolinite suspensions. This indicates that VO^{2+} groups are located onto surface hydroxyls inside the kaolin particles.

In natural kaolins, Mn^{2+} and VO^{2+} ions trapped inside kaolin particles are fingerprints of growth conditions of kaolinite: sorbed Mn^{2+} ions on lateritic kaolinites are indicative of redox changes during soil differentiation; the presence of sorbed VO^{2+} ions indicates that sedimentary kaolinites have suffered a significant exchange with reduced diagenetic fluids.

(1) Muller J. P. and Calas G. (1991) Keller Kaolin 90 Symposium, W. Bundy and H. H. Murray eds., Clay Miner. Soc. (accepted); (2) Muller J. P. and Calas G. (1991) Geochim. Cosmochim. Acta (submitted).

MÖSSBAUER SPECTRA OF KAOLINITE, HALLOYSITE AND THE FIRING PRODUCTS OF KAOLINITE: Murad E. and Wagner U.

Lehrstuhl für Bodenkunde, T. U. München, D-8050 Freising-Weißenstephan, Fed. Rep. Germany

22 kaolinites that differ widely in their degree of structural order (Hinckley indices between 0.30 and 1.55) and Fe contents (0.15 to 1.29 wt %), 3 halloysites, and the products of firing one kaolinite to 1350°C in steps of 50°C were studied by Mössbauer spectroscopy at room temperature. Selected samples were also studied at 120 and 4.2 K.

Mössbauer spectroscopy showed that the majority of samples had noticeable proportions of their Fe contents (over 50 % in one case) in the divalent state. The determination of the Mössbauer parameters was complicated by the generally low Fe contents, which leads to the development of slow paramagnetic relaxation, and by the presence of possibly interfering mineral constituents in some samples. "Best values" for Fe²⁺-free kaolinite are a temperature-independent quadrupole splitting of 0.51 mm/s and an isomer shift of 0.35 mm/s relative to metallic Fe. The Fe²⁺ components - where present - in kaolinite have a quadrupole splitting of 2.54 mm/s at room temperature and an isomer shift of 1.11 mm/s. The Mössbauer parameters of halloysite do not differ noticeably from those of kaolinite.

Interferences from associated Fe oxides can be avoided by their selective removal, or they can be taken into account separately by carrying out measurements at low temperatures. Mössbauer spectra taken at 4.2 K allowed the identification of goethite in kaolins of complex mineralogy at concentrations as low as 0.1 %.

The parameters change drastically upon firing. Mössbauer spectra reflect the mineralogy of the products as well as the temperature and redox conditions during firing, and may therefore serve for an assessment of these. Both metakaolin and mullite were also prone to paramagnetic relaxation within the full range of Fe substitution encountered in the studied kaolinites.

SURFACE FREE ENERGIES OF KAOLINITES: Murphy K., van Oss C. J., and Giese R. F., Geology-SUNY, 4240 Ridge Lea Road, Amherst, NY 14226

The outer cleavage surfaces of kaolinite crystals, unlike 2:1 minerals, are of two different types: one is a plane of hydroxides and the other is a plane of oxygens. The physical and chemical reactions of these two types of surface with water, other liquids and colloids should be very different. Unfortunately, kaolinite does not form sufficiently large crystals to allow one to isolate either the hydroxide surface or the oxygen surface for experimentation. The best we can do is to examine the totality of the surface properties of (powdered) kaolinite samples. In theory, the total surface free energy of a kaolinite sample is an average of the free energies of the two cleavage surfaces plus the lateral edges, each weighted by its relative surface area. To a first approximation, the contribution of the lateral surfaces can be neglected.

The surface tension of a solid is related to the surface free energy by: $\gamma = -\frac{1}{2}\Delta G^{\text{TOT}}$. The surface tension, γ , has an apolar component, γ^{LW} , and a polar component, γ^{AB} , which represents the Lewis acid/base character of the surface. The AB component, in turn, consists of two parameters; γ^{\ominus} for the Lewis acid and $\gamma^{\omin�}$ for the Lewis base strength.

The values of the surface tension components and parameters were determined for Georgia well-crystallized kaolinite (KGa-1) and several kaolinite samples obtained from Georgia Kaolin. The experiments involved determining the rate of capillary rise of the $< 2 \mu\text{m}$ fraction through a thin, uniform layer of the kaolinite sample which was deposited from water suspension upon a glass slide. The cosine of the contact angle is obtained via the Washburn equation. Four liquids were used for the wicking experiments: two apolar (α -bromonaphthalene and di-iodomethane), and two polar (water and ethylene glycol). The contact angles for these liquids were used to solve the Young equation for each kaolinite sample.

The values of γ^{LW} for all samples range between approximately 34 and 36 mJ/m²; these are smaller than values found for smectites and are closer to talc and pyrophyllite. All samples are weak Lewis acids ($\gamma^{\ominus} < 0.1 \text{ mJ/m}^2$), and are strong Lewis bases. The Lewis basicity varies from approximately 35 mJ/m² to as much as 50 mJ/m². This variation may be due to differences in the defect structure of the different kaolinite samples or to the presence of small amounts of smectite or other impurities covering the kaolinite particles. KGa-1 has the largest value of $\gamma^{\omin�}$ yet observed for a kaolinite.

Curiously, liquid formamide exhibited an anomalously high rate of capillary rise in wicking experiments for all kaolinites examined; this behavior may be related to the formation of a formamide:kaolinite intercalate at the mineral surfaces and edges, though the origin of the increase in capillary rise is not obvious.

EVIDENCE OF DISSOLUTION AND PRECIPITATION ON GIBBSITE USING ATOMIC FORCE MICROSCOPY: Nagy K. L., Dept. Geol. & Geophy., P.O. Box 6666, Yale Univ., New Haven, CT 06511 (now at Exxon Prod. Res. Co., P.O. Box 2189, Houston, TX 77252); Hochella M. F., Jr., Dept. Geol., Stanford Univ., Stanford, CA 94305; Blum A. E., U.S. Geol. Survey, MS 420, 345 Middlefield Rd., Menlo Park, CA 94025; Lasaga A. C., Dept. Geol. & Geophys., P.O. Box 6666, Yale Univ., New Haven, CT 06511

Gibbsite crystal surfaces reacted in dilute aqueous solutions at 80°C and pH 3 (1) were examined using atomic force microscopy (AFM) for evidence of dissolution and precipitation. Although measurable dissolution and precipitation rates had been obtained over a range of solution saturation states, SEM images of the reacted surfaces could not be used to identify features indicative of either reaction, with the exception of images of a few dissolved grains over a specific range of undersaturation. Fundamental surface features caused by dissolution and growth of a crystal are generally below the resolving capability of the SEM.

Steady-state reaction rates of synthetic gibbsite (1-10 μm blocky grains) were obtained in stirred-flow reactors at saturations equivalent to $-1.1 \text{ kcal/mol} \leq \Delta G_R \leq +0.47 \text{ kcal/mol}$ (where ΔG_R is the Gibbs free energy of reaction, and $\Delta G_R = 0$ at equilibrium) for the reaction: $\text{Al}(\text{OH})_3 (\text{s}) + 3\text{H}^+ \rightleftharpoons \text{Al}^{3+} + 3\text{H}_2\text{O}$. Dissolution rates increased with increasing undersaturation according to a sigmoidal function of ΔG : the rates varied linearly with ΔG_R near equilibrium, increased sharply over the range $-0.50 \text{ kcal/mol} \leq \Delta G_R \leq -0.20 \text{ kcal/mol}$, and were constant at $\Delta G_R \leq -0.50 \text{ kcal/mol}$. Precipitation rates increased linearly with increasing ΔG_R . SEM images of samples at $\Delta G_R \leq -0.20 \text{ kcal/mol}$ contained rare large-scale etch pits on only a few grains.

In an attempt to differentiate reacted surfaces and to identify mechanisms that could explain the observed functional dependencies of the rates on ΔG , we examined the starting material and three of the experimentally reacted gibbsite samples using a Digital Instruments Nanoscope II AFM at the Center for Materials Research at Stanford University. Gibbsite grains were dispersed in methanol on a sample mount and examined using a 200 μm Si_3N_4 tip in constant force (variable height) mode. The starting gibbsite exhibited numerous linear ledges with lengths up to a few hundred nm. The ledges were 1 to 3 nm high and spaced at intervals of ~10 to 100 nm. Sublinear ledges of similar length but smaller vertical relief (< 0.5 nm) also were observed. Dissolved surfaces had linear ledges and appeared mottled or hummocky with holes that did not conform to any crystallographic outlines. Hole depths were generally $\leq \sim 1$ nm. No evidence for etch pits was observed on grains from a sample in which etch pits were observed at the μm scale by SEM. However, the small number of grains examined with AFM does not preclude the occurrence of etch pits at the nm scale. Surfaces of seven grains from a sample on which precipitation occurred contained striking hexagonal steps with heights of ~1 to 4 nm, and diameters of ~2 to 8 nm. In most cases, these steps were suggestive of two-dimensional growth although one image was suggestive of spiral growth. Arrays of steps forming long linear ledges were not observed.

The AFM observations support dissolution and precipitation processes involving lateral retreat and growth of steps with some evidence for reaction controlled by other mechanisms (etch pits in the dissolved samples and spiral steps in the precipitated samples). However, the dependencies of the overall rate laws on ΔG_R coupled with the AFM observations suggest that the surfaces are sufficiently rough to provide numerous high energy sites at which dissolution and precipitation can proceed. Surficial dislocation outcrops do not provide the only sites for dissolution and growth, however they can be the predominant reaction sites over specific ranges of ΔG_R . In fact, they explain the observed abrupt increase in dissolution rate as the undersaturation exceeds -0.20 kcal/mol. Most importantly, the AFM observations provide evidence for distinct differences between the two types of reacted surfaces that is not obtainable using SEM. This application of AFM to natural samples potentially could be useful for mapping fluid-flow patterns and determining mineral growth/dissolution histories in near surface crustal environments.

1: Nagy K. L. and Lasaga A. C., 1991, *Geochimica et Cosmochimica Acta* (in press).

HYDROPHOBIC NATURE OF ORGANO-CLAYS AS A LEWIS ACID/BASE
 PHENOMENON: Norris J., Giese R., Costanzo P. M., and van Oss
 C. J., Geology-SUNY, 4240 Ridge Lea Road, Amherst, NY 14226

It has been recognized for some time that the replacement of exchangeable inorganic cations of smectites by organic cations (e.g., alkyl ammonium cations) increases the adsorption capacity of the treated clay for a wide range of organic molecules. This increased adsorption is due to what has traditionally been rather vaguely described as "hydrophobic binding". In a surface thermodynamic sense, this consists of the interfacial interactions between two low-energy surfaces, or between one low and one high energy surface, immersed in water. The free energy of adsorption of a molecular species on a solid surface, immersed in a liquid, is proportional to the interfacial tension between the solid and the liquid. This interfacial tension has two contributors: electrodynamic interactions (the Lifshitz-van der Waals or LW component, γ^{LW}) and polar, or electron donor and electron acceptor interactions (the Lewis acid/base or AB component, γ^{AB}). The AB component is specified by two parameters, one for the electron donor activity, γ^{\ominus} , and the other for the electron acceptor activity, γ^{\oplus} .

Changes of the surface thermodynamic properties of two clay minerals (SWy-1 and Laponite) resulting from the exchange of inorganic cations by an organic cation were investigated. The exchange was effected by dipping oriented clay films, sedimented on glass slides, into a 0.1M solution of an organic salt. This resulted in a clay film whose external surface was populated by the organic cations. After drying, contact angles were measured for a number of test liquids and these angles were used with the Young equation to determine values of the surface tension components and parameters. The organic cations were tetramethyl (TMA), octyl (OA), decyl (DEA), dodecyl (DOA), hexadecyltrimethyl (HDTMA) and trimethylphenyl (TMPA), where A stands for the ammonium group. The surface tension components (in mJ/m^2) are listed below.

		Amm	TMA	OA	DEA	DOA	HDTMA	TMPA
SWy-1	γ^{LW}	41.7	41.5	40.9	41.7	39.6	40.0	41.3
	γ^{\oplus}	0.7	3.0	0.8	0.3	0.3	0.4	3.1
	γ^{\ominus}	36.2	12.9	12.6	10.0	6.0	8.7	9.7
Laponite	γ^{LW}	42.5	44.4	42.1	41.4	41.5	43.0	
	γ^{\oplus}	1.5	1.5	1.0	0.8	0.9	0.7	
	γ^{\ominus}	30.7	31.2	24.2	24.3	24.5	24.7	

As seen in the table, there was very little change in the surface tension component values for Laponite when converted to the organo-form. All of the organo-SWy-1 samples had substantially the same γ^{LW} as the untreated ammonium (Amm) saturated clay. The values of the Lewis base parameter, γ^{\oplus} , for SWy-1 decreased dramatically upon conversion to the organo-form. The Lewis acid parameter, γ^{\ominus} , remained small (i.e., $\gamma^{\ominus} < 1 \text{ mJ/m}^2$) except for TMA and TMPA which had values of about 3 mJ/m^2 . The "hydrophobic binding" of organo-SWy-1 results from the reduced Lewis base activity of the treated clay. Further, the selectivity of organo-clays for different adsorbents, and especially from different solvents, is likely to be related to the values of the Lewis acid/base parameters of the organo-clay, the adsorbent and the solvent. The principal driving force is the hydrogen-bonding component of the energy of cohesion of water.

EQUILIBRIUM AND SPECTROSCOPIC CHARACTERIZATION OF Co(II) SORPTION SITES ON KAOLINITE SURFACES

P.A. O'Day, G.A. Parks, and G.E. Brown, Jr.
School of Earth Sciences, Stanford University, Stanford CA 94305 USA

The uptake of metal ions from aqueous solution by reactive surface sites on clay minerals is an important geochemical process in many natural systems at low temperature. Co(II) sorption on kaolinite was investigated by laboratory solution equilibrium studies and X-ray Absorption Spectroscopy (XAS) at ambient conditions to try to characterize specific sites of metal sorption on the kaolinite surface. We compared Co(II) sorption as a function of pH, ionic strength of a background electrolyte, and particle size among three chemically pure kaolinites of differing degrees of crystallinity (as determined by bulk XRD analyses), ranging from low to very high crystallinity [1]. The kaolinite samples contain small amounts of TiO₂ (< 2 wt. %) as rutile or anatase particles, but chemical analyses suggest minimal isomorphous substitution within the kaolinite structure. Surface areas (measured by N₂ BET) of different particle size fractions were used to determine initial Co(II) concentrations (10⁻³ - 10⁻⁴ M) which would give similar Co(II) surface sorption densities (Γ) as a function of pH on all three kaolinites. Kaolinite fractions were equilibrated with pH-adjusted Co(NO₃)₂ solutions for 24-36 hours and Co(II) uptake from solution was measured radiometrically. Desorption of Co(II) by addition of acid and equilibration for 36-72 hours was not complete, suggesting a small fraction of Co(II) in strongly bound sites. Under acidic to neutral conditions (pH \approx 3 - 7), uptake of Co(II) by kaolinite varies with changes in ionic strength of the supporting electrolyte in the range of 0.01 to 1.0 M. Above pH 6-7, Co(II) sorption is not affected by ionic strength and is remarkably uniform despite differences in kaolinite crystallinity. For the <2 μ m kaolinite fraction, this change in sorption behavior occurs at Γ of about 0.35 - 0.4 μ mol m⁻². For particles of larger size (5 - 50 μ m), change in sorption behavior occurs at a higher Γ (0.8 - 1.0 μ mol m⁻²). Previous study of Cu(II), Pb(II), and Cd(II) uptake on kaolinite of surface area near to our <2 μ m fraction showed a similar change in sorption behavior at $\Gamma \approx$ 0.4 μ mol m⁻²[2].

These results suggest at least two types of sorption sites or processes[2,3] probably associated with kaolinite edge and (001) face sites. Edge and face areas estimated from electron micrographs of kaolinite particles and bulk BET surface area, together with theoretical crystallographic considerations [3], suggest that a single edge site is responsible for metal ion sorption at low pH. We propose that metal ion sorption on kaolinite under acidic conditions takes place by outer-sphere complexation of the metal ion with a terminal Si-OH edge site. At higher pH, solution behavior and XAS results indicate dominantly inner-sphere complexation [4], probably with Al-OH and Al-OH₂ sites. At values of Γ nearing monolayer coverage, XAS results indicate large Co(II) clusters and longer range ordering similar to that of Co(OH)₂(s), suggesting polymerization or formation of a hydroxide-like phase on Al-OH (001) faces. These conclusions indicate that the reactive sites responsible for sorption on kaolinite and the type of sorption complex which forms vary with changing solution conditions and metal ion surface coverage. With increasing pH, the sorbed ion changes from a weakly-bound, outer-sphere complex associated with edge sites to specifically-bound, inner-sphere multinuclear complexes probably associated with both edge and face sites which grow in size with increasing sorption density.

[1] Kaolinite samples and chemical analyses provided by H. May (U.S.G.S.) are gratefully acknowledged.

[2] Schindler, P.W., Liechti, P., and Westall, J.C. (1987) *Netherlands J. Agri. Sci.* 35, 219-230.

[3] Sposito, G. (1984) *Surface Chemistry of Soils*, Oxford Univ. Press, 234 p.

[4] O'Day, P.A., Brown, G.E., Jr., and Parks, G.A. (1991) *X-ray Absorption Fine Structure*, Hasnain, S.S. (ed.), 260-262.

ENVIRONMENTAL ASPECTS OF SILICA MINERALS IN CLAYS AND SEDIMENTS

I. Edgar Odom and Jessica M. Elzea

American Colloid Company, 1500 West Shure Drive, Arlington Heights, IL 60004

McCrone Associates, Inc., 850 Pasquinelli Drive, Westmont, IL 60559

Since OSHA made a trigger decision and declared crystalline silica minerals (quartz, cristobalite, tridymite) regardless of their particle size to be probably carcinogenic to humans based on very limited research data by IARC, the types and amounts of silica minerals in clays, sediments and natural zeolites have come under great scrutiny by both producers and users. It is highly important that mineralogists involved in the study of clays and zeolites correctly define the exact nature of silica minerals present. For example, many laboratories now performing commercial silica mineral analyses mistakenly apply the name cristobalite to opaline silica (Opal-CT) common with alpha quartz in fuller's earths, bentonites, diatomaceous earths and some natural zeolites. Microscopic, X-ray and thermal data provide conclusive proof that the so called cristobalite referred to above is disordered opaline silica of very low temperature origin. Crystalline silica is regulated as a carcinogen, disordered or amorphous silica is not.

In the alteration of volcanic glass to montmorillonite, there is an excess of Si. This Si precipitates as poorly ordered SiO_2 (Opa-CT or opaline silica). Biogenic silica is another source of opaline silica or Opal CT. The two sources may give rise to slightly different forms of disordered silica. The transformation of disordered opaline silica minerals to quartz with age has been well documented. This agrees with the occurrence of trace amounts of opaline silica in Cretaceous bentonites, whereas bentonites, fuller's earths and some zeolites of Tertiary or younger age may contain significant amounts. The commercial importance of some fuller's earths and bentonites are enhanced by the presence of opaline silica, and the use of these materials in certain consumer products presents little, if any, health risk to humans.

Whether silica minerals are or are not carcinogenic to humans, for regulatory reasons, the forms of silica minerals in clays and sediments should not be loosely called something they are not. There is no evidence at the present time that disordered opaline silica minerals pose any health risk. While it is well known that silicosis may be caused by excessive inhalation of silica (farmers, granite workers, foundry workers), cancer deaths among this group do not appear to be above the normal when cancer causing factors such as smoking are considered.

ILLITE AGE ANALYSIS: A METHOD FOR INTERPRETING SHALE K/Ar AGES

D. R. Pevear, Exxon Production Research Co, Box 2189, Houston, TX 77001

W. C. Elliott, Geol. Sciences, Case Western Reserve University, Cleveland, OH 44106

Illite Age Analysis (IAA), our application of the K/Ar radiometric dating technique, provides both integrated age of diagenesis and mean age of illite in the source terrane from shale samples. K/Ar ages of micaceous minerals in shales most always show finer size fractions to be younger than coarser fractions, even younger than depositional age. This has led to the assumption that shale is a mixture of detrital and diagenetic phases, the former older than the age of deposition, the latter younger. Most attempts to physically separate the diagenetic material from the detrital, in order to obtain the age of diagenesis, have not been very successful. Even the finest size fractions appear to be mixtures of detrital and diagenetic phases, therefore the dates obtained are not particularly useful. Illite Age Analysis has solved this problem. Using IAA, the measured age of diagenetic illite can be compared with that forward-modeled by W-L Huang's experimental kinetics for the smectite-to-illite reaction; any discrepancy between the calculated and measured date is used to adjust the kinetic model. IAA assumes that illite in shales is a mixture of diagenetic (young) illite, in mixed-layer illite / smectite (I / S) and discrete detrital (old) illite derived by erosion. Laboratory processing gives size fractions with widely varying amounts of each end-member and therefore widely varying K/Ar ages. Modeling of the XRD patterns of each fraction using NEWMOD permits quantitative determination of end-member proportions. Plots of K/Ar age vs. that percent of total illite which is diagenetic are linear confirming the two-component model; extrapolation to 0% and 100% detrital illite gives ages for the diagenetic and detrital end-members.

Initial testing of IAA was done using core from an Alaska North Slope well containing shales interbedded with bentonites. The bentonites consist of I/S with 70% illite layers and lack detrital illite -- therefore they are entirely of one end-member and all fractions give the diagenetic K/Ar age of ~30 my. This age provides an independent measure of the age of the diagenetic end-member as determined by IAA of adjacent shales. The 300'-thick cored interval consists of the "Pebble Shale" (Ellesmerian provenance) and overlying bentonitic, Albian-Aptian of Brookian provenance. The extrapolated diagenetic end-member value for each of four shale samples has the same intercept within the 90% confidence limit of the least-squares regression. For all of these the IAA diagenetic age is ~30 my, confirmed by the bentonites and predicted by kinetic modelling. On the other hand, the age of the detrital end-member of the "Pebble Shale" (350 my) is much older than that of the overlying Brookian-sourced shale (~120 my), confirming derivation of the former from an Ellesmerian source (Canadian Shield). The numeric difference between the provenance age and the diagenetic age of a single sample (Illite Age Gap) is controlled by the regional rates of uplift, erosion and burial, and for these two shale units (325 vs. 95 my) indicates a major tectonic reorganization associated with opening of the Canada Basin, uplift of the Brooks Range, and establishment of a foreland basin-type setting.

Petrogenetic Significance of Kaolinite Nucleation and Growth on Pre-existing Mica in Sandstones and Shales

D.R. Pevear, R.E. Klimentidis & G.A. Robinson, Exxon Production Research Co, Box 2189, Houston, TX 77001

Biotite and muscovite 00L surfaces serve as preferred nucleation sites for authigenic kaolinite in sandstones, shales and bentonites. Kaolinite grows with 00L parallel to that of mica and apparently nucleates within slit-like intercleavage micropores; mica structure may serve as a template for growth of the first hydroxide sheet of kaolinite. Continued intercleavage growth physically expands the mica until the mica-kaolinite stack may consist almost entirely of vermicular kaolinite; however, all the original mica remains, obscurely intergrown with kaolinite. XRD patterns show sharp hkL peaks typical of "well-crystallized" kaolinite. TEM and EMP show the mica to be unaltered other than probable loss of K from exposed surfaces. The texture we report has often been described as "mica altering to kaolinite", but our study, and that of Crowley (1), show mica is largely unaltered.

Many features typical of authigenic kaolinite in sedimentary rocks are explained by the above growth mechanism. The pronounced vermicular habit of pore-filling kaolinite almost always forms by expansive intercleavage growth on a mica substrate. The replication, throughout the vermicular stack, of initial irregularities in the mica (giving the vermicules a set of grooves perpendicular to 00L) shows the profound effect of the mica surfaces on growth and that there is no edge growth. We call such "grooved" crystals "Kopy-Kat" kaolinite. Edge-expanded "bow-tie" micas with kaolinite are also a manifestation of this growth mechanism. Very large (sand-size) kaolinite vermicular xls. and composite pseudo-crystals in sandstones indicate a mica substrate; careful petrographic examination generally reveals thin mica layers, greatly expanded from the initial detrital mica. The highly localized nature of pore-filling diagenetic kaolinite in sandstones may be due to its nucleation in only those pores where the dissolving feldspar contained small amounts of sericite which could serve to nucleate kaolinite growth. The 10Å interlayers often described in TEM lattice images of commercial kaolins hint, as was suggested long ago by Hinckley (2), that kaolinite growth, in general, is facilitated by nucleation on mica. The mica within kaolinite stacks may serve to nucleate illite growth during continued diagenesis. We have seen entirely similar relations between chlorite and mica; it is unclear if the expansive intercleavage chlorite was initially kaolinite.

Since mica is unaltered during kaolinite growth, we are not necessarily looking at crystallization from fluids out of equilibrium with mica, as suggested by those interpreting this texture as mica altering to kaolinite. In the bentonites of our study (Pierre Shale) expansive kaolinite growth in volcanic biotite has compressed the smectite, which must then have been present before kaolinite. The growth of kaolinite in mica, without mica alteration, in a smectite-dominated bentonite suggests fluids on a mica-kaolinite phase boundary. Apparently, metastable smectite is dissolving and more stable kaolinite is nucleating on the mica substrate. Lastly, certain features of illite 00L XRD patterns, such as the broad 001 peak in the absence of peak shift to lower angles (predicted by calculations for thin crystallites assuming only mica layers) and the high low-angle background, can be calculated by NEWMOD assuming 5% kaolinite interlayers; as a long shot - - possibly kaolin may coat the surfaces of illite crystallites.

(1) Crowley S.F. (1991) *Clay Minerals*, v. 26, p.91-103

(2) Hinckley D.N. (1961) PhD Thesis, Penn. State Univ.

RECENT ADVANCES IN INTERCALATED
CLAY CATALYSTS

Thomas J. Pinnavaia
Department of Chemistry and
Center for Fundamental Materials Research
Michigan State University
East Lansing, MI 48823

After having the been the subject of relatively intense catalytic research for nearly a decade, smectite clays continue to be an important class of materials for the rational design of heterogeneous catalysts capable of addressing a broad spectrum of organic chemical conversions. Other materials such as layered double hydroxides and layered silicic acids also have appeared on the scene which promise to take the field in new directions. This lecture will present an overview of some of these recent new advances. The main topics will include the design of organo clays for triphase catalysis, the synthesis of super gallery pillared clays, and tubular silicate-layered silicate intercalation compounds with novel microporosity for potential shape selective reactions. Fundament aspects of the pillaring reactions of smectites, layered double hydroxides, and silicic acids, particularly those factors relevant to the design of stable super gallery derivatives, also will be discussed.

CHARACTERIZATION OF FLY ASH AND THE IMMOBILISATION OF Pb AND Zn
WITH CLAY MINERALS

Adrian Plüss and *Ray E. Ferrell, Jr

Laboratory for Clay Mineralogy, Geotechnical Engineering
Swiss Federal Institute of Technology (ETH), 8092 Zürich
*Department of Geology & Geophysics, Louisiana State University,
Baton Rouge, Louisiana, U.S.A., 70803

Since filter-dust from the incineration of municipal solid waste (MSW) contains leachable heavy metals such as Pb, Cd, Zn and Cu, these materials require treatment before their ultimate disposal in landfills. One treatment is a washing process, where mainly soluble salts are washed out. Other procedures attempt to stabilize the heavy metals in the waste by producing a glass or by reaction with cement or a reactive clay prior to burial.

Two different types of fly ash, a filter-dust from an electrostatic precipitator and a fly ash from a flue gas cleaning system, have been studied by X-ray image analysis techniques in an electron microprobe. The crystalline materials in the ashes were revealed by X-ray powder diffraction techniques to be gypsum, anhydrite, quartz, halite, sylvine, calcite and ettringite. X-ray element mapping and image analysis methods have shown, that the heavy metals, especially lead, are present as: (1) individual, essentially pure small particles with particle sizes between 1-10 μm , as (2) pure, small areas within larger, heterogeneous glassy particles and (3) disseminated in varying amounts within or on the surface of glassy particles and other aggregates. Semi-quantitative elemental analysis indicate that lead, zinc, copper, chromium, tin, antimony, and titanium are present as oxides or hydroxides, rather than chlorides, sulfides, or carbonates. The thorough characterization of the fly ash is essential to understanding the reactions of the waste during stabilization and subsequent potential leaching by groundwater.

Leaching tests with percolation columns were applied for the evaluation of zinc- and lead-elution. The leaching was carried out with a constant solid-liquid-ratio. The fly ash was percolated seven times to develop the heavy metals elution. 20-, 30-, and 40-weight% substitution of calcium-bentonite and Opalinus clay were added to the fly ash: Zn-adsorption to bentonite-substitution ranged between 58%, 70% and 79% and Pb-adsorption between 43%, 43% and 59%. The adsorption for Pb with Opalinus clay ranged between 29%, 60% and 51%. Compacting the fly ash-bentonite mixture with proctor standard energy, the permeability is reduced from 10^{-7} m/s (pure fly ash) over 10^{-8} m/s (30-weight% bentonite substitution) to 10^{-9} m/s (with a 40-weight% substitution).

The immobilisation of heavy metals with clay minerals is obtained by the adsorption of the heavy metals with the clay minerals. The question remains open, if the reduction of the water flow in the compacted fly ash/clay-mixture has any influence on the adsorption of the heavy metals.

The Illite/smectite Geothermometer--Considerations and Case-History Studies in Hydrocarbon-Bearing Rocks of Miocene to Mississippian in Age

Richard M. Pollastro

U.S. Geological Survey, P.O. Box 25046, MS 960, Denver, Colorado 80225

Over the past decade, empirical relationships between clay minerals and temperature have provided a basis for the use of clay minerals as geothermometers. The utility of clay-mineral geothermometry has been applied mainly to diagenetic, hydrothermal, and metamorphic settings in an attempt to better understand the thermal histories of migrating fluids, hydrocarbon source beds, and ore and mineral formation.

Quantitatively, the most important diagenetic clay mineral reaction in sedimentary rocks is the progressive transformation of smectite to illite via mixed-layer illite/smectite (I/S). Changes in the proportion of illite and smectite (expandability), and ordering of I/S, as determined from X-ray powder diffraction profiles, correspond to changes in temperature due to burial. Although the smectite-to-illite reaction may be influenced by several factors, it appears to be strongly controlled by temperature. Studies show that the model proposed by Hoffman and Hower (1) is applicable in burial diagenetic settings from about 3 to 300 Ma. Reliability of the I/S geothermometer is, however, dependent upon a good understanding of the rock's original clay-mineral composition and burial and temperature histories (2).

In particular, changes in I/S are useful in the exploration for hydrocarbons because of the coincidence between the temperatures for the conversion from random-to-ordered I/S and those for the onset of peak, or main phase, oil generation. Common approaches utilizing the I/S geothermometer in diagenetic studies are 1) well profiles of I/S through several thousand feet of sedimentary rock, 2) I/S analyses of samples from a particular rock or bed in numerous wells at various depths, and 3) thermal history of a region from I/S analyses of outcrop and well samples.

The I/S geothermometer is commonly compared with other inorganic and organic geothermometers. Siliceous rocks of the Miocene Sisquoc and Monterey Formations, California, provide both I/S and silica geothermometers; temperatures derived from these geothermometers show good agreement in several wells having different geothermal gradients. Temperatures determined from I/S geothermometry in Lower Tertiary and Upper Cretaceous rocks of the Wagon Wheel No. 1 well, northern Green River basin, Wyoming, agree with those determined from vitrinite reflectance and fluid inclusions. These paleotemperature interpretations help explain gas generation and subsequent zones of overpressuring in the Pinedale anticline area.

Although the proportion of illite in I/S and ordering of I/S in hydrocarbon-productive chalk of the Upper Cretaceous Niobrara Formation, Denver basin, is variable because of its multiple sources, I/S formed in bentonite beds of similar origin shows progressive diagenetic changes in the proportion of illite and changes in ordering that can be directly correlated with thermal history. Thus, I/S in bentonites is useful for predicting the thermal maturity of hydrocarbons generated from the Niobrara in the region.

Sandstone and shale of the Permian upper part of the Minnelusa Formation, Powder River basin, Wyoming, and of Springeran and Morrowan age rocks of the Anadarko basin, Oklahoma, contain random I/S in wells at depths that correspond to calculated paleotemperatures <100 °C; similarly, only ordered I/S is found in wells at depths where calculated paleotemperatures are equal or greater than 100-110 °C. Thus, the Hoffman and Hower model seems to also apply well into the Paleozoic era.

References: (1) Hoffman, J., and Hower, J., 1979, in *Aspects of Diagenesis*, SEPM Spec. Pub. 26, p. 55-79; (2) Pollastro, R.M., 1990, in *Applications of Thermal Maturity Studies to Energy Exploration*, RMS-SEPM, p. 1-18.

Origin and Genesis of Clay Minerals at the Cretaceous/Tertiary Boundary Interval, U.S. Western Interior

Richard M. Pollastro and Bruce F. Bohor, U.S. Geological Survey, P.O. Box 25046, MS 960, Denver, Colorado 80225

Ancient coal-forming environments, particularly in Cretaceous and Tertiary peat swamps of the Rocky Mountain region, have preserved beds of altered airfall volcanic ash called tonsteins. These low-energy environments also allowed for the preservation of a distinct claystone couplet that formed from a unique airfall material at the Cretaceous/Tertiary (K/T) boundary. This well-preserved claystone couplet in Western Interior coal deposits records the details of a catastrophic event that terminated the Cretaceous Period.

The K/T interval in the U.S. Western Interior is represented by a 2 to 3-cm-thick claystone unit composed of two distinct clay layers overlain by a thin lignite bed. The boundary interval at these nonmarine sites differs significantly from K/T intervals described in marine sections. The more distal location of the marine sites from the source crater and greater susceptibility to reworking and detrital contamination in the marine environment are largely responsible for these differences. Additionally, many mineralogic and chemical components and textures of the K/T claystones are unique to this unit -- they differ from those in tonsteins and detrital clay beds within, or adjacent to, the boundary interval (1). Mineralogic, textural, and chemical evidence strongly favor the interpretation that these thin couplet layers are altered fallout ejecta resulting from the impact of an extraterrestrial bolide into siliceous crust (1, 2, 3, 4).

The impact sequence inferred from the two-layer claystone at Western Interior sites consists of two phases: a fireball-ejection-plume cloud and a melt-ejecta cloud. First, a fireball cloud was ejected above the atmosphere at high angles and high velocity, while a lower velocity, low-angle cloud of melted target rock was ejected slightly later and transported through the atmosphere. The melt-ejecta cloud deposited a blanket of melted target rock that contained minor bolide contamination, microtektites, and some shocked grains from near-surface target rock. The fireball cloud circled the earth and subsequently deposited a thin, iridium-enriched layer of condensed bolide glass, magnesioferrite-bearing clasts, and shocked minerals on top of the more localized melt-ejecta blanket layer. K/T sites in the Western Interior were probably close to the impact site because they display both ejection layers as a couplet and have the largest shocked grains of all sites globally; marine K/T sites, more distant from the crater, consist mainly of the fireball ejecta and contain shocked grains that are smaller than those found at Western Interior sites (3).

The clay minerals that formed in these two distinct layers are largely a function of the original composition and vitreous state of the fallout materials. The fireball layer is now mainly smectitic and formed from the alteration of glassy mafic material from the asteroidal bolide; a few kaolinite vermicules and graupen-like, kaolinitic clasts of altered silicic target melt are commonly mixed within the layer. The substantial iridium anomaly, the presence of high-Ni magnesioferrite crystals, and the overall geochemical signature support a vaporized bolide origin for the major portion of this layer (3).

The lower ejecta layer represents melted silicic target rock that is altered mainly to kaolinite with some smectite or mixed-layer illite/smectite. It also contains hollow spherules, dispersed shocked quartz grains, and a subdued iridium anomaly. The lower layer is characterized by an imbricate fabric of glass shards, bubbles, and spheres that are altered to clay and other diagenetic minerals (1, 2). In this layer, most of the vitreous components initially crystallized as "cabbage-like" microspherules of halloysite, probably from an allophane precursor. During subsequent burial and diagenesis, the metastable halloysite was converted to kaolinite. Minor smectite also formed during alteration of the glass. The crystallinity of kaolinite and illitization of smectite varies locally and is probably controlled by subsequent burial-diagenetic conditions. Original glassy droplets that display spherical and other splash-form morphologies resembling microtektites are altered to (or replaced by) various secondary minerals. These spherules were probably deposited as impact glass droplets (microtektites) and altered to their present chemical and mineral compositions by the local diagenetic environment.

References: (1) Pollastro, R.M., and Pillmore, C.L. (1987) *J. Sedim. Petrol.*, 57, 456-466; (2) Bohor, B.F. (1990a) *Tectonophysics*, 171, 359-372; (3) Bohor, B.F. (1990b) *Geol. Soc. Amer., Spec. Paper 247*, 335-342; (4) Sigurdsson, H., et al. (1991), *Nature*, 349, 482-487.

BEIDELLITE FROM THE BLACK JACK-TRADE DOLLAR MINE AND NEARBY
DELAMAR SILVER MINE

James L. Post and Barrett L. Cupp

Civil Engineering Department, California State University,
Sacramento, CA 95819
DeLamar Silver Mine, P.O. Box 52, Jordan Valley, OR 97910

The many clay seams in these mines were first described by Lindgren for the Geological Survey in 1899. Then, a specimen of "leverrierite" was sent to the U.S. National Museum, and later identified as beidellite by Nagelschmidt in 1938. The clay seams were formed during hydrothermal alteration in rhyolite and volcanic ash overlying granodiorite and along basalt structures. Separate species of monomineralic clay include beidellite, illite, halloysite, kaolinite and dickite. Ordered mixed-layer illite-beidellite is present in large amounts. The country rock is Mg-deficient and, thus, aluminous smectites are present.

Beidellite specimens from the Black Jack-Trade Dollar mines also contain orthoclase and fluorite, where the DeLamar mine beidellite is associated mainly with quartz and halloysite or kaolinite. The Al_2O_3 contents of the beidellite range from about 26 to 32 percent, and some Fe-beidellite also is found.

The DeLamar beidellite measured LL is 109 and PL is 35 whereas the optimum moisture content for the ASTM modified compaction test is only 15.7%. The maximum expansion pressure was about 9.3 kgf/cm² at 24.3% moisture content, from 9.4% air-dry content. The measured Al_2O_3 content of the beidellite is a linear function of the near infrared combination band position, as with other dioctahedral smectites, which range from 4455 for Fe-smectite to 4580 cm⁻¹ frequency for beidellite.

The basal spacing of the beidellite is very sensitive to humidity and temperature, normally about 15.05Å, going to 9.62Å at 300°C, and readily rehydrating after heating to 550°C.

Illite/Smectite Geothermometry of the Oronto Group, Southern Lake Superior Basin, Michigan

Kirsten L. Price and S. Douglas McDowell

Michigan Technological University

Characterization of the thermal history of the Lake Superior basin is an important component in assessing the potential for hydrocarbon reserves in the region. Samples from the Freda, Nonesuch, and Copper Harbor Formations of the middle Proterozoic Oronto Group are being investigated using XRD techniques on the less than 2 micron fraction of shale, silt and sandstone lithologies. Sampling thus far encompasses the area from the Presque Isle River to the vicinity of Calumet in Michigan's upper peninsula. Samples include outcrop as well as core from drill holes up to 4000 feet in depth.

Authigenic phases in the Freda and Nonesuch Formations include mixed layer illite/smectite and chlorite. Preliminary analyses of core near White Pine using methods described by Moore and Reynolds (1989)¹ and Srodon (1984)² indicate a regular trend with increasing depth from I/S with approximately 25% expandable layers to pure illite with only a hint of expandable layers. Examination of the illite 001 peak from core samples suggests an increase in illite crystallite size and crystallinity with depth. In the White Pine area illite is the dominant authigenic component of the Nonesuch Formation, while surface samples near Calumet indicate the persistence of expandable phases in the underlying Copper Harbor Formation.

Burtner and Warner (1986)³ demonstrated the decrease in I/S expandability as a function of T_{max} values derived from Rock Eval pyrolysis techniques; T_{max} values of 435 °C to 450 °C correspond to I/S expandabilities ranging from 30% to less than 10%. Results from XRD analyses of I/S within the Nonesuch are entirely consistent with T_{max} values of 435 °C to 440 °C reported by Pratt et al. (1991)⁴ from the Presque Isle and White Pine area.

Investigation of the clay mineralogy of the Oronto Group will continue with particular emphasis on both lateral and vertical variations. Future studies will include SEM and TEM analyses as well as the development of a thermal history model to consider both burial history and thermal effects associated with native copper mineralization of the underlying basalts. Acknowledgement is made to the Donors of The Petroleum Research Fund, administered by the American Chemical Society, for the support of this research.

¹Moore, D.M. and Reynolds, R.C. (1989) Oxford University Press, Inc. New York.

²Srodon, J. (1984) *Clays and Clay Minerals*, vol. 32, no. 5, p. 337-349.

³Burtner, R.L. and Warner, M.A. (1986) *Clays and Clay Minerals*, vol. 34, no. 4, p. 390-402.

⁴Pratt, L.M., Summons, R.E. and Hieshima, G.B. (1991) *Geochim. et Cosmochim. Acta*, vol. 55, p. 911-916.

RIETVELD REFINEMENT OF A *I1b*-2 CLINOCHLORE

John F. Rakovan and Stephen Guggenheim, Dept. of Geological Sciences, University of Illinois at Chicago, Chicago, Illinois 60680.

Single-crystal x-ray and Rietveld powder x-ray methods were used to study a clinochlore-*I1b* from West Chester, Pa., with a composition of $(\text{Mg}_{4.54}\text{Al}_{1.01}\text{Fe}_{0.26}\text{Cr}_{0.02})(\text{Si}_{2.93}\text{Al}_{1.07})\text{O}_{10}(\text{OH})_8$. The single crystal used was large (4 x 4 x 0.5 cm) and provided material for both methods. Precession patterns showed a dominant one-layer *I1b* polytype coherently intergrown with a minor two-layer *I1b* phase. The crystal was powdered by using an iron file, and a spray drying technique produced a random powder mount. Powder patterns showed no apparent two-layer phase present; thus, the Rietveld refinement procedures did not include the two-layer polytype.

The one-layer clinochlore-*I1b*-2 was refined by the Rietveld method to a final weighted residual, R_{wp} , of 0.089 in space group $C2/m$ with unit cell parameters of $a = 5.327 \text{ \AA}$, $b = 9.228 \text{ \AA}$, $c = 14.317 \text{ \AA}$, and $\beta = 96.85^\circ$. Octahedral bond distances, $\text{M1} = 2.09 \text{ \AA}$, $\text{M2}, 3, 4 = 2.02 \text{ \AA}$, are considered reasonable, whereas tetrahedral bond distances ($\text{T1} = 1.69 \text{ \AA}$) are not. Individual T-O bond distances varied from 1.55 \AA to 1.75 \AA . Fourier-difference maps showed tetrahedral cation and basal oxygen locations for the two-layer polytype superimposed on the silicon and basal-oxygen planes of the one-layer structure. The octahedral sheets in the two polytypes appear identical. It is likely that systematic errors affecting cation and anion positions in the tetrahedral sheet are related to the overlapping electron densities in the x-ray data for the two polytypes.

Results show that there is no apparent structural degradation from the use of a file and that spray drying is effective in producing a random powder mount. Furthermore, it appears possible to use Rietveld data to extract structural information for a coherently intergrown phase, if the minor phase is sufficiently similar to the input model in its structure.

One- and Three-Dimensional X-Ray Powder Diffraction Studies of Illite/Smectites Subjected to Different Sample Preparation Methods.

R. C. Reynolds Jr.

Department of Earth Sciences
Dartmouth College
Hanover N.H. 03755

Paul Nadeau and his coworkers demonstrated that mixed-layered illite/smectite crystallites could be disassembled into small particles that are much thinner than the X-ray coherent domain sizes of these minerals in oriented aggregates. Since those findings were published, some clay scientists and geochemists have been concerned that standard methods of separating and preparing clay-size fractions of sedimentary rocks for X-ray diffraction analysis produced artifactual structures that do not represent the natural character of the minerals. This question is addressed by the studies reported here.

Ten bentonites were studied by X-ray powder diffraction methods. These range from 12% to 100% expandable and include the ordering types $R=0$, $R=1$, and $R>1$. Diffraction patterns were obtained from rock fragments mounted in epoxy and ground flat, freeze-dried $<1\mu$ fractions prepared as randomly oriented powders, and $<1\mu$ fractions dispersed in water and oven-dried on glass slides. All specimens were solvated by the ethylene glycol vapor method.

The basal diffraction series (2 to $19^\circ 2\theta$) is sensibly identical for the three preparations from each sample. In fact, even line breadths are unaffected by preparation methods, indicating that either the crystallites did not come apart, or if they did, went back together to produce the same mean MacEwan crystallite thicknesses. No evidence supported the speculation that the one-dimensional structure of illite/smectite is modified by these laboratory procedures.

Three-dimensional diffraction studies indicate no preparation-specific modifications of rotational order/disorder, based on the similarity of the $k \neq 3n$ reflections (or their absence) on the diffraction patterns from the rock and powder pairs. More importantly, the degree of modulation of the 20; 13 band into discrete reflections is unaffected by dispersion and particle-size fractionation, demonstrating that the frequency of turbostratic displacements within the three-dimensional crystallites is not easily subject to modification. The modulation of the 20; 13 band is, however, well correlated with respect to percent expandability as deduced from the 00/ patterns, suggesting that turbostratic displacements occur at and are limited to the expandable interlayers of the illite/smectite crystallites.

STRUCTURAL AND COMPOSITIONAL VARIATIONS IN LOW-GRADE
METAMORPHIC ILLITE AND CHLORITE FROM THE BELT SUPERGROUP,
MONTANA AND IDAHO

Pete Ryan and Gray Thompson, University of Montana, Missoula,
Montana, 59812

Structural and compositional variations in coexisting illite and chlorite in the Proterozoic Belt Supergroup were studied over a wide range of low-grade burial metamorphic conditions. Samples were collected from the eastern portion of the basin where Belt rocks are thin and shallowly-buried, from the western portion of the basin where the thickness of the Belt exceeds 15,000 meters and burial depth was great, and from intermediate localities. The maximum temperature attained by eastern samples was 80° C, and that attained by western samples was 350°-400° C.

Chlorite in the eastern samples is predominantly of the I Ib polytype, with traces of the Ib polytype. Chlorite from all other samples is completely of the I Ib polytype. Chlorite in the eastern samples is mixed-layer chlorite/smectite (C/S) with 6% smectite layers. Both the proportion of chlorite layers in C/S and chlorite crystallite thickness increase westward with metamorphic grade. Eastern chlorites are Mg-rich, whereas higher-grade chlorites are richer in Fe.

Illite from eastern samples is mixed-layer illite/smectite (I/S) with 2% smectite layers. Both the proportion of illite layers in the I/S and illite crystallite thickness increase westward with metamorphic grade. The proportion of 2M₁ illite polytype increases westward from <10% to >95% with metamorphic grade.

The data suggest that I Ib chlorite and I/S with <2% smectite layers formed at a temperature ≤80° C in eastern samples, and that the 1Md illite polytype is stable or persists for long times at a temperature ≤80° C.

RESPIRABLE QUARTZ DETERMINATION
IN KAOLIN BY X-RAY DIFFRACTION METHODS

Timothy L. Salter and William E. Riley

Thiele Kaolin Company, P.O. Box 1056, Sandersville, GA 31082, USA

Recent Occupational Health and Safety Administration (OSHA) regulations require labeling of materials which contain known or suspected carcinogens at a concentration of 0.1%, or greater. Crystalline silica has been classified as a Group 2A substance (probably carcinogenic to humans) by the International Agency for Research on Cancer, and materials containing 0.1% quartz or any other silica polymorph must be labeled as potentially carcinogenic under current OSHA standards. This regulation covers many clays and other fine-grained natural materials, and has created an analytical problem in the detection and quantitation of quartz at 0.1%.

A method has been developed which permits quantitation of quartz in natural and processed kaolin at 0.1% and below. X-ray diffraction was chosen for quantitation to provide the best compromise between sensitivity and ability to discriminate quartz (and other silica polymorphs) from amorphous silica and other silica bearing minerals. The method developed involves addition of known quantities of a quartz standard to prepared kaolin and measurement of the intensity of the (101) diffraction peak. After removing the background, the integrated area of the diffraction peak is proportional to the quartz content. The linear relationship between peak area and quartz content extends over the interval considered (0.1% to 0.5% added quartz). The intercept of the quantitation line extrapolated to 0% added quartz is the quartz content of the original kaolin. The quantitation line can be used to determine the quartz contents of unknown kaolins. Quartz contents for kaolins range from <0.1% for the fine-grained fraction of water processed kaolin to >1% for crude kaolin.

Complicating circumstances in quartz analysis include the difficulty in detecting the quartz peak at such low abundances, and overlaps between kaolinite and mica diffraction peaks and the quartz (101) diffraction peak. The first difficulty is overcome by reducing the focusing circle of the diffractometer to a minimum, maximizing the intensity of the diffracted X-ray beam, and by counting for long time intervals at each 20 increment. The second circumstance is removed by treating the kaolin at 580°C for 30 minutes to destroy kaolinite peaks without producing mullite. There is presently no satisfactory means to remove overlapping diffraction peaks from illite and other mica minerals: if any diffraction peak at 1.0 nm is detected, the quantitation attempt must be discontinued. Less intense quartz diffraction peaks are not suitable for quantitative determination at 0.1% because their low intensities result in prohibitively long counting times.

Overview of Interactions of Organic and Inorganic Contaminants with Soils and Clays

B. L. Sawhney

Department of Soil and Water, The Connecticut Agricultural
Experiment Station, 123 Huntington Street, New Haven, CT 06511

Increasing concern about ground water contamination with industrial and agricultural chemicals disposed or applied to the soil requires that we understand their interactions with soils and their constituents. During the past decade, a large number of investigations have been carried out on reactions and movement of many of the 126 organic priority pollutants, 24 metals and 4 inorganic ions included in the U.S. EPA's target compound list (TCL). In this review are discussed sorption reactions and mechanisms of both ionic and nonionic organic compounds, and sorption and precipitation reactions of metals with soils as they relate to their concentrations in the aqueous phase which ultimately determines their movement to ground water.

The uptake of ionic organic compounds by soils and clays is well understood while that of nonionic compounds is incompletely understood. The cationic compounds are known to sorb by ion exchange with the cations in soil and clays. The sorption of anionic compounds is extremely limited in these systems because of sparsity of exchangeable anions. The uptake of nonionic organics involves several mechanisms: sorption by organic matter, sorption on clay surfaces and diffusion into interparticle pores. In addition, the presence of redox-active metal cations which promote catalytic properties of clays, such as polymerization of phenols, and of surface functional groups which promote coupling reactions with organics, further enhance the uptake of organic contaminants. In efforts to attenuate the movement of organic pollutants to ground water, their reactions with synthetic clays and with chemically modified clays have been investigated both in the vapor and the aqueous phases. The uptake of metals by soils and clays occurs by sorption and/or precipitation. These interactions have been investigated under different pH and redox conditions. Attempts to predict their concentrations into solution generally involve models based upon solubility product of the likely precipitated compounds. Finally, the role of clay liners from the natural clays and the development of liners from synthetic and modified natural clays in attenuating movement of pollutants to ground water are discussed.

FAR INFRARED SPECTROSCOPY OF MIXED-LAYER ILLITE/SMECTITES

Paul A. Schroeder

Department of Geology and Geophysics, Yale University, P.O. Box 6666, New Haven, CT 06516

Investigation of the far infrared (IR) spectra of mixed-layer illite/smectites indicates the presence of torsional mode absorption bands associated with fixed interlayer potassium sites. By contrast, hydrated montmorillonitic interlayer sites are transparent in the far IR. The intensity of bands for interlayer cation sites is related to both the magnitude and site of negative layer charge within the 2:1 layer structure. The bimodal nature of spectra of illite/smectite leads to the suggestion that two fixed potassium environments occur in the illite structures studied. These two environments are influenced by octahedral composition. The interlayer torsional modes at 112 and 89 cm^{-1} represent fixed potassium sites influenced respectively, by an Al-rich, high charge dioctahedral layer and a heterogeneous aluminum-iron-magnesium, low charge layer. A general trend of increasing absorption of the 112 cm^{-1} band relative to the 89 cm^{-1} band is observed in a typical illite/smectite burial diagenetic sequence in Miocene shales from the Gulf of Mexico sedimentary basin. An increase in absorbance of both bands is also seen with an increase in degree of illitization and the amount of fixed potassium in the illite/smectite. These observations are consistent with a concept of shales undergoing illitization during burial diagenesis by both the collapse of high charge smectite layers to form illite layers and the formation by recrystallization of new high charge (-1.0) illite layers.

TRACE ELEMENT ANALYSIS OF ATMOSPHERIC AEROSOLS USING A SYNCHROTRON X-RAY FLUORESCENCE MICROPROBE

D. G. Schulze¹, R. H. Grant¹, S. R. Sutton², and M. L. Rivers²¹ Agronomy Department, Purdue University, West Lafayette, IN 47907² Geophysical Sciences Department, The University of Chicago, 5734 South Ellis Avenue, Chicago, IL 60637

Atmospheric aerosol particles were collected 5 km southeast of Vincennes, Indiana from 3 air masses. Two had arrived within 3 days from either Canada or the Gulf of Mexico, while one had resided over the Midwest for more than 4 days. The particles were analyzed on the synchrotron x-ray microprobe on beamline X26A at the National Synchrotron Light Source, Brookhaven National Laboratory. Analyses of filters containing >7, 7-3.3, and <1.1 μm (aerodynamic diameters) aerosol fractions were made using 5 and 10 μm x-ray beam spot sizes and 1D and 2D scans.

The aerosol samples contained Fe, Ti, Mn, Ni, Cu, Zn, Pb, and Sr in general agreement with the expected composition of a combination of crustal and anthropogenic sources. Cu was one of the most variable elements, both among air masses and among size fractions of the same air mass. Cu concentration in the aerosols of the air mass coming from Canada was about an order of magnitude less than in the air mass from the Gulf of Mexico or the air mass resident over the Midwest. The size distribution of Cu, in conjunction with the air mass trajectory analysis, indicated a combination of both local and distant sources.

Preliminary results of 2D scans of the >7 μm fraction of a Midwest aerosol showed Ca, Fe, Mn, and Ti rich areas of the filter were usually coincident, but the Cu distribution suggested that Cu sometimes occurs as relatively Cu-rich particles. The 2D scans of the <1.1 μm fraction from the same air mass showed areas where Ca, Fe, Ti, and Cu were highly associated, while other areas showed Mn and Zn to be highly associated.

FAULT GOUGE CLAY DATES - HOW MEANINGFUL ARE THEY?

Shafiqullah, M and PE Damon, Department of Geosciences, University of Arizona, Tucson, AZ 85721

K-Ar dating technique and thermo-mineralogy of fault gouge clays can become important tools in solving some tectonic problems. Authigenic submicron illite found in fault gouge clays has a high K-Ar closure temperature. We estimate the closure temperature to be about 200 °C and 180 °C for cooling rates of 100 °C/Ma and 10 °C/Ma respectively. Thus, K-Ar dating of illite provides an ideal geochronometer.

Characterization of the mineral assemblage by electron microscopy and X-Ray diffraction provides information concerning the thermal and chemical environment. Smectite clays above 70 °C rapidly absorbs potassium to form mixed-layer illite-smectite assemblage. Above 180 °C, if sufficient iron and magnesium are available to form chlorite, the assemblage becomes illite-chlorite, whereas above 230 °C the assemblage becomes white mica-chlorite.

Sampling is critical. It is essential to know what is being collected and how to isolate contaminants related to the footwall, hangingwall and extraneous clayey minerals. The authigenic component is normally very fine grained (<0.1 micron) and the proportion of authigenic illite increases with decreasing grain size. Hence, submicron clays appear to yield consistent K-Ar dates. However, if the detrital and authigenic illite components are of similar size, or detrital core with illitic overgrowth is present, the detrital component tends to contribute toward older dates. Scatter of K-Ar dates on fault gouges in the literature appear to be due to improper sampling or incomplete separation of detrital and authigenic components.

When the dates on coeval samples with different K contents do not agree within experimental limitations or structural-stratigraphic constraints, the basic assumptions of the K-Ar method are not met. In such a case, ^{40}K vs ^{40}Ar and $^{40}\text{Ar}/^{36}\text{Ar}$ vs $^{40}\text{K}/^{36}\text{Ar}$ isochron methods have limited usefulness in explaining the scatter as well as the isochron age (Shafiqullah and Damon, 1974) from an evaluation of K-Ar isochron methods.

Shafiqullah, M., and P. E. Damon, 1974. Evaluation of K-Ar isochron methods: *Geochim. et Cosmochim. Acta*, v.38, p.1341-1358

INTERACTION BETWEEN CHLOROHYDROCARBON AND HEAVY CATIONS IN THE
CLAY INTERLAYER: AN EXAMPLE OF SYNERGISTIC EFFECT

Darsa P. SIANTAR and José J. FRIPIAT

Department of Chemistry and Laboratory for Surface Studies, University of Wisconsin-
Milwaukee, P.O. BOX 413, Milwaukee, Wisconsin 53201

The adsorption of cis-1,2-dichloroethylene (CDE) on hectorite exchanged with Hg^{2+} , Cd^{2+} , Ag^+ , and Na^+ has been studied by measuring simultaneously the CDE adsorption and water desorption isotherms and by recording the infrared (IR) spectrum of the adsorbed phase. The clay was outgassed at room temperature before the adsorption experiment under such conditions that the interlayer cations remain hydrated. In this situation, there is a competition between the hydration water and CDE but the number of water molecules displaced is much less than the number of CDE adsorbed.

The adsorption process of CDE is not purely physical since, upon long outgassing, the characteristic IR bands of CDE although much weakened, are still observable in the Hg^{2+} and Cd^{2+} clays. The association between CDE and the cation may result from dipole-cation interaction or through the interaction of the double $>\text{C}=\text{C}<$ bond with the cation (as known, for instance, for Hg^{2+}). A Raman active band is observed, showing that the symmetry of the molecule has changed upon adsorption.

Completely dehydrated clays do not adsorb CDE even if some residual chemisorbed CDE is trapped in the interlayer. The adsorption of the chlorohydrocarbon is enhanced by the presence of heavy cations, such as Hg^{2+} or Cd^{2+} suggesting a synergistic effect between both organic and inorganic pollutants.

INFLUENCE OF CITRIC ACID AND GLYCINE ON KINETICS OF MERCURY (II) ADSORPTION BY KAOLINITE: Singh, J. and Huang, P.M., Department of Soil Science, University of Saskatchewan, Saskatoon, Sask., Canada.

Interactions between sediment particulates and metals play an important role in the regulation of dissolved metal concentrations in freshwaters. The extent of the association of Hg with sediment particulates is controlled by the nature and properties of sediments and ionic factors. This investigation was carried out to study the effect of different concentrations of citric acid and glycine, which are common in freshwaters, on the kinetics of the adsorption of Hg by kaolinite under various pH conditions. The data indicate that Hg adsorption by kaolinite in different concentrations of citric acid and glycine obeyed multiple first order kinetics. Citric acid had a significant retarding effect on both the fast and slow adsorption process at pHs 6.0 and 8.0, while it had a significant promoting effect on the fast and slow adsorption process at pH 4.00. In the presence of 10^{-3} and 10^{-2} M citric acid at pH 4.00, Hg was present mainly as Hg citrate complexes. The kaolinite surface carried net positive charge at pH of 4.00, the Hg citrate complexes thus could be adsorbed by kaolinite. In addition, citrate was also adsorbed on the kaolinite surface and the residual COOH group of the citrate adsorbed on Kaolinite would serve as the new adsorption sites for the mercury. Therefore, the rate of Hg adsorption by kaolinite increased with increasing citric acid concentration at pH 4.00. At pHs of 6.00 and 8.00, kaolinite surface carried net negative charge and Hg citrate complexes also apparently had negative charge. Therefore, the rate of adsorption of Hg decreased in the presence of citric acid. The amount of citric acid adsorbed by the kaolinite was also minimum due to the repulsion of the negatively charged surface of kaolinite and citrate in this pH range. Glycine had a very pronounced enhancing effect on the rate of Hg adsorption by kaolinite during the fast process. The rise in pH of the system further increased the effect of glycine on Hg adsorption. The rate of the fast adsorption of Hg by kaolinite significantly increased as the concentration of glycine increased from 0.00 to 10^{-2} M over the pH range of 4.00 to 8.00, indicating that compared with $\text{Hg}(\text{OH})_2$, the Hg-glycinate species has a higher affinity towards the surface of kaolinite. The magnitude of the retarding/promoting effect of citric acid and glycine upon the rate of Hg adsorption was evidently dependent upon the pH, structure and functionality of organic acids, and molar ratios of the organic acid/Hg. The data obtained suggest that low-molecular-weight organic acids merit close attention in studying the kinetics and mechanisms of the binding of Hg by sediment particulates and the subsequent food chain contamination.

THE EFFECTS OF BURIAL DIAGENESIS ON THE TEXTURE, MINERALOGY AND PROPERTIES OF SOURCE ROCKS FROM THE PERMIAN BASIN.

Sivagnanam Sivalingam, Texas Tech University, Lubbock, Texas.

The fabric of organic rich shales are affected by the type and amount of clay minerals, amount of organic matter and the degree of diagenesis. Precipitation of diagenetic minerals such as pyrite, quartz, calcite and dolomite within the shale affected the texture drastically. This caused an increase in shale density, reduction in porosity and permeability. Fissile shales were altered to dense massive calcareous shale. Shale intervals with higher amount of organic material seem to have experienced a lower degree of diagenesis. In certain shale intervals fissility is enhanced by epitaxial growth of clay minerals.

The diagenetic transformation of clay minerals within the shales causes a variation in clay morphology, reduction in cation exchange capacity, reduction in geocatalytic properties and the release of ions due to substitution within the lattices. Shales with randomly mixed illite/smectite clays have higher CEC and greater geocatalytic properties compared to the ordered R3 type illite/smectite clays. The reduction in the CEC is related to the decrease in the amount of smectite and a decrease in surface area due to precipitation of diagenetic minerals within the clay aggregates. The reduction in the specific catalytic activity is related to a reduction in Bronsted and Lewis acidity.

The interrelationship between the texture and primary migration within source rocks, the development of seals due to precipitation of diagenetic minerals and the unreliability of pore pressure prediction using shale density will be presented.

ANALYTICAL ELECTRON MICROSCOPY OF ILLITE/SMECTITE CLAYS FROM THE PERMIAN BASIN.

Sivagnanam Sivalingam and Necip Guven, Texas Tech University, Lubbock, Texas.

The most abundant clay minerals in the source rocks of the Atokan and Wolfcampian ages from the Permian Basin are illite/smectite clays.

The illite/smectite clays in the Atokan shales from the Northwestern shelf are less mature than the Wolfcampian shales, consisting of a mixture of RO and RI phases with about 45 to 75% illite. The Wolfcampian shales from the Delaware Basin, Midland Basin and Southern Shelf contain R3 ordered phase with about 70 to 95% illite component. Precipitation of diagenetic minerals such as quartz, pyrite and carbonate minerals are common in the more mature shales. Destruction of clay minerals was also observed within the calcareous shale sequence.

The Atokan clays and Wolfcampian clays show different morphology. Under SEM the Atokan clays shows a cornflake texture whereas the Wolfcampian clays shows a platy habit. Under TEM the Atokan clay aggregates occur as subrounded smooth lamellar aggregate whereas the Wolfcampian clay occurs as dense domained and subrounded aggregates.

The Atokan clays which have a higher percentage of smectite component shows a higher amount of octahedral AL and Fe compared to the Wolfcampian clays. There is an increase in both tetrahedral and octahedral substitution in the Wolfcampian clays. The octahedral charge is largely created by Mg substitution and the tetrahedral charge by Al substitution for Si. The amount of K⁺ in Atokan clays (RO and R1) ranges between 0.32 to 0.42 whereas the amount of K⁺ averages about 0.61 (R3, Welch A) and to a high of 0.77 in clays with 95% illite.

The lattice fringes of Atokan clays show true mixed layering whereas the more mature Wolfcampian clays shows packets of discrete illite with structural discontinuity between them. Two models of illitization, transformation-recrystallization and neoformation-recrystallization will be discussed.

ESTIMATION OF GIBBS FREE ENERGY OF FORMATION OF CLAY MINERALS USING CALCULATED BINDING ENERGIES

M. Slaughter
Department of Chemistry and Geochemistry
Colorado School of Mines
Golden, CO 80401

Jae-Young Yu
Department of Geology
Gangwon National University
Chuncheon 200-701, The Republic of Korea

ABSTRACT

The determination of clay stabilities as a function of chemical environment and composition requires free energies of formation. Experimental free energies of formation for good reasons are frequently seriously in error or are not practical to measure. Expressions may be derived for the clay minerals, relating calculatable partial binding energies to Gibbs and Helmholtz free energies of formation. Using partial molar free energies of substituent groups such as AlO_2^- for SiO_2 one may calculate the free energies of any clay composition, if accurate free energies of formation are available for a few end member minerals.

The Gibbs free energies of formation of clay minerals are estimated from the calculated binding energies by the equation $\Delta G_{f,298}^\circ = kE_{\text{cal}} + C$, where $\Delta G_{f,298}^\circ$ is the standard Gibbs free energy of formation, E_{cal} is a calculated partial binding energy, k is a scaling factor and C is a correction term. The scaling factor, k , is determined only by the kind of interlayer cations. The correction term C is a function of the octahedral composition. The Gibbs free energies of formation of clay minerals estimated by the above equation are quite accurate.

The Gibbs free energies of formation show a parallelism among phases having the same octahedral chemical composition, indicating that the scaling factor k is valid. Iso-compositional clay phases makes the correction term C constant, as well as the scaling factor k , and allows determination of relative stabilities. Using partial molar free energies for structural groups such as $\text{MgO}_{1.5}^-$ or $\text{Fe}^{2+}\text{O}_{1.5}^-$ relative to $\text{AlO}_{1.5}$, give good estimates of the free energies of any nonstoichiometric clay phase.

Parameters and equations are presented to calculate the Coulomb, Pauli repulsion and London energies for partially ionic complex silicate and oxide structures for all crystal systems. The parameters are ionicities, ionic charges, electronegativities, Pauli radii, ion polarizabilities, ionization energies and electron affinities. Some parameters for clays derive from the ionic part of the binding energies of pyrophyllite, muscovite and paragonite. The precision of ionic binding energy is ± 0.1 kcal or 0.001% of the total ionic binding energy.

PARTIAL BINDING ENERGIES AND STRUCTURAL PROPERTIES OF THE HEULANDITE/CLINOPTILOLITE SERIES

M. Slaughter

Department of Chemistry and Geochemistry
Colorado School of Mines
Golden, CO 80401

Jae-Young Yu

Department of Geology
Gangwon National University
Crunchcon 200-701, The Republic of Korea

ABSTRACT

Clinoptilolite and heulandite are nearly isostructural. The principal difference is not just the amount of aluminum and divalent cations such as Ca^{2+} in the structure. Although these two factors affect the thermal stability and ion exchange properties, one of the most important factors in determining the properties of heulandite/clinoptilolite is the substitution of Al in the layer- or sheet-linking tetrahedra, which in heulandite violates the so-called aluminum avoidance rule. Binding energy calculations show that a structure with Al in adjacent layer-linking tetrahedra is the lowest energy structure for heulandite at ambient temperatures, when Ca and/or Sr are the charge balancing cations. Such an arrangement minimizes the Coulomb energy of the structure. Clinoptilolites, which do not have Al concentrated in the linking tetrahedra should have low Ca/Sr content and/or low Al content.

The Al-substituted sheet-linking tetrahedral oxygens, where both tetrahedra are substituted, binds strongly to divalent cations, inhibiting the replaceability of Ca^{+2} in heulandite. Reduced substitution in the linking tetrahedra enhances the replaceability of cations of clinoptilolite, because of reduced Coulomb attraction between charge balancing cation and framework oxygens. The differences in thermal properties of heulandite and clinoptilolite correlate with the lower energy associated with the aluminum substituting in the sheet-linking tetrahedra, the proportion of K^+ relative to Ca^{2+} and Na^+ in the exchange positions and only secondarily with Si content. Increasing the amount of K^+ at the exchange sites increases the thermal stability of both heulandite and clinoptilolite, because of increased Pauli repulsive forces. Pauli forces prevent collapse of K-saturated heulandite and clinoptilolite. The large Coulomb forces at higher temperatures cause collapse of the sheet-linking tetrahedral oxygens around the dehydrated Ca^{+2} , causing the collapse of the structure. The structural properties of haulandite/clinoptilolite suggest that Ca^{2+} is the structure determining element in natural systems.

Experimental Determination of the Stability and Rate of Precipitation of Authigenic Illite: J.S.Small

Dept. of Geology, University of Manchester, Manchester, M13 9PL U.K.

Illite precipitation experiments have been performed between 200°C and 250°C at 500bars using Dickson fluid-sampling bombs. Dissolution of an amorphous Al/Si gel in an initial solution of K-oxalate produces conditions supersaturated with respect to illite, and results in mass precipitation of lath and fibrous-type illites. The morphology and composition of this synthetic illite are highly representative of authigenic sandstone illite.

The precipitation of illite from solution has been directly monitored by fluid sampling at up to 12 intervals during an experiment and subsequent measurement of solute concentration and quench pH. The pathway of fluid composition during illite precipitation and its relationship to the timing of precipitation has been compared to the existing (a_K/a_{H^+} vs. a_{SiO_2}) stability diagram. This reveals that fibrous and lath-shaped illites are associated with precipitation outside the illite stability field under conditions of K-feldspar and zeolite stability. However, the final steady state fluid composition, assumed to represent equilibrium, coincides with buffering by illite/K-feldspar. In contrast, platy illite formed in KCl solution precipitates from solution within the established limits of illite and muscovite stability.

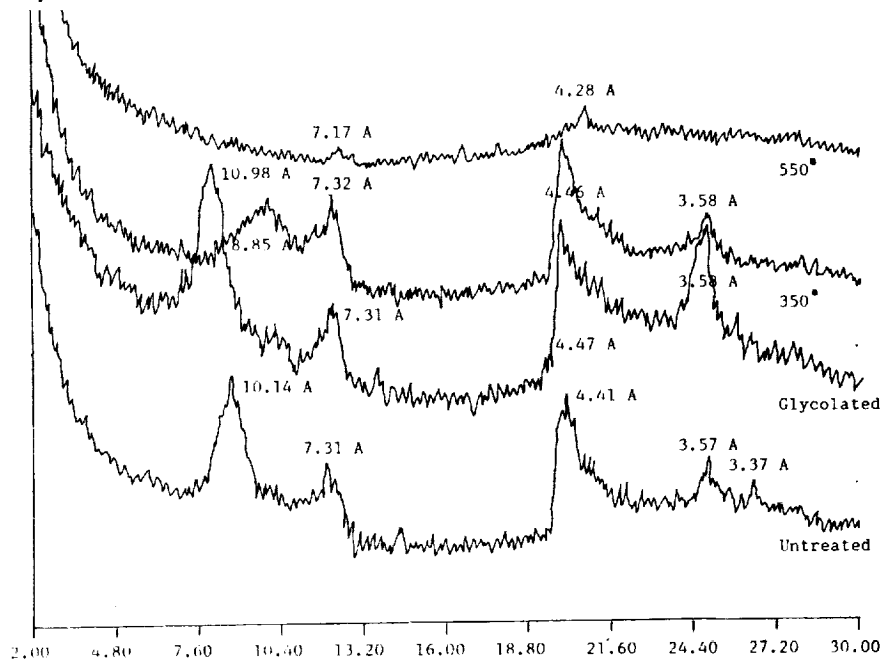
Al and K solute concentrations during illite precipitation show a pronounced decrease with time until a steady state, equilibrium concentration is reached. This concentration vs time data can be used to measure illite precipitation rate. The oversaturation of Al and K with time conform to a first order rate equation when allowance is made for decreasing fluid volume during sampling, and for an increase in effective surface area for nucleation as illite precipitates. Precipitation rate measured at 200°, 230° and 250°C define a linear Arrhenius function which when extrapolated to reservoir temperatures at an appropriate fluid/rock ratio is consistent with the time/temperature of formation of authigenic sandstone illite constrained by K/Ar dating methods. This result implies that the first appearance of neofomed illite in a burial sequence is kinetically controlled by burial and thermal histories.

HALLOYSITE; PRODUCT OF CALCIUM-RICH PLAGIOCLASE ALTERATION, RIVERSIDE COUNTY, CALIFORNIA. Matthew C. Taylor and Richard W. Berry

Dept. of Geol. Sciences, San Diego State Univ., San Diego, CA 92182

A Mesozoic gabbro consisting of calcic plagioclase, olivine, pyroxene, amphibole and spinel was itself intruded during late Mesozoic by granite pegmatite. The study area is located northeast of Anza in Riverside County, California. The intrusion is irregular, occurring as an assemblage of small dikes, sills and pods, often a few centimeters wide but occasionally widening to several meters. Host gabbro is highly altered between pegmatite strands and to a distance of at least 10 meters on either side of the dike complex. A trench exposed altered gabbro to a depth of approximately 11 meters below surface but full depth of the alteration zone is unknown. Discontinuous exposures suggest the zone of alteration extends for the entire 1.5 to 2 kilometer extent of contact between pegmatite and gabbro.

Gabbro is altered to fine grained powdery grey to white material. Barely enough original material remains to identify it. Pseudomorphs after parent minerals are sufficiently strong to maintain their integrity but are very weakly held together, one to another, making the alteration zone soft. Pseudomorphs after calcic plagioclase were separated, analyzed by x-ray diffraction and found to be halloysite (see below). Pseudomorphs after mafic minerals were shown to consist of smectite, also by x-ray diffraction analysis. Clay minerals in adjacent pegmatite "pockets" are smectite. Most, but not all "pockets" have been ruptured. Halloysite and smectite do not ordinarily occur as mineral associates. A single hydrothermal fluid may have interacted with different parent minerals to produce smectite and halloysite pseudomorphs in contact with each other. Alternatively, two pulses of alteration (one associated with initial pegmatite intrusion and a second associated with pocket rupture) may have been responsible for the two remarkably different clay mineral pseudomorphs. Until more than one pulse of hydrothermal alteration is clearly documented, the hypothesis attributing primary control of alteration product mineralogy to parent mineralogy is favored.



AUTHIGENIC MUSCOVITE $^{40}\text{AR}/^{39}\text{AR}$ ISOTOPIC ANALYSES AS A TOOL FOR
TIMING PRESSURE SOLUTION IN THE JURASSIC NORPHLET FORMATION
Thomas, A.R.¹, Dahl, W.M.², Hall, C.M.³, and York, D.³

- 1) Texaco EPTD, 3901 Briarpark, Houston, Tx. 77042
- 2) Texaco USA, 400 Poydras St., New Orleans, La. 70130
- 3) Univ. of Toronto, Dept. of Physics, Toronto, Ont. M5S 1A7, Canada

The Texaco Mobile Bay Block 872 #1 Well, Offshore Alabama, was drilled in 1988 and penetrated a highly stylolitized Upper Norphlet Formation sandstone at 22500 ft. subsea. The quantity of stylolites contained in this well is anomalously high for the trend. Three morphologies of authigenic muscovite are associated spatially with the stylolites:

- * **large 1M muscovite** (1 cm. long, 0.2 cm. wide) found along vertical offsets in the stylolites,
- * **pore-filling muscovite** (30 to 50 micron sized aggregates) currently found within 5 cm. of the stylolites,
- * **muscovite pods** (30 to 50 micron sized aggregates) contained within the insoluble residue of the stylolite seams.

Because the Norphlet contains essentially no detrital muscovite, authigenic muscovite growth appears to be linked chemically and spatially to stylolitization and pressure solution of potassium feldspar.

Eight stylolite bearing sandstone thin sections were selected for neutron activation and $^{40}\text{Ar}/^{39}\text{Ar}$ analyses. Ages were assigned to each muscovite morphology by laser fusing areas of the thin section ≥ 50 microns in diameter. Thirty seven total analyses illustrate that each muscovite morphology grew at a different time:

- * large 1M muscovite - 54 \pm 14 million yr.
- * pore-filling muscovite - 73 \pm 24 million yr.
- * muscovite pods - 83 \pm 18 million yr.

A burial history curve for the well indicates the onset of stylolitization, as indicated by authigenic muscovite growth, occurred at 12000 to 13000 ft. Age sequence and textural similarity substantiate the theory that the muscovite pods are relict pore fills which accumulated in the insoluble residue during stylolitization. Age data indicate this style of authigenic mica growth continued until 17000 to 18000 ft. burial depth where the large 1M muscovite, growing normal to the plane of maximum compressive stress, began to dominate the pore-filling morphology. The fundamental change in mica growth style and the comparative abundance of the large 1M muscovite morphology is presumed to indicate the onset of intense stylolitization.

The age bracket of the large 1M muscovite marks an organic maturity range just beneath the top of the dry gas window. Gas leakage occurring at this time would not only have promoted stylolitization through temporary fluctuations in reservoir fluid pressure/overburden pressure, but also would account for the gas-water contact which is currently located well above the deepest pyrobitumen-stained Norphlet Formation sandstone.

NON-FACIES SELECTIVE CLAY PARAGENESIS OF SANDSTONE RESERVOIRS, FULLER RESERVOIR FIELD, WIND RIVER BASIN, WYOMING: THOREZ, J., Liege State University, Liege, Belgium; BOSSIROY, D., INIEX, Liege, Belgium; FLORES, R.M., and KEIGHIN, C.W., U.S. Geological Survey, Box 25046, Federal Center, Denver, CO 80225

Facies analyses of cores from the Paleocene Fort Union Formation in Fuller Reservoir field, Wind River Basin, Wyoming, recognized fluvial channel, crevasse splay, delta front, and offshore lacustrine sandstone reservoirs. Clay minerals of these facies-reservoir types were analyzed to determine their paragenesis.

The less-than-2-m clay fraction was extracted from these sandstone reservoirs and prepared as oriented aggregates. The samples were X-rayed in air dried, glycolated, and heated (325°-500°C) states. Complementary tests, including attack with boiling 4N HCl followed by hydrazine saturation (kaolinite "crystallinity") and Li-saturation for identification of swelling components, were performed to yield more accurate qualitative analyses. X-ray diffraction analyses indicated a complex clay composition with a predominant kaolinite component that comprised well-crystallized kaolinite (Kt), disordered kaolinite (Kd), and dickite (D). Minor components were chlorite (C) and illite (I). Chlorite consisted of degraded Fe-chlorite or neoformed Mg-chlorite. Illite consisted of mixed layer illite-smectite (I/S) containing less than 50% swelling layers. These clays are a combination of illite with montmorillonite (cf. I/M) and illite with beidellite interlayers (cf. I/Bei); the former represents neoformed "hairy" illite in sandstone pores, whereas the latter reflects a transitional degradational stage in the weathering of parent (feldspar) silicate structure. Also present were traces of mixed-layer (10-14C) material that was made up of illite layers and distended interlayers behaving like chlorite.

Quantitative analyses of clay components do not indicate a relationship between clay paragenesis and reservoir types. This may be due to complex diagenetic history, which includes provenance-inherited clays (I, Kd, C, and 10-14C), in situ weathering (I/Bei), and in situ neoformation (I/M with "hairy" illite, Kt, D, and Mg-chlorite).

QUANTITATIVE WHOLE ROCK DETERMINATION OF CLAY MINERALS IN SANDSTONES BY COMBINED XRD/TG/EWA

D.M. Thornley & T.J. Primmer

B.P. Research Centre, Sunbury-on-Thames, Middx, TW16 7LN, U.K.

Current methods of quantitative clay mineral analysis of whole rock samples often provide little more than an estimate of clay mineral abundances, especially if the total clay mineral content comprises <10% (wt/wt) of the sample. Thermogravimetry evolved water analysis (TG/EWA), combined with X-ray diffraction (XRD) data, allows more accurate, quantitative determination of absolute abundances of clay minerals in the whole rock to be made.

The TG/EWA system incorporates a high precision thermobalance linked to a water specific infra-red detector. This is used to analyse quantitatively the clay mineral dehydroxylation water evolved from the whole rock when heated from 300°C to 900°C. This data can be combined with data from XRD analysis of a separated clay size fraction, to determine quantitatively clay mineral abundances in the whole rock sample.

Artificial sand/clay mineral mixtures with known amounts of different clay minerals (chlorite, illite and kaolinite) were prepared such that total clay concentrations did not exceed 10% (wt/wt). Results show that, compared to the amount of that clay mineral weighed into the mixture, the accuracy of calculated clay mineral abundances are influenced by,

1. The degree of accuracy in determining the relative proportions of the respective clay minerals in the clay size fractions by XRD.
2. The assumed water content of each individual clay mineral.
3. The measured evolved water content of the clay mineral/sand mixture.

Errors induced in (1) were found to far outweigh errors in (2) or (3). In minimising these errors, determinations accurate to better than 5% (relative) for a given clay mineral could be made at absolute concentrations as low as 2% (wt/wt). This constitutes a dramatic improvement over that currently achieved by routine XRD analysis of whole rock samples.

SYNTHESIS OF SMECTITE FROM A VOLCANIC GLASS, CLAY MINERALS AND ROCKS AT 1 ATM.: Tomita K., Yamane H., and Kawano M., Institute of Earth Sciences, Faculty of Science, Kagoshima University, 1-21-35 Korimoto, Kagoshima-shi, 890 Japan

Smectite and various zeolites were formed from a volcanic glass, clay minerals such as kaolinite, sericite, pyrophyllite, talc and chlorite, and rocks such as granites, andesites and a basalt as the products of the reaction with NaOH solution at 90~100°C under atmospheric pressure. Formation conditions of smectite and various zeolites were restricted by the ratio of the amount of starting material(g) to NaOH(g) in the solution. In an experiment where a pumice of 1~2mm size was used as a starting sample, smectite was formed on the surface of the pumice, and zeolites were formed in the vesicles in the pumice. When 0.02~0.03g of volcanic glass was boiled in the 100ml of 2M~3M NaOH solution, smectite was formed well after 30~40 hrs. boiling. When 0.03g of kaolinite was boiled in the 100ml of 2M~3M NaOH solution, smectite was formed well after 30~60 hrs. boiling. When sericite or pyrophyllite was used as a starting material, a similar result was obtained. When talc was used as a starting material, stevensite was formed after reaction of a short time. Smectite was also formed from granites, andesites and a basalt as reaction products respectively. Powdered and block samples of these rocks were used for the experiments. When 0.02~0.03g of powdered granite was boiled in the 100ml of 3M NaOH solution, smectite was formed after a 30~50 hrs. reaction, and only zeolites were formed after a 90 hrs. reaction. When a block sample of granite was boiled in the 100ml of 2M NaOH solution, smectite was not formed after a 5 day reaction and smectite was formed on the surface of only plagioclase after a 16 day reaction. Only zeolites were formed after a 100 day reaction. When 0.03g of powdered andesite was boiled in the 100ml of 3M NaOH solution, smectite was formed after a 32 hr. reaction, and only zeolites were formed after a 60 hr. reaction. When a block sample of andesite was boiled in the 100ml of 2M NaOH solution, smectite was formed in the cracks of pyroxenes and in the ground mass after a 5 day reaction, and smectite was formed on the surface of plagioclase after an 8 day reaction. Only zeolites were formed on the surface of plagioclases.

OXIDATION OF PHENOL IN ACIDIC AQUEOUS SUSPENSIONS OF MANGANESE OXIDES.

Ukrainczyk, L. and McBride, M.B.

Department of Soil, Crop and Atmospheric Sciences, Cornell University, Ithaca, NY 14853.

Phenol (benzenol) oxidation by three synthetic manganese oxides (buserite, manganite, and feitknechtite) has been studied in aerated, aqueous, acidified, suspensions. The rate of reaction was pH dependent. It was greatly enhanced for pH below 4, where diphenoquinone and p-benzoquinone were identified as the initial products. The initial reaction rate was correlated with standard oxidation potential (E°) of the oxides following the order: feitknechtite > manganite > buserite. A more gradual process of phenol oxidation after the initial reaction was influenced by electrochemical properties of the solution: high soluble manganese activity and increase in pH adversely affected reaction rates. Thus the reactivity of the oxides for this slower reaction was related to their stability and possibly the ability to readsorb Mn(II), following the order: buserite > manganite > feitknechtite.

The results indicate that thermodynamic and electrochemical data for oxides and phenols are useful in predicting under which conditions phenols can be oxidized by a given system.

TEXTURAL AND COMPOSITIONAL VARIATIONS IN SIZE FRACTIONATED AUSTRALIAN KAOLINS.

Philippa J.R. Uwins & Ian D.R. Mackinnon

Electron Microscope Centre, University of Queensland, Queensland, 4072, Australia

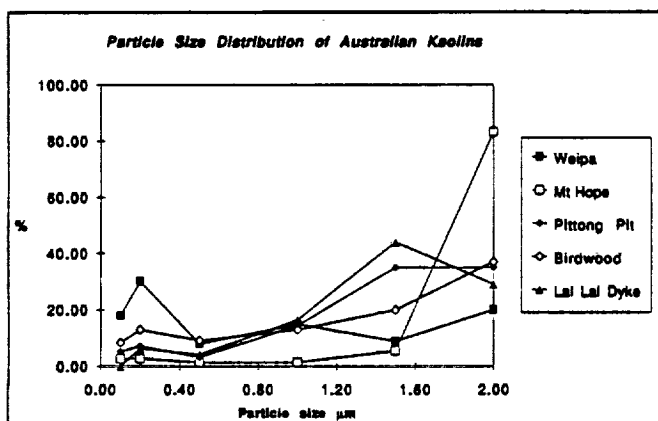
Kaolinites from different geological environments have nominally different properties such as particle size distribution, shape, degree of crystallinity and impurities. These properties influence the quality of commercial kaolinites and determine the nature of kaolin uses such as paper coatings, fillers, ceramics or refractories. Because of the abundance of kaolin deposits in Australia, a comprehensive microstructural study (SEM, TEM, HRTEM, AEM and XRD) has been initiated of Australian kaolins, from commercial and undeveloped sequences covering a wide range of geological environments. This study aims to gain an understanding of the textural, compositional and particle size variations between and within the different kaolin deposits. In addition, relationships between the parent rock, particle size distribution, morphology, degree of structural order and chemistry may significantly influence downstream processing such as intercalation efficiency.

Samples from six localities have been examined using a JEOL 6400F SEM, JEOL 890F SEM, JEOL 4000 FX AEM, and Hitachi 200kV TEM. These localities cover a wide range of depositional environments and geological timescales:

1. Weipa (Queensland) sedimentary; Late Cretaceous/Early Tertiary.
2. Lal Lal dyke (Victoria) residual; altered Devonian dyke.
3. Mt Hope (South Australia) residual; deep insitu weathering of Archaen granite gneiss.
4. Birdwood (South Australia) residual; altered biotite schist.
5. Pittong Pit (Victoria) residual; altered Devonian granodiorite.
6. Lal Lal Pit (Victoria) residual; altered Devonian granodiorite.

Distinct textural differences in each deposit can be clearly seen; in some cases, the current fabric closely resembles the parent source. For example, the Birdwood deposit retains a microfolded schistose fabric even though the original biotite schist has completely altered to kaolinite. Significant morphological variation can be observed between deposits and within size fractions of a given deposit. The Pittong Pit samples show ragged and embayed crystallites, while those from the nearby Lal Lal dyke have well defined platy morphologies.

Particle size distributions were determined for six fractions of each deposit by repeated centrifuging and subsequent SEM and TEM imaging. The particle size distribution for each deposit is shown in Figure 1. In general, most deposits show a predominant particle size in the 0.5 to 2.0 μm range with the exception of the Mt Hope and Weipa samples. For Mt Hope, most particles (80%) are > 2 μm , while for the Weipa deposit, > 50% of the particles are < 0.5 μm in size.



Particle crystallinities as measured via XRD and calculated using the methods of Plançon and Zacherie (1990) show variation between deposits. For example, all samples show both single and bi-phase defect structure in different size fractions. Single phase fractions show a range of layer values from 23 to 45. Calculated Hinkley Indices for all samples show little variation (ranging from 1.3 to 1.7) in any size fraction. Particle crystallinity determinations by Plançon and Zacherie are clearly more effective than HI values in providing distinguishing criteria which can be related to bulk physical properties.

"CRYSTALLINITY" AND INTERCALATION RELATIONSHIPS IN SIZE FRACTIONATED AUSTRALIAN KAOLINITES.

Uwins, P.J.R.,¹ Mackinnon, I.D.R.¹ & Thompson, J.G.²

¹Electron Microscope Centre, University of Queensland, Queensland, 4072, Australia

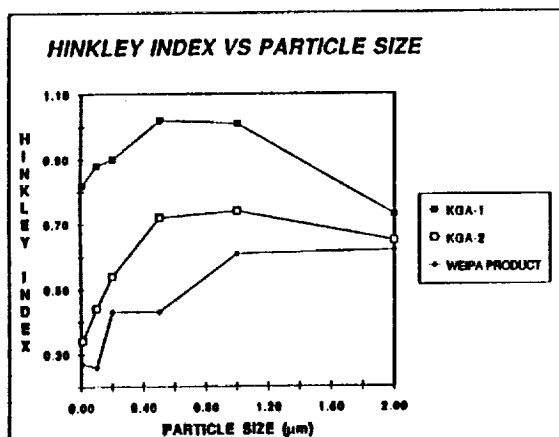
²Research School of Chemistry, Australian National University, Canberra, ACT 2600, Australia

The physical properties of kaolinites influence not only the commercial viability of a particular deposit (e.g., brightness, rheology, particle size distribution, crystallinity) but also the chemical and surface properties of the bulk product. In an earlier comparative study of Weipa and Georgia kaolins, it was found that the effectiveness of intercalation with N-Methylformamide (NMF) varied between and within deposits. The efficiency of reaction was measured via a number of parameters, including the percentage of unreacted kaolinite in the intercalated product. To better appreciate the relationship between kaolinite physical properties and the mechanisms of clay-polymer intercalation, clays from four other Australian deposits have been compared with those of this earlier study.

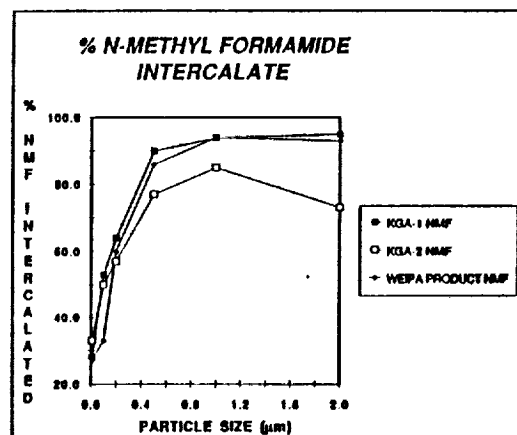
Samples from sedimentary and residual deposits ranging in age from Archean to Early Tertiary have been analysed using HRTEM, AEM, SEM and XRD. In each case, particle size, shape, crystallinity and degree of intercalation with NMF have been determined by a combination of these techniques. Each sample was weighed and separated into six size fractions by repeated centrifuging. The resulting size fractions were weighed to determine the proportion of each bulk product with a specific size distribution.

Six fractions from three samples, Weipa, KGa-1, and KGa-2 and three fractions from the remaining samples were chosen for preliminary analysis and XRD traces were collected in order to determine crystallinity using both the Hinkley Index and the Expert system of Plançon and Zacherie, 1990. In all samples the crystallinity decreased with decreasing particle size in the less than 0.5-1 μ m fraction and this appears to be independent of the parent source rock (Fig. 1).

Each sample was then intercalated with N-methylformamide via hydrazine hydrate to determine the effect of parent source, particle size and crystallinity on intercalation. Particle size appears to provide a stronger control on intercalation than the degree of structural order, since almost 100% yields of intercalated product can be achieved using a certain size fraction (approx. 2 μ m) of both highly crystalline kaolinite and poorly ordered kaolinite (Fig. 2); small size fractions on the other hand, irrespective of crystallinity, had lower yields for NMF. Preliminary results also show that the HI values of kaolinite remaining in the intercalated product, is in general higher for intercalated size fractions than for the original size fractionated starting material. This observation implies that the degree of crystallinity is not a decisive parameter for the determination of intercalation yields on kaolinites. In addition particle shape characterised by both TEM and SEM does not tend to reflect the degree of structural order or the ability to intercalate.



1



2

**Artificial weathering of biotite and phlogopite on ultrathin sections;
studied in HRTEM**

H. Vali, R. Hesse and H. Kodama

**Department of Geological Sciences, McGill University,
3450 University Street, Montreal, Quebec, Canada H3A 2A7**

***Land Resource Research Centre, Agriculture Canada, CEF
Ottawa, Ontario, Canada K1A 0C6.**

Ultrathin sections (700-800Å thick) of resin-embedded biotite and phlogopite (<2µm fraction) were cut with an ultramicrotome. For artificial weathering the sections are transferred onto grids with formvar and carbon supported film as substrate and treated with a 0.1 M CaCl₂ solution for 2-12 hours at 60 °C and up to 4 days at room temperature. Intercalation of n-alkylammonium ions makes direct imaging of expandable interlayers in HRTEM possible (Vali and Hesse, 1990). The exchange of interlayer cations and the chemical composition of individual particles were determined using a JEOL 100 CX TEM at 100 kV equipped with an energy-dispersive X-ray detector.

The untreated natural sample of biotite (Renfrew County, Ontario) and phlogopite (Burgess, Ontario) revealed no expandable component on ethylene glycol or glycerol solvation in XRD. However, after octadecylammonium ($n_c = 18$) treatment, 10 to 30% of the layers expanded forming random mixed-layers with the non-expanded 10 Å layers. The proportion of expanded layers increased after CaCl₂ treatment. A complete expansion of all layers in the samples could not be achieved. The expanded and non-expanded components usually occurred as coherent sequences up to hundreds of layers thick within individual particles. However, a small proportion of random mixed-layer structures was also observed. Since the micro-environmental conditions for all particles in a section are about the same, different responses of individual layers to a given chemical reaction appear to be controlled more by variation in chemistry than by the kinetics of the reaction.

Comparison between naturally weathered biotite or phlogopite, (Jefferson vermiculite: Brinton's Quarry, Pennsylvania and Llano vermiculite: Texas, CMS sample VTA-1), with the artificially weathered materials revealed significant differences in morphology and expansion behavior of the two sets of samples. Artificially weathered biotite and phlogopite did not respond to heptylammonium ($n_c = 7$) exchange, whereas natural vermiculite expanded easily. No dissolution of layers has been observed in these weathering experiments of biotite and phlogopite. However, for the natural samples a dissolution and reprecipitation mechanism cannot be excluded. Based on chemical composition, the interlayer charge of biotite and phlogopite is 1 per [O₁₀(OH)₂]. Surprisingly, n-alkylammonium exchange gave the same XRD patterns for natural vermiculites as for phlogopite suggesting that the interlayer charge of these vermiculites is higher (close to 1?) than previously assumed.

Vali, H. and Hesse, R. (1990) Amer. Miner., 75, 1443-1446.

Combined TEM observation of layer structure and surface microtopography applied to study the crystal growth mechanism of clay minerals.

H. Vali, R. Hesse and J. Środoń*

**Department of Geological Sciences, McGill University,
3450 University Street, Montreal, Quebec, Canada H3A 2A7**

*** Centre de Géochimie de la Surface CNRS, 1 Rue Blessig,
67084 Strasbourg, France**

The layer arrangement and surface morphology of smectite, illite and S/I mixed layers were studied using HRTEM, freeze-etching and metal-decoration techniques [1, 2, 3].

Treatment of smectite/illite samples with n-alkylammonium ions revealed three different types of interlayer spacings corresponding to: (1) a non-expanded component, (2) a high-charge expanded component, and (3) a low-charge expanded component. They are identified respectively as: (1) illite interlayers, (2) illite interlayers expanded by alkylammonium cation, (3) smectite interlayers. The identification of (2) is based on: (i) groups of high-charge expanded layers made visible in pure illite samples with alkylammonium treatment; (ii) the calculation of expandability from HRTEM images, which give numbers unacceptably higher than obtained by other HRTEM and Pt/C-shadowing techniques, if both (2) and (3) were regarded as smectite, [4]; (iii); significantly decreased K^+ content after alkylammonium exchange.

Comparison of layer structure imaged in ultrathin sections with the surface morphology observed on freeze-etch replicas suggests that the smectite to illite conversion through intermediate S/I mixed layers during burial diagenesis is a dissolution and reprecipitation mechanism. A layer-by-layer transformation of smectite layers to illite by potassium fixation appears unlikely. Individual smectite layers which are common in shallow subsurface samples do not occur in the samples from greater depths. Individual double layers which correspond to Nadeau's thinnest illite fundamental particles are present in the samples from intermediate and great depths.

Replicas of hydrated freeze-etched and gold-decorated hydrothermal illite revealed that a large variation exists in both shape and size of individual particles. Rhombohedron-shaped growth forms were present in addition to lath-shaped and pseudohexagonal ones. These individual crystal types occurred in a variety of particle sizes (50 Å to 2 μm) suggesting that they grew independently. The conversion of one type to another would require dissolution and reprecipitation. Both dissolution and crystal growth features are observed in the same specimens.

[1] Vali, H. and Bachmann, L. (1988) *J. Colloid Interf. Sci.*, 126, 278-291.

[2] Vali, H. and Hesse, R. (1990) *Amer. Miner.*, 75, 1443-1446.

[3] Vali, H., Hesse, R. and Kohler, E. (1991) *Amer. Miner.*, in press.

[4] Środoń, J., Andreoli, C., Elsass, F. and Robert, M. (1990) *Clays Clay Miner.* 38, 373-379.

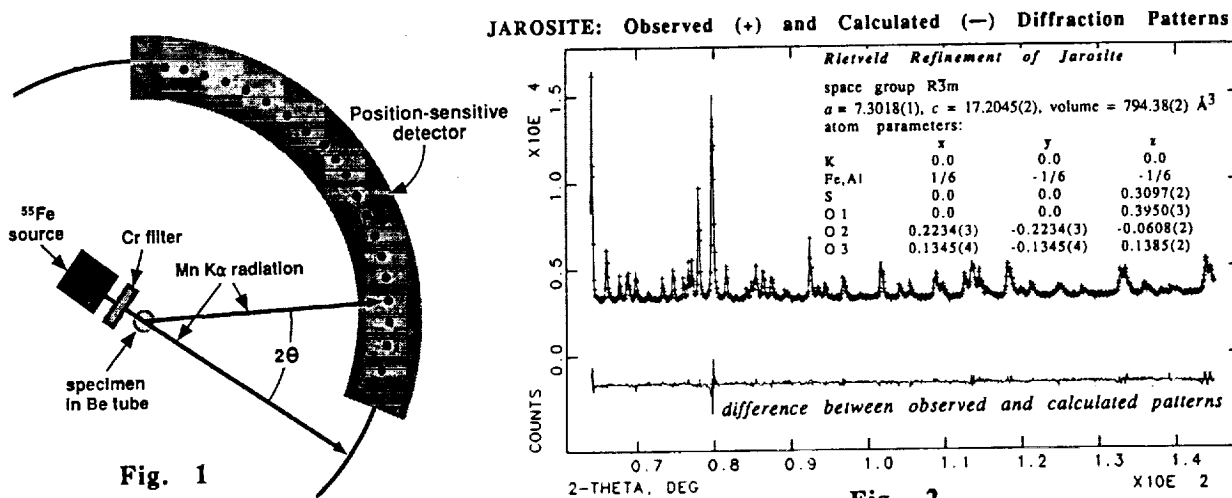
INTEGRATED XRD AND XRF DATA FROM A SINGLE INSTRUMENT FOR PLANETARY-SURFACE EXPLORATION

D. Vaniman, D. Bish, and S. Chipera

Earth and Environmental Sci. Div., Los Alamos National Lab., Los Alamos, NM 87545

The Viking mission to Mars demonstrated geochemical exploration by XRF. The instrument flown on Viking was relatively crude compared with current technology, but it was powerful enough to provide some of the most important information about the martian surface: the great similarity between the two chosen landing sites, the surprising abundances of S and Cl, the dominance of Fe-rich basaltic rocks at the landing sites, and the strong evidence of hydrous alteration. Missing from the Viking lander, however, was an instrument to determine the mineralogy into which this chemistry is cast. Without such instrumentation, it has proven very difficult to determine the alteration mineralogy that is so critical in deciphering the present and past surface environments on Mars.

A simple, single instrument for combined XRD and XRF analysis is shown in Fig. 1 (the XRD mode is illustrated). For XRD analysis, this instrument might use a Cr-filtered ^{55}Fe isotopic X-ray source for Mn $K\alpha$ radiation, a blade-type position-sensitive detector, and Debye-Scherrer geometry built around a spinning Be sample tube. For XRF, the Cr filter is removed from the ^{55}Fe source, an additional higher-energy source is unshielded, and additional detectors are used. This is only one of many possible configurations, combining minimal power requirements, accurate XRD and XRF data collection, rugged construction, and few moving parts.



Collection of both XRD and XRF data from a single sample provides simultaneous chemical and mineralogic data; these data can be used to constrain the modes derived from chemical data and to correlate quantitative chemistry and mineralogy as a set of simultaneous linear equations, the solution of which can lead to full characterization of the sample. The use of Rietveld methods for XRD data analysis can provide a powerful tool for quantitative mineralogy [1] and for obtaining crystallographic data on complex minerals (e.g., the possible Martian mineral jarosite, Fig. 2). Rietveld methods applied to the XRD data will provide (1) enhanced accuracy for quantitative mineralogy, (2) a capability for crystal-chemical characterization of unstable minerals in their natural environment, and (3) a capability to recognize and characterize previously unknown minerals.

[1] Vaniman, D. T., D. L. Bish, and S. J. Chipera, 1991, Lunar and Planet. Sci. XXII, 1429-1430.

SEPIOLITE AT THE SURFACE OF YUCCA MOUNTAIN, NEVADA

D. Vaniman, D. Bish, S. Chipera, and M. Ebinger

Earth and Environmental Sciences Division, Los Alamos National Laboratory, Los Alamos, NM 87545

Sepiolite with intergrown calcite occurs in complex laminae within faults and in slope-parallel carbonate-plugged horizons at the surface of Yucca Mountain. Opal-CT and opal-A are associated with the sepiolite-plus-calcite assemblages, but opal is seldom if ever intergrown with the sepiolite. The commonest occurrences of sepiolite assemblages are as (1) multiple generations of fibrous laminae, (2) clasts of these laminae that have been reworked into other, later-formed laminae, and (3) concentric ooid rims. Within the slope-parallel carbonate-plugged horizons that are distant from the faults, the development of sepiolite-plus-calcite assemblages is not as extensive as it is within the faults. Within the faults, the occurrence of sepiolite fibers in pods up to 1 mm wide and 1 cm long indicates that the mineral is authigenic rather than detrital.

Petrographic, X-ray diffraction, and electron microprobe studies of the sepiolite within the faults suggest a range of compositions that may be sensitive to the timing and environment of sepiolite formation (Table 1). Sepiolite within the most recent laminae is a relatively pure Si-Mg form (columns 1 and 2), whereas some earlier-formed laminae (column 3) include sepiolite that is Al,Fe-rich and some sepiolite from portions of the silicified tuff wall-rock of the fault (column 4) is relatively Al-rich.

Table 1: Electron Microprobe Analyses of Sepiolite from Fault-filling Laminae (Columns 1-3) and from Silicified Tuff Wall-rock (Column 4)

	1	2	3	4
	<u>1-T13a-2b</u>	<u>1-T13a-4b</u>	<u>1-T11a-4b</u>	<u>4-T11a-3c</u>
SiO ₂	56.6	56.3	55.0	53.7
Al ₂ O ₃	0.37	0.66	1.21	2.26
Fe ₂ O ₃	<0.04	<0.04	4.60	<0.03
MnO	<0.12	<0.12	<0.11	<0.11
MgO	24.0	23.1	19.4	22.4
CaO	0.22	0.15	0.29	<0.12
Na ₂ O	0.21	<0.14	0.47	<0.15
K ₂ O	<0.12	<0.12	0.30	<0.11
H ₂ O*	18.5	19.7	18.8	21.6

*H₂O estimated by difference, assuming 100% totals.

The occurrence of authigenic sepiolite, calcite, and opal in the laminated deposits is in accord with deposition by desiccation of trapped solutions. Source waters for these solutions are attributable to high-CO₂ soil-zone water equilibrated with siliceous igneous rocks at low temperature [1]. Such an origin is also in accord with stable isotope studies that suggest a meteoric origin for waters that precipitated the calcite in these deposits [2].

[1] Garrels R.M. and F.T. Mackenzie (1967) Origin of the chemical compositions of some springs and lakes, *Equilibrium Concepts in Natural Water Systems*, Amer. Chem. Soc., Washington, D.C., pp. 222-242; [2] Quade J. and T.E. Cerling (1990) Stable isotopic evidence for a pedogenic origin of carbonates in trench 14 near Yucca Mountain, Nevada, *Science* 250, 1549-1552.

CLAY AND VITRINITE KINETIC MODELS B Velde

Dept. Geology ENS, 24 rue Lhomond, 75005 Paris, France

A two step reaction model is used to simulate clay diagenesis in the smectite-to-illite conversion. Loss of smectite content of the aggregate clay edifices is modelled and compared to change in vitrinite reflectance. Determination of clay compositions is made using decomposition methods on the composite, assymetric illite peak found near 10A.

Calculated examples compared to sedimentary series with complex burial histories show that the clay composition - vitrinite reflectance correlations allow one to estimate the burial history and heating rate of sedimentary series with reasonable accuracy. Appropriate nomograms are given.

The last stages of I/S to illite transfer are easily followed as well as the increase in grain size of the micaceous illite particles. The illite peak is resolved into two bands, one showing the small grain size fraction, the other the coarse micaceous fraction.

Use of the results presented allows one to estimate the geologic history of rocks hitherto considered to reside in the limbo between sedimentary and metamorphic domains.

CLAY STABILITIES UNDER SHOCK PRESSURE B Velde, et al.

Dept. Geology ENS, 24 rue Lhomond, 75005 Paris, France

The shock pressure transformation of kaolinite and smectite (montmorillonite) have been investigated under laboratory conditions. Shock pressures of 20 to 40 GPa were employed to obtain the crystalline to diaplectic glass transition. Infrared spectra of the shock products were used to identify and characterize the materials. It is seen that the clays change in ways quite similar to those of tectosilicates (quartz and feldspars) by a mixed phase shock pressure region where crystals and glass are found together. Kaolinite changes in the 20 to 30 GPa region whereas smectite changes abruptly near 25 GPa. The stability of these two clay minerals can be considered to indicate ranges to be expected for clays found in meteorites, ie. iron serpentines and smectites.

N92-10254

UV, VISIBLE, AND NEAR-IR REFLECTIVITY DATA FOR MAGNETIC SOILS/ROCKS FROM BRAZIL.

R. K. Vempati¹, R. V. Morris¹, H. V. Lauer², Jr. and J. M. D. Coey³.

¹ Code SN2, NASA-Johnson Space Center, Houston TX 77058, ²LESC, Houston TX 77058, and ³Dept. Pure and Applied Physics, Trinity College, Dublin, Ireland.

Recent studies indicate that certain Brazilian tropical soils have saturation magnetizations (J_s) greater than $1 \text{ Am}^2 \text{ kg}^{-1}$ (kg of Fe_2O_3) (1-2), which is sufficiently large to satisfy the magnetic constraints for the Martian regolith. The objective of this study is to obtain UV, visible, and near-IR reflectivity spectra for several magnetic Brazilian soils/rocks and compare them to corresponding data for Mars to see if these materials satisfy both magnetic and spectral constraints for Mars.

Table 1. Selected mineralogical properties of some Fe-rich Brazilian soils/rocks.

Sample	Color	Mineralogy	J_s^\dagger $\text{Am}^2 \text{ kg}^{-1}$	$^4\text{T}_{1g}$ nm
B7	dark brown	pyrophyllite, kaolinite, gibbsite, Al-hematite , maghemite	8.1	870
B9	brown	kaolinite, gibbsite, hematite , maghemite	14.4	870
M1	reddish brown	<i>hematite</i> , maghemite, Al-goethite , gibbsite	3.9	860
QF 4ar‡	burnt orange	<i>goethite</i> , <i>hematite</i> , pyrophyllite, gibbsite	1.7	900
QF 2dr‡	chocolate brown	hematite , magnetite, kaolinite, gibbsite	31.1	850

† data adapted from study 1 and 2; J_s values reported is per kg of Fe_2O_3 and ‡ ground rock samples. **Bold** and *italicized* letters indicate the predominant and second dominant Fe oxides, respectively.

Selected physical properties of the magnetic Brazilian soils/rocks are given in Table 1. The reflectivity spectra of the B7, B9, M1, and QF 2dr samples show the spectral signature of hematite, *e.g.*, the presence of the $^4\text{T}_{1g}$ crystal-field band at $\sim 870 \text{ nm}$. This is the case even though Mössbauer data indicate M1 contains about 70% Al-goethite. The reason for the optical dominance of hematite in M1 is not clear, but it may be a particle-size effect and/or a coating phenomena. For QF 4ar, the presence of the $^4\text{T}_{1g}$ crystal field band at 900 nm and a nearly-resolved $^4\text{T}_{2g}$ band near 640 nm are consistent with the spectral signature of goethite. We see no spectral evidence for maghemite even though its presence is indicated (1) The reflectivity in the near-IR decreases in the order QF 4ar, M1, B9, B7, and QF 2dr from approximately 50 to 7%. This range results from particle-diameter and mineralogical differences among the samples; *e.g.*, the presence of magnetite in QF 2dr undoubtedly contributes to its low reflectivity. The presence of bands near 1400 nm and 1900 nm for samples M1 and QF 4ar indicate optically significant amounts of H_2O - and/or OH-bearing phases.

The presence of a very shallow band near 860 nm in Martian spectral data has been attributed to crystalline hematite (3). In general, the spectral features resulting from ferric crystal-field transitions are much better defined in the spectra of the magnetic Brazilian soils/rocks than in Martian spectral data. Presumably, this results from a relatively higher proportion of crystalline ferric oxides for the former. The apparent masking of the spectral signature of maghemite by hematite or goethite for the Brazilian samples implies the magnetic and spectral constraints for Mars can be decoupled. That is, maghemite may be present in magnetically-significant but optically-insignificant amounts compared to crystalline hematite. The data for sample M1 show that the positive spectral evidence for hematite on Mars does not exclude the presence of other crystalline ferric oxides.

REFERENCES

- (1) Allan, J. E. M., Coey, J. M. D., Resende, M. and Fabris, J. D.. (1988) *Phys. Chem. Minerals*, **15**, p. 470-475.
- (2) Resende, M., Allan, J. E. M. and Coey, J. M. D. (1986) *Earth and Planet Sci. Lett.*, **78**, p. 322-326.
- (3) Morris, R. V. and Lauer, H. V. Jr. (1990) *J. Geophys. Res.*, **95**, p. 5101-5109.

N92-10255

SYNTHESIS AND PROPERTIES OF Ti-SUBSTITUTED GOETHITES AND HEMATITES.

R. K. Vempati¹, R. V. Morris¹, H. V. Lauer², Jr., and J. DeHart¹.¹NASA-Johnson Space Center and ²Lockheed Engineering and Sciences Company, Houston, TX 77058.

Titanium is the second most abundant transition element next to Fe in terrestrial soils, and the Viking mission soil analyses at two sites indicated that this is true also for Martian soils. The presence/association of Ti in soil goethites and hematites has been documented in terrestrial environments (1-3), which suggests the formation of these minerals authigenically in the pedogenic environments. The objective of this study was to synthesize Ti-substituted goethites and hematites and to characterize them using x-ray diffraction (XRD), thermogravimetric analysis (TGA), coulometry, optical and Mössbauer spectroscopies, and magnetic data in order to determine the evidence for Ti substitution in the Martian spectral data.

Titanium-substituted goethites containing 0 to 4 percent Ti were synthesized in the laboratory under alkaline conditions. Corresponding Ti-hematites were made by heating the sample at 650°C for 24 h. The Fe and Ti contents were analyzed using an electron microprobe. The color of the unsubstituted goethite was yellow and became darker with increasing substitution; Ti hematites were dark red irrespective of Ti substitution. No XRD peak shifts resulting from Ti substitution were observed for both oxides. The half-line widths of 110 and 111 XRD Ti-goethite peaks were in the range of 0.254 to 0.211 and 0.297 to 0.211 °2θ, respectively which indicate well-crystallized oxides. The TGA analysis of Ti-goethites in He gas, showed that the dehydroxylation temperature increased from 269°C for unsubstituted to 290°C for the 4 mole percent Ti samples, providing evidence for the Ti substitution in goethite structure. Total water analysis was ~11%, which is the stoichiometric value within the error. Room temperature Mössbauer spectroscopy showed that the hyperfine splitting value (B_{hf}) decreased from 38.4 T for unsubstituted to 37.3 T for the 4 mole percent Ti-goethites; the full peak width at half height (FWHH) increased with increasing Ti-substitution which further confirms the incorporation of Ti in the crystal lattice. The room temperature Mössbauer spectroscopy for Ti-hematites showed no differences in B_{hf} values. At 11K, the Ti-substituted hematites underwent a Morin transition at a temperature less than 260° K value for the unsubstituted hematite which suggests the presence of Ti in the hematite structure. The reflectivity spectra of the Ti-substituted goethites and hematites showed that the $^4T_{1g}$ crystal field band occurred at ~920 and ~860 nm, respectively, independent of Ti content. The $^4T_{2g}$ band for the unsubstituted goethite was observed at ~670 nm and the position of this band was also unaffected by Ti content.

This study provides evidence that up to 4 mole percent can be incorporated into the goethite structure during the low temperature synthesis. Because the spectral data in the visible and near-IR are not sensitive to the degree of Ti-substitution in goethites and hematites, such data cannot likely be used to infer the presence or absence of Ti substitution in Martian hematites and goethites.

REFERENCES

1. Fritzpatrick R. W. and Le Roux J. (1975) *Proc. Int. Clay Conf., Mexico City*. Appl. Publ., Wilmette, Ill., p. 585-599.
2. Fritzpatrick R. W. Le Roux J. and Schwertmann U. (1978) *Clays Clay Minerals*, vol. no. 26, p. 189-201.
3. Tessens E. and Zauyah S. (1982) *Soil Sci. Soc. Am. J.*, vol. no. 46, p. 1103-1106.

CLAY MINERALS IN SUBDUCTION ZONES - ROLE OF INTERLAYER WATER

Peter Vrolijk, Exxon Production Research Co., P. O. Box 2189, Houston, TX 77252-2189

Dehydration of clay minerals in subduction zones in particular, and sedimentary rocks in general, strongly influences the geochemistry of pore waters. For example, in the Barbados accretionary prism (ODP Leg 110), active fault zones and the décollement zone contain fluids anomalously depleted in chloride and enriched in ^{18}O . Because the sedimentary section contains abundant smectite, dehydration of smectite is inferred to be the principal contributor to the geochemically altered fluids.

Although the anomalous chloride concentrations are explained by dilution of pore waters by fresh interlayer water, the observed enrichment of pore waters in ^{18}O could result from loss of interlayer water if the fractionation of oxygen isotopes between interlayer and pore waters was sufficiently large (on the order of 3-5‰) or by dissolution of smectite and precipitation of illite during smectite-illite transformation. Because in theory it is conceivable that interlayer water is enriched in ^{18}O relative to pore waters (considering hydrogen bonding to tetrahedral layers and creation of hydration sheaths around interlayer calcium atoms), it is difficult to distinguish waters modified by loss of interlayer water from those influenced by smectite-illite reactions. For the fluid migration problem posed for Barbados, distinguishing these two sources is important for understanding migration distances and fluid sources.

To solve this problem of fluid sources, experiments were performed to determine the oxygen and hydrogen isotope composition of interlayer water of Na- and Ca-montmorillonite (cation exchanged SWy-1). Rather than trying to completely extract interlayer water from the samples, the isotopic composition was determined by preparing a completely dehydrated clay sample by gentle heating in a vacuum. A specified amount of clay was then placed in a glass equilibration vessel with a specified amount of water of known isotopic composition and a small amount of CO_2 gas. The mixture was placed in a controlled temperature bath at temperatures of 2, 5, 10, 25, and 50°C , smectites were allowed to expand, and isotopic equilibrium between interlayer water, pore water, and CO_2 was established. CO_2 was extracted and analyzed to determine the change in the isotopic composition of pore water, from which the isotopic composition of interlayer water was then computed. The procedure for determining the hydrogen isotope composition was identical except H_2 was used instead of CO_2 and Hokko beads, platinum-impregnated teflon beads, were added to the experiment to catalyze hydrogen isotope exchange.

The experimental results indicate that interlayer water is depleted in ^{18}O by 1‰ at 10°C and 0.2‰ at 50°C . There is no difference in fractionation between Na- and Ca-montmorillonite, indicating insignificant effect of bonding to interlayer cations. Although many other techniques suggest that interlayer water is structured, these data suggest that interlayer water is less structured than pore waters. This dilemma may be resolved by postulating that interlayer water is highly structured in the plane of the interlayer, but because of the tight space constraints, there is little opportunity for structuring in the third dimension. Hydrogen isotope experiments are somewhat scattered and indicate either no fractionation between interlayer and pore waters or a slight enrichment of interlayer waters in deuterium, consistent with fractionation expected for hydrogen bonding of water to tetrahedral oxygen atoms.

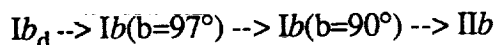
For the Barbados accretionary prism, the results indicate that the geochemically anomalous pore fluids observed in the décollement zone must be derived from smectite-illite reactions occurring at deeper structural levels rather than *in situ* dewatering of clays. In fact describing a single source of the anomalous fluids permits me to calculate that 10-20% of the fluid in the décollement is derived from deeper levels, based on mass balance calculations of the chloride and oxygen isotope budgets.

CHLORITE POLYTYPISM - A POSSIBLE GEOTHERMOMETER?

Jeffrey R. Walker

Department of Geology and Geography, Vassar College, Poughkeepsie, NY 12601

Since the first systematic studies of chlorite polytypes it has been suggested that the stability of the various polytypes may be a function of the temperature at which the mineral formed. The proposed sequence of chlorite polytypes stability is:



The transition from type I to type II is inferred to occur at around 200°C. The suggestion that this sequence represents increasing stability in response to increasing temperature appears to be confirmed in studies of sedimentary and metamorphic chlorites, however, few studies have been completed in which polytypes of chlorite in a specific suite of samples have been determined and correlated with the temperature of their formation. A review of the reported occurrences of type I chlorite indicate that other factors, including grain size of the host rock, may be as important, if not more so, than temperature in controlling the stability ranges of these polytypes.

Results of systematic studies in areas of very low-grade metamorphism, prehnite-pumpellyite and lower grades of metamorphism in northern Maine and sub-greenschist metamorphism in the Salton Basin, suggest that type II chlorite may be stable at temperatures well below 200°C and that it may form as the initial chlorite phase without passing through any intermediate polytypic stages. In northern Maine, where some have suggested temperatures could have been as low as 80°C, IIb chlorite in metavolcanic rocks is derived from a chlorite/smectite precursor whereas in metasedimentary rocks it is found at the very lowest grades with no immediate precursor. In metasedimentary rocks of the Salton Basin, chlorite appears at around 135°C and, although it has some interstratification of 7Å layers, it is the IIb polytype. Detrital influence can be ruled out as a source for the type II chlorite in both examples, particularly in the case of the volcanic rocks.

AUTHIGENIC CLAY MINERALS IN RESERVOIR SANDSTONES OF THE PERMIAN DELAWARE MOUNTAIN GROUP, WEST TEXAS

Walling S.D. and Tieh T.T., Department of Geology
Texas A&M University, College Station, TX 77843

Reservoir sandstones of the Guadalupian Delaware Mountain Group in the subsurface of Reeves County, Texas are very fine-grained and subarkosic in composition. Samples from cored intervals, ranging in depth from 600 to 2500 meters, were selected and studied for diagenetic alterations and their effect on reservoir rock properties. The major episodes of diagenesis include: early cementation, formation of secondary porosity by dissolution, and clay authigenesis preceding hydrocarbon emplacement.

Authigenic clay minerals are pervasive in these sandstones and comprise from 1 to 10% of the bulk rock volume. X-ray diffraction analyses of clay concentrates indicate that chlorite is the most abundant clay mineral, with lesser and variable amounts of mica/illite. Heat treated samples show intensification of the chlorite 1.4 nm reflection and collapse of higher order peaks. Stronger even- versus odd-ordered x-ray reflections combined with elemental analysis from energy dispersive spectroscopy (EDS) indicate that the chlorite is iron-rich. In some samples shifts in peak positions occurred after heating, suggesting the presence of an interstratified variety of chlorite. Scanning electron and optical microscopic analyses indicate that authigenic clays typically consist of thin (<0.2 μm) interlocking platelets which occur as both pore-lining and pore-filling aggregates.

The low permeability and high fluid saturation of these sandstones are to a large extent controlled by the abundance and nature of occurrence of the authigenic clay minerals. Pore filling clay segment the pore spaces into micropores, thereby decreasing permeability and increasing water saturation. An understanding of the clay mineralogy, texture, and nature of occurrence is fundamental to the design of an efficient enhanced oil recovery program.

A Stepwise-Dissolution Technique for Potassium-Argon Analysis of Clays

J. M. Wampler¹ and A. A. Hassanipak²

¹School of Earth and Atmospheric Sciences, Georgia Institute of Technology, Atlanta, GA 30332-0340.

²Mining Engineering Department, Faculty of Engineering, Tehran University, Tehran, Iran.

Clay samples commonly are mixtures of crystals having different origins and different ages. Thus, conventional potassium-argon analysis of clay samples often results in an apparent age that is intermediate between the ages of two potassium-bearing components (or intermediate among the ages of multiple potassium-bearing components). The ^{40}Ar - ^{39}Ar age-spectrum method is sometimes useful for interpretation of the ages of components present in a mixture, but loss of ^{39}Ar owing to the recoil energy imparted to the ^{39}Ar atoms as they are formed severely limits the usefulness of this technique for clay samples. The loss of ^{39}Ar is particularly severe in the case of mixed-layer clays having high expandability.

There are considerable differences in the rates of dissolution of clays in acid solution, and, in particular, differences in the rates of extraction of potassium from different structural sites in potassium-bearing clays (1). Furthermore, Thompson and Hower (1) presented evidence that the rate "constant" for removal of potassium from particular structural sites in glauconitic material is not dependent on grain size. Our own work has shown that the rates of release of radiogenic argon by thermal decomposition of clays (in vacuum) depend on the composition of the clay and on the expandability of mixed-layer clays and that these rates of argon release do not depend on grain size. However, neither in our work nor in that of Thompson and Hower (1) was it possible to measure both potassium and argon as the clay decomposed.

We have developed a technique for isotopic measurement of the argon released from clay samples as they slowly decompose in hydrochloric-acid solution in an evacuated apparatus. The acid solution moves slowly over the clay and drains to a reservoir, from which it may later be evaporated to a reflux condenser for another step in the extraction. The potassium dissolved during each step may be isolated from that dissolved during subsequent steps, so the technique permits stepwise potassium-argon analyses that provide "age spectra" for which the independent variable is the degree of chemical decomposition over time (rather than the degree of thermal decomposition over time as in ^{40}Ar - ^{39}Ar work). We expect that the technique will be particularly useful for study of age relationships in mixed-layer glauconite/smectite and illite/smectite. We also expect the method to be useful in cases where a relatively small amount of detrital illite occurs in, and disproportionately affects the conventional apparent age of, clay that is largely authigenic.

(1) Thompson G. R., and Hower J. (1973) *Geochim. Cosmochim. Acta*, vol. 37, no. 6, p. 1473-1491.

CATALYTIC TRANSFORMATIONS OF AMINO ACIDS BY BIRNESSITE AS INFLUENCED BY PYROGALLOL: M. C. Wang, Dept. of Soil Science, National Chung Hsing Univ., Taichung, Taiwan 40227, Republic of China

Abiotic transformations of selected amino acids as catalyzed by birnessite and the role of pyrogallol in the transformations were studied in systems free of microbial activity. Among the systems studied, the decarboxylation of the birnessite-cysteine system was the most pronounced, while that of the birnessite-methionine system was the least. The amount of CO_2 released from the former was 1.5 times of that released from the latter. The deamination of the birnessite-cysteine system was the most pronounced, while that of the birnessite-proline system was the least. The amount of NH_3 released from the former was 3.4 times of that released from the latter. Birnessite catalyzed the desulfurization of methionine and cysteine to release SO_4^{-2} in the supernatants of the reaction systems. The amount of SO_4^{-2} released from the birnessite-cysteine system was 140 times of that from the birnessite-methionine system. The data indicate that the role of pyrogallol in the decarboxylation, deamination, and desulfurization of selected amino acids as catalyzed by birnessite was promotion, inhibition, and nil, respectively.

Mechanism on Formation of Birnessite in Alkali Media

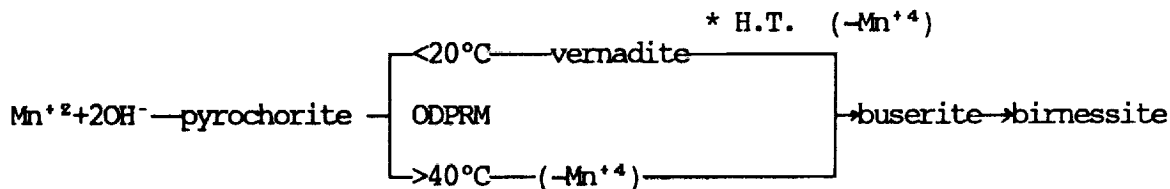
Ming K. Wang and Deng S. Young

Department of Agricultural Chemistry

National Taiwan University

The results of this study proved that earlier synthetic birnessite concept should be changed. Literatures suggested and emphasized that oxygen gas bubble into manganese (II), rate was 1.5 liters/minute, and birnessite synthetic temperature was lower than room temperature. This study recommended that right condition to synthesis birnessite could be changed to higher than room temperature. $Mn(NO_3)_2$ and NaOH solutions bubbled with N_2 gas, before these solutions mixed together. In order to obtain a pure pyrochroite [$Mn(OH)_2$], it is necessary to bubble with N_2 gas, to reduce the soluble oxygen contents in solutions. Thus, no competition of hausmannite was produced at high temperature. Mechanism of birnessite formation through the oxidation of pyrochroite can be proposed as following path way:

Oxidation-Deprotonation Reaction Model (ODPRM)



Where, Symbol of (vernadite) denotes that vernadite is a metastable manganese oxide mineral. Thus, formation of birnessite may or may not path through vernadite.

Vernadite can be considered as a proto-buserite.

* H.T. : Vernadite sample aged at high temperature.

The results of this study also suggested that formation of birnessite is necessary through the oxidation of pyrochroite pathway. On the other hand, the method of reduced $KMnO_4$ solutions, boiled at high temperature, synthetic products may be precipitated as T(2,n) type manganese oxide with a complicated tunnel structure. It may not produce birnessite.

This synthetic study also extended and implicated that manganese and pyrolusite was the major manganese minerals developed at acidic soils. Vernadite can be predicted to form under pergelic and cryic of soil temperature at alkaline soils, and birnessite formed at hyperthermic of tropical high pH soils .

NATURE OF OH-AL POLYMERS IN COMMERCIAL AND LABORATORY PREPARED SOLUTIONS

Weizi Wang and Pa Ho Hsu

Department of Environmental Sciences, Rutgers, The State University of New Jersey, New Brunswick, NJ 08903-0231

Eight commercial OH-Al solutions were characterized using kinetics of Al-ferron color development, kinetics of H^+ back neutralization, and Al-27 NMR spectrometry. Basic Al sulfates were precipitated by addition of sodium sulfate, and characterized using XRD and kinetics of acid dissolution. A series of OH-Al solutions prepared in laboratory by partially neutralizing $AlCl_3$ solutions with dilute NaOH were characterized similarly for comparison.

The results show that the OH-Al polymers in commercial solutions are distinctly different from those in laboratory prepared solutions. Seven of the eight commercial solutions are dominated by polymers of gibbsite-fragment structure. Al-13 polymers of Keggin structure are the dominant species in laboratory prepared solutions when freshly prepared, but slowly convert to gibbsite-fragment structure with time.

ONCE A PIONEER ALWAYS A PIONEER

Charles E. Weaver, School of Earth and Atmospheric Sciences,
Georgia Institute of Technology, Atlanta, GA.

During the 1950's, I was fortunate in being able to help pioneer in the development of the field of the clay (physil) petrology of shales. As no one else is interested I will spend the 1990's pioneering the neglected field of the clay (physil) petrology of carbonates. Authigenic/diagenetic clay minerals (physils) are common in carbonate rocks and grow from ions generated both internally and externally. These clay minerals (physils) provide information on the original composition of the rock, environments, fluid chemistry, time of fluid movement, solution, recrystallization, dolomitization, stylolitization, temperature, and burial and tectonic history.

TIMING OF KAOLINITIZATION IN HARD KAOLINS OF THE HUBER FORMATION IN CENTRAL AND EASTERN GEORGIA: TRACE FOSSIL MICROTERTURES DOCUMENTED BY SCANNING ELECTRON MICROSCOPY

Harold Webb and E. Kent Sprague

ECC International, P.O. Box 471, Sandersville, GA 31082
McCrone Associates-Atlanta, Inc., 1412 Oakbrook Dr., Norcross, GA 30093

Trace fossils (burrows) created by both deposit and suspension feeding organisms are quite common in commercial grade hard kaolin occurrences of central and eastern Georgia. High concentrations of these burrows can extend throughout a mineable stratum of kaolin both vertically (3 - 15 m) and laterally (100's of meters). Two ichnogenera dominate the deposits: Planolites and Palaeophycus. Palaeophycus, though abundant, has not been documented previously, and this is the first report of its presence in the Huber Fm. This suite of trace fossils has been consistently associated with estuarine, marginal marine, or intertidal facies in modern- and paleo-environmental studies.

Controversy exists as to whether kaolinitization was in situ on crystalline rocks of the Piedmont, or post-depositional in the basin. Examination of economic kaolin ore samples by scanning electron microscopy and in hand specimen reveals that animal burrows are preserved in extremely fine detail. The observed preservation features, dense packing of burrows and smooth curvilinear axes of burrows seen in hand specimen clearly indicate the sediment was deposited and worked by organisms as kaolinite grains, not as lithic fragments.

Several physical features of economic kaolin ores constrain the timing of kaolinitization to the in situ model. In many of the burrows original sculptings of the organism are well preserved down to 0.05mm. Textures observed by scanning electron microscopy document that the original sedimentary microtexture of kaolinite grains was displaced as the organism plowed through the soft sediment. Boundaries between the burrows and the substrate are distinct; the texture of the biogenically reworked material is different from that of the less disturbed substrate. Burrows are smoothly curvilinear, indicating the animals did not encounter rock fragments during excavation. Vertical and horizontal limbs of the burrows remain cylindrical and have not been physically altered by compaction or diagenesis.

A detailed examination of trace fossils found in economic kaolin deposits of central and eastern Georgia indicates that kaolinitization took place in situ in the Piedmont. Many of the hard kaolins have a bioturbate texture throughout. The bioturbate texture and preserved burrows are restricted to soft muddy environments high in organic content (3% to 10%) at the time of deposition. In contrast, lithic fragments, which would be indicative of the post-depositional kaolinitization model, could only have been a minor component of the sediment.

Paleoenvironmental Implications of Lacustrine Clay Minerals from the Double Lakes area, Southern High Plains, Texas.

Daniel M. Webster and Blair F. Jones, U.S. Geological Survey, 432 National Center, Reston, VA 22092

Major-element chemical and X-ray diffraction analyses of ultrafine (<0.1 μm) fractions of Pleistocene-Holocene lacustrine sediments from the Double Lakes Formation, Southern High Plains, Lynn County, Texas, suggest that the clay minerals reflect periodic variations in paleolake conditions. Above a Cretaceous marine-shale substrate dominated by well-crystallized aluminous dioctahedral smectite, the clay-mineral assemblages of the younger lacustrine sediments show cyclic changes believed to be related to changes in hydrologic environment. The cycles apparently represent evaporatively induced salinity shifts from brackish to saline (perennial), or ephemeral (playa) lake conditions, as inferred from the predominance of sepiolite, interstratified Mg-smectite, and palygorskite, respectively. Two of at least four cycles show a complete sequence from low to high lake level and return to playa conditions. Between sediment units clearly dominated by a single clay-mineral species are intervals containing variable mixtures of chain-structure clays and smectite; sepiolite and interstratified Mg-smectite do not occur exclusively. Chemically, the highest ratios of silica to alumina are associated with the sepiolite and the greatest values of the Mg/Al ratio are correlated with Mg-smectite prominence. Pulses of detritus associated with overland runoff or wind are indicated by concentrations of illite and minor kaolinite, as evidenced by high K and Al contents. Spring deposits (tufas) in a principle drainageway near the lake suggest inflow from groundwater has had a major effect on the formation of chain-structure clays.

SEDIMENTARY STRUCTURE IN GRAY KAOLINS OF GEORGIA

G. Norman White¹, J. B. Dixon¹, R. M. Weaver² and A. C. Kunkle²
¹Dept. of Soil and Crop Sciences, Texas A & M University,
College Station, TX 77843-2474 and ²J. M. Huber Corp., Huber, GA
31298

The depositional environment and the post depositional history of most of the Georgia kaolin deposits are unknown due to the lack of visible depositional features in the relatively homogeneous white kaolin deposits. X-ray radiography is a technique in which spatial differences in composition within a sample are measured by the differences in absorption of X-rays as they penetrate the sample. The technique has been applied to the study of sedimentary structure since it was introduced by Hamblin (1). No reports have been published of the application of radiography to the study of sedimentary structure in kaolins.

Gray kaolin cores from two Cretaceous sites and one Tertiary site in Twiggs and Wilkinson Counties, Georgia, were examined by X-ray radiography to determine the processes of formation of the deposits. Earlier reports on the same cores had shown that regions of all three cores had undergone recrystallization of the sulfides and that the kaolinite in one of the Cretaceous cores and the Tertiary core had been recrystallized (2,3). Radiographs from the Cretaceous site which had not been recrystallized show thin laminar bedding in the gray kaolin. This sedimentary layering is visually observed only in the underlying red kaolin but continues without interruption into the overlying gray kaolin. Sedimentary structure was not observed at a Tertiary site and in sections of the core from another Cretaceous site where kaolinite was recrystallized to large vermiforms. These findings suggest that the Cretaceous kaolins probably were deposited as a kaolinite-iron oxide mixture in a reducing environment free of subsequent physical and biological mixing. Recrystallization of kaolinite may have destroyed sedimentary structures in part or all of the other two kaolin cores.

REFERENCES

1. Hamblin, W. K. (1962) *J. Sedimen. Petrol.*, vol. 32, p.201-210.
2. White, G. N., Dixon, J. B., Weaver, R. M., and Kunkle, A. C. (1991a) *Clays and Miner.*, vol. no. 39, p.70-76.
3. White, G. N., Dixon, J. B., Weaver, R. M., and Kunkle, A. C. (1991b) *Clays and Clay Miner.*, (accepted).

TEXTURAL CHANGES AND NUCLEATION DURING THE EARLY STAGES OF ILLITIZATION: AN EXPERIMENTAL STUDY

Gene Whitney¹ and Bruce Velde²

¹U.S. Geological Survey, MS 904, Box 25046, Denver, CO 80225

²Département de Géologie, École Normale Supérieure, Paris 75231, France

Experiments were performed to investigate the textural changes which occur in interstratified illite/smectite (I/S) during the early stages of illitization. K-saturated smectite (Wyoming bentonite SWY-1, < 0.1 μm fraction) was treated hydrothermally in 1N NaCl for 7 days at temperatures from 200 to 450°C to produce I/S with 100% to 40% smectite layers. A precisely weighed aliquot of each sample and the starting material was dispersed in distilled water and sonified for one minute. A drop of each suspension was placed on a graphite-coated grid for transmission electron microscope (TEM) analysis. The suspensions were sufficiently dilute to minimize overlap of particles on the grid, and the resulting mounts provided oriented (flat-lying) particles that could be counted and measured (length, width, aspect ratio, and area).

We observed the following: (1) The total number of particles per milligram of sample decreased as the proportion of illite layers increased. (2) There was no significant change in length, width, aspect ratio or area of the particles until approximately 50% illite layers were present. (3) Particles became progressively more euhedral with increasing proportion of illite layers, but no lath-shaped particles appeared until approximately 50% illite layers were formed. (4) Particles exhibited higher relief in the TEM images with increasing illite proportion, suggesting that the particles were getting thicker. Near 50% illite layers, individual particles sometimes appear to be a mosaic of large and small particles in face-to-face contact. (5) Thickness of a few particles (considered to be "as-grown crystals") were measured using lattice fringe imaging, and some were up to four layers thick in the most illitic samples (Alain Baronnet, personal communication).

The mechanism for nucleation of illite layers within a compact smectite mass appears to be either by topotactic nucleation on or between smectite 2:1 layers, or by overgrowth of small smectite flakes residing on the surface of larger smectite particles. If illite nucleates in this way, the energy barrier for nucleation is near zero and nucleation of new illite layers may proceed easily during the early (R0) stage. Nucleation occurs at random sites within smectite stacks, thus creating the random (R0) stacking arrangement observed in shales and bentonites. In addition, some early-formed, low-charge "illite" layers may actually be a two-layer packet consisting of an inherited smectite 2:1 layer and a neoformed illite 2:1 layer. These data suggest that illitization may begin in a very different way in compact, smectite-rich mudrocks than in open, water dominated systems such as sandstones or hydrothermal veins with no smectite precursor. Without a smectite precursor, there is no mechanism by which R0 I/S may be produced. In addition, the precise rate at which the R0 stage of illitization proceeds in a compact smectite mass may be a complex function of the composition and particle size distribution of the original smectite, the extent of compaction, fluid:solid ratio, temperature and fluid chemistry.

DETRITAL KAOLINITE IN SANDSTONES OF THE ANCESTRAL YUBA RIVER (EOCENE), SIERRA FOOTHILLS, CALIFORNIA

James L. Wood
Unocal Science and Technology, 376 S. Valencia Ave., Brea, CA 92621

The origin of kaolinite in early Eocene fluvio-fan delta deposits of the lone Formation of California continues to be controversial. In an effort to distinguish detrital from diagenetic kaolinite in these rocks, a comparative study utilizing SEM, thin section petrography, and XRD techniques was conducted on fluvial deposits of a major lone Basin tributary, the ancestral Yuba River, and potential source rocks, the severely leached tropical soils developed on Mesozoic basement rocks which appear to have mantled the entire region and directly underlie the fluvial channels. The sands of the stream deposits are predominantly comprised of quartz and kaolinitic soil or pedogenic aggregates ("mudballs") derived from local kaolinitic paleosols. Kaolinite microtextures differ from one mudball to the next, an important feature which distinguishes them from pore-filling diagenetic clay. Reflecting the diversity of weathered rock types which contributed detritus to the streams, the variable textural characteristics of detrital mudballs are produced by variations in platelet size, arrangement (stacked vs random), amount of microporosity, inherited textures from lithic precursors, and patterns of iron oxide staining imparted while in the soil environment. Due to inherent microporosity, the mudballs are deformable and formed pseudomatrix upon deposition although their spherical shape is sometimes preserved. The sands often display mudball rich laminae while other laminae are mud free. In better sorted sands, the mudballs having a lower bulk density are consistently of a larger diameter than quartz grains. A particularly distinctive form of kaolinite forming sand sized grains is a resilient pseudomorphous replacement of mica "books" (previously called anauxite) derived from weathered granitic and metamorphic sources.

In sands of low order streams (tributaries draining a small area), microtextures of kaolinite clasts are more homogeneous and are mineralogically and texturally similar to those of the underlying kaolinitic paleosol. The heterogeneity of kaolinite microtextures increases in the downstream direction due to the greater diversity of soil debris in higher order streams. Well rounded voids found in kaolinite matrix mud are interpreted as preserved air bubbles trapped by cohesive mud at the time of deposition. This texture can be reproduced in the laboratory with kaolinite to water volume ratios of approximately 1:1 suggesting a stream system choked with muddy sediment.

The distinctive morphologies and textures of kaolinite observed in sandstones of the ancestral Yuba River and the lone Basin conform to the criteria defined as "detrital clay" as established by Dickinson (1) and Wilson and Pittman (2). Other features which suggest that post-depositional weathering in these rocks has been minor or nil are the preservation of small scale sedimentary structures and the presence of pristine minerals which are ordinarily unstable in an oxidizing environment, eg. hornblende, biotite, feldspar, and glass shards.

Identical clay textures interpreted here as detrital were also observed in sandstones of other kaolinitic fluvial deposits: Silverado/Santiago Formations (Paleocene - Eocene) of Southern California, Morley Formation (upper Cretaceous) of New Zealand, and the Buffalo Creek Formation (upper Cretaceous) of Georgia. While a modern analogue of a depositional system comprised of sediments described here is difficult to find, during the period from the upper Cretaceous through the middle Eocene, a unique time of globally warm climatic conditions, stream systems similar to the ancestral Yuba River transporting detritus derived from tropical soils may not have been uncommon.

Dickinson, W. R., 1970 *Jour. Sed. Petrology*, v. 40, p. 695-707.

Wilson, M. D., and Pittman, E. D., 1977 *Jour. Sed. Petrology*, v. 47, p. 3-31.

TRANSMISSION ELECTRON MICROSCOPY STUDY OF IMPLANTED MICA

Q. Xu¹, W.A. Chiou², C. Templier³, F. G. Karioris¹ and L. Cartz¹

1. Department of Mechanical Engineering, Marquette University, Milwaukee, WI 53233
2. Department of Materials Science and Engineering, Northwestern University, Evanston, IL 60208
3. Department of Physics, University of Poitiers, Poitiers, France

Anomalous reversible thermal expansion, as much as 300% upon heating to 600°C in some mica structures has long been known. To simulate this property as a potential thermal actuator, natural muscovite implanted with a noble gas (Helium or Argon) has been investigated by thermomechanical analysis and transmission electron microscopy. The muscovite-helium gas composite has an enhanced thermal expansion coefficient of approximately $10^{-4} \text{ }^\circ\text{C}^{-1}$, about 10 times greater than that of unimplanted muscovite at 600°C along the (000 ℓ) direction. Transmission electron microscope observation of the implanted muscovite mica at room temperature shows typical lenticular flaws. These lenticular flaws are believed to be gas bubbles induced by the implanted ions since no such features can be found in unimplanted samples. Upon heat treatment of implanted specimens, the shape and size of these induced lenticular flaws become somewhat irregular and extended. The transmission electron microscope study also suggests that these noble gases are implanted along (000 ℓ) cleavage planes.

TRANSMISSION ELECTRON MICROSCOPY AND THERMAL EXPANSION BEHAVIOR OF BIOTITE AND PHLOGOPITE MICAS

X. Yang¹, W-A. Chiou², F. G. Karioris¹ and L. Cartz¹

1. Department of Mechanical Engineering, Marquette University, Milwaukee, WI 53233
2. Department of Materials Science and Engineering, Northwestern University, Evanston, IL 60208

Gas bubbles or lenticular flaws in biotite and phlogopite micas have been investigated by X-ray diffraction, thermomechanical analysis and transmission electron microscopy to understand the thermal expansion behavior of these minerals. Phlogopite has an abrupt thermal expansion at about 100°C, and as much as 200% at 600°C, and is reversible up to 950°C with hysteresis. Biotite has a higher thermal expansion of 280% at 700°C, but the abrupt expansion occurs at about 680°C and is irreversible. Gas bubbles, typically spherical in shape, of different sizes ranging approximately from 50 nm to 700 nm, can be observed in phlogopite specimens at room temperature as well as those heated up to 950°C. In contrast, random but evenly distributed open pores and micro-cracks were found in heat treated (950°C) biotite while there were typical gas bubbles in biotite at room temperature. Information obtained from electron microscopy and electron diffraction suggests that gas or vapor inclusions in biotite have escaped through open pores after heat treatment in agreement with the irreversible thermal expansion behavior.

SIGNIFICANCE OF OXYGEN ISOTOPE TEMPERATURES OF SEA-FLOOR
HYDROTHERMAL SMECTITE

Hsueh-Wen Yeh
Hawaii Institute of Geophysics
SOEST
University of Hawaii

Smectite is a common constituent of sea-floor metalliferous sediments and probably wide spread in most part of deep-sea basement. The most famous occurrence is the greenish smectite of the hydrothermal mounds on the south flank of Galapagos spreading center.

They are generally dioctahedral Fe-smectite and nontronite with high Fe/Al ratios. Available pb isotope data indicate significant input of "basaltic" pb, while REE reveal seawater signature. Oxygen isotope temperature of the smectite fall overwhelmingly in the range of 20° to 50°C, although a low of 0°C and a high of 275°C have also been found. These oxygen isotope data thus establish unequivocally the hydrothermal origin of these smectite, except the one with an isotopic temperature of 0°C. However, by defining hydrothermal smectite as the smectite of which chemical components are thoroughly or partly from products of hydrothermal sea water/basalts interaction, a case can be made to include the one with 0°C isotope temperature on the basis of chemical evidence.

The significance of these isotope temperatures is not obvious. The smectite are undoubtedly precipitate from solution which is a mixture of normal seawater and altered seawater (hydrothermal fluid). The proportions of these two end members for sure vary from mostly hydrothermal fluid to mostly normal seawater. Other important factors in appreciating the significance of the isotope temperature are variation in ratios of hydrothermal to hydrogenous constituents and in distances between sites of hydrothermal reaction and sites of precipitation. This communication will focus on discussing the relationship between the isotopic temperatures and aforementioned factors.

GEOMETRICAL STRUCTURE SYNTHESIS AND STABILITY OF DIOCTAHEDRAL CLAY MINERALS, INCLUDING THE WATER STRUCTURE OF HYDRATED MONTMORILLONITE

Jae-Young Yu
Department of Geology
Gangwon National University
Chuncheon 200-701, The Republic of Korea

M. Slaughter
Department of Chemistry and Geochemistry
Colorado School of Mines
Golden, CO 80401

ABSTRACT

Equations are presented to determine the atomic coordinates, cell dimensions and interaxial angles of dioctahedral three-layer clays and micas. The simulated structures and cell parameters are accurate to within experimental error for several published structures. Only the chemical composition is needed to determine the structure in the a-b plane. The c-dimension is determined by calculating binding energies as a function of $d(001)$ to find the minimum energy dimension. The structural synthesis method provides fairly accurate structures for 1M and 2M1 dioctahedral phyllosilicates having random or ordered aluminum-substituted tetrahedral cation configurations. Because the method requires no initial knowledge of atomic coordinates or cell parameters, one can generate the structures of non-stoichiometric clay minerals, such as montmorillonite illite and mixed layer clay minerals.

Three interlayer cation/two-water-layer structural models for smectite taken or altered from previous studies have cations and waters occupying different positions. One model (Model I) is the cation/water structure for vermiculite. Another (Model III) was proposed for smectite. The third model (Model II) has the structure between Models I and III. Binding energy calculations show that montmorillonite is most stable when it has Model II type hydrated interlayer structure. Model II hydrated interlayer structure has the interlayer cations occupying the center of the tetrahedral triads and has the interlayer water molecules occupying the positions over the octahedral cations. Model I has too much repulsion among cations and tetrahedral layer oxygens. Model III has low hydrogen bond energies between the hydrogens of the water molecules and the basal oxygens of the tetrahedral layer.

Comparing calculated binding energies of mixed layer illite/montmorillonite (I/S) phases having the same chemical composition, stability of an I/S phase varies as a function of the tetrahedral cation configuration and interlayer cation population. Phases having a random tetrahedral cation configuration are more stable at lower temperatures than phases having an ordered one. A montmorillonitic layer of I/S has greater stability with a homogeneous interlayer cation population than with a heterogeneous one. Interlayer cations of heterogeneous populations produce an interlayer structure with weaker hydrogen bonds and less stable hydration shells. The binding energies show no significant difference among the I/S phases having different layer stacking sequences. The stability of ordered layer mixing and layer stacking sequences are most likely related to the surface energies of I/S particles.

Multiple-Site Modeling of Metal Ion Adsorption on Specimen and Soil Layer Silicates

Zachara, J.M., Cowan, C.E., and Smith, S.C.
Geosciences Department, Pacific Northwest Laboratory
Richland, WA 99352

Metal cation (Me) adsorption on 2:1 layer silicates exhibits complex behavior over ranges in pH and ionic strength as a result of the variable contributions of ion exchange to fixed charge sites and surface complexation to edge sites. This presentation will describe the application of a site-binding model containing fixed-charge (X⁻) and hydroxylated edge sites (AlOH, SiOH) to metal cation (Cd, Co) sorption data on smectite (SWy-1) and two low carbon smectitic soil isolates in Na⁺ and Ca²⁺ electrolytes. The model was used to explore the relative contributions of ion exchange and edge site complexation to metal ion binding. Calculations were performed within the code FITEQL. Edge reactions were described using the triple-layer model (TLM) and an inner-sphere Cd complex on AlOH sites and outer-sphere complexes on SiOH sites. The complexation reactions were parameterized using Cd sorption data on silica and alumina. Site concentration estimates for the smectite sorbents were based on external surface area (N₂) and ion exchange data over a range in pH. Ion exchange reactions for NaX, MeX₂, and CaX₂ were described in half-reaction format, and constants for the exchange reactions were fit using Me sorption data in either Na⁺ or Ca²⁺ electrolyte. The experimental Me sorption data could be adequately described over ranges in pH and electrolyte concentration using a combination of ion exchange complexes on fixed-charge sites (MeX₂) and an inner-sphere complex (AlOMe) on edge AlOH. Complexation of Me to edge SiOH was not calculated to be important. The calculated contribution of AlOH edge-site complexation of Me was significant, and increased with increases in pH and ionic strength. Good predictions of Me sorption in mixed electrolytes were obtained using half-reaction exchange constants derived from single-electrolyte systems. Consistent with experiments in which Me sorption on the smectitic soil isolates exhibited "oxide-like" behavior, edge sorption reactions were computed to be more important for the soil smectites than for SWy-1 because of their greater external surface area (i.e., more AlOH sites).

Effect of Cations on the Relation Between Swelling Pressure and Interlayer Distance in Montmorillonite

Fushan Zhang, Philip F. Low, and Charles B. Roth

Department of Agronomy, Purdue University, West Lafayette, IN 47907

To study the effect of interlayer cations and electrolyte concentration on the long-range forces between silicate layers, the relation between the interlayer distance, λ , and the swelling pressure, Π , was determined for Li-, Na- and K- saturated Upton montmorillonite in chloride solutions of the respective cations. The concentration of the solutions was usually 10^{-4} M but was varied in the case of LiCl. Oriented gels of the samples were placed in an environmental chamber mounted on a X-ray diffractometer and compressed between a N_2 -gas piston and a porous membrane in contact on its underside with a solution exposed to the outside atmosphere. After equilibrium at each of several successively higher value of Π , which equalled the applied pressure, λ was determined by X-ray diffraction. The results of these measurements showed that the relation between Π and λ was the same for all cations. Also, under a given value of Π , the value of λ for Li-montmorillonite remained essentially constant with increasing LiCl concentration until the concentration reached 10^{-1} M, where it decreased significantly. These observations can not be explained by DLVO theory. It is postulated that the predominate force between the layers of montmorillonite is due to the rearrangement of water molecules near their surfaces.

Sorption and Desorption of Quaternary Amine Cations on Clays

Z. Z. Zhang and D. L. Sparks

Dept. of Plant and Soil Sciences, University of Delaware, Newark, DE 19717

The adsorption of organic cations on clays was first studied by Hendricks¹. It has been shown that organic cations are generally preferentially adsorbed over metal cations and that the adsorption of organic cations can be used to measure the cation exchange capacity of the clay² as well as to determine the specific surface area³.

It is well known that the organic cations on the exchange sites render the clay surfaces rather hydrophobic. This property makes the organo-clay attractive to poorly water soluble organic compounds. More recently, several investigators have suggested the application of organo-clay to environmental problems, such as water treatment, spill control, tank and landfill liners, and waster stabilization^{4,5,6}. Before the organo-clay can be successfully used for these environmental problems, however, the following questions must be addressed: 1. How much of the organic cations are being adsorbed on clays and how much are remaining in solution? 2. Are the adsorbed organic cations easily removed from clay surfaces in the presence of excess electrolyte?

The present study was conducted to investigate the sorption and desorption of several quaternary amines on Na and Ca montmorillonite using a titration procedure developed by Furlong and Elliker⁷. Adsorption of amines was conducted at an ionic strength of 0.01 M, and desorption of amines was studied by adding excess electrolyte to increase the concentration of the metal cations tenfold compared with adsorption. We found that the selectivity coefficient for the exchange reaction decreases as the amount of amines added increases. Furthermore, the selectivity coefficient for the desorption process is at least 10 times higher than that for the adsorption process, indicating that the exchange reaction is essentially irreversible.

References

1. Hendricks, S.B. (1941). *J. Phys. Chem.*, 45, 65-81.
2. Hang, P.H. and G.W. Brindley. (1970). *Clays Clay Miner.*, 18, 203-212.
3. Greenland, D.J. and J.P. Quirk. (1964) *J. Soil Sci.*, 15, 178-191.
4. Mortland, M.M., S. Shaobai, and S.A. Boyd. (1986). *Clays Clay Miner.*, 34, 581-585.
5. Smith, J.A., P.R. Jaffe, and C.T. Chiou. (1990). *Environ. Sci. Technol.*, 24, 1167-1172.
6. Cadena, F. and R. Garcia. (1990). *Environmental Progress*, 9, 245-253.
7. Furlong, T.E. and P.R. Elliker. (1953). *J. Dairy Sci.* 36, 225-234.

THE NATURE OF THE SURFACE CHARGE ON KAOLINITE: CONSTRAINT OF SURFACE CHARGE DENSITY: Zhou Z. and Gunter W. D., Oil Sands and Hydrocarbon Recovery, Alberta Research Council, P. O. Box 8330, Station F, Edmonton, Alberta Canada T6H 5X2

It is well known that kaolinite carries a negative charge on its basal faces and a variable charge on its edges. The negative charge on the basal faces is commonly attributed to the isomorphous substitution of Si^{4+} by Al^{3+} , and is thus considered as a constant structural charge; whereas the charge on the edges is due to protonation/deprotonation of surface hydroxyl groups and therefore depends on the solution pH and ionic strength (1,2,3). Discussion has been centered on the concept of constant structural charge on the basal surface (e.g. 4,5).

In this communication, the origin of the surface charge of kaolinite is discussed in light of surface charge density. Based on the concept of constant basal surface charge and the geometry of kaolinite, the charge density on the edge faces of kaolinite has been calculated. Both published and newly measured cation exchange capacity (CEC) and potentiometric titration data on kaolinites (KGa-1, Cornwell, Greenbushes, Cornish) were used for the calculation. The charge density on the edge of kaolinite, calculated as such, can be as high as $-2,250 \text{ mCm}^{-2}$, and is one order of magnitude greater than that of either alumina or silica under the same solution conditions. This surface charge density requires ionizable surface site concentrations as high as $1.5 \times 10^{19} \text{ m}^{-2}$ which would exceed the total surface hydroxide concentration of either silica or alumina (6).

From the consideration of surface charge density, it is obvious that the ionization of edges alone can not explain the magnitude of changes in the CEC and net surface proton charge density observed in many experiments. Thus, the basal surface must also be ionizable and contribute to these changes. For well crystallized Georgia kaolinite (KGa-1), such a contribution from the basal faces can be described well by a site dissociation model similar to that for mica surface (7). This model predicts a largely negative charge on the basal surface of kaolinite. But the magnitude of the negative charge depends on the pH and ionic strength of solution. The assumption of constant structural charge on the basal surface seems not necessary for well crystallized kaolinite. A site dissociation model of basal surfaces, along with amphoteric edges, can simulate most of the surface properties of kaolinite.

REFERENCES

1. van Olphen H.(1951) Disc. Fara. Soc., vol.11, p.82-84.
2. Schofield R.K. and Samson H.R.(1954) Disc. Fara. Soc., vol.18, p.135-145.
3. van Olphen H.(1977) Clay Colloid Chemistry, 2nd Ed., John Wiley, NY, 318pp.
4. Ferris A.P. and Jepson W.B.(1975) J. Coll. Interf. Sci., vol.51, p.245-259.
5. Bolland M.D.A., Posner A.M., and Quirk J.P.(1976) Aust. J. Soil Res., vol. 14, p.197-216.
6. Schindler P.W.(1981) In Adsorption of Inorganics at Solid-Liquid Interfaces, M.A. Anderson and A.J. Rubin eds., Ann Arbor Science, p.1-49.
7. Scales P.J., Griesser F., and Healy T.W.(1990) Langmuir, vol.6, p.582-589.

V92-10256

CLAY MINERALS IN PRIMITIVE METEORITES AND INTERPLANETARY DUST

I. M. E. Zolensky and L. P. Keller, Planetary Science Branch, NASA Johnson Space Center, Houston, TX 77058.

INTRODUCTION. Many meteorites and interplanetary dust particles (IDPs) with primitive compositions contain significant amounts of phyllosilicate minerals, which are generally interpreted as evidence of protoplanetary aqueous alteration at an early period of the solar system [1]. These meteorites are chondrites (near solar compositions) of the "carbonaceous" and "ordinary" varieties. The former are subdivided (according to bulk composition and petrology) into CI, CM, CV, CO, CR, and "ungrouped" classes. IDPs are extraterrestrial particulates (typically under 100 μm in dia.), collected in the stratosphere, which have chemical compositions indicative of a primitive origin; they are typically distinct from the primitive meteorites. Characterization of phyllosilicates in these materials is a high priority because of the important physico-chemical information they hold.

Although we are still at a rudimentary level of understanding, we know that the most common phyllosilicates present in chondritic extraterrestrial materials are serpentine-group minerals, smectites, and micas [1-7]; other types of phyllosilicates have been rarely reported [8]. We discuss these phyllosilicates separately below and in an accompanying abstract [9]. We then describe the interpretation of their occurrence in meteorites and IDPs and what this indicates about the history of their parent bodies, which are probably the hydrous asteroids.

SERPENTINE. A very wide variety of serpentine group minerals (including cronstedtite, greenalite, antigorite, and chrysotile) occur in CI-, CM-, CO-, CV-(rarely), CR- and ungrouped carbonaceous chondrites as well as chondritic IDPs [1-5, 7]. In CM and CO carbonaceous chondrites serpentines are essentially the only phyllosilicate present; in the other materials serpentines are often intergrown with saponite; in CI chondrites and in a single chondritic IDP, serpentine is coherently intergrown with saponite [10,11]. Serpentine is reported from two CV chondrites, Mokoia and Allende, where it is observed in coherent intergrowths with Na-phlogopite. In CM chondrites and some IDPs, serpentine is coherently intergrown with the sulfide-hydroxide mineral tochilinite. The compositional range of these serpentines varies more widely than in terrestrial samples, from 20 to 80 mole % Fe [12]. This wide compositional range is probably due to the a similarly wide compositional variety of precursor minerals available on the protoplanetary bodies. The grain size of serpentine in extraterrestrial materials ranges up to only 1 μm ; observed morphologies are spongy, platy, flaky, and cylindrical. Because of the fine-grained nature of these serpentines more detailed mineralogical characterizations have rarely been attempted, but are clearly the next required step in this work.

SMECTITES AND MICAS. Smectites are found in CI-, CV-, CR-, and ungrouped carbonaceous chondrites, ordinary chondrites, and IDPs. Micahs are apparently confined to the CV chondrites. We present a fuller description of extraterrestrial smectites and micahs in the accompanying abstract [9].

PHYLLOSILICATE FORMATION IN EXTRATERRESTRIAL ENVIRONMENTS. Phyllosilicates are important indicators of the chemical environment on hydrous primitive solar system bodies (probably main belt and outer belt asteroids). The presence of serpentine and smectite replacing olivine, pyroxene, and glass indicates episodes of aqueous alteration on hydrous asteroids at an early period in their history [1]. The oxygen fugacity characteristic of alteration on hydrous asteroids thus appears to have varied depending on the location and time (e.g. CI chondrites record increasing $f\text{O}_2$ through time [13]). The temperatures of alteration fluids were in the range 0 to 150°C, depending upon the specific phyllosilicate assemblages. Calculated fluid pHs vary from 7 to 10 for serpentine/saponite assemblages, and 7 to 12 for serpentine-dominated assemblages [13]. Additional work characterizing the exact mineralogy of these phyllosilicates will serve to further constrain the nature of the mineralizing fluids.

REFERENCES. [1] Zolensky and McSween (1988) in *Meteorites and the Early Solar System*, 114. [2] Keller and Buseck (1990) *GCA* 54, 1155. [3] Zolensky and Lindstrom (1992) *Proc. 22nd Lunar Planet. Sci. Conf.*, in press. [4] Zolensky (1991) *Meteoritics*, in press. [5] Tomeoka and Buseck (1990) *GCA* 54, 1745. [6] Keller and Buseck (1990) *GCA* 54, 2113. [7] Tomeoka and Buseck (1985) *GCA* 49, 2149. [8] Reitmeijer (1991) *Earth Planet. Sci. Letts.* 102, 148. [9] Keller and Zolensky (1991) this volume. [10] Tomeoka and Buseck (1988) *GCA* 52, 1627. [11] Keller *et al.* (1991) *Meteoritics*, in press. [12] Browning *et al.* (1991) *Lunar Planet. Sci. Conf. XXII*, 145. [13] Boucier and Zolensky (1991) *Meteoritics*, in press.

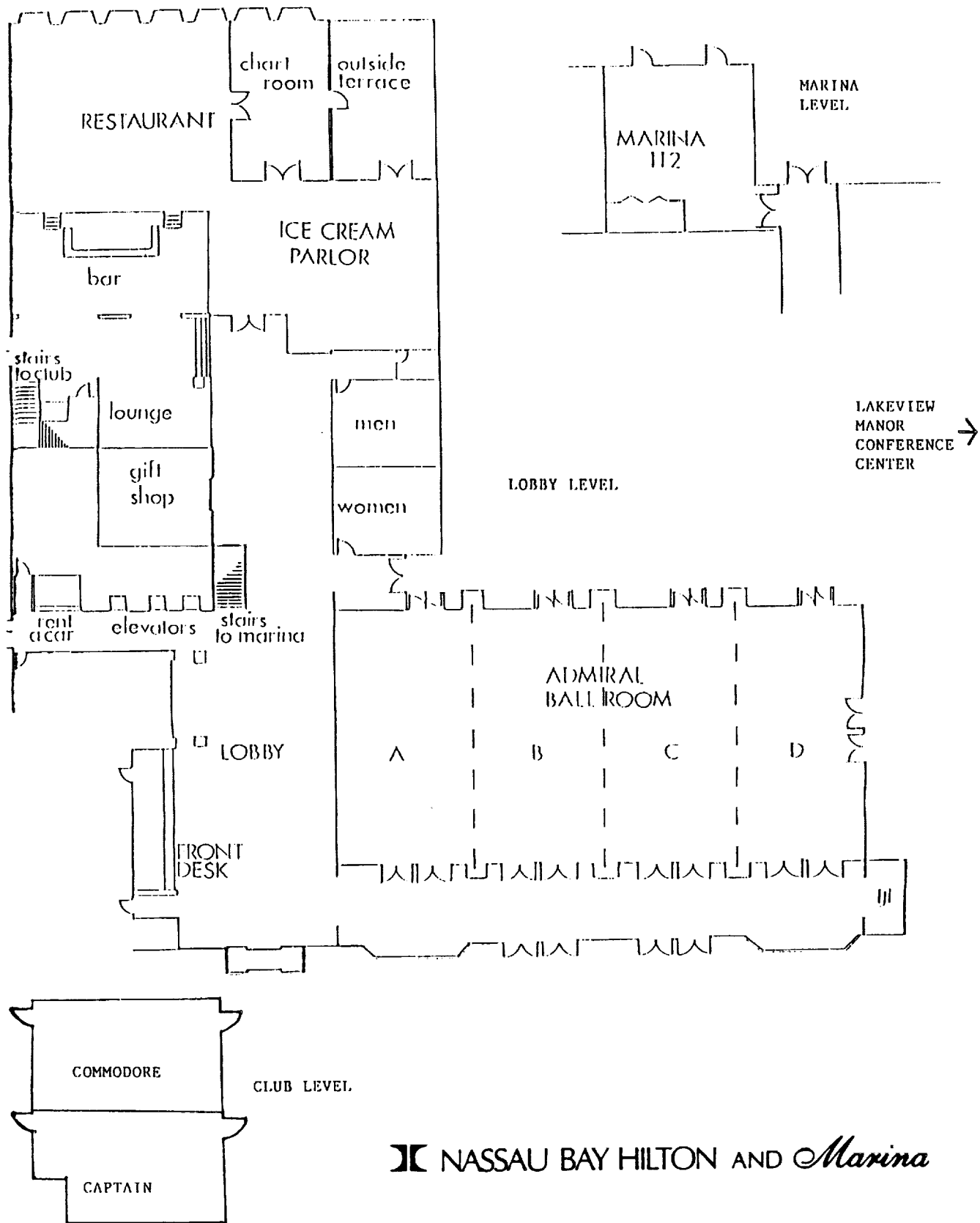
Author Index

Agresti D. G.	1	Chiou W.-A.	176, 177
Allard T.	116	Chipera S.	157, 158
Allen C. C.	2	Chipera S. J.	29
Allen F.	3	Chisholm Brause C. J.	30
Altaner S. P.	4, 35, 110	Clauer N.	31, 32
Anderson D. M.	5	Clayton T.	72
Aochi Y.	47	Coey J. M. D.	161
April R. H.	6, 73	Conradson S. E.	30
Aronson J. L.	35, 42, 98	Cook R. J.	33
Awwiller D. N.	7	Cornachione H. S.	34
		Costanzo P. M.	121
Baker J. C.	8, 9, 24	Cown C. E.	180
Banin A.	10	Coyne L. M.	17
Barnes H. L.	85	Cupp B. L.	130
Baron J.	80		
Bates J. K.	111	Dahl W. M.	148
Bechtel A.	11	Dahlgren R. A.	18, 19
Beebe S. L.	73	Damon P. E.	139
Bell J. F. III	12	Daniels E. J.	35
Bentzon M. D.	107	de Bakker P. M. A.	20
Berry R. W.	147	Dec S. F.	53
Bertolino S. R.	13	de Caritat P.	36
Bertsch P. M.	113	De Grave E.	20, 37
Bish D.	63, 64, 157, 158	DeHart J.	162
Bish D. L.	14, 15, 16, 29, 84	Dixon J. B.	38, 173
Bishop J. L.	17	Donahoe R. J.	94
Blum A.	40, 83	Duplay J.	54
Blum A. E.	120	Durand C.	39
Boettinger J. L.	18, 19	d'Uston C.	90
Bohor B. B.	129		
Bonté Ph.	82	Eberl D.	100
Bossiroy D.	149	Eberl D. D.	40, 41
Bowen L. H.	20	Ebinger M.	158
Boyd S. A.	21, 81	Eggleton R. A.	62
Bradley C. R.	111	Eller P. G.	30
Bradley J. P.	111	Elliott W. C.	42, 124
Bronnimann C. E.	53	Elzea J. M.	43, 123
Brown G. E. Jr.	122	Evlanov E. N.	90
Browne P. R. L.	67		
Burkett P. J.	22	Fallick A. E.	44, 74
Burns R. G.	23	Faraj B. S. M.	45, 46
Buscher T. C.	30	Farmer W. J.	47
		Fendorf S. E.	48
Calas G.	116, 117	Feng X.	58
Carmichael D. C.	24	Ferrell R. E. Jr.	49, 127
Carter J. J.	25	Fialka B. N.	102
Cartz L.	176, 177	Finkelstein D. B.	50
Casal B.	56	Fisher D. S.	23
Cases J. M.	26	Fishman N. S.	51
Cetin K.	27	Fitch A.	52
Charlet L.	109	Fitzgerald J. J.	53
Chermak J. A.	28	Flores R. M.	149

Foh J.	90	Jager H.	90
Follmer L. R.	79	Jaynes W. F.	81
Forster H. S.	60	Jéhanno C.	82
Fripiat J. J.	140	Johnson W. H.	79
Fritz B.	54	Johnsson P.	83
Froget L.	82	Jones B. F.	172
		Jones R. C.	16, 84, 108
Gan H.	55	Jørgensen S. S.	92
Garcia-Ponce A.-L.	56		
Gassman P. L.	57	Kacandes G. H.	85
Gierke J. S.	34	Kankeleit E.	90
Giese R.	100, 121	Kawano M.	86, 151
Girard J.-P.	58	Keighin C. W.	149
Glasmann J. R.	59	Keller D. M.	6
Glese R. F.	119	Keller L. P.	87, 184
Glikson M.	46	Keppens E.	32
Goldberg S.	60	Kevan L.	88
Golden D. C.	61	Khoury H. N.	45
Gooding J. L.	10	Khromov V.	90
Grant R. H.	138	Klimentidis R. E.	4, 89, 125
Grimley D. A.	79	Klingelhofer G.	90
Guggenheim S.	62, 132	Knudsen J. M.	90
Gunter W. D.	183	Koch C. B.	91, 92, 107
Guthrie G.	63, 64	Kocsardy E.	93
Guyen N.	143	Kodama H.	155
		Kornegay C. J.	94
Hall C. M.	148	Kralik M.	95
Hamza A. I.	53	Krishnamurti G. S. R.	96
Happ J. W.	65	Kump L. R.	85
Harper D. A.	66	Kunkle A. C.	173
Harvey C. C.	13, 67		
Hassanipak A. A.	68, 166	Lander R. H.	4
Haszeldine R. S.	44	Lanson B.	97
Hauff P.	69	Lasaga A. C.	120
Hay R. L.	70	Lauer H. V. Jr.	61, 161, 162
Heick E. L.	60	Leckie R. M.	50
Held P.	90	Le Dred R.	80
Hesse R.	155, 156	Lee M.	98
Hillier S.	71, 72	Lee S. Y.	99
Hluchy M. M.	73	Li Z.	100
Hochella M.	83	Liu J.	70
Hochella M. F. Jr.	120	Lo P.-H.	101
Hogg A. J. C.	74	Longo J. M.	76
Holland K.	75	Longstaffe F. J.	66, 102
Hsu P. H.	169	Lou G.	103
Huang P. M.	96, 103, 141	Low P. F.	181
Huang W. L.	76, 89	Lundegard P. D.	104
Hueckel T.	77	Lynch F. L.	105
Huff W. D.	27		
Huggett J.	78	Ma C. M.	77
Hughes R. E.	79, 115	Macaulay C. I.	44
Hutcheon I.	36	Maciel G. E.	53
Huve L.	80	Mackinnon I. D. R.	8, 9, 45, 46, 62, 153, 154

Madé B.	54	Robin E.	82
Madsen F. T.	106	Robinson G. A.	125
Madsen M.	90	Rocchia R.	82
Madsen M. B.	107	Roth C. B.	181
Malengreau N.	117	Roy-Paulsen N. O.	107
Malik H. U.	108	Ruiz-Hitzky E.	56
Manceau A.	109	Ryan P.	134
Martin K. R.	9		
Martin P.	80	Saehr D.	80
Matthews J. C.	110	Salter T. L.	135
Mazer J. J.	111	Savin S. M.	58
McBride M. B.	152	Sawhney B. L.	47, 136
McDowell S. D.	34, 131	Schroeder P. A.	137
Mermut A. R.	112	Schulze D. G.	138
Miller W. P.	113	Schuraytz B. C.	114
Ming D. W.	61, 114	Sennett P.	3
Moore D. M.	79, 115	Shaffer N. R.	93
Morris D. E.	30	Shafiqullah M.	139
Morris R. V.	1, 161, 162	Sharpton V. L.	114
Morup S.	107	Shelfer T. D.	1
Mukhin L. M.	90	Sheppard R. A.	51
Muller J.-P.	116, 117	Siantar D. P.	140
Murad E.	118	Sigurdsson H.	82
Murphy K.	119	Singh J.	141
Murray H. H.	13	Sivalingam S.	142, 143
Myer L. R.	25	Slaughter M.	144, 145, 179
		Small J. S.	146
Nagy K. L.	120	Smirnov G. V.	90
Norris J.	121	Smith R. J.	24
Nüesch R.	106	Smith S. C.	180
		Southard R. J.	19
O'Day P. A.	122	Sparks D. L.	48, 182
Odom I. E.	43, 123	Sposito G.	25
		Sprague E. K.	43, 171
Parks G. A.	122	Srodon J.	41, 156
Pearson M. J.	74	St. Arnaud R. J.	112
Pevear D. R.	76, 89, 124, 125	Stevenson C. M.	111
Pieters C. M.	17	Stille P.	32
Pimperl M. M.	1	Stucki J. W.	55
Pinnavaia T. J.	126	Sutton S. R.	138
Plüss A.	127		
Pollastro R. M.	128, 129	Taylor M. C.	147
Post J. L.	130	Teucher R.	90
Price K. L.	131	Thiry M.	69
Prilutski O. F.	90	Thomas A. R.	148
Primmer T. J.	150	Thompson G.	134
		Thompson J. G.	154
Rakovan J.	132	Thorez J.	149
Reynolds R. C. Jr.	133	Thornley D. M.	150
Riley W. E.	135	Tieh T. T.	101, 165
Ripmeester J. A.	103	Tomita K.	86, 151
Rivers M. L.	138	Tomplier C.	176
Robb G. A.	102	Turner C. E.	51

Ukrainczyk L.	152	White G. N.	173
Uwins P. J. R.	9, 153, 154	Whitney G.	174
		Williams L. B.	49
Vali H.	155, 156	Wills E. L.	1
Van Alboom M.	37	Wood J. L.	175
Vandenbergh R. E.	20		
Vaniman D.	157, 158	Xu Q.	176
van Oss C. J.	100, 119, 121		
Velde B.	159, 160, 174	Yamane H.	151
Vempati R. K.	161, 162	Yang X.	177
Villieras F.	26	Yey H.-W.	178
Vistisen L.	107	Ylagan R. F.	4
Vrolijk P.	163	York D.	148
		Young D. S.	168
Wadleigh M. A.	66	Yu J.-Y.	144, 145, 179
Wagner U.	118	Yuretich R. F.	50
Walker J. R.	75, 164		
Walling S. D.	165	Zachara J. M.	180
Walshe J. L.	36	Zelazny L. W.	57
Wampler J. M.	68, 166	Zhang F.	181
Wang M. C.	167	Zhang Z. Z.	182
Wang M. K.	168	Zhou Z.	183
Wang W.	169	Zolensky M.	184
Weaver C. E.	170	Zolensky M. E.	87
Weaver R. M.	173	Zubkov B.	90
Webb H.	171	Zuchniewicz J.	90
Webster D. M.	172		

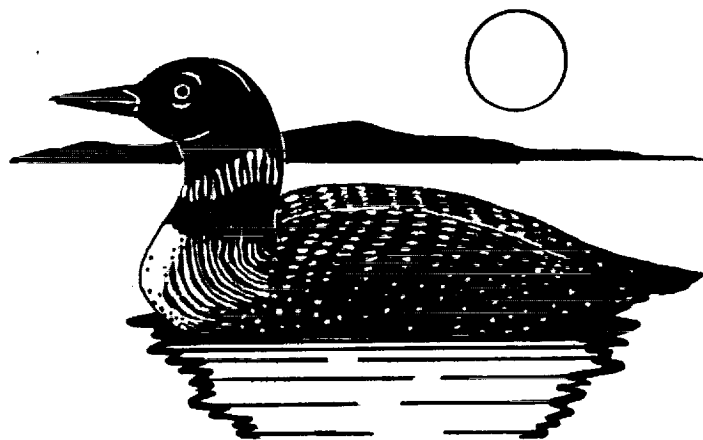


NASSAU BAY HILTON AND *Marina*

The Clay Minerals Society 29th Annual Meeting

November 1-6, 1992 Minneapolis, Minnesota

Joint CMS-SSSA Meeting



General Co-Chairmen:

**Jerry Bigham 614-292-2001
Wayne Hudnall 504-388-1344**

Program Chairman:

Darrell Schulze 317-494-8062



The Clay Minerals Society



SOIL SCIENCE
SOCIETY OF AMERICA